

**Table 4-16. Thermal-Hydrologic Variables Predicted with the Multiscale Thermal- Hydrologic Model at 610 Locations in the Potential Repository**

Thermal-Hydrologic Variable	Drift-Scale Location at Which Predicted
Temperature	Near-field environment host rock (5 m [16 ft] above crown)
	Near-field environment host rock (mid-pillar at potential repository horizon)
	Maximum lateral extent of boiling
	Upper drift wall (crown of the drift)
	Lower drift wall (below invert)
	Drift wall (perimeter average)
	Drip shield (perimeter average)
	Drip shield (upper surface)
	Waste package (surface average)
	Invert (average)
Relative humidity	Drift wall (perimeter average)
	Drip shield (perimeter average)
	Waste package
	Invert (average)
Liquid saturation (matrix)	Drift wall (perimeter average)
	Drip shield (perimeter average)
	Invert
Liquid-phase flux	Near-field environment host rock (5 m [16 ft] above crown)
	Near-field environment host rock (3 m [10 ft] above crown)
	Drift wall (crown)
	Drip shield (crown)
	Drip shield (upper surface average)
	Drip shield (lower side at the base)
	Invert (average)
Gas-phase air-mass fracture	Drift shield (perimeter average)
Gas-phase pressure	Drift shield (perimeter average)
Capillary pressure	Drift shield (perimeter average)
	Invert (average)
	Drift wall (crown; in matrix)
	Drift wall (crown; in fractures)
Gas-phase (water vapor) flux	Drift wall (perimeter average)
Gas-phase (air) flux	Drift wall (perimeter average)
Evaporation rate	Drift shield (crown)
	Drift shield (perimeter total)
	Invert (total)

are run for 31 locations spaced throughout the potential repository area (Figure 4-65) for a range of thermal loading values that represents the influence of edge-cooling. Variability of the hydrologic properties at the scale of the potential repository is represented by the 31 locations (CRWMS M&O 2000cf, Section 5.1.1).

The other three types of models, which are thermal conduction-only models, are required to account

for the influence of three-dimensional mountain-scale heat flow and three-dimensional drift-scale heat flow on drift-scale thermal-hydrologic behavior. Further details on these thermal-conduction-only models, the method used to modify the two-dimensional thermal-hydrologic model results to reflect the three-dimensional scale effects, and the representation of air spaces in the drifts are provided in supporting documentation (CRWMS M&O 2000cf, Sections 6 and 7.1).

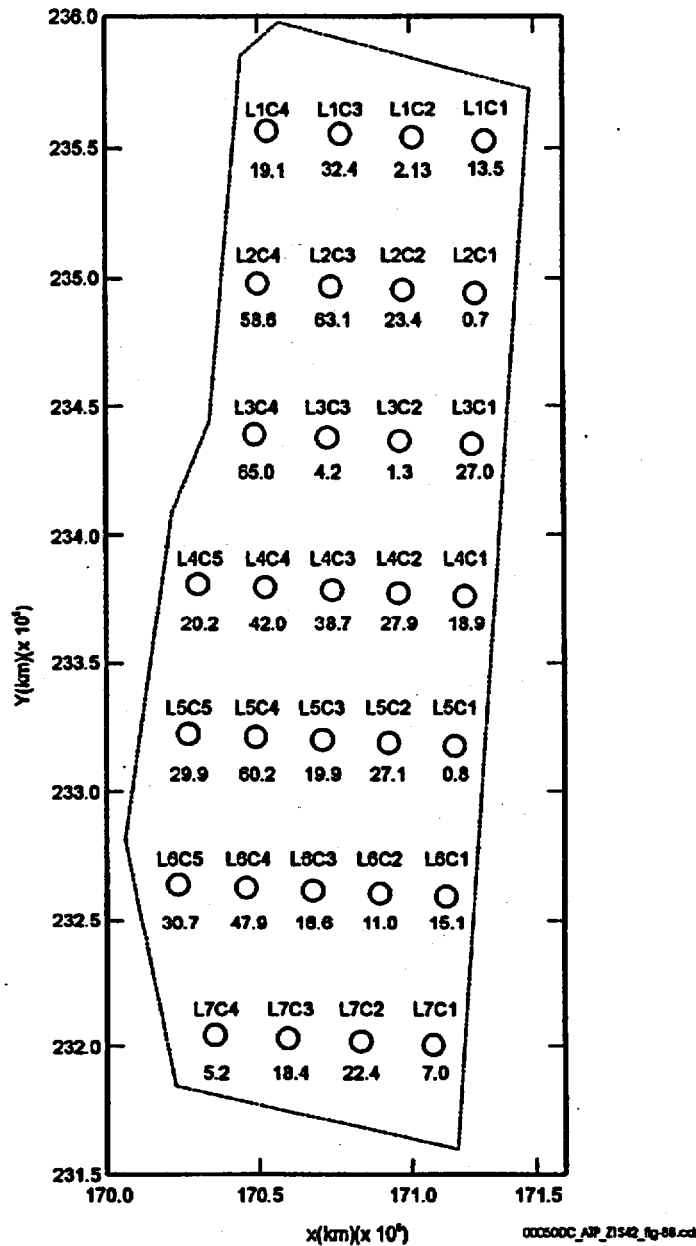


**Figure 4-65. Layout of the Potential Repository Used in the Multiscale Thermal-Hydrologic Model**  
These 31 locations (labeled L1C1 through L7C4) represent the overall repository in the multiscale thermal-hydrologic model. Detailed modeling is performed for each location to predict temperature and humidity conditions in the emplacement drifts. These models are combined with larger (but coarser) drift-scale and mountain-scale models to incorporate the effects of large-scale features of the site and the repository layout. The values posted at each location are the net infiltration values for the glacial-transition (long-term) climate state. Source: CRWMS M&O 2000as, Figure 3-70.

In the multiscale thermal-hydrologic model, the waste package sequence is explicitly modeled in a drift segment and repeated hundreds of times throughout the footprint of the potential repository. Model geometry is consistent with the design basis described in this report. The emplaced waste packages fall into several categories, representing those that would contain (1) pressurized water reactor spent nuclear fuel, (2) boiling water reactor spent nuclear fuel, (3) DOE high-level radioactive waste, and (4) DOE (naval) spent nuclear fuel. All waste packages are emplaced at the same time and follow the same average thermal decay function (as a percentage of initial heat output). The 70 percent heat-removal efficiency and the 50-year ventilation period are applied uniformly throughout the potential repository footprint. The overall average areal mass loading of the potential repository for multiscale model applications is 60 MTHM/acre.

Figure 4-65 illustrates the potential repository footprint used in the model; this footprint closely approximates the actual plan view of the perimeter within which waste would be emplaced. Thirty-one locations are shown, which represent the lateral variability in hydrologic properties, stratigraphic thickness, and boundary conditions.

Major results of the multiscale thermal-hydrologic model summarized in this section are based on the higher-temperature thermal operating mode described in Section 2. During the preclosure period, host rock temperatures remain below the boiling point for the mean- and upper-infiltration flux cases, while boiling occurs in the host rock for the lower-flux case.

The expected duration of temperatures above the boiling point of water (96°C [205°F]) on the surfaces of the waste packages varies for three main reasons: (1) location within the repository layout, (2) spatial variation in the infiltration of recharge water at the ground surface, and (3) variability in the heat output of individual waste packages. The repository edges would cool first because they lose heat to the cooler rock outside the layout. The repository center would cool more slowly because heat flow would be limited mainly to the upward and downward directions. Water percolating downward through the

host rock in response to infiltration at the ground surface would hasten cooling of the repository; locations with greater percolation will cool sooner. There will be relatively large variations in the heat output of individual waste packages depending on the type and age of the waste they contain. Each of these effects is represented explicitly in the multiscale thermal-hydrologic model, and the results of this model are used in TSPA.

During the preclosure period, peak waste package temperatures of 100°C (212°F) for the mean flux case, and 110°C (230°F) for the low flux case, are expected to occur at 10 to 15 years; peak drift-wall temperatures of 86°C (187°F) for the mean flux case, and 96°C (205°F) for the low flux case, are expected to occur at 20 to 25 years. Edge-cooling effects will not strongly affect preclosure temperatures.

During the postclosure period, peak waste package temperatures of 128° to 178°C (262° to 352°F) for the mean flux case, 127° to 189°C (261° to 372°F) for the low flux case, and 124° to 173°C (255° to 343°F) for the high flux case are expected to occur at 60 years. The difference in peak waste package temperature between the hottest and coldest waste packages for the mean flux case would be approximately 50 C° (90 F°). During the very early postclosure period, edge-cooling will have a small effect on temperatures. By 100 years, the influence of edge-cooling will be considerable, with waste package temperatures varying by 65 C° (117 F°) (98° to 163°C [208° to 325°F]) from the edge to the center of the potential repository for the mean flux case.

A typical waste package under nominal conditions would have an average surface temperature above the boiling point of water for about 1,000 years (CRWMS M&O 2000cf, Figure 6-50). For the mean infiltration case, the average temperature on the surfaces of all 21-PWR waste packages would cool to below the boiling point of water after about 1,400 years. Lower infiltration rates could increase the time until the waste packages cool to this temperature. Depending on the infiltration rate and the location in the repository, the time to cool could be less; for example, for the mean infiltration rate a 21-PWR waste package located on the edge of the

repository would cool to below the boiling temperature of water within about 300 years. For brevity, these ranges are described elsewhere in this report as "from hundreds to thousands of years."

Liquid-phase flux in the host rock above the drift would be influenced by dryout and heat pipe activity. Heat pipe behavior can increase the liquid-phase flux in fractures to well above the ambient percolation flux. However, the duration of this effect would be greatly decreased in this design in comparison with the repository design used for the Viability Assessment (CRWMS M&O 1998g, Chapter 3, Section 3.5.4). For the higher-temperature operating mode, the increased liquid-phase flux is calculated to last for less than 600 years (the duration of the present-day climate period).

The maximum lateral extent of boiling temperatures (away from the drift wall) is a good indication of spatial extent of dryout around the emplacement drifts. The lateral extent of boiling would be greater for the low infiltration-flux case than for the mean or upper-flux cases. For the hottest waste package location and the lower flux distribution, the maximum lateral extent of boiling would be 18 m (59 ft); because the drifts would be 81 m (266 ft) apart, a maximum of approximately 44 percent of the potential repository area would exceed the boiling point. If the estimated infiltration increases, this percentage would decrease.

There is a much greater difference in dryout behavior (as evidenced by the maximum lateral extent of boiling and by relative humidity reduction) between the mean and low infiltration-flux cases than between the mean and upper flux cases. Therefore, if one considers a percolation threshold above which rock dryout becomes substantially limited by percolation, the threshold would be near the mean infiltration-flux case. Larger values of the percolation flux greatly limit the calculated extent of boiling temperatures and rock dryout.

#### **4.2.2.3.3 Drift-Scale Thermal-Hydrologic-Chemical Processes and Models**

Figure 4-40 shows schematically the relationships between thermal-hydrologic and geochemical processes in the zones of boiling, condensation,

and water drainage in the rock surrounding the potential repository, particularly in the rock above the emplacement drifts. The emphasis in this section is on the changes in flow properties of the host rock due to these processes. Modeling of thermal-hydrologic-chemical effects on the aqueous chemistry of seepage water and gas composition in the potential repository host rock is described in Section 4.2.3.3.

Changes to hydrologic properties were evaluated using the thermal-hydrologic-chemical model. The thermal-hydrologic-chemical models account for two-dimensional heat and mass transfer within the drifts and in the surrounding rock, using separate continua in the rock to represent the connected network of fractures and the rock matrix in which the fractures reside (CRWMS M&O 2000a1, Section 3.2.3.4.2). The thermal-chemical model component is implemented using TOUGHREACT, a heat transfer, mass transfer, and reactive-transport code. The model is used to calculate dissolution and precipitation of minerals that could change the porosity and permeability of the fracture system (CRWMS M&O 2000a1, Section 3.2.3.4.3).

Thermal-hydrologic aspects of the model, such as the heating rate, ventilation, infiltration flux, and other boundary conditions, are identical to the thermal-hydrologic models discussed previously in this section. Discretization of the model domain is illustrated in Figure 4-66. Several cases were evaluated for different infiltration conditions (i.e., lower, mean, and upper) using the same climate-change scenarios used for the unsaturated zone flow model (BSC 2001o, Section 6.3).

The dual-permeability method was selected for modeling thermal-hydrologic-chemical processes. This is an important selection because a realistic representation of chemical interactions between fractures and the rock matrix depends on realistic representation of hydrologic interactions. The active fracture model is used (Liu et al. 1998; CRWMS M&O 2000bq, Section 6.4.5). Each matrix gridblock and each fracture gridblock has its own pressure, temperature, liquid saturation, water and gas chemistry, and mineralogy. Water-mineral reactions are considered to take place

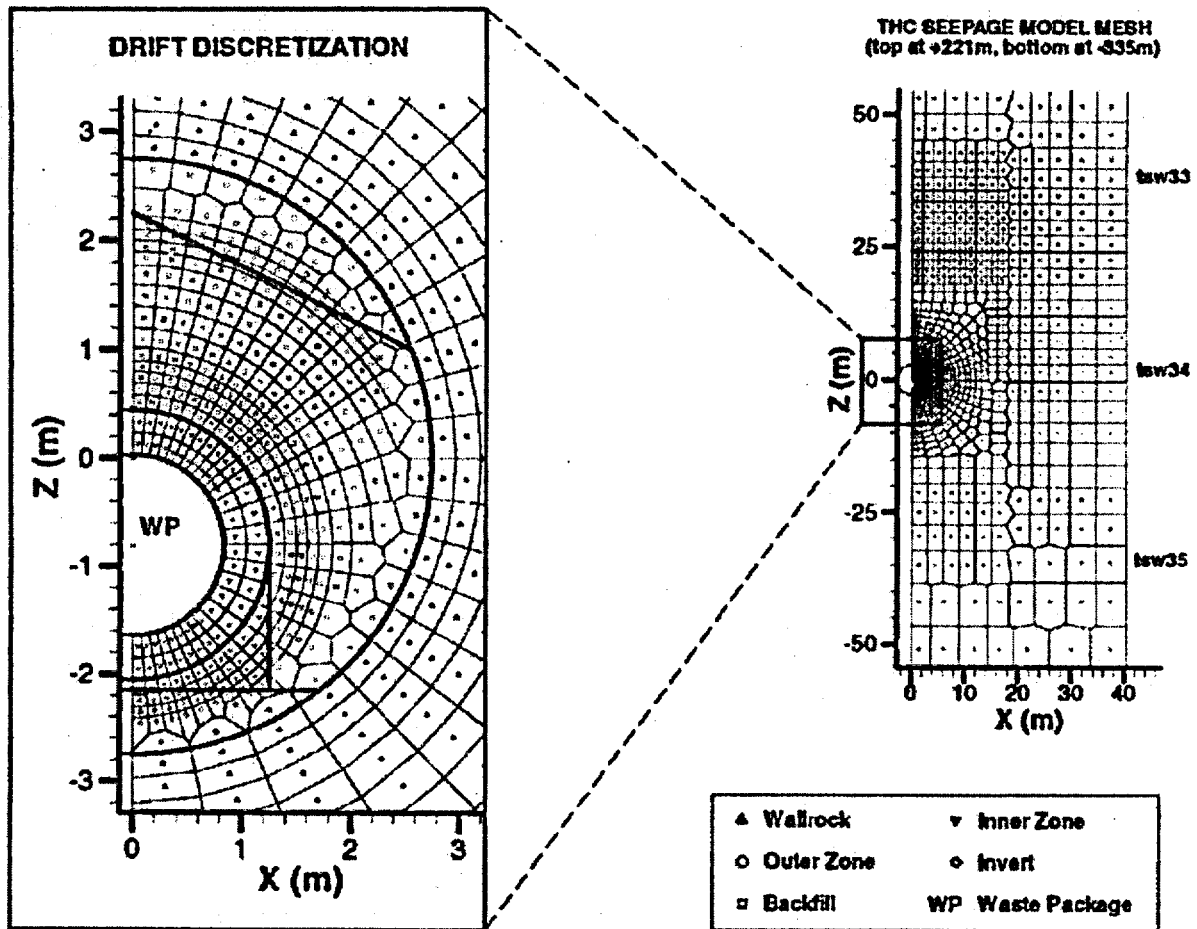


Figure 4-66. Thermal-Hydrologic-Chemical Seepage Model Mesh Showing Hydrogeologic Units in Proximity of the Drift, and Blowup Showing Discretization of In-Drift Design Components

The hydrogeologic units shown are the Topopah Spring Tuff upper lithophysal (tsw33), middle nonlithophysal (tsw34), and lower lithophysal (tsw35) units. These model grids are for simulations with backfill. The model results are used to predict thermal, hydrologic, and chemical conditions at the drift wall, rather than inside the drift. The results are therefore considered applicable to the design without backfill. THC = thermal-hydrologic-chemical. Source: CRWMS M&O 2000c, Figure 3.10-6.

under either kinetic or equilibrium conditions, using simulation methods similar to those described by Reed (1982) and Steefel and Lasaga (1994). Because the dissolution rates of many mineral-water reactions are quite slow, most phases are treated using pseudo-order reaction kinetics.

As stated in Section 4.2.2.2.1.3, the initial water and gas chemistry selected for use in the thermal-hydrologic-chemical model is based on the chem-

ical composition of matrix pore water collected from Alcove 5 (BSC 2001a, Sections 4.1.3 and 6.1.2). Although the rock permeability of the matrix is many orders of magnitude smaller in the matrix than in the fractures, the TSPA-SR thermal-hydrologic-chemical model assumes that infiltrating water in the fractures has the same composition as matrix pore water. This is justified in that the chloride-sulfate-type matrix-derived pore water composition is more concentrated in total dissolved minerals. The actual water compo-

sition within fractures tends to be more dilute (i.e., bicarbonate-type water). For all thermal-hydrologic-chemical modeling, the initial water composition is set to be the same in the fractures and matrix throughout the model domain (BSC 2001o, Section 4.1.3). Thermal-hydrologic-chemical model simulations were repeated with two sets of rock minerals to evaluate the sensitivity of calculated results to the mineral assemblage selected (BSC 2001o, Section 6.2). A full-simulation case included the major minerals found in the fractures and matrix of all rock units that are likely to be thermally perturbed based on mineral occurrence in deeper zeolitized units. A limited-simulation case included those minerals needed to represent basic aspects of Drift Scale Test data, such as pH and gas-phase carbon dioxide, while neglecting other species, such as silicates, ferric minerals, and fluorides. Details on derivation of model inputs, the numerical model and supporting sensitivity studies are provided in *Drift-Scale Coupled Processes (DST and THC Seepage) Models* (BSC 2001o, Sections 4.1 and 6.2).

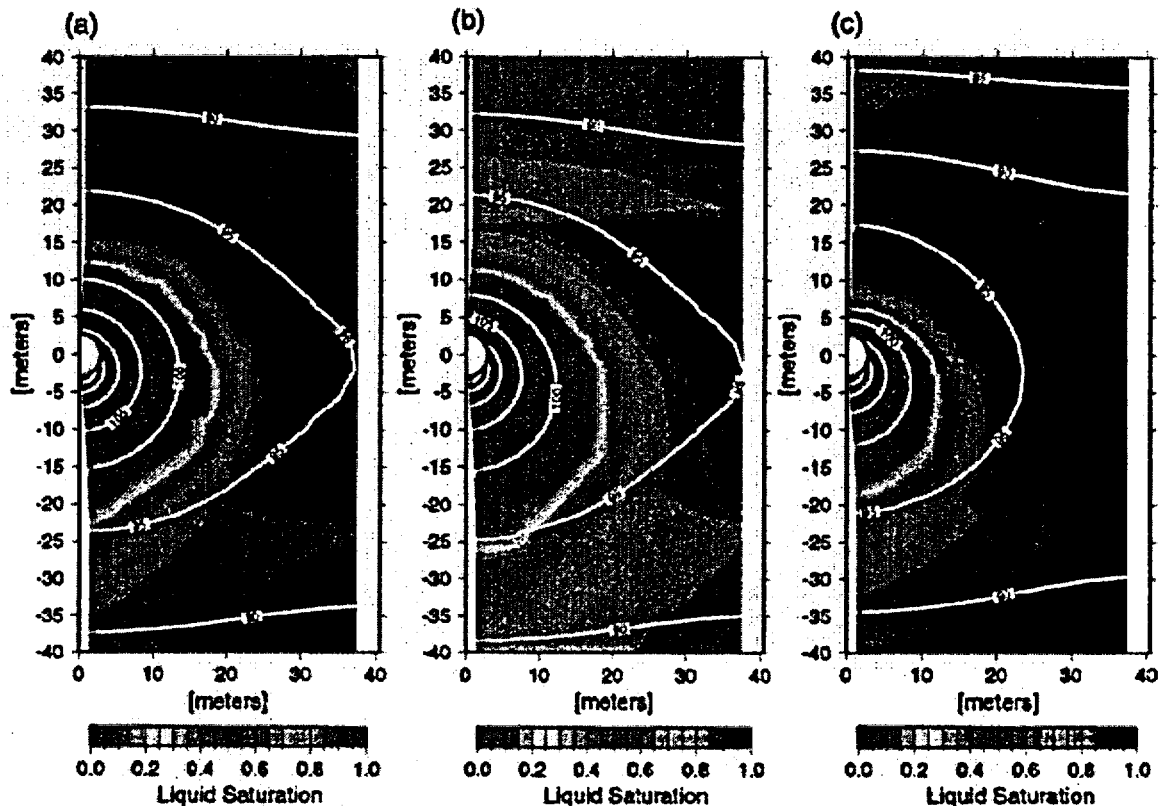
Thermal-hydrologic-chemical model results consist of projections for the composition of water and gas that may enter the emplacement drifts for 100,000 years, including a 50-year preclosure period with ventilation. Figure 4-67 shows liquid saturation and temperature in the rock around the drifts at 600 years for the three infiltration conditions (i.e., lower, mean, and upper). This is the approximate time of the maximum extent of dryout for each infiltration case investigated. Note that these models predict conditions that would be encountered near the center of the potential repository, and that cooler conditions would be found near the edges.

Time histories for gas-phase carbon dioxide concentration, pH, chloride concentration, and total dissolved carbon concentration are predicted for the several locations in the host rock at the drift wall (CRWMS M&O 2000c, Figures 3.10-8 to 3.10-11). These results are summarized in Section 4.2.3.3, where they are used as boundary conditions for the physical and chemical environment in the emplacement drifts.

Comparison with data from the Drift Scale Test shows that the limited simulation (calcite, silica, and gypsum minerals only) matches observed chemical data more closely than the full simulation (including silicates, iron, and fluorides). However, for longer duration of reflux and boiling, as would be encountered in the potential repository, the system may trend toward the chemistry of the more complex full simulation.

Porosity changes in the rock matrix and fractures are directly related to volume changes from mineral precipitation and dissolution. Changes in fracture permeability are approximated using a parallel-plate model approach with fractures of uniform aperture (Steefel and Lasaga 1994, p. 556). Matrix permeability changes are calculated from changes in porosity using the Carmen-Kozeny relation (Bear 1988, p. 134). Capillary pressure in the matrix and fractures is modified using the Leverett scaling relation (Slider 1976, pp. 290 to 297), as previously mentioned in Section 4.2.1.3.2.

The calculated changes in fracture porosity for rock near the emplacement drifts, for the full simulation, at a simulation time of 10,000 years, are shown in Figure 4-68 for the three infiltration conditions (i.e., lower, mean, and upper). The fracture porosity change is expressed as a percentage of the initial porosity. Maximum porosity decrease is predicted for the high-infiltration case, predominantly above the drift. For all cases, the porosity change is relatively small (less than 1 percent of the initial porosity). For the limited simulation, porosity decrease results mainly from calcite precipitation, as was interpreted from the Drift Scale Test simulations. For the full simulation, the fracture porosity change is dominated by zeolite reactions. Because the fracture porosity changes are small compared to total fracture porosity, permeability changes are negligible and thermal-hydrologic processes will not be significantly affected by mineral precipitation or dissolution (CRWMS M&O 2000a, Section 3.2.3.4.3).



000500C\_ATP\_21842\_fig-36.m

Figure 4-67. Contour Plot of Modeled Liquid Saturations and Temperatures in the Matrix at 600 Years (Near Maximum Dryout) for Three Infiltration Rate Scenarios

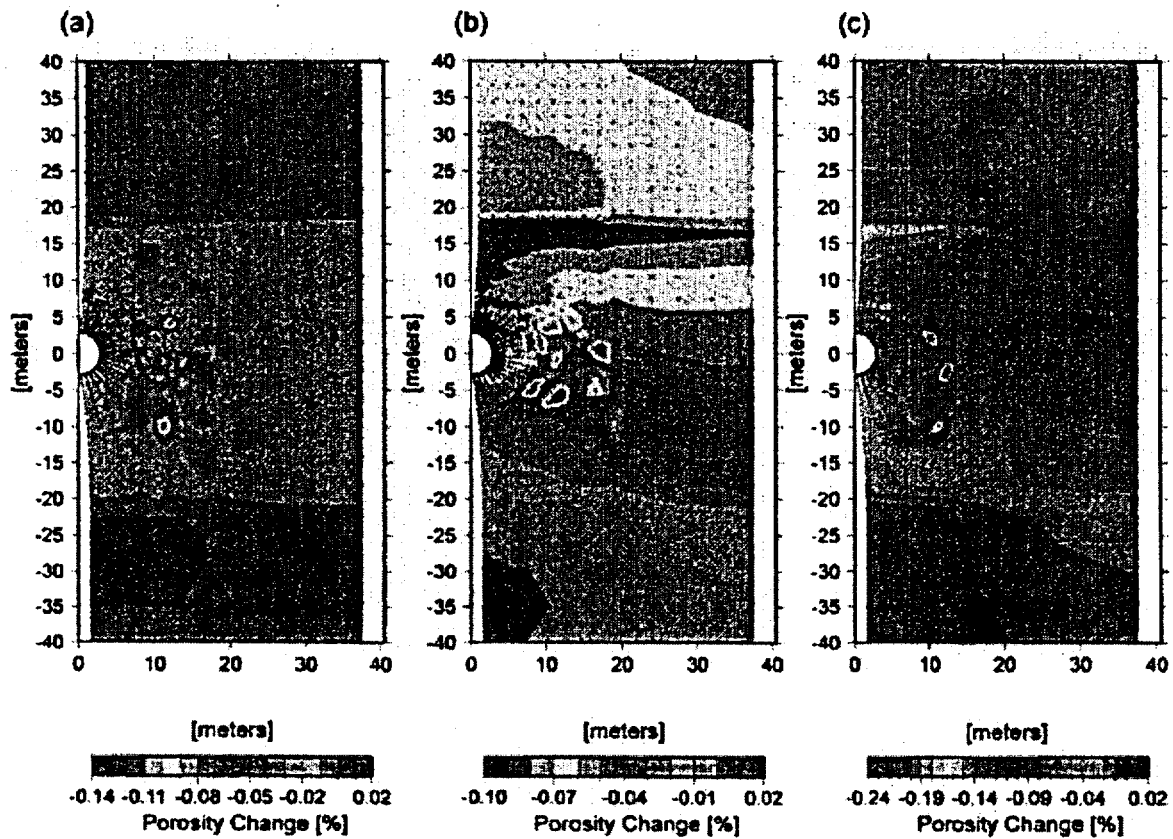
The lower, mean, and upper infiltration rate scenarios are developed for the unsaturated zone flow model to represent the uncertainty of present-day and predicted future infiltration rates. The contour plots shown are (a) lower, (b) mean, and (c) upper scenarios (calcite-silica-gypsum system). The white contour lines show temperature in °C. The white half-circle in each plot is the drift outline, and the models are laterally symmetrical about the drift center. Source: CRWMS M&O 2000c, Figure 3.10-7.

#### 4.2.2.3.4 Drift-Scale Thermal-Hydrologic-Mechanical Processes and Models

The drift-scale thermal-hydrologic-mechanical modeling in support of the TSPA accomplishes two objectives. This section emphasizes the potential effect on hydrologic properties in the surrounding rock resulting from thermal-mechanical changes, specifically potential effects on permeability. The drift degradation analysis presented in Section 4.2.3.3.5 assesses thermally caused movement of blocks on fractures intersecting the drift and the

potential for rockfall to affect the engineered barrier system.

Most prior thermal-mechanical modeling had the objective of determining the evolution of stresses in the near-field rock, in order to estimate the requirements for rock support in the emplacement drifts. These models treated the rock as a continuum and conservatively assumed that the mid-pillar locations were symmetry boundaries. This assumption is conservative (produces higher calculated stresses) because the overall repository footprint can expand due to the heating. The move-



000600C\_ATP\_Z1842\_1p-38

Figure 4-68. Contour Plot of Calculated Total Fracture Porosity Change at 10,000 Years for Three Infiltration Rate Scenarios

The lower, mean, and upper infiltration rate scenarios are developed for the unsaturated zone flow model to represent the uncertainty of present-day and predicted future infiltration rates. The contour plots shown are (a) lower, (b) mean, and (c) upper scenarios (full simulation). Red areas indicate the maximum decrease in porosity as a result of mineral precipitation. The white half-circle in each plot is the drift outline, and the models are laterally symmetrical about the drift center. Source: CRWMS M&O 2000c, Figure 3.10-12.

ment of rock blocks at fractures was captured in the continuum models by the rock mass properties, such as the coefficient of thermal expansion (the fractional expansion of the rock per degree of temperature rise). Measurements of this coefficient depends on the size of the sample, with the coefficient decreasing as the scale moves from core to small blocks to small field tests and then to large field tests (CRWMS M&O 1999m, Table 9-3). The decrease in expansion coefficient can be attributed to the increased number of fractures which can accommodate expansion of the rock blocks. The results of the modeling indicate that horizontal

compressive stresses increase more than vertical compressive stresses during the thermal pulse, due to the stiff boundary conditions at the mid-pillar locations.

In this analysis supporting the TSPA-SR model, the distinct-element code 3DEC is used to simulate normal and shear displacement and other behavior on discrete fractures in the rock mass surrounding the drift (CRWMS M&O 2000a, Section 3.5.2). Fracture orientations and fracture densities are represented and discretized (gridded) in three dimen-

sions. Fracture orientations are based on field observations (Albin et al. 1997). Joint and rock-mass properties used in the calculation are based on field and laboratory studies of rock and fracture behavior, such as those by Barton et al. (1985) and Olsson and Brown (1994). Fracture densities are based on the assumption that only a few well-connected fractures are mechanically and hydrologically active (CRWMS M&O 2000al, Section 3.5.2).

Calculated joint deformations are used to compute permeability deformation values over a period of 1,000 years to capture the effects of heating and cooling. The mathematical formulation is described in the *Near-Field Environment Process Model Report* (CRWMS M&O 2000al, Section 3.5.2.3). Using this formulation, shear deformation always produces an increase in permeability, while normal deformation will increase permeability if the fracture opens and decrease permeability if the fracture closes. In general, fracture closing is expected during the heating phase in response to thermal expansion, while fracture opening occurs during cooling, the effects of shear displacements notwithstanding.

The results of the calculation (CRWMS M&O 2000al, Section 3.5) are that the major thermal-mechanical effect on fracture permeability occurs during cooldown due to both shear and normal deformation. Shear deformation of fractures during the cooldown causes permeability of the fractures in a region within two drift diameters of a drift wall to increase in permeability as much as an order of magnitude. Specifically, shear deformation on vertical fractures during cooldown produces the maximum amount of permeability change. Farther away from the drift wall, smaller increases in permeability (a factor of five) may occur on vertical fractures (CRWMS M&O 2000al, Section 3.5.3).

Results also indicate that normal deformation of fractures causes permeability to increase but to a lesser degree than shear deformation. Normal deformation during heating causes permeability to decrease significantly within one drift diameter of the drift wall. During cooldown, some vertical

fractures above the drift open, thus increasing the permeability by a factor of two from the ambient values (CRWMS M&O 2000al, Section 3.5.3).

Ambient fracture permeability at the repository horizon is high, greater than  $10^{-13}$  m<sup>2</sup> (100 millidarcy) (CRWMS M&O 2000ch, Table 5). *Near-Field Environment Process Model Report* (CRWMS M&O 2000al, Section 5.5) concludes that the potential order of magnitude increase in permeability due to shear movement is not likely to significantly affect seepage.

#### 4.2.2.3.5 Limitations and Uncertainties

As discussed in Section 4.1.1.2, uncertainties are an inherent component of the TSPA method. Uncertainty is introduced through the conceptual model selected to characterize a process, as well as the mathematical, numerical, and computational approaches used to implement the model. Uncertainty is also introduced from imperfect knowledge of important parameters used for input to the models (e.g., physical properties).

The DOE has performed several supplemental activities to address uncertainties and limitations in the TSPA-SR model. Additionally, as noted in Section 4.1.4, the DOE is evaluating the possibility for mitigating uncertainties in modeling long-term repository performance by operating the design described in this report at lower temperatures. Consequently, some of the models describing the effect of decay heat on water movement have been updated since the TSPA-SR model. Some alternative conceptual models have been implemented, and sensitivity analyses conducted to address parameter and model uncertainties. These supplemental model analyses are summarized in *FY01 Supplemental Science and Performance Analyses* (BSC 2001a, Section 1; BSC 2001b, Section 1).

**Mountain-Scale Thermal-Hydrologic Model—**The unsaturated zone flow model is the basis for the mountain-scale thermal-hydrologic model. Therefore, uncertainties associated with the unsaturated zone flow model also pertain to the mountain-scale model (see Section 4.2.1.3). The spatial resolution of the numerical mountain-scale thermal-hydrologic model is large enough that it

limits the interpretation of calculated temperature, saturation, and fluxes within the emplacement drifts and in the host rock near the drift openings. Consequently, the multiscale thermal-hydrologic model, with a finer spatial scale than the mountain-scale model, is used for these purposes.

**Multiscale Thermal-Hydrologic Model—**Two categories of model uncertainties are defined for the multiscale thermal-hydrologic model: (1) uncertainties related to thermal-hydrologic modeling and (2) uncertainties related to the multiscale estimation methodology.

The unsaturated zone flow model provides an important basis for the multiscale thermal-hydrologic model. Consequently, uncertainties associated with the flow model are propagated to the multiscale thermal-hydrologic model. Uncertainties related to the special features of the unsaturated zone seepage process model are not incorporated in the TSPA-SR model. As discussed in this section, the TSPA-SR model uses a conservative approach for calculating seepage during the thermal pulse, based on the percolation flux (5 m [16 ft] above the drift openings) and calculated by the multiscale thermal-hydrologic model. Although this is considered to be a conservative approach (leading to overestimated thermal seepage into drift openings), model improvements have been suggested such as discrete representation of flow focusing along faults and fractures and representation of episodically increased flow in the host rock (BSC 2001a, Section 4.3.5.6).

The percolation flux contains uncertainties related to mean, high, and low infiltration flux conditions, temporal variability (e.g., changes in climate), and spatial variability (e.g., repository cooling at the edges). The principal effects of these uncertainties on TSPA are related to the timing for cooling and return of moisture to the in-drift environment. Differences in timing of hundreds to a few thousands of years (as discussed in Section 4.2.2.3.2) will have a minor impact on the estimated longevity of the drip shield and waste package (with expected lifetimes greater than 10,000 years calculated in the TSPA-SR model). Another uncertainty is the arrangement and heat output of

different types of waste packages, either in a lower- or higher-temperature operating mode. An arrangement of waste types with different heat output is used in the multiscale model, but the extent to which this is representative of repository conditions is uncertain, pending final decisions on repository design and operations parameters.

Uncertainties related to the multiscale estimation methodology include the effects of mountain-scale gas-phase convective circulation and the movement of water vapor along the axis of emplacement drifts from warmer to cooler regions. The TSPA-SR modeling approach did not include heat transfer by these mechanisms, probably resulting in overestimation of predicted temperatures and the duration of the thermal pulse.

Supplemental studies have added insight to some uncertainties and limitations identified with the TSPA-SR model. Approaches included alternative thermal property sets representing lithophysal tuff, Monte Carlo simulations of spatially heterogeneous fracture properties, simulation of a through-going vertical fracture zone intersecting the drift opening, and decreased thermal loading representing a lower-temperature operating mode (BSC 2001a, Sections 4.3.5.3, 4.3.5.4, and 4.3.5.5). Specific studies included:

- Alternative thermal seepage models incorporating the effects of flow focusing and episodicity (BSC 2001a, Section 4.3.5). The results support previous TSPA-SR analyses that found thermal seepage to be negligible for the relatively small values of seepage that may occur.
- Representation of fractures by spatially heterogeneous properties (BSC 2001a, Section 5.3.1.4.2).
- Evaluation of the bulk permeability of the host rock, the thermal conductivity of the lithophysal Tptpl unit and the invert, and the effects of lithophysal porosity of the Tptpl unit on vapor storage and heat capacity (BSC 2001a, Sections 5.3.1.4.1, 5.3.1.4.7, 5.3.1.4.8, 5.3.1.4.9, and 5.3.1.4.10).

- Evaluation of mountain-scale gas-phase convective process and the movement of vapor along the axis of the emplacement drifts (BSC 2001a, Sections 5.3.1.4.4 and 5.3.2.4.6).

Supplemental studies substantiate the overall model and analytical results of the TSPA-SR model, providing quantification of uncertainty either quantitatively or qualitatively. Thermal-hydrologic-chemical and thermal-hydrologic-mechanical processes will not significantly affect temperature or relative humidity within the emplacement drifts (BSC 2001a, Sections 5.3.1.4.5 and 5.3.1.4.6). In evaluating a lower-temperature operating mode, supplemental studies show thermal perturbations to be less than in the higher-temperature operating mode (BSC 2001b, Sections 3.2.2.6 and 4.2.2).

**Drift-Scale Thermal Hydrologic-Chemical Processes Model**—Uncertainties exist in the chemical parameters used to describe mineral precipitation and dissolution. Temperatures and flow rates are better constrained than other parameters of these models. Geochemical reactions are strongly influenced by temperature, the presence of water, and mass transport; so while the spatial distribution of mineral precipitation and dissolution is considered to be representative, the quantities minerals formed or dissolved at a given time and location are more uncertain. Furthermore, the potential for rapid boiling in the rock to cause mineral behavior outside the range of the models is recognized.

The assumed initial water and gas compositions as well as the geochemical conceptual model may also introduce uncertainty. Uncertainty is also recognized in the relationship used to determine fracture permeability based on changes in fracture porosity. These model uncertainties affect predictions of host rock pore water chemistry and changes in permeability in the host rock caused by thermal-hydrologic-chemical processes.

Model parameters, such as the effective reaction rates, are calibrated to results from field thermal tests, including the Drift Scale Test. Comparison of model predictions to geochemical data is important

for confidence building, and such comparisons have shown that the model is reasonable. Results from the full simulations yield higher pH values than measured in water samples from the Drift Scale Test, which results from a greater calculated reaction rate for feldspars. Therefore, porosity changes as a result of feldspar alteration in the potential repository host rock will probably be slower than predicted, suggesting that the TSPA-SR model gives an upper bound on such changes.

Supplemental studies have added insight to some uncertainties and limitations identified with the TSPA-SR thermal-hydrologic-chemical process and abstractions. These activities included a range of different input data and assumptions, such as host rock mineralogy and thermodynamic input data (BSC 2001a, Sections 4.3.6.3.1 and 6.3.1.6). Studies included:

- Supplemental model validation activities of water and gas compositions conducted for Drift Scale Test results (BSC 2001a, Sections 4.3.6.3.1 and 4.3.6.9)
- Supplemental sensitivity studies of different initial water and gas boundary conditions (BSC 2001a, Section 4.3.6.5)
- Simulated evolution of water and gas compositions in the lower lithophysal as well as the middle nonlithophysal tuff unit (BSC 2001a, Section 6.3.1.4.3).

These additional drift-scale thermal-hydrologic-chemical model simulations support the TSPA-SR evaluation, concluding only negligible changes in fracture permeability resulting from thermal-chemical rock and water interactions (BSC 2001a, Sections 4.3.6.7.4 and 4.3.6.9).

**Drift-Scale Thermal-Hydrologic-Mechanical Processes and Models**—The thermal-hydrologic-mechanical model, used in the TSPA-SR model, used a simplified thermal history to calculate results (CRWMS M&O 2000a1, Section 3.5). Coupling the model to the multiscale thermal-hydrologic model has been suggested as a model improvement. Uncertainties in the TSPA-SR

thermal-hydrologic-mechanical model also include mechanical boundary conditions, joint and block properties, block geometry, and the calculation of permeability change due to aperture change.

The model domain for drift-scale near-field thermal-mechanical models is bounded by the mid-pillar locations between the emplacement drifts. For stress calculations, using a zero lateral displacement boundary condition at this location would be conservative (i.e., producing greater horizontal compressive stress) because in reality the entire repository layout can expand, allowing some displacement of the mid-pillar locations during the heating period.

The thermal-hydrologic-mechanical model used in the TSPA-SR model imposed boundary conditions equal to the ambient in situ stress (CRWMS M&O 2000a, Section 3.5). This is nonconservative (producing smaller stresses) because it is equivalent to assuming that more lateral displacement of the repository layout would occur. An alternative method would calculate the overall large-scale repository response in a coarsely gridded model and use the results to develop time-dependent displacement and stress boundary conditions for a drift-scale model. An additional advantage of this method would be the ability to consider the variability of the thermal-hydrologic-mechanical response due to proximity to an edge of the repository.

The joint and rock mass properties are based on field and laboratory studies (CRWMS M&O 2000a, Section 3.5.2). As discussed in Section 4.2.2.3.4, the effective thermal expansion coefficient depends on the size of the sample because of the tendency for fractures to deform in response to thermal stress changes. A similar situation exists for discrete fracture models because the rock between the discretely modeled joint may also include fractures. Also, the input values used for joint friction and cohesion are both variable and uncertain. Possible model improvements include adjusting the model grid for more gradual transitions in block sizes, also using site-specific fracture mapping data to develop the block sizes and shapes.

Supplemental studies have added insight to some uncertainties and limitations identified with the TSPA-SR thermal-hydrologic-mechanical process evaluation. Two models were used to assess selected uncertainties related to thermal-hydrologic-mechanical processes: a revised and extended discrete fracture (distinct element) analysis and a fully coupled thermal-hydrologic-mechanical continuum model (BSC 2001a, Section 4.3.7). These studies evaluated different boundary conceptual models, a simplified cubic-block conceptual model, and alternative empirical nonlinear relationships to calculate permeability change from porosity change (BSC 2001a, Section 4.3.7). Sensitive parameters were identified (e.g., residual permeability and rock stiffness) and conclusions are similar to those reached for the TSPA-SR model: permeability changes are within the range of the ambient seepage model, and thus uncertainty is already captured in the TSPA-SR model (BSC 2001a, Section 4.3.7.5).

#### 4.2.2.3.6 Alternative Conceptual Processes

As with limitations and uncertainties, some of the following alternative conceptual models have been implemented or addressed in supplemental uncertainty analyses. These results are summarized in *FY01 Supplemental Science and Performance Analyses* (BSC 2001a, Section 1; BSC 2001b, Section 1).

**Mountain-Scale Thermal-Hydrologic Model and Multiscale Thermal-Hydrologic Model—**Alternative conceptual models can be organized in several categories: representation of fractured rock in numerical models, selection of representative property values, the potential for permanent changes in those properties from the effects of heating, and alternative models implemented to quantify uncertainties.

The host rock is represented in the mountain-scale and multiscale models as a continuous porous medium, although the rock contains discontinuities such as fractures and fracture zones. An alternative model represents the fractures discretely, and the resulting discrete fracture model approach has been applied to example problems (Hardin 1998, Section 3.3.3). The approach is very computation-

ally intensive and probably not practical for drift-scale and mountain-scale calculations. In addition, the number of interconnected fractures present in the host rock is so large that features of the network can be represented by a continuous medium (Section 4.2.1.3.1.1). Use of the discrete fracture model approach has been limited to modeling studies that support understanding of thermal-hydrologic processes.

Another category of alternative models involves the manner in which the network of fractures in the host rock is represented by a continuous medium. The thermal-hydrologic models described here represent fracturing using a dual-permeability continuum approach, based on the active fracture concept, which is also used in the unsaturated zone flow model (Section 4.2.1.3.1.1). The dual-permeability approach controls the movement of liquid and gas between fractures and the adjacent intact rock. Other available approaches include dual-porosity models and the equivalent single-continuum model (Hardin 1998, Section 3.3). The need for dual-permeability has been demonstrated by comparison to field thermal test data (Hardin 1998, Section 3.4); other approaches have been determined to provide less realism than the dual-permeability approach.

Alternative models for potential permanent changes in thermal and hydrologic properties of the host rock may be summarized as follows:

- Heating, cooling, and resulting water movement occur in a system with fixed thermal and hydrologic properties (such as porosity, permeability, and thermal conductivity). Properties of the rock may vary with temperature and water saturation but return to pre-repository values after the temperature returns to ambient levels.
- The same processes occur, but thermal effects permanently alter certain properties of the host rock through the action of coupled processes. For example, thermal-hydrologic-chemical coupling may change the hydrologic properties because of dissolution and precipitation of minerals in different regions.

The understanding of thermal-hydrologic-chemical effects on flow is summarized in Section 4.2.2.3.3. The model results indicate that changes in fracture porosity and permeability caused by chemical dissolution and precipitation will be minor compared to total porosity and permeability; hence, the first conceptual model (i.e., stationary properties) is selected as the most credible. This is the conceptual basis for both the mountain-scale thermal-hydrologic model and the multiscale thermal-hydrologic model.

As noted in the previous Section 4.2.2.3.5, supplemental studies have addressed additional alternative models:

- Supplemental studies implemented an alternative seepage method. Instead of using percolation flux as input to the seepage abstraction model, the unsaturated zone seepage model is used, incorporating new models for focusing seepage flow along discontinuities (e.g., faults) and episodic flow (BSC 2001a, Section 4.3.5).
- Supplemental studies implemented effects of mountain-scale gas-phase convective circulation and the movement of water vapor along the axis of emplacement drifts from warmer to cooler regions (BSC 2001a, Sections 5.3.1.4.4 and 5.3.2.4.6).
- Supplemental studies implemented effects of vapor storage and altered heat capacity within lithophysal cavities (porosity) of the Tptpl unit (BSC 2001a, Sections 5.3.1.4.1 and 5.3.1.4.9).
- Sensitivity studies incorporated drift-scale heterogeneity such as the influence of drift-scale heterogeneity of fracture properties, including permeability, porosity, and capillary properties (BSC 2001a, Section 5.3.1.4.2).

Supplemental analyses employing alternative models substantiate the overall model and analytical results of the TSPA-SR model (BSC 2001b, Sections 3.2.2 and 4.2.2).

**Drift-Scale Thermal-Hydrologic-Chemical Processes and Models**—A model proposed by Matyskiela (1997) suggests that silica precipitation in the rock matrix adjoining fractures will strongly reduce the permeability of the matrix, resulting in significantly decreased imbibition of percolating waters. The time required for strong sealing by silica was estimated for volcanic glasses under saturated conditions. Matyskiela (1997) observed complete filling of pore spaces with silica at fracture-matrix interfaces around a basaltic magma intrusion, the 50-m (160-ft) wide Papoose Lake sill, in the Paiute Ridge area of the Nevada Test Site. He estimated that fracture flow could be enhanced five times in magnitude with the sealing of the matrix pores (Matyskiela 1997, pp. 1117 to 1118). Formation of a silica cap by plugging of fractures with siliceous minerals, as predicted by recent simulations conducted for the potential repository at Yucca Mountain (Hardin 1998, Section 8.5.1), is the opposite behavior. More recent simulation modeling (CRWMS M&O 2000a, Section 3.3.3.5) has shown that fracture plugging will be of limited importance, given estimated fracture porosity of 1 percent.

Lichtner et al. (1999) showed that for a given matrix porosity, fracture plugging depends on the fracture porosity and the particular silica mineral that precipitates. The two-phase numerical simulation results suggest that at distances of tens of meters from the larger Paiute Ridge intrusion in their study, prolonged boiling conditions were established for times on the order of several thousands of years. Amorphous silica, with its higher solubility, is more readily transported by water and therefore produces the largest decrease in porosity, followed by chalcedony and quartz. For substantial sealing of fractures, a very small value of the fracture porosity is necessary. Lichtner et al. (1999) questioned the conclusions of Matyskiela (1997).

Comparison of the geochemical environment around a potential repository at Yucca Mountain with the geochemical environment around a basaltic magma intrusion is provided in supporting documentation (CRWMS M&O 2000c, Section 3.10.9). As discussed in Section 4.2.2.3.3, models of permeability changes due to mineral precipitation indicate that any such changes will be

minimal. The sealing effects of silica deposition will probably be less developed at Yucca Mountain because (1) devitrified tuff reacts slowly compared with volcanic glass, (2) unsaturated fractures have less wetted surface area, and (3) the silica concentration in condensate draining through fractures will probably be limited by reaction rate processes.

As noted in Section 4.2.2.3.5, supplemental studies have addressed additional alternative models, including:

- Alternative initial water and gas compositions boundary conditions (BSC 2001a, Section 4.3.6.5)
- Alternative representation of the host rock, including the explicit representation of the Tptpl lithophysal unit mineralogy (BSC 2001a, Section 6.3.1.4.3).

Supplemental analyses employing alternative models substantiate the overall model and analytical results of the TSPA-SR model (BSC 2001b, Section 3.2.4.2).

**Drift-Scale Thermal-Hydrologic-Mechanical Processes and Models**—Alternative approaches fall into two categories: continuum versus discrete fracture models and method of coupling thermal-mechanical results to hydrologic flow. Both continuum and discrete fracture models have been used on the project. The continuum approach is satisfactory for calculating spatially averaged stress fields but is unable to resolve fracture displacements that affect permeability. The discrete fracture method can calculate movement of a significant number of representative fractures, which can then be related to permeability change.

Fracture displacement through normal or shear movement results in aperture change. The aperture change can be used to calculate both fracture porosity and fracture permeability, based on assumptions about fracture geometry. The approach used in Section 4.2.2.3.4 was to calculate fracture permeability change directly from fracture aperture change, using an empirical relationship based on laboratory studies. An alternative approach, used for thermal-hydrologic-chemical

modeling in Section 4.2.2.3.3, assumes a fracture geometry (parallel plates) and calculates permeability change from theoretical considerations.

As noted in Section 4.2.2.3.5, supplemental studies have addressed additional alternative models, including:

- A revised and extended distinct element analysis and a fully coupled thermal-hydrologic-mechanical continuum model (BSC 2001a, Section 4.3.7)
- A simplified cubic block conceptual model and alternative empirical nonlinear relationships to calculate permeability from porosity (BSC 2001a, Section 4.3.7).

Conclusions from the supplemental studies are similar to those reached for the TSPA-SR model: permeability changes are within the range of the ambient seepage model, and thus uncertainty is already captured in the TSPA-SR model (BSC 2001a, Section 4.3.7.5).

#### **4.2.2.3.7 Model Calibration and Validation**

**Mountain-Scale Thermal-Hydrologic Model—**There are no directly applicable data for validation of the mountain-scale response to thermal loading associated with the potential repository. However, numerical models of geothermal and petroleum systems can be validated from a wealth of field-scale testing and geothermal production data. The validity of mountain-scale model predictions is demonstrated by corroborative results from the modeling of analogue systems, from previously published unsaturated zone modeling studies, and from field-scale thermal tests in the Exploratory Studies Facility.

Table 4-15 in Section 4.2.2.3.3 lists selected geothermal systems (and, where available, analyses of those systems) that are comparable to the mountain-scale model. Applications for thermal-hydrologic modeling include detailed studies of the genesis, production history, and future performance of geothermal fields. Justification for the modeling approaches used in the mountain-scale thermal-hydrologic model is found in the

successful modeling of fluid and heat transport in large natural subsurface systems for which extensive field data are available. The magma intrusion analogues for thermal-hydrologic-chemical processes are discussed in Section 4.2.2.3.5. In addition, models for the recently completed Single Heater Test (Tsang and Birkholzer 1999) and the ongoing Drift Scale Test (CRWMS M&O 2000c, Section 2.2.4) use the same approach and input data as the mountain-scale model. In summary, the mountain-scale thermal-hydrologic model is considered valid because of its similarity to the models developed for field tests and the demonstrated validity of the geothermal analogue models.

**Multiscale Thermal-Hydrologic Model—**The multiscale thermal-hydrologic model uses a method based on industry-standard finite-difference software that includes both mass and energy balances. Model documentation addresses input data, assumptions, initial and boundary conditions, software, uncertainties, and other information required to replicate the model results.

Several validation approaches are used for the multiscale thermal-hydrologic model, including comparison of thermal-hydrologic modeling with results from the Large Block Test and the Drift Scale Test and comparison of multiscale thermal-hydrologic model results with mountain-scale thermal-hydrologic simulation, as described below. These comparisons are discussed in more detail in supporting documentation (CRWMS M&O 2000cf, Section 6.13).

**Thermal-Hydrologic Models of the Large Block Test—**A similar modeling approach was used to simulate the entire history of the Large Block Test (CRWMS M&O 2000cf, Section 6.13.1). As an example of model comparison with data, Figure 4-69 shows simulated borehole temperature profiles compared to observed temperatures. Evaluation of goodness-of-fit to measured temperatures shows accuracy of a few degrees Celsius.

Figure 4-70 shows the simulated and measured liquid-phase saturation profiles along another borehole in the Large Block Test. The simulated dryout zone develops more slowly than observed, but the

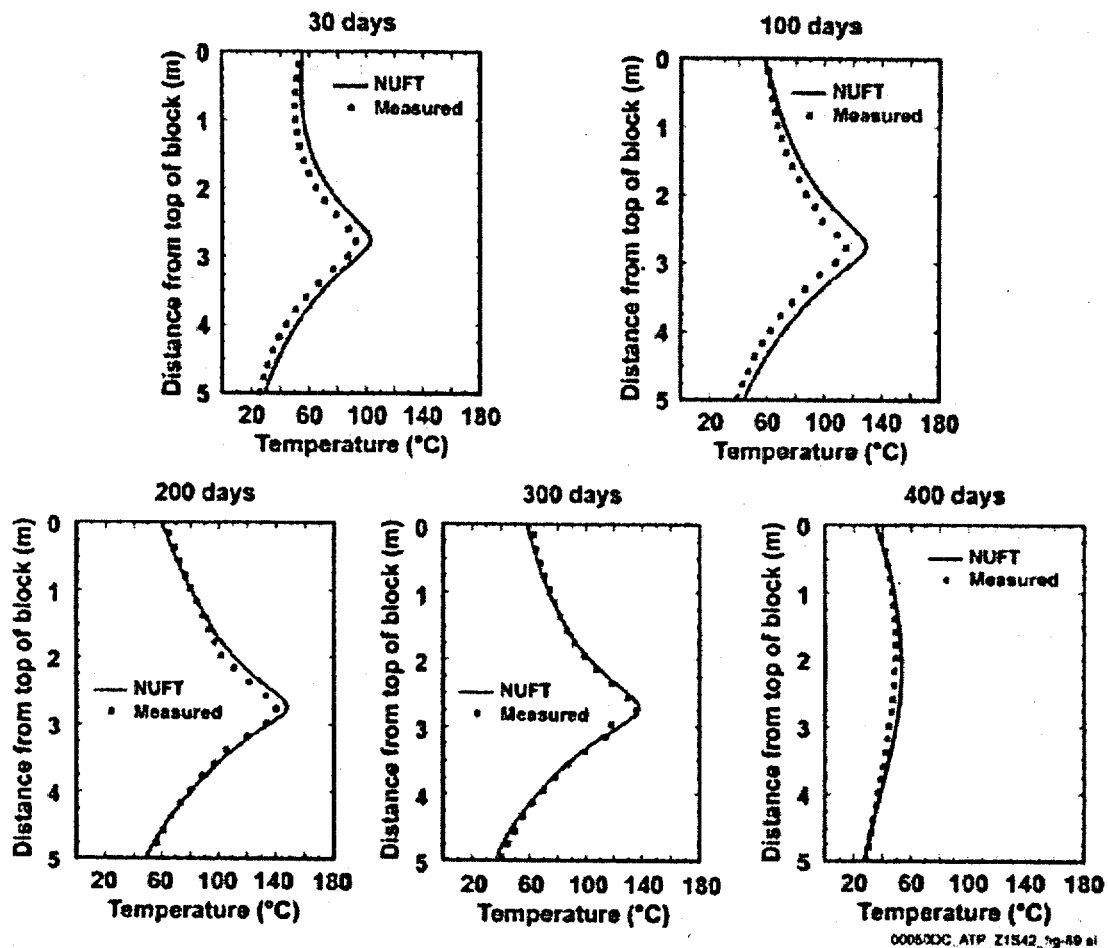


Figure 4-69. Comparison of Simulated and Measured Temperature Profiles along Large Block Test Borehole TT1, at Five Times from 30 to 400 Days

See Figure 4-45 for the location of Borehole TT1. Source: CRWMS M&O 2000cf, Figure 6-65.

difference resolves with time. At later times, the model is in close agreement.

**Thermal-Hydrologic Models of the Drift Scale Test**—Thermal-hydrologic modeling of the Drift Scale Test heating period, from startup to the present, was compared to observations (CRWMS M&O 2000cf, Section 6.13.2). As an example of model comparison with data, Figure 4-71 compares the simulated and measured temperatures along an observation borehole. The model results are in close agreement with measured temperatures, only slightly overpredicting temperatures in the dryout zone and slightly underpredicting temperatures in the sub-boiling zone.

In general, close agreement with observed temperature in the sub-boiling zone indicates that heat flow there is dominated by conduction and that the value of thermal conductivity is reasonable. Close agreement in the region close to the heated drift indicates that (1) thermal radiation is adequately represented inside the heated drift, (2) heat flow in the boiling and above-boiling zones is dominated by conduction, and (3) the value of thermal conductivity in this region is reasonable.

**Comparison of the Multiscale Thermal-Hydrologic Model with the Mountain-Scale Numerical Model**—Figure 4-72 compares the drift-wall temperature predicted by the multiscale thermal-hydrologic model with temperatures predicted by east-west cross-sectional mountain-scale thermal-

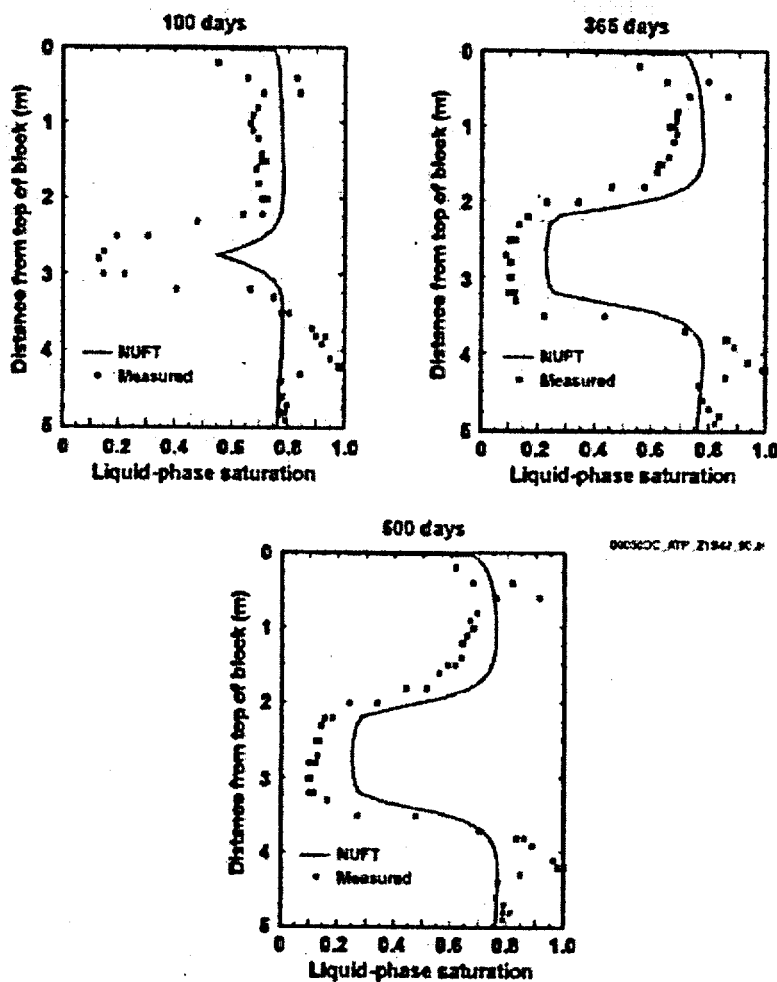


Figure 4-70. Comparison of Simulated and Measured Liquid-Phase Saturation Profiles along Large Block Test Borehole TN3, at Three Times from 100 to 500 Days  
See Figure 4-45 for the location of Borehole TN3. Source: CRWMS M&O 2000cf, Figure 6-66.

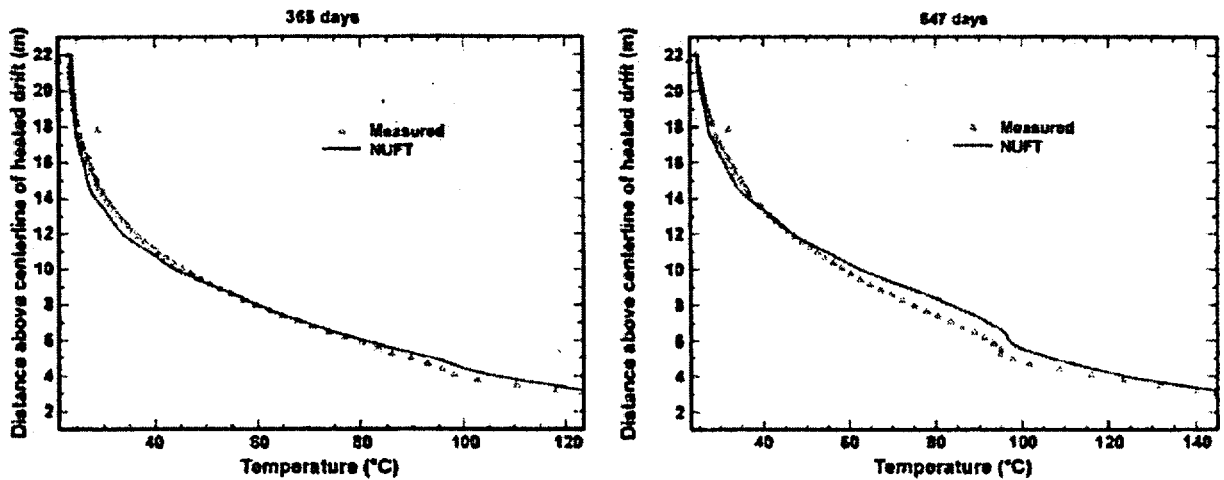
hydrologic models (for details, see CRWMS M&O 2000cf, Section 6.13.3). The mountain-scale thermal-hydrologic model is coarsely gridded, so the comparison is limited to drift-wall temperature from the multiscale thermal-hydrologic model vs. drift temperature from the mountain-scale thermal-hydrologic model.

Before comparing the two approaches (Figure 4-72), it is important to discuss other differences in the models. Differences between the multiscale model and mountain-scale modeling approaches include:

- The temperature predicted by the mountain-scale model is for a grid block that occupies

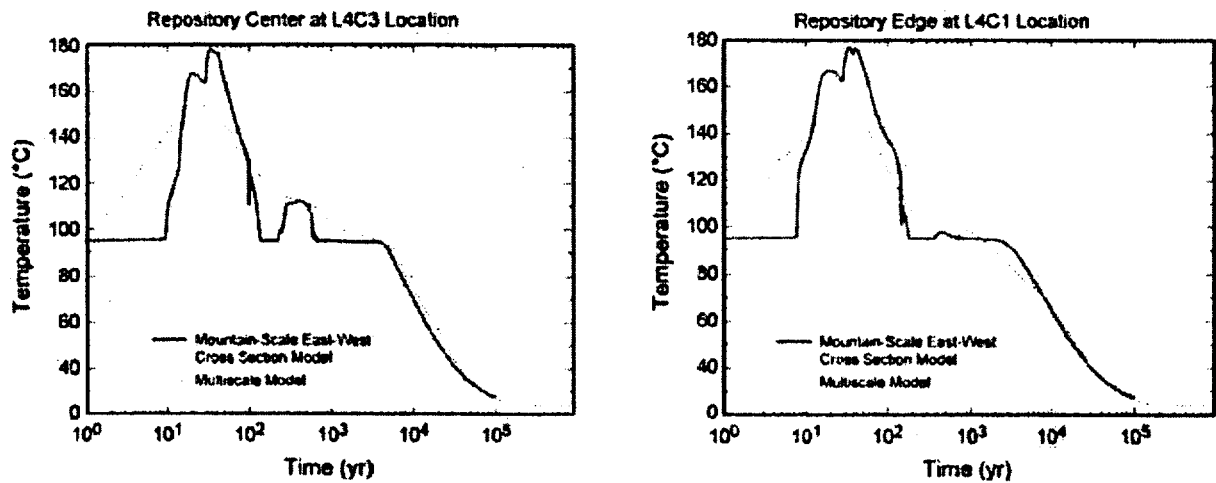
an entire drift, so it produces a lumped representation of drift temperature, whereas the multiscale model resolves temperature differences within the drift.

- The mountain-scale thermal-hydrologic model uses a line-averaged heat source that axially smooths the differences between hotter and cooler waste package locations.
- The initial areal power density (at emplacement) in the multiscale thermal-hydrologic model is 92.3 kW/acre, compared to 99.4 kW/acre in the mountain-scale thermal-hydrologic model.



00050DC\_ATP\_Z1S42\_fig-91.ai

Figure 4-71. Comparison of Simulated and Measured Temperatures along Single Heater Test Borehole ESF-HD-137 at 365 and 547 Days  
Source: CRWMS M&O 2000cf, Figure 6-67.



00050DC\_ATP\_Z1S42\_fig-92.ai

Figure 4-72. Drift-Wall Temperature Predicted by the Multiscale Thermal-Hydrologic Model Compared to the Temperature Predicted by an East-West Cross-Sectional Mountain-Scale Thermal-Hydrologic Model  
L4C1 and L4C3 locations are shown in Figure 4-65. Source: CRWMS M&O 2000cf, Figure 6-68.

- The mountain-scale thermal-hydrologic model representation of the heated footprint of the potential repository extends slightly further to the west than in the multiscale thermal-hydrologic model.

Near the center of the potential repository, the approaches predict nearly the same duration of boiling (Figure 4-72, left). Near the edge, the mountain-scale model predicts a longer duration of boiling (Figure 4-72, right). During the post-boiling period, the temperatures predicted by the approaches are in close agreement. During the early heating period, the coarse gridding of the mountain-scale model cannot capture the more rapid changes that the multiscale model predicts. Also because of the coarse gridding, the mountain-scale model tends to overpredict heat pipe behavior. Given the differences in technical approach, the models are in reasonable agreement throughout much of the thermal evolution of the potential repository.

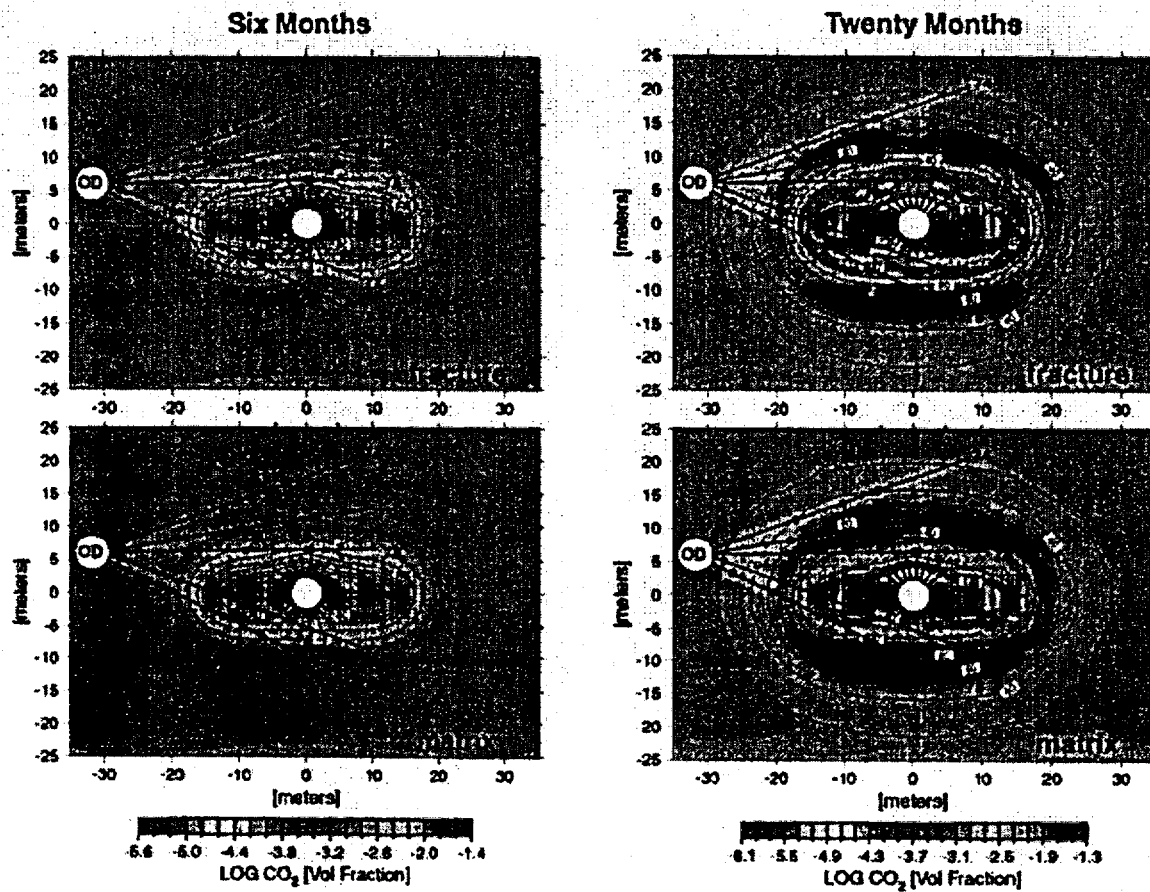
**Drift-Scale Thermal-Hydrologic-Chemical Processes and Models—Comparison of model predictions with data from the Drift Scale Test involves (1) modeled patterns of fracture drainage compared to locations where water has been collected during the test, (2) comparison of carbon dioxide concentrations from gas samples, and (3) comparison of the evolution of water composition in boreholes sampled over time.**

Simulated distributions of temperature and carbon dioxide concentration are shown in Figure 4-73 for the limited simulation approach (Case 2). The comparison shows that the simulations follow general trends in measured carbon dioxide concentration (CRWMS M&O 2000c, Figure 3.10-5). Two exceptions were when heater power loss occurred temporarily and when the gas samples were acquired at boiling temperatures and condensation occurred during the sampling. Detailed comparison of the modeling results and the measured carbon dioxide concentration data is discussed in *Drift-Scale Coupled Processes (DST and THC Seepage) Models* (BSC 2001o, Section 6.2.7.2).

The simulated pH of water in fractures is shifted to pH 6.5 from an initial pH of approximately 8.3, with the lowest pH values predicted where carbon dioxide concentration is greatest. The predicted shift in pH is similar to that observed in water samples collected from the Drift Scale Test. Chloride concentrations in waters collected from hydrology boreholes are considerably more dilute (a factor of 5 to 10) than the matrix pore water predicted by the modeling. Other species, such as calcite and silica, show similar trends in the modeled fracture water compositions compared to measured water compositions.

In the model simulations, calcite is the major phase forming in the zone above the heaters, although the quantity of calcite is small. Amorphous silica also precipitates but is less abundant than calcite. Direct observation of calcite precipitation or dissolution has yet to be observed in the Drift Scale Test, which is ongoing. However, other indications, such as the composition of water samples, provide indirect evidence for calcite precipitation. Fracture porosity changes predicted for the Drift Scale Test after 20 months are very small (on the order of 0.01 percent of the initial fracture porosity). Such small changes would likely have no measurable effect on the hydrologic properties of the rock.

**Drift-Scale Thermal-Hydrologic-Mechanical Processes and Models—Model calibration and validation of fracture displacements due to heating and cooling is done using laboratory and field test results. Calibration includes normalizing models to test results and using observations to determine physical phenomena needed in the models. An example of the latter is the observation of sharp movements in multipoint-borehole-extensometer data at specific times; this observation has resulted in the adoption of a discrete fracture conceptual model in Section 4.2.2.3.4. Validation is the comparison of calculated results to test data, with the calculations being done independent of the test data themselves. Both continuum models and discrete fracture models have been compared to test data from the Large Block Test, the Single Heater Test, and the Drift Scale Test; these tests are described in Section 4.2.2.2.3.2.**



00050DC\_ATP\_Z1S42\_fig-38.m

Figure 4-73. Simulated CO<sub>2</sub> Volume Fractions in Fractures and Matrix after 6 Months and 20 Months of Heating During the Drift Scale Test

The white labels indicate locations of isotherms (in °C). These isotherms correspond approximately to the distribution of volume fraction of CO<sub>2</sub>, shown by the color contours. The white circle in the center of the plot is the heated drift diameter. "OD" indicates the observation drift from which Boreholes 74 through 78 extend (see Figure 4-52 for the location of these boreholes). Sampling locations in those boreholes are plotted with black dots. Source: Adapted from BSC 2001o, Figures 5 and 6.

#### 4.2.2.4 Total System Performance Assessment Abstraction

Because of the limited thermal effect on water movement at large distances, the mountain-scale thermal-hydrologic model results are not directly included in the TSPA. Abstraction of thermal-hydrologic model results for the TSPA was therefore based on the near-field behavior predicted by the multiscale model.

The mountain-scale thermal-hydrologic model shows that the impacts of repository heating on

temperature, saturation, and liquid flux in the unsaturated zone will have limited duration and will be limited to the repository area. Some effects, such as elevated liquid flux associated with heat pipe activity, will be limited to the vicinity of the emplacement drifts. Also, mineralogical alteration of the overlying and underlying hydrogeologic units will be minimal with preclosure ventilation. Accordingly, the thermal-hydrologic effects on far-field flow and transport are not currently considered in the TSPA (CRWMS M&O 2000c, Table 3.13-2).

The purpose of the report *Abstraction of NFE Drift Thermodynamic Environment and Percolation Flux* (CRWMS M&O 2000cc) is to abstract the multiscale, process-level thermal-hydrologic model results (CRWMS M&O 2000cf) so that they can be implemented in the TSPA model. The purpose of the abstraction is to simplify the detailed thermal-hydrologic description of the potential repository that is produced by the multi-scale model. An averaging process ("binning") is used to compute these quantities, based on a subdivision of the repository footprint that preserves a wide range of thermal-hydrologic variability. Multiscale model results used directly in support of the TSPA-SR model include waste package temperature, relative humidity at the waste package surface, and the percolation flux in the host rock 5 m (16 ft) above the emplacement drift. Temperature and relative humidity are used for the corrosion model, and percolation flux is used for the seepage model. Time-histories of waste package temperature, percolation flux, evaporation rates, and maximum and minimum waste package surface temperatures are also provided (CRWMS M&O 2000cc, Section 6.3). The abstraction of thermal-hydrologic data represents the potential variability and uncertainty in thermal-hydrologic conditions. It provides a quantitative description of thermal-hydrologic variability (i.e., from variability in the host rock unit, edge proximity, waste package type, infiltration rate, and climate state) and also incorporates uncertainty associated with the infiltration (i.e., lower, mean, and upper).

Abstraction of predicted water and gas compositions for the mean infiltration rate (with climate change), including both limited and full mineral suite simulations, is summarized in Section 4.2.3.4. Also, since the predicted thermal-hydrologic-chemical coupled effects on flow properties are relatively small, the effects on seepage are not included in the TSPA-SR.

The abstracted seepage model used in TSPA-SR performance assessment calculations did not include changes in permeability due to thermal-mechanical effects. This approach was based on *Near-Field Environment Process Model Report* (CRWMS M&O 2000a, Section 5.5) and was

confirmed by supplemental TSPA analyses (BSC 2001a, Section 4.3.7.4.4).

#### 4.2.3 Physical and Chemical Environment

The lifetimes of the drip shield and waste package will depend on the environmental conditions to which they are exposed: the in-drift physical and chemical environment (CRWMS M&O 2000a, Section 3.3). Once a waste package is breached, the transport of radionuclides released from the waste form also depends on the environment in the emplacement drifts.

This section describes estimates of how the physical and chemical conditions in the drifts are expected to evolve with time, based on the thermal operating mode described in Section 2. The description is based on the estimated response of the host rock to heating and on data concerning behavior of the engineered materials used to construct the potential repository. The estimates are based primarily on results from laboratory and field-scale testing, supplemented by observations from natural and man-made analogues.

As noted in Section 4.1.4, the DOE is evaluating operation of the repository at lower temperatures. Operating the repository at lower temperatures may change the evolution of the physical and chemical conditions in the drifts described in this section. The data and analytical results presented in this section reflect the effects of higher-temperature operating mode conditions, specifically the process models and abstractions employed in the TSPA-SR model (CRWMS M&O 2000a). Alternative thermal operating modes and supplemental uncertainty evaluations related to the in-drift physical and chemical environment models are described and summarized in *FY01 Supplemental Science and Performance Analyses*, (BSC 2001a, Sections 6.3.3., 6.3.4, 7.3.1, 7.2.4, and 10.3.4; BSC 2001b, Sections 3.2.4.2 and 4.2.4).

Results of the in-drift models used directly in the TSPA-SR model include time-dependent estimates of the infiltration rate, temperature, and relative humidity at the drift wall, as well as the evolution of the chemical conditions at the drift wall over four discrete time periods: (1) preclosure,

(2) boiling, (3) transitional cooldown, and (4) extended cooldown (CRWMS M&O 2000a, Section 3.3.3.4.2).

**Physical Environment**—The physical environment is described by the evolution, with time, of thermal-hydrologic conditions in the emplacement drifts. Estimation of the temperature, relative humidity, and rate of evaporation at locations throughout the potential repository is described in Section 4.2.2. The results show that every location in the potential repository could evolve from very dry conditions at temperatures greater than boiling to cooler conditions and increasing humidity. Differences between locations are limited mainly to the timing of these changes—for example, the duration of boiling temperatures on the waste package will depend on its location in the repository layout, local infiltration flux, and the heat output of individual waste packages (see Section 4.2.2.3.2). Cooling, and return of moisture to the emplacement drifts, would occur hundreds to a few thousands of years sooner at the edges of the potential repository, compared with the center. Cooling also would occur sooner at locations where there is greater recharge of water from the ground surface.

The potential for liquid water seepage into the emplacement drifts is described in Section 4.2.1. Seepage is combined with temperature, relative humidity, and evaporation rate to represent the physical environment for the engineered barriers in the TSPA-SR. Diversion of seepage by the drip shield and waste package is described in Section 4.2.5. The potential for condensation under the drip shield during the thermal period is also discussed in that section. A model of the flow of liquid water through breaches in the drip shield and waste package is used to assess advective releases of radionuclides in TSPA-SR. Thermal-hydrology, seepage, and water diversion model results that were developed in Sections 4.2.1, 4.2.2, and 4.2.5 are implicit in the following description of the physical and chemical environment and are not discussed further in this section.

The physical environment also includes the potential for rockfall, which could damage the drip shields or waste packages. The effects of rockfall are estimated based on observations from site char-

acterization and use approaches that represent the effects of heating and seismic loading. Estimates of block size and rockfall frequency have been used to design the drip shield, which is designed to withstand rockfall over its design lifetime and thereby protect the waste package. The approach to estimating rockfall events is also described in this section.

**Chemical Environment**—Important processes affecting the chemical environment include evaporation and condensation of water, the formation of salts, and the effects of gas composition. During the thermal period, relative humidity will likely control the equilibrium solution chemistry and is therefore a principal descriptor of the chemical environment. The approach to analyzing the chemical environment involves several types of predictions:

- Composition of water and gas in the host rock around the drifts that can enter drift openings
- Composition of waters within the drifts that can further evaporate and form precipitates and salts
- The effect of microbial activity on the chemical environment
- The effects of engineered materials such as steel and cement
- The chemical environment at the surfaces of the drip shield and waste package.

These analyses are complementary and together describe the in-drift chemical environment as it is represented for performance assessment. Each is either incorporated explicitly in TSPA-SR or has been considered to have minor consequences to system performance and is excluded from consideration. The approach for each analysis is described in the following sections.

#### 4.2.3.1 Conceptual Basis

This section describes the conceptual models that form the basis for analytical treatment of processes

in TSPA. Although the descriptions may contain statements that appear to be definitive, it is important to recognize that there are uncertainties associated with the selection of appropriate conceptual models. Alternative conceptual models are discussed in Section 4.2.2.3.7. Model results based on the selected conceptual models are generally considered to be best estimates, incorporating uncertainty, such that the models are suitable for use in TSPA.

#### **4.2.3.1.1 Conceptual Basis for the Composition of Liquid and Gas Entering the Drifts**

**Composition of Liquid Seepage**—The chemistry of waters in the host rock will act as a boundary condition on the in-drift chemical environment (CRWMS M&O 2000a1, Section 3.4.2). During the thermal pulse, water vapor will move away from the heated drifts while liquid water percolates downward and replaces the water that evaporates in a thermal refluxing process (Section 4.2.2). The percolating waters will contain dissolved chemical species, such as sodium, calcium, sulfate, chloride, carbonate, and silica (CRWMS M&O 2000a, Section 3.3.3.4.2). When evaporation occurs, the chemical species will be left behind in the rock as precipitated minerals and salts.

The areal extent of the dryout zone produced by the higher-temperature operating mode would shrink as the heat output from the waste packages decreased with time. This will cause the region of boiling conditions to slowly converge on the drift openings. Liquid water will tend to sweep through formerly boiling regions, redissolve precipitates and salts, and move them closer to the openings. Soluble salts will tend to be concentrated near the openings. Depending on local hydrologic conditions, this process could cause seepage to be concentrated in soluble salts relative to the ambient (preheating) water composition.

With seepage, salts such as calcium carbonate and sodium chloride can form in the drifts (for example, from dripping and evaporation) directly on the drip shield or waste package. In the TSPA-SR model, only a fraction of the waste package locations in the repository would be

affected by seepage (Section 4.2.1), especially during the thermal pulse when the conditions are relatively dry (Section 4.2.2). Without seepage, the effects of chemical processes in the host rock on the in-drift chemical environment will be limited to the gas composition. Seepage will be more likely in the future as the climate changes to the cooler, wetter, glacial-transition conditions discussed in Section 4.2.1. However, by the time the effects of this climate change propagate down to the host rock, cooldown will have progressed so that the drip shield temperature will be below boiling throughout the potential repository (CRWMS M&O 2000cf, Section 6.11.4).

After cooldown, and after soluble salts precipitated during the thermal pulse are redissolved and remobilized, the composition of seepage water will become increasingly similar to the ambient percolation in the host rock units. Some minerals precipitated during the thermal pulse may be stable, or slow to dissolve, but effects from such minerals are incorporated into the thermal-hydrologic-chemical model (BSC 2001o, Section 6.1).

**Composition of the Gas Phase**—The gas-phase composition in the host rock will also act as a boundary condition on the in-drift chemical environment (CRWMS M&O 2000a, Sections 3.3.3.2.3 and 3.3.3.4.2). The gas composition will initially be similar to atmospheric air, but during the thermal pulse, the gas phase will be strongly modified by evaporation of water and by interaction with carbon dioxide in waters and carbonate minerals (BSC 2001o, Section 6.2.7.2). Change in the in-drift gas flux and composition will affect water pH, including water that may occur on the surface of the drip shield or waste package (CRWMS M&O 2000ck, Section 6.2.4; CRWMS M&O 2000a, Section 3.3). Relationships among thermal, hydrologic, and chemical processes in the host rock around the drift openings, and within the drifts, are depicted schematically in Figure 4-74.

Evaporation of water from heating of the host rock will cause much of the dissolved carbon dioxide to be released as gas (the remainder will be precipitated as carbonate minerals). The gaseous carbon dioxide will form a broad halo around the drift openings that encompasses the cooler region where

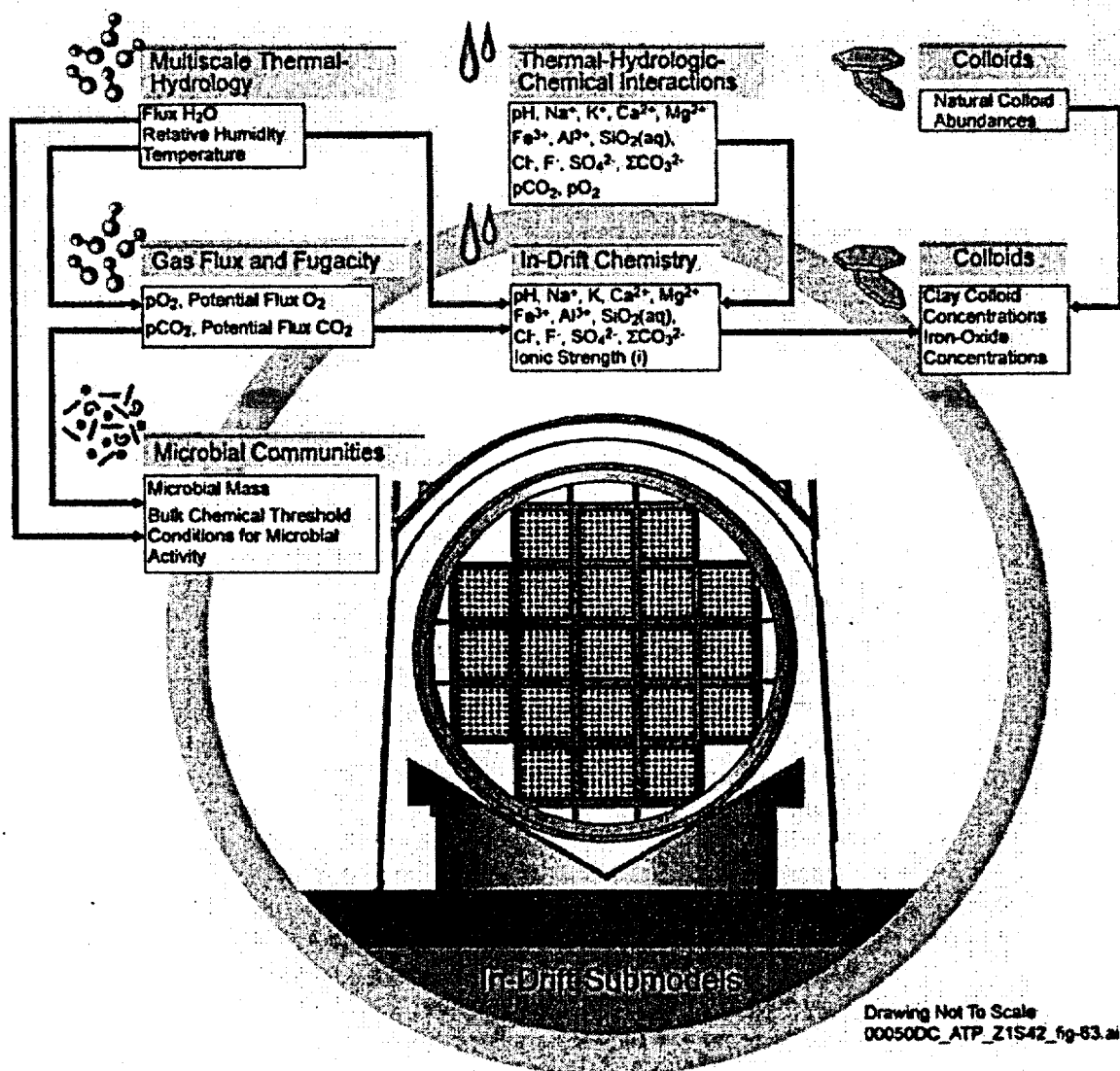


Figure 4-74. Emplacement Drift Cross Section Showing the Processes Considered in the Evolution of the Physical and Chemical Environment, and in the Transport of Radionuclides, within the Emplacement Drifts

Source: Modified from CRWMS M&O 1998g, Chapter 4, Figure 4-1.

water vapor condenses. Condensate will be enriched in carbon dioxide and slightly acidified (CRWMS M&O 2000a1, Section 3.6.4.2). In the zone of evaporation closer to the drift openings, calcite and other carbonate minerals will be precipitated but may be redissolved later during cooldown when liquid water returns. Oxygen will exhibit simpler behavior because it is less soluble in water and forms different kinds of minerals. Analyses of uncertainty and the thermal sensitivity of chemical conditions within the drifts are

described in *FY01 Supplemental Science and Performance Analyses* (BSC 2001a, Section 6.3).

#### 4.2.3.1.2 Conceptual Basis for Evolution of the Chemical Environment for the Engineered Barriers

At low relative humidity, any minerals or salts that exist in the emplacement drifts will be dry. These minerals and salts may be introduced as ventilation dust, from evaporation of construction water, or

from the occurrence of seepage when the drifts are hot and dry. As the relative humidity increases during cooldown, salts will condense to trap water vapor from the air (deliquescence) and form brine. Minerals and salts may occur on a small scale, for example, an evaporated droplet on the surface of the drip shield. Eventually, increasing humidity will cause the brines to capture more water vapor and become diluted. Seepage (where it occurs) will flush soluble salts from the drifts and redissolve the less soluble minerals. After the thermal period, the composition of waters and gases in the emplacement drifts will return to ambient (preheating) conditions (CRWMS M&O 2000as, Section 3.1.2.5.1).

**Minerals and Salts Formed by Evaporation—**Temperatures well above the boiling point of pure water (96°C [205°F] at the potential repository elevation), and associated low relative humidity, will persist hundreds to thousands of years after emplacement, depending on the location within the repository layout, the local infiltration flux, and the heat output from individual waste packages, as discussed in Section 4.2.2.3.2. These conditions are conducive to evaporation. Seepage into the drifts during this period, if it occurs, may be transient, but the nonvolatile dissolved constituents will accumulate in the drifts as salts and minerals. These solids will include soluble salts with the potential to form brines when relative humidity increases to approximately 50 percent and greater (CRWMS M&O 2000as, Section 3.1.2.5.1). Another source of minerals and salts is dust on the drip shield or waste package surfaces, which could be derived from the rock or from aerosols introduced from the atmosphere by ventilation during the preclosure operational period (CRWMS M&O 2000ck, Section 6.2).

**Composition of Waters in the Emplacement Drifts—**Temperature and humidity would be slowly varying in the repository, so equilibrium relationships will apply between brine concentration and relative humidity. Thus the relative humidity, which is readily predicted from thermal-hydrologic calculations (Section 4.2.2), is a good estimator of brine composition (CRWMS M&O 2000ck, Section 6.4). As noted previously, all waste package locations will evolve to high rela-

tive humidity, but at different rates, so the effect on TSPA is limited mainly to the timing of changes in equilibrium brine composition and seepage.

Where seepage occurs, the rate of seepage entering the drift during cooldown will eventually exceed the rate of evaporation in the drift as the thermal output decays (CRWMS M&O 2000cl, Section 6.2). When this happens, liquid water will begin to flow through the drift. Any brines present will tend to be diluted and flow out of the drifts with the seepage. If seepage is flowing into the drift, then considerable dilution of brines has probably occurred already from the associated humidity. Therefore, the details of seepage mixing with pockets of brine are not critical to predicting the chemical environment.

**Microbial Activity in the Emplacement Drifts—**Microbial activity is important primarily because of the potential for microbially influenced corrosion of the waste package. Microbes may also increase the rates of degradation for other engineered materials and can contribute to radionuclide transport. Bacteria and fungi, including molds, occur naturally in the host rock and would also be introduced by repository construction and operation. Because of dryness and elevated temperature, heating the rock at the potential repository will arrest microbial activity for time periods on the order of hundreds of years. However, heating will redistribute water so that cooler locations are wetter, which will locally increase the microbial activity. Factors that will limit microbial activity include elevated temperature, low humidity, and availability of nutrients and energy from engineered materials. Engineered materials such as steel may provide metabolic energy sources and limiting nutrients, such as phosphate. Measures to control the use of organic materials during construction and operation will also limit microbial activity (CRWMS M&O 2000as, Section 3.1.2.4).

#### **4.2.3.1.3 Conceptual Basis for the Effects of Engineered Materials on the Chemical Environment**

Engineered materials have the potential to affect the chemical environment as they degrade. Drip shield and waste package materials will degrade

slowly, and the effects on oxygen availability will be minor. Structural steel in the emplacement drifts will corrode and consume more oxygen, depending on the relative humidity. Cementitious grout will be used to anchor rock bolts in a portion of the potential repository (CRWMS M&O 2000cg) and may contribute cement leachate to the chemical environment.

**Degradation of Steel and Alloys**—Measured penetration rates for the titanium drip shield and the Alloy 22 waste package outer barrier are small (see Section 4.2.4). These materials obtain corrosion resistance from a passive layer of oxides on the exposed surfaces. The rate of oxygen consumption from maintaining the oxide layer is directly related to the penetration rate.

Steel will be used in roof supports, rails, and beams in the invert that support the drip shields and waste packages (see Section 2.4). These are preclosure structural applications; the steel will readily degrade during the postclosure period when humidity returns. Steel corrosion will begin when the temperature is near boiling and much of the air is displaced by water vapor. The steel is likely to corrode relatively quickly, within a few hundreds to thousands of years. While it is active, steel corrosion may affect the oxygen budget in the emplacement drifts (CRWMS M&O 2000cm, Section 6.2.2).

**Cementitious Materials**—Cement that will be used in rock bolt installation (like all Portland-based cements) is an assemblage of minerals and other phases, some of which dissolve to produce highly alkaline leachate. The composition of leachate will be determined by the solubilities of cement mineral phases. The phases present in "fresh" cement are more alkaline than those in aged cement because of carbonation and other processes (CRWMS M&O 2000cg, Section 5.3.1). Therefore, the leachate composition can be bounded using readily available information on cement composition. Several factors will act to limit the quantity and quality of leachate produced, including cement carbonation, low grout permeability, limited exposure to seepage flux, and neutralization of leachate by carbon dioxide in the

drift environment (CRWMS M&O 2000cg, Sections 6.3.1 and 6.7.5).

**Colloidal Particles Produced by Degradation of Engineered Materials**—Colloidal particles are important as carriers for radionuclides, particularly isotopes of relatively insoluble elements, such as americium and plutonium. These radionuclides are transported very slowly (or not at all) in groundwater, except for colloidal modes of transport. Colloid generation and radionuclide transport are discussed at length in Sections 4.2.6, 4.2.7, 4.2.8, and 4.2.9. Colloids derived from the host rock will be present in seepage water. Additional colloids will be generated from degradation of engineered materials in the potential repository, including waste forms and other materials within the waste package (CRWMS M&O 2000cn, Section 6.1; CRWMS M&O 2000cg, Section 6.6).

Engineered materials in the emplacement drifts will consist mainly of corrosion-resistant alloys, cement, crushed rock, and steel. Corrosion products of titanium and Alloy 22 are mechanically stable (hence the corrosion resistance of these materials) and are unlikely to form significant colloids. Degradation of cementitious materials can form colloids (Hardin 1998, Chapter 6), but the usage of cement and its exposure to seepage will be limited. The invert ballast material will be crushed tuff derived from the host rock (see Section 2.4.1); the resulting colloids will be similar to colloids introduced with seepage. By contrast, steel in the emplacement drifts will be an abundant source of ferric-oxide colloids that are potentially important for radionuclide transport.

It is anticipated that quantities of colloids will be mobilized as a result of alteration of both the high-level radioactive waste and spent nuclear fuel waste forms. Colloid abundance within a breached waste package will depend on the extent of waste form alteration and the alteration products formed from in-package steel components. Colloid abundance and stability also depend on many environmental factors, including the ionic strength, pH, cation concentrations, colloid content of groundwater entering the waste package from the drift, presence of fulvic and humic acids, and microbe fragments (CRWMS M&O 2000co,

Section 1). The colloid source term and transport models are described in Sections 4.2.6 and 4.2.7 of this report, respectively.

**Contribution of Engineered Materials to Microbial Activity**—As stated previously, microbial activity is important primarily because of the potential for microbially influenced corrosion of the waste package; microbial activity may also increase the rates of degradation for other engineered materials and contribute to radionuclide transport. Microbes exploit chemical reactions (oxidation-reduction) that are rate-limited under abiotic conditions by providing faster alternative reaction pathways that also support cell-building and energy production (CRWMS M&O 2000cp, Section 6.3.1.1). Engineered materials include metals, which are important sources of reactants for these chemical reactions.

Engineered materials in the emplacement drifts will consist mainly of corrosion-resistant alloys, steel, cement, and crushed rock. Each of these can interact with microbes in particular ways, but steel will probably be the most important contributor. Steel will oxidize completely in the first few hundred years after sufficient humidity returns to the in-drift environment; after that, it will contribute little to microbial activity.

#### 4.2.3.1.4 Conceptual Basis for the Environment on the Surfaces of the Drip Shield and Waste Package

**Behavior of Water on the Barrier Surfaces**—The environments on the surfaces of the drip shield and the waste package will determine the potential for corrosion processes and the penetration rates. Surface chemical conditions will be controlled by temperature, humidity, gas-phase composition (especially oxygen and carbon dioxide), the composition of dripping water, and the minerals and salts that may be deposited.

During the thermal pulse, the drip shield will be warmer than the surrounding in-drift environment in some instances, and the local relative humidity at the surface will be lower than the average humidity in the drift. Under these conditions, any water on the drip shield would tend to evaporate,

resulting in concentration of aqueous solutions and precipitation of minerals and salts (CRWMS M&O 2000ck, Section 6.2.3).

The titanium and Alloy 22 surfaces will react with atmospheric oxygen to form thin, resistant layers of metal-oxides (corrosion processes and rates are discussed in Section 4.2.4). These oxide layers will be mechanically stable and chemically unreactive, which confers corrosion resistance to these materials. Because the oxides are chemically inert compared to other species in the environment, they are assumed to not contribute to the chemical evolution of aqueous solutions on the barrier surfaces (CRWMS M&O 2000ck, Section 5).

Waste packages under intact drip shields will be exposed to moisture and chemical species. Humidity will penetrate the air gap between the waste package and drip shield, although the increase of relative humidity at the waste package surface will be delayed because of the warmer temperature there (CRWMS M&O 2000ck, Section 6.2.3). Moisture will form thin films on the surfaces by adsorption or capillary condensation (CRWMS M&O 2000ck, Section 6.3). Minerals and salts will be present in small quantities from dust and aerosols transported in the drift air (CRWMS M&O 2000ck, Section 6.1). If a drip shield is breached, seepage can contact the underlying waste package, which can lead to additional precipitation of minerals or salts on the waste package surface. As the waste package cools, less evaporation will occur on the surface, and accumulation of minerals or salts will be increasingly unlikely.

**Potential for Acidic Conditions**—There are two mechanisms by which acidic conditions could occur on the surfaces of the drip shield or waste package: radiolysis and localized corrosion. Neither mechanism will be important in the potential repository.

Radiolysis (outside the waste package) will be caused by gamma radiation that penetrates the waste package wall and interacts with air and moisture in the environment to produce small amounts of hydrogen peroxide (CRWMS M&O 2000n, Section 3.1.6.6) and possibly other species, such as

nitric acid. Radiolysis inside the waste package is discussed in Section 4.2.4. Several factors will limit the effect of radiolysis on the environment at the waste package and drip shield surfaces. The rate of gamma radiation from spent fuel and other waste forms will decline steeply within the first 1,000 years from the decay of relatively short-lived fission products. Only a small portion of the gamma radiation from the waste package will interact with the air space between the waste package and drip shield; much of this radiation will penetrate the drip shield or be absorbed within it. Acidic compounds formed in the drift environment during the thermal period will likely condense on cooler surfaces such as the drift wall and not on the drip shield or waste package, which will be warmer than their surroundings. If acidic compounds tend to precipitate on surfaces, then the drip shield will afford some protection to the waste package. Finally, the drip shield and waste package materials are resistant to attack by products of radiolysis (Section 4.2.4).

Localized corrosion can, in principle, cause acidic conditions to develop in cracks, crevices, or interfaces where exposure to the bulk chemical environment in the drifts is limited (CRWMS M&O 2000ck, Sections 6.5 and 6.6). Corrosion modes are discussed at length in Section 4.2.4, and localized corrosion is found to be of minor importance for titanium and Alloy 22.

#### **4.2.3.1.5 Conceptual Basis for Rockfall on the Drip Shield**

Fractures intersecting emplacement drifts can form "key blocks" that may become dislodged and fall directly onto the drip shields. Key blocks typically form at the crown of the existing excavations, are of minor size, and fall immediately after excavation, prior to ground support installation (CRWMS M&O 2000a, Section 3.3.1). In the design described in Section 2.4.4, the drip shield segments will be pinned together to prevent movement (with allowance for longitudinal thermal expansion and seismic strain). Structural bracing will provide capacity to resist permanent deformation from rockfall. The drip shield segments will have overlapping and interlocking joints to impede water leakage, even with small displacements between

segments. The connections between segments will tend to stiffen the structure, so that loads will be shared by adjacent segments. Determination of the size distribution for rock blocks that may fall on the drip shield and analysis of the structural response of the drip shield to rockfall are ongoing activities for which preliminary results are presented in Section 4.2.3.3.5.

### **4.2.3.2 Summary State of Knowledge**

#### **4.2.3.2.1 Composition of Liquid and Gas Entering the Drifts**

**Ambient Water Composition in the Unsaturated Zone**—As discussed in Section 4.2.2.1.3, infiltrating water chemistry could be chosen from either the pore water chemistry in the unsaturated zone at or above the repository horizon or from a more dilute composition found in the perched water or saturated zone. These are referred to as a chloride-sulfate-type water composition and a bicarbonate-type water composition, respectively. As discussed in Section 4.2.2.3.3, the thermal-hydrologic-chemical model assumes the chloride-sulfate-type water as the basis for the initial ambient water composition in fractures in the unsaturated zone.

**Composition of Evaporatively Concentrated Waters**—Laboratory evaporation tests have been performed using both types of waters to investigate the effects of partial evaporation on solution chemistry and to determine which minerals and salts form as the waters are evaporated completely (CRWMS M&O 2000cg, Section 6.5.2). The bicarbonate-type water has been shown to evolve by evaporative concentration to a brine with high pH, whereas the chloride-sulfate-type water evolves to a brine with a nearly neutral pH. The chloride, sulfate, and nitrate concentrations in these waters tend to increase linearly with evaporation, and precipitate only in the later stages, because they are highly soluble. The major differences in behavior are attributed to the relative abundance of bicarbonate and carbonate among the anions present.

Studies of saline lakes in the western United States show that alkaline sodium-carbonate brines of the type that were produced from bicarbonate-type

water in laboratory tests occur in nature (CRWMS M&O 2000cl, Section 6.1.2). Many of these waters occur in volcanic geology similar to Yucca Mountain and have high silica content. These waters also are typically enriched in chloride and sulfate. Similarly, carbonate-poor brines of the type that were produced from matrix pore water in laboratory tests also occur in nature, such as those resulting from evaporation of sea water.

Water samples collected from the rock, in field-scale thermal tests performed at Yucca Mountain, are analogous to waters that would form during the heating of the host rock around the potential repository. The waters were collected where fractures intersected boreholes; therefore, they represent fracture waters that could potentially seep into repository drifts. The composition of such waters has varied with location, temperature, and other conditions but is dominated by condensation and interaction with fracture minerals (CRWMS M&O 2000cg, Section 6.5). The water compositions show that calcite present in the fractures is more readily dissolved than clays, feldspars, quartz, or other forms of silica. The noncalcite constituents of the waters are present in relative amounts that are similar to perched water and water found in well J-13, referred to hereafter as J-13 water (CRWMS M&O 2000cg, Section 6.5). The overall rate of condensation in these tests greatly exceeds the rate of water input from natural percolation, so the waters are dilute. Mixing of condensate with matrix pore waters was limited over the duration of the field tests but may be important over hundreds or thousands of years. From this discussion, it is appropriate to consider a range of water compositions, including bicarbonate-type and chloride-sulfate-type waters, for estimating the effects of evaporatively concentrated water and projecting the evolution of the in-drift chemical environment (CRWMS M&O 2000cg, Section 6.7.4.6).

**Ambient Gas Composition**—The natural composition of the gas phase in the unsaturated zone at Yucca Mountain is similar to atmospheric air, except that the carbon dioxide concentration is elevated by a factor of three. Elevated carbon dioxide is associated with soil processes near the ground surface and is commonly observed in nature. At other locations where there is more plant

activity, the carbon dioxide activity in the subsurface may be an order of magnitude greater than at Yucca Mountain (CRWMS M&O 2000cg, Section 6.2). The oxygen concentration throughout the unsaturated zone is apparently close to atmospheric, indicating there are no natural processes that consume oxygen at rates nearing the rate of potential supply from the ground surface.

Analysis of radiocarbon data from the site, from sampling of pore gas in surface-based boreholes and analysis of core samples, has been used to investigate the natural processes that deliver carbon dioxide to the unsaturated zone (CRWMS M&O 2000cg, Section 6.2). The influx of carbon dioxide dissolved in infiltrating waters, plus that transported in the gas-phase, has been estimated from isotopic mass balance to be in excess of 500 mg carbon dioxide per square meter per year. The results indicate that carbon dioxide is transported in the unsaturated zone by percolating waters and by gas-phase processes, such as barometric pumping.

**Effects of Heating on Gas Composition**—With heating of the potential repository, carbon dioxide will be released to the gas phase from evaporating matrix pore water (CRWMS M&O 2000al, Sections 3.3.1.2 and 3.3.3). At the same time, the humidity will increase with temperature, and water vapor will displace the air. This will initially cause increased carbon dioxide activity, as observed in field thermal tests, relative to the ambient level for the unsaturated zone. Years later, the carbon dioxide activity will decrease as the temperature approaches 96°C (205°F) (the boiling point at the potential repository elevation) and air is displaced by water vapor. Eventually, during cooldown, the carbon dioxide concentration in the emplacement drifts will approach the ambient level for the unsaturated zone.

Gas-phase convection during the thermal pulse will have an important impact on the fluxes of carbon dioxide and oxygen to the emplacement drifts and on the resulting gas-phase concentrations available for chemical reactions. As the host rock heats up, and the humidity increases, the density of the gas phase will decrease, and buoyant convection may occur. Buoyant convection can occur in porous

media, and has been interpreted as the cause for thermal effects associated with hot springs and igneous intrusions (Turcotte and Schubert 1982, pp. 367 to 370). Convection could circulate gas in the unsaturated zone, and thereby move air into the emplacement drifts, decreasing the humidity and increasing the availability of carbon dioxide and oxygen during the thermal pulse (CRWMS M&O 2000cg, Section 6.2.2.2). Increased availability of carbon dioxide will have the effect of buffering evaporatively concentrated, alkaline solutions, particularly above pH 10 (CRWMS M&O 2000cg, Section 6.7.5.3). Increased availability of oxygen will lessen the impact of steel corrosion on the in-drift chemical environment (CRWMS M&O 2000cg, Section 6.3.2.2).

The gas-phase concentration of carbon dioxide in the emplacement drifts during the thermal pulse will also be augmented by liquid water percolation in the host rock. As waters percolate downward toward the potential repository, carbon dioxide will exsolve because its solubility decreases with increasing temperature. If the waters are evaporatively concentrated, more carbon dioxide may be produced. The concentration of carbon dioxide species in such waters can be inferred from the composition of perched waters sampled from field thermal tests (CRWMS M&O 2000cg, Section 6.5) and is predicted using the approach described below.

**Approach to Modeling the Composition of Liquid and Gas Entering the Drifts**—The modeling approach for seepage and gas-phase composition during the thermal period couples thermal-hydrologic processes with both liquid and gas-phase chemistry. Temperature and evaporative concentration are determined from thermal-hydrology, while dissolution and precipitation reactions are modeled simultaneously (CRWMS M&O 2000c, Section 3.10.5). The thermal-hydrologic-chemical modeling approach is integrated with the unsaturated zone flow model (Section 4.2.1) because the same rock properties and boundary conditions are used. The same coupled model is used in Section 4.2.2 to evaluate the potential for coupled effects on hydrologic properties.

As noted previously, every location in the potential repository will be subject to similar evolution of thermal-hydrologic and chemical processes, but the timing of these processes will depend on local conditions. The principal factors that will control timing are edge versus center locations in the potential repository layout and the local percolation flux (CRWMS M&O 2000cg, Section 6.1). Based on similarity of the process evolution at different locations, it is possible to represent thermal-hydrologic-chemical behavior using a limited set of chemical computational models. The major drawback of such an approach is uncertainty of hundreds to thousands of years in the timing of thermally driven changes in chemical conditions. This uncertainty corresponds to the predicted variability in the duration of elevated temperature on individual waste packages, as discussed in Section 4.2.2.3.2.

For developing and validating this model, results from the Drift Scale Test constrain the thermal-hydrologic response, gas composition, and composition of liquid water in fractures for the first few years of repository evolution. Longer-term evolution is predicted by extrapolation. The concentrations of carbon dioxide and oxygen depend on thermally driven gas-phase circulation, and a range of models and properties are considered and compared (CRWMS M&O 2000cg, Section 6.2).

Water and gas compositions are predicted at the drift wall to represent effects of processes in the host rock and used as boundary conditions for processes in the drift (CRWMS M&O 2000c, Section 3.10.5). These predictions are then used as boundary conditions on a different model for in-drift processes, which uses an approach formulated to accommodate evaporatively concentrated waters with high ionic strength (CRWMS M&O 2000cg, Section 6.7.4.6; CRWMS M&O 2001b, Section 1). Evaluation of the carbon dioxide and oxygen budgets for chemical processes occurring in the drifts and the surrounding host rock shows that chemical reactions will probably not strongly perturb conditions in the surrounding rock (CRWMS M&O 2000cg, Section 6.7). The concentrations of carbon dioxide and oxygen will be uniform within the drift air-space (although

relative humidity will vary with temperature) because gas-phase diffusion and convective mixing are rapid compared to the potential rates of consumption of these reactants. Finally, alternative chemical boundary conditions for water composition (i.e., bicarbonate-type and chloride-sulfate-type waters) are used to reflect the present state of knowledge of mobile waters in the host rock (CRWMS M&O 2000cg, Section 6.7.4).

#### 4.2.3.2.2 Evolution of the Chemical Environment

The following discussion describes the summary state of knowledge for processes that will affect the bulk chemical environment in the emplacement drifts. This environment is distinguished from local conditions associated with cracks and crevices, microbial colonies, and within layers of engineered material degradation products.

**Minerals and Salts Formed by Evaporation—**As Yucca Mountain waters are evaporated to dryness, various minerals and salts are formed in sequence as the solution conditions exceed their solubility constraints. The formation of brines by evaporative concentration of natural waters can be conceptualized as a series of chemical divides, which are caused when salts with limited solubility drop out of solution (CRWMS M&O 2000ck, Section 6.5). The concept of chemical divides is straightforward. When a salt such as calcium sulfate is precipitated from solution during continual evaporation, one or the other of the component species (i.e., calcium or sulfate) will be effectively removed from the water. The remaining one will jointly determine what precipitates next, and so on, in a series of chemical divides. (The situation is more complex for solutions with multiple soluble species, as discussed below.) The complete precipitation of all limited-solubility species is observed in natural waters that have been concentrated by evaporation, such as Owens Lake in southeastern California (CRWMS M&O 2000ck, Section 6.5).

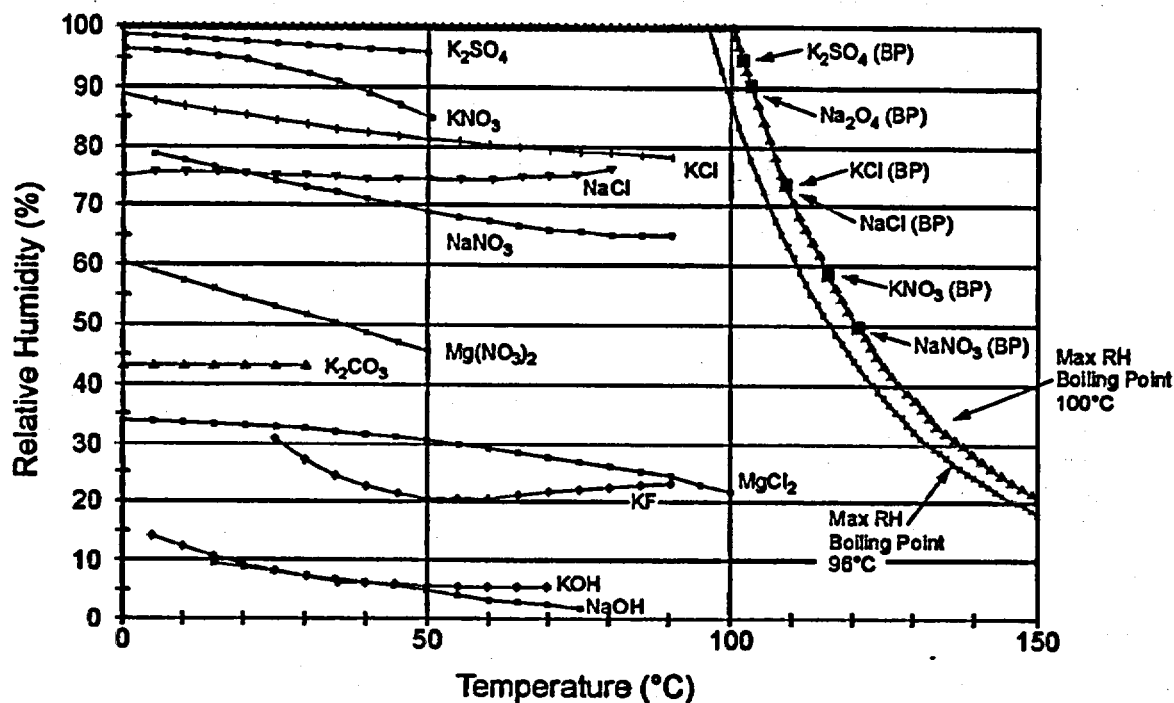
As discussed previously, for particular conditions of temperature and relative humidity, there is a specific extent of evaporative concentration for Yucca Mountain waters, such that the solution is in

moisture equilibrium with the gas phase. In other words, the solution will either evaporate or absorb moisture from the air until equilibrium is reached. This equilibrium behavior is well known and has been observed in laboratory tests (CRWMS M&O 2000ck, Section 6.6). Below a critical value of the relative humidity, or deliquescence point, the solution evaporates completely and the resulting salts remain dry. Colligative behavior is observed when solutions are concentrated by boiling; the boiling temperature increases with solution concentration until a limit is reached and the salt precipitates. The deliquescence point and the boiling point have been measured for a number of solutions of pure salts, as shown in Figure 4-75. Various salts exhibit different behavior, but solutions of salts with lower deliquescence points have consistently higher boiling points.

During cooldown of the potential repository, dissolution of salts will occur rapidly when the relative humidity exceeds the critical value for each salt present. Rapid dissolution is consistent with the observation that puddles of dissolved salt (primarily sodium chloride) occur overnight on salt flats when the relative humidity exceeds the deliquescence point for sodium chloride, but the temperature remains above the dew point (CRWMS M&O 2000cl, Section 6.1.4.2). These puddles can then dry up during the day when the relative humidity decreases.

Laboratory evaporation tests have been used to identify the minerals and salts that could form in the emplacement drifts. Tests were conducted using two different water compositions: a bicarbonate-type water and a chloride-sulfate-type water (CRWMS M&O 2000cg, Section 6.5). Evaporation was performed at below-boiling conditions (85°C [185°F]) to represent the behavior of slowly migrating waters in the engineered barrier system. At this temperature, the assemblage of mineral phases resulting from evaporation is controlled by precipitation kinetics. It is thought that the assemblages are representative of potential repository conditions.

The first set of tests using bicarbonate-type water (similar to water from well J-13) showed that the salts formed during complete evaporation included



000500C\_ATP\_Z1S42\_87b.cdr

Figure 4-75. Deliquescence Points (Expressed as Relative Humidity) and Boiling Points for Several Pure Salts

This figure plots handbook data for the equilibrium relative humidity, as a function of temperature, for saturated aqueous solutions of some pure salts. Some of these may be present in the emplacement drifts, and these data represent minimum relative humidity conditions when aqueous conditions can occur. Each data curve probably terminates at the boiling curves to the right, but these are gaps in the available handbook data at intermediate temperatures. BP = boiling point; RH = relative humidity. Source: CRWMS M&O 2000ck, Figure 8.

niter, halite, thermonatrite, calcite, and silica (CRWMS M&O 2000cg, Section 6.5). Calcium and magnesium precipitated as carbonates early in the evaporation process, while halite and niter, being more soluble, precipitated when evaporation was nearly complete. The precipitates formed are sensitive to the concentration of carbon dioxide in the environment, which affects the pH environment. The tests provided no evidence of hydroxide precipitates, which would indicate very high pH. When the tests were repeated with tuff particles mixed with the water, similar results were obtained.

Test results for the chloride-sulfate-type water (similar to matrix pore water or sea water)

concluded that chloride and sulfate are the major anionic brine constituents, and that carbonate species are substantially less important (CRWMS M&O 2000cg, Section 6.5). As the water was evaporatively concentrated, the pH decreased to approximately 6 or lower. On complete evaporation, chloride and sulfate salts (such as halite and gypsum) predominated. In summary, test results show that calcium and magnesium carbonates, if present, will precipitate early in the evaporation process, while halite and niter are among the last salts to form. Other, additional chloride and sulfate salts will precipitate from chloride-sulfate-type waters.

**Composition of Waters in the Emplacement Drifts**—Throughout most of the repository performance period, composition of water in the drifts will be similar to that of ambient percolation in the host rock. During the thermal pulse, development of brine compositions that could potentially accelerate corrosion of the drip shield and waste package will depend on the chemical composition in late stages of evaporation.

In the laboratory tests described previously, evaporation of the bicarbonate-type water (similar to J-13 well water) produced a carbonate-rich brine that was highly concentrated in sodium, chloride, sulfate, carbonate, and silica. The pH increased to at least 10 and possibly higher as evaporation progressed. Evaporation of chloride-sulfate-type water (similar to matrix pore water or sea water) produced a carbonate-poor brine that was concentrated in sodium, chloride, sulfate, calcium, and magnesium (CRWMS M&O 2000cg, Section 6.5). Other dissolved components that can be enriched in natural brines include fluoride, bromide, strontium, phosphate, and boron (CRWMS M&O 2000cg, Section 6.1). Laboratory test results have shown that fluoride is not concentrated in brines representing Yucca Mountain waters, probably because these waters contain sufficient calcium and sodium to precipitate fluoride minerals (CRWMS M&O 2000cg, Section 6.5). Other components of natural brines (bromide, strontium, phosphate, and boron) are trace constituents in Yucca Mountain waters and are unlikely to achieve significant concentrations. Thus, the major chemical constituents of concentrated brines in the potential repository drifts will be sodium, calcium, magnesium, chloride, sulfate, and nitrate. For high-pH carbonate-rich brines, silica species and carbonate will also be present.

Brine compositions are outside the range that can be calculated exactly with widely used chemical activity models (i.e., much greater than 1 molal ionic strength). Accordingly, descriptions of brine behavior are more empirical, particularly with multiple dissolved species (not a single salt). The Pitzer approach (CRWMS M&O 2000cl, Section 6.4.2; CRWMS M&O 2000cg, Section 6.7.3) is based on observations of analogous ion interac-

tions and for simulating brine behavior at ionic strengths as high as 10 molal.

**Microbial Activity in the Emplacement Drifts**—Laboratory testing, combined with microbial test results in the scientific literature, show that threshold conditions for microbial activity and growth are relative humidity above 90 percent, and temperature below 120°C (248°F) (CRWMS M&O 2000cg, Section 6.4.5.1). Field investigations have been performed at Yucca Mountain and at nearby Rainier Mesa to characterize microbial populations in situ (CRWMS M&O 2000cg, Section 6.4). Additional microbial observations from the exploratory tunnels at Yucca Mountain are underway.

Site characterization investigations have shown that in situ microbial growth and activity are limited by availability of water and nutrients, particularly phosphate and organic carbon. In the potential repository environment, microbial activity will also be limited by temperature and radiation (CRWMS M&O 2000cg, Section 6.4). Water will be locally available during the repository thermal evolution, as discussed previously. Phosphate is a trace constituent of J-13 water, probably because the Topopah Spring Tuff contains apatite, a phosphate mineral. Organic carbon may be limiting for some classes of organisms, such as molds, but microorganisms that fix carbon from carbon dioxide are common in rock samples obtained underground at Yucca Mountain; therefore, a source of organic carbon is not required for bacterial growth and activity. Temperature will decrease over time, so microbial activity will be possible within a few hundred years after permanent closure. Radiation from the waste package may sterilize the surrounding environment, but the shielding effect of the host rock will ensure that nearby microbes can recolonize the emplacement drifts. From this discussion, it is evident that microbial activity will occur in the emplacement drifts. The effects of microbial activity on the degradation of the waste package outer barrier material are discussed in Section 4.2.4.3.3. The potential effects on radionuclide transport are discussed in Section 4.2.7.

**Approach to Modeling the Evolution of the In-Drift Chemical Environment**—In this approach,

relative humidity is used as a "master variable" to control the evolution of brines. Initially, the formation of minerals and salts, as seepage waters are evaporated to dryness, is modeled using a normative approach based on the laboratory tests described previously (CRWMS M&O 2000cg, Section 6.5). As relative humidity increases in the emplacement drifts, the salts formed by evaporation gradually become brines and are diluted. For the salts formed from evaporation of bicarbonate-type water (similar to J-13 well water), and considering the behavior of the salts separately and without interaction, deliquescence begins at relative humidity of 50 percent (CRWMS M&O 2000ck, p. 75 and Figure 8). At a greater value of relative humidity, all the salts are considered to be dissolved, and further changes in solution composition are calculated using the Pitzer modeling approach (or other more widely used modeling approaches) as the environment approaches ambient (preheating) conditions. If seepage occurs, it either evaporates completely, forming minerals and salts, or it is partially evaporated and the evaporative concentration effect is accommodated in the chemical modeling approach (CRWMS M&O 2000cg, Section 6.5).

To evaluate the effects of microbial activity on the bulk chemical environment while taking into account the importance of engineered material degradation, an approach is used that incorporates energy balance and mass balance. Threshold conditions determine when microbial growth and activity can resume, then degradation rates for the materials present in the in-drift environment determine the biomass that can be supported. The result of this calculation can be compared with other descriptors of the in-drift environment to assess whether microbial effects are significant (CRWMS M&O 2000cg, Section 6.4).

The same threshold conditions apply to the onset of microbially influenced corrosion of the waste package. While the drip shield and waste package materials are included in the energy- and mass-balance approach, the corrosion rates are developed directly from laboratory tests (see Section 4.2.4).

#### 4.2.3.2.3 Effects of Engineered Materials on the Chemical Environment

**Degradation of Steel and Alloys**—The product of drip shield corrosion is predominantly titanium dioxide. Alloy 22 corrosion produces oxides of major components nickel, chromium, iron, and molybdenum. These oxides tend to be chemically inert and do not react with other chemical species in the drift environment. They will accumulate slowly, corresponding to general corrosion rates on the order of 10 to 1,000 nm/yr (0.0000004 to 0.00004 in./yr) (see Section 4.2.4). This will consume oxygen at a rate that is negligible compared with the rate of gas flux through the drift openings (CRWMS M&O 2000cg, Section 6.3).

Steel corrosion products are insoluble ferric-oxides or oxyhydroxides. The concentration of ferric iron for aqueous solutions in equilibrium with hematite, goethite, and other iron oxides is very small, comparable to the concentration associated with iron-bearing nontronite clays (CRWMS M&O 2000cg, Section 6.7).

The rate of degradation for structural carbon steel, for vapor-phase conditions representative of the drift environment, has been measured for many samples, at different temperatures, in close proximity to different solutions conditions, such as pH and chloride concentration (CRWMS M&O 2000cg, Section 6.3). The measured penetration rates are on the order of tens to hundreds of microns per year. The corresponding consumption rates for oxygen are comparable to the convective flux of oxygen through the drift openings during the time period when this corrosion will occur.

Corrosion products can increase in volume, and particles can move in the drifts, potentially changing flow characteristics. These effects are neglected because the liquid flux in the drifts will be orders of magnitude smaller than the flow capacity, and redistribution of particulate matter can therefore have only a minor impact on the flow.

**Effects of Cementitious Materials**—A modified Type-K (Portland-based) expansive cement would be used for rock bolt anchorage in the potential

repository. The mix will contain silica fume, plasticizer, and a low water-cement ratio to promote strength, durability, and low permeability ( $10^{-19} \text{ m}^2$ ).

The alkaline composition of leachate from rock bolt cement grout will be bounded by equilibrium with portlandite. This approximation is conservative because portlandite will be carbonated over tens or hundreds of years from exposure to carbon dioxide in the gas phase. This behavior is known to occur with long-term exposure of concrete to air (CRWMS M&O 2000cg, Section 6.3).

**Colloidal Particles Produced by Degradation of Engineered Materials**—The following paragraphs describe laboratory data and field analogue data that are used to estimate the importance of ferric colloids for radionuclide transport.

Naturally percolating, mobile fracture waters have not been intercepted or sampled in the host rock, so groundwater analogues have been used to estimate colloid concentrations in seepage water. Colloids have been sampled by pumping of groundwater from 18 well intervals, from the saturated zone, at or near Yucca Mountain. The concentrations of particles in different size ranges were determined by instrumental analysis (CRWMS M&O 2000cg, Section 6.6). It is assumed that these results are analogous to unsaturated zone fracture waters in the potential repository host rock because the waters are derived from broadly similar rock types and likely have similar compositions. Accordingly, colloids are probably of similar types, consisting mainly of clays and silica.

It is noted that for more concentrated waters with greater ionic strength, such as will be produced by evaporative concentration during the thermal pulse, colloid concentrations are suppressed (Section 4.2.6). As the solution concentration increases, colloid stability decreases (i.e., the maximum possible concentration of colloids, which may vary for different sizes).

Production of colloids from engineered materials will be dominated by steel corrosion products, as

discussed previously. The maximum concentration of ferric colloids in seepage waters can be estimated using the groundwater analogue. The affinity of these colloids for radionuclides has been measured in the laboratory (CRWMS M&O 2000cg, Section 6.6). Ferric-oxide colloids were shown to have high affinity for plutonium and americium.

**Application to Modeling the Effects of Engineered Materials**—The effects of steel on oxygen consumption in the drifts, and radionuclide transport, are modeled using the available information. Consumption of oxygen by steel is modeled by applying the average of measured corrosion rates, subject to a condition that the onset of steel corrosion occurs when the relative humidity is 70 percent. Consumption of oxygen by titanium and Alloy 22 corrosion, and the effects of cementitious materials on the bulk chemical environment, are not included in performance analyses, based on the previous discussion.

Use of groundwater colloids as an analogue for the concentration of ferric-oxide colloids in the drifts is conservative because pumping wells are highly dynamic, and not all colloids in the drift will be ferric-oxide or derived from steel. Also, different types of colloids become unstable in certain pH ranges (point of zero charge), and ferric-oxide colloids are unstable near pH 8, which is very close to the predicted pH of seepage. Use of laboratory test data for radionuclide affinity is also a conservative approach because smaller distribution coefficients would probably be observed in chemical systems with more components, containing anions and cations that could compete with radionuclides for sorption sites.

It is noted that the majority of ferric-oxide corrosion products in the drifts will be immobile in the drift environment and yet exposed to seepage water so that released radionuclides can be immobilized by sorption. The potential for retardation by corrosion products in the drifts was not incorporated into the TSPA-SR model but has been considered in supplemental studies. This supplemental evaluation is described further in Section 4.2.7.

#### 4.2.3.2.4 Environment on the Surfaces of the Drip Shield and Waste Package

**Behavior of Water on the Barrier Surfaces**—As discussed previously, the deliquescence point defines the minimum relative humidity at which a salt will absorb water from the atmosphere and form a concentrated brine. Figure 4-75 shows deliquescence points for a number of pure salts as functions of temperature. Among the salts which have been identified from evaporation of representative waters, sodium nitrate has the lowest deliquescence point (50 percent). Humidity corrosion of the drip shield and waste package can therefore begin at a relative humidity of 50 percent. This is conservative because deliquescence apparently occurs at greater humidity for mixtures of salts. For example, the deliquescence point for a mixture of salts evaporated from J-13 well water can be inferred from the observed boiling point of a concentrated brine representing the result of evaporating a bicarbonate/carbonate solution. The boiling point for such a brine is approximately 112°C (234°F) (CRWMS M&O 2000ck, Section 6.12.5), which is less than the boiling point of a saturated sodium nitrate solution (Figure 4-75). This means that humidity corrosion of the drip shield or waste package is not actually likely to occur until relative humidity reaches a value greater than 50 percent.

**Potential for Acidic Conditions**—Inorganic acids could form in small quantities from chemical evolution of brines, or they could be produced in conjunction with localized corrosion processes. These acids, such as hydrochloric acid, have known vapor pressures and will tend to evaporate over time, especially at elevated temperature (CRWMS M&O 2000ck, Section 6.10).

**Application to Modeling the Environment on Barrier Surfaces**—Consideration of the environment on the drip shield and waste package surfaces is limited mainly to identifying the value of relative humidity at which corrosion will begin. Humidity corrosion begins at 50 percent relative humidity, which is conservative, as discussed previously. The relative humidity is determined from thermal-hydrologic predictions that represent the metallic barriers explicitly.

Once corrosion begins, the water composition is estimated using the approach described previously for the in-drift chemical environment. Possible water compositions range from a concentrated sodium nitrate brine to dilute bicarbonate-type or chloride-sulfate-type waters. The corrosion rates used with these water compositions in the TSPA-SR model are based on laboratory-measured corrosion data for several different water compositions ranging from dilute bicarbonate-type water to concentrated brine, including elevated temperature conditions and both acidified and basified compositions (CRWMS M&O 2000ck, Section 6.12). The selection of these water compositions for corrosion test conditions is central to the approach for representing environmental conditions on the surface of the drip shield and waste package.

Considering the factors limiting production and deposition of inorganic acids and hydrogen peroxide, radiolysis outside the waste package is considered to be of minor importance to corrosion and is not considered in the performance analyses.

#### 4.2.3.2.5 Rockfall on the Drip Shield

The geotechnical parameters required to predict rockfall include data and information collected either by field mapping or by laboratory testing. Joint mapping data for the subunits that constitute the emplacement horizon of the potential repository have been collected from the Exploratory Studies Facility, including the ECRB Cross-Drift (CRWMS M&O 2000e, Section 4.1). Joint strength parameters, including cohesion and friction angle, have been developed from laboratory shear strength test data from core samples and are used to predict both the size and number of fallen rock blocks (CRWMS M&O 2000e, Section 4.1). Rock density data and intact rock elastic properties are used to assess seismic effects and to determine the load applied to the drip shield; these data have also been obtained from laboratory tests performed on core samples (CRWMS M&O 2000e, Section 4.1).

Key block analysis in underground excavations located in jointed rock masses has been considered for a number of design situations. Deterministic methods of block theory in rock engineering were advanced by Warburton (1981) and Goodman and

Shi (1985). The literature provides examples for deterministic analysis of the maximum block size, given the spacing and orientation of three joint sets, and the excavation size and orientation. Subsequent work by other authors has been oriented toward probabilistic risk assessment of key block failure (CRWMS M&O 2000e, Section 6.3). These more recent methods are considered suitable for the analysis of densely jointed and faulted rock masses (i.e., greater than three joint sets) where planar joint surfaces can reasonably be assumed. Such conditions typically exist in the potential host rock units at Yucca Mountain. The probabilistic approach used in the TSPA-SR model is distinguished from traditional key block analysis because it not only assesses the maximum size of key blocks, but it also predicts the number of potential key blocks that will be formed in a certain length of tunnel for any tunnel orientation.

#### 4.2.3.3 Process Model Development and Integration

The discussion of the physical and chemical environment is divided into five parts: (1) the chemical composition of seepage water and gas flux into the emplacement drifts (these are near-field conditions and are bounding conditions to the chemical and physical environment for the engineered barriers); (2) the chemical environment in emplacement drifts; (3) the effects of engineered materials on the chemical environment; (4) the chemical environment on the surfaces of the drip shield and waste package; and (5) the model for the rockfall on the drip shield.

##### 4.2.3.3.1 Modeling the Composition of Liquid and Gas Entering the Drifts

**Thermal-Hydrologic-Chemical Seepage Model Approach**—This section discusses implementation of the thermal-hydrologic-chemical seepage model. The unsaturated zone flow model and the drift seepage model, which are the bases for thermal-hydrologic modeling, are discussed in Section 4.2.1. This model predicts, at the drift scale, the composition of seepage and the associated gas-phase chemistry for 100,000 years, including the effects of heating.

The effects of heating on gas composition are important for predicting the composition of incoming seepage. The concentration of carbon dioxide in the immediate vicinity of the drift openings will decrease because of displacement and dilution by water vapor. This will be accompanied by decreased carbon dioxide activity in any associated seepage, which will cause pH to increase. In the zone of condensation further from the drift openings, carbon dioxide enrichment will occur, causing pH to decrease. Diffusivity for gaseous species is much greater than for aqueous species, and transport is more rapid. The result is that the region affected by changes in gas composition will be larger than that affected by changes in liquid-phase transport.

Flow of information from various models and data sources to the thermal-hydrologic-chemical seepage model is shown in Figure 4-76. The model uses input from modeling of the Drift Scale Test, the unsaturated zone flow model (CRWMS M&O 2000c), and other sources of geochemical data (CRWMS M&O 2000a, Section 3.3). These inputs ensure consistency between the thermal-hydrologic-chemical seepage model and the other models and data used to calculate drift seepage and the movement of water in response to heating. Other model inputs, including reactive surface areas of minerals, fracture-matrix interaction area, and the mineral volume fractions, are estimated from observed data (CRWMS M&O 2000a, Section 3.2.2).

Comparison with observations from the Drift Scale Test (CRWMS M&O 2000ch) and sensitivity studies on mineral assemblages and water compositions were used to guide development of the model. An example of the comparison of model results and observed data is shown in Figure 4-77. Evolution of the concentration of carbon dioxide in the gas-phase, over time, is compared with model results at four sampling intervals in the Drift Scale Test. For some data, calculated results are shown for nearby points in the model grid. For example, locations labeled "above" or "below" are calculated somewhat above or below the sampled location in the test. Similarly, locations labeled "center" or "end" were calculated near the center or the far end, respectively, of the sampled loca-

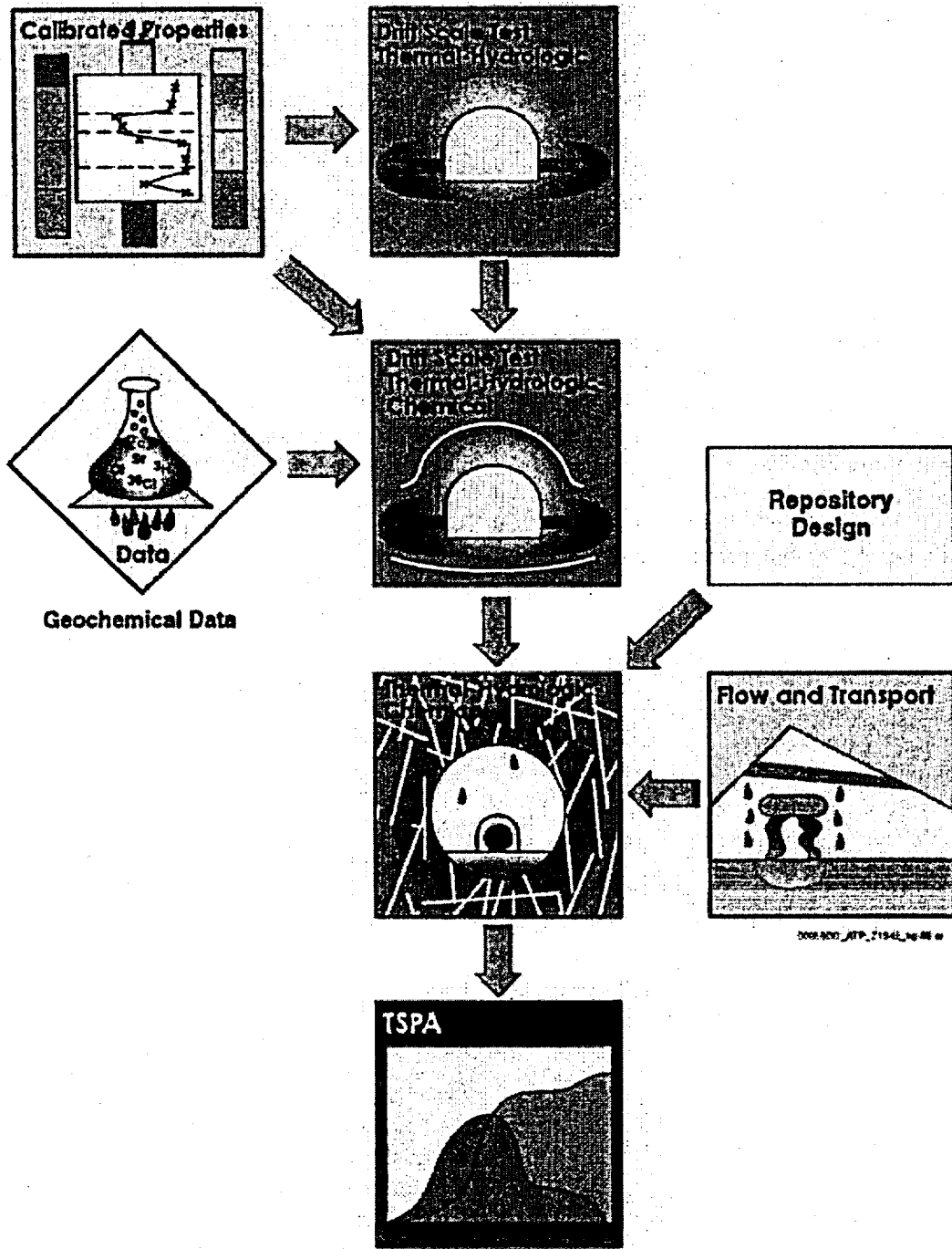


Figure 4-78. Model Diagram Relating Inputs and Outputs for the Thermal-Hydrologic-Chemical Seepage Model, with the Thermal-Hydrologic Drift Scale Test Model, Thermal-Hydrologic-Chemical Drift Scale Test Model, Calibrated Properties Model, Unsaturated Flow and Transport Model, Other Data Input, and Design Information

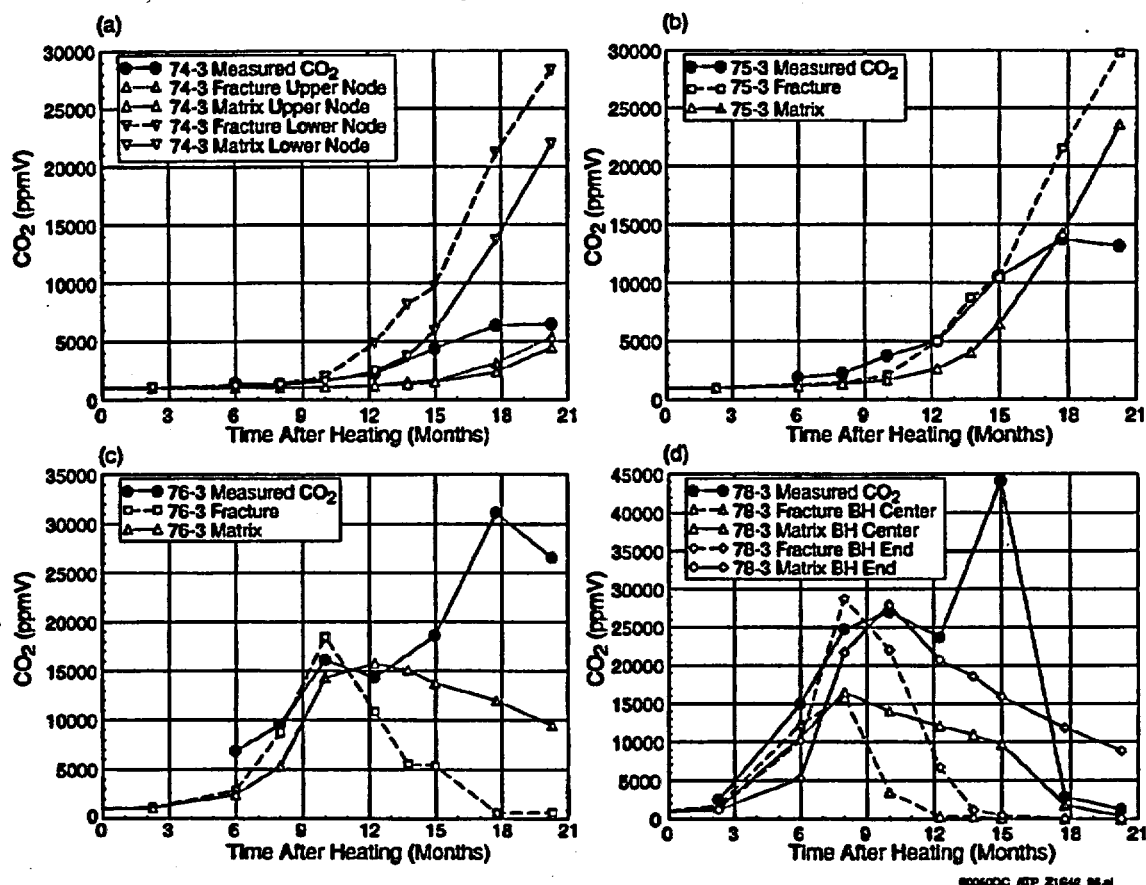


Figure 4-77. Comparison of Modeled Carbon Dioxide Concentrations in Fractures and Matrix to Measured Concentrations in Boreholes for the First 21 Months of the Drift Scale Test

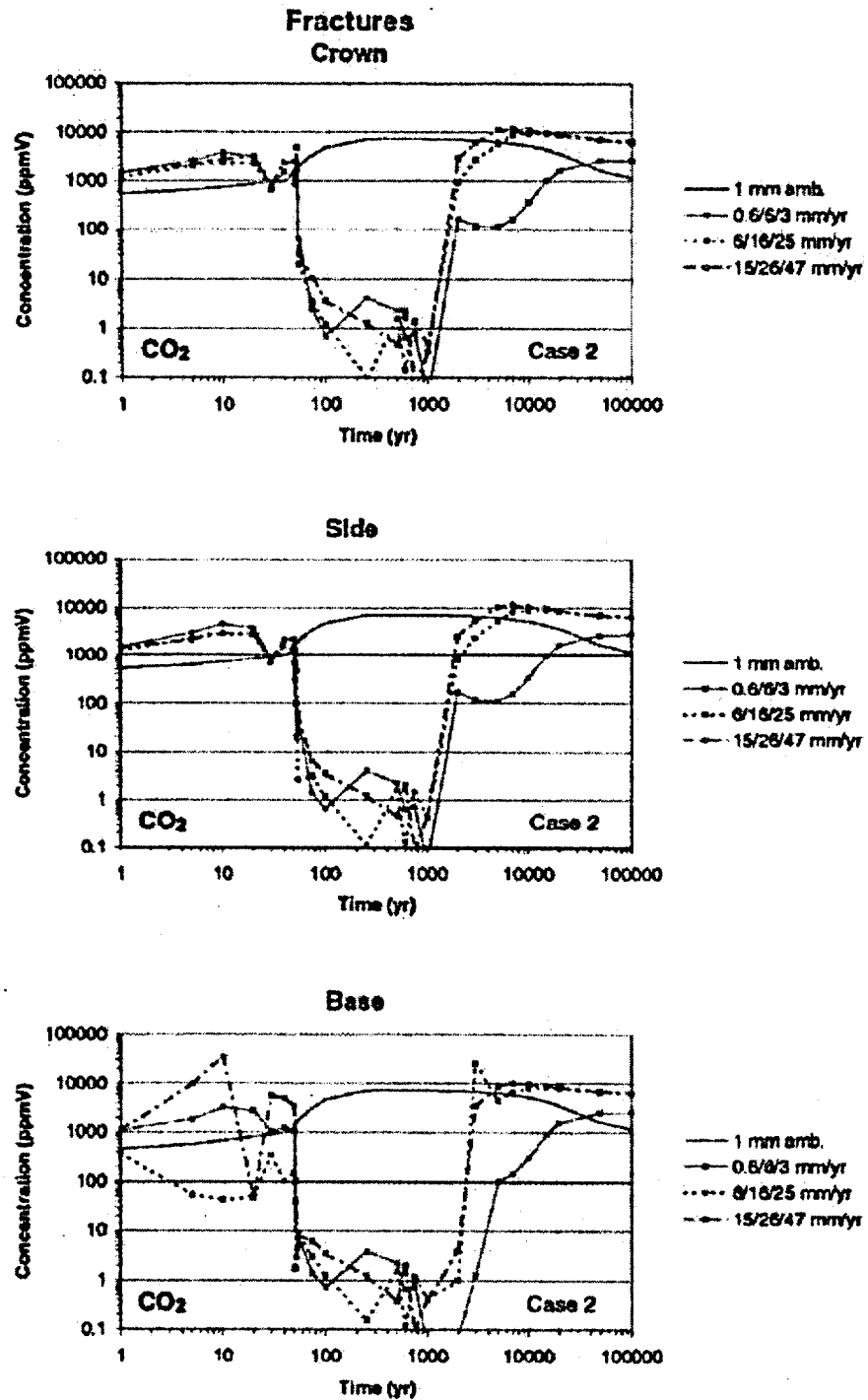
(a) Borehole interval 74-3. (b) Borehole interval 75-3. (c) Borehole interval 76-3. (d) Borehole interval 78-3. Measured data are plotted with black dots; calculated results are shown using other symbols. The model results are from the grid points in the model domain closest to the sampling intervals. The predictive model is based on a limited mineral assemblage that includes calcite, gypsum, and silica phases. See Figure 4-52 for the location of Boreholes 74, 75, 76, and 78. Source: BSC 2001o, Figure 10.

tion. There are comparable trends between the test data and the calculations, and agreement is obtained in an average sense throughout much of the time period modeled.

**Thermal-Hydrologic-Chemical Seepage Model Results**—The model incorporates elements of the repository thermal operating mode nominally described in Section 2 to represent waste package heating over time, changes in heating from ventilation, heat transfer within the drift, and thermal-hydrologic-chemical processes (CRWMS M&O 2000al). As an example of model results, time profiles for gas-phase carbon dioxide concentra-

tions at three locations around the drift, for one simulation using chloride-sulfate-type water, are shown in Figure 4-78. Carbon dioxide concentrations in fractures decrease significantly during dryout and increase again during rewetting. The increase during rewetting is caused by the dissolution of calcite deposited during dryout and by heating of ambient percolation and condensate waters as they approach the drift opening (the solubility of carbon dioxide in water decreases as temperature increases).

Using the chloride-sulfate-type water as the initial condition, the chloride concentration in fracture



0000131\_AFP\_ZTV42\_0068.A

**Figure 4-78. Time Profiles of Modeled Carbon Dioxide Concentrations in the Gas Phase in Fractures at Three Drift Wall Locations for Different Climate Change Scenarios**

The climate change scenarios are indicated as net infiltration flux values (in mm/yr) for the present-day, monsoonal, and glacial-transition climate states (calcite-silica-gypsum system). For all scenarios, the transitions between these sites occur at 600 and 2,000 years. Source: BSC 2001o, Figure 40.

water immediately above the drifts is estimated to increase approximately fourfold from evaporative concentration. Higher concentrations could occur below the drifts. Upon rewetting, chloride concentrations are estimated to decrease to near-ambient values. The results indicate that seepage water should not be concentrated more than approximately one order of magnitude in chloride, compared to the ambient pore water. For the same simulation, the estimated pH for waters reaching the drift wall ranges from near-neutral (pH 7.2 to 8.3) to sub-alkaline (pH 8.6 to 9.0), depending on the chemical system properties used in the calculation, such as mineral assemblage and gas-phase carbon dioxide (CRWMS M&O 2000a1, Section 3.3; CRWMS M&O 2000c1).

#### 4.2.3.3.2 Modeling the Evolution of the In-Drift Chemical Environment

Three complementary modeling approaches are used to describe the formation and behavior of salts under different relative humidity conditions:

- **Normative Precipitates and Salts Model**—Based on empirical data, this model is used to estimate which minerals and salts will form when waters are completely evaporated.
- **Low-Relative-Humidity Salts Model**—The low-relative-humidity salts model describes the behavior of salts when relative humidity is less than 85 percent.
- **High-Relative-Humidity Salts Model**—The high-relative-humidity salts model calculates water composition and dissolution/precipitation reactions for solutions that can occur when relative humidity is greater than 85 percent.

These models are used to determine the timing of in-drift environmental conditions that permit aqueous corrosion and to estimate the composition of waters that can transport released radionuclides.

**Normative Precipitates and Salts Model**—For waters having compositions similar to either bicarbonate-type water or chloride-sulfate-type water, a set of precipitates is identified that is consistent

with the laboratory test data discussed previously. This model describes an assemblage of precipitates formed by complete evaporation. It is approximate in that the laboratory tests may not exactly duplicate evaporation conditions in the potential repository. It is supported by arguments based on thermodynamic data, which indicate that:

- Thermonatrite and calcite are favored over hydroxides such as portlandite because of the presence of sufficient carbon dioxide in the environment.
- Anhydrite is favored to form over gypsum (both forms of calcium sulfate) for the humidity conditions that will be present in the drifts.
- Thenardite (sodium sulfate) and calcite are a more stable assemblage than thermonatrite and anhydrite.

The final species considered in the assemblage is amorphous silica (silicon dioxide), which was detected in all the laboratory samples derived from the bicarbonate-type water. The presence of the tuff would allow for more geochemical processes, such as formation of clays, cation exchange, and silicate buffering associated with tuff dissolution (CRWMS M&O 2000cg, Section 6.5).

**Low-Relative-Humidity Salts Model**—This model begins at a point in time during the thermal period when the emplacement drifts are dry and at low humidity. Incoming seepage (if it occurs) is completely evaporated, and the salts and minerals that form are determined from the normative approach. As relative humidity continues to increase over time, the salts are allowed to dissolve according to their deliquescent behavior. The amount and composition of brine produced are controlled by the solubilities of the salts and the fraction of each salt that is allowed to dissolve. For the nitrate salts, the entire amount is allowed to dissolve when the relative humidity reaches 50 percent. For the remaining salts, the fraction dissolved is abstracted from the individual salt properties. For simplicity in performance assessment analyses, all of the remaining salts are modeled to dissolve exponentially from zero to

unity as relative humidity increases from 50 percent to 85 percent. The timing of relative humidity evolution at different locations in the potential repository is obtained from thermal-hydrologic calculations (Section 4.2.2). At 85 percent relative humidity, all the accumulated soluble salts are considered to be completely dissolved.

**High-Relative-Humidity Salts Model**—The high-relative-humidity salts model is used for relative humidity greater than 85 percent, conditions for which soluble salts are fully dissolved and the relative rates of evaporation and seepage control the aqueous chemistry. Modeling the behavior of concentrated aqueous solutions (greater than 1 molal ionic strength) is performed using a Pitzer approach, implemented using the EQ3/6 chemical modeling code (CRWMS M&O 2000cl, Section 6.4.2). A modified Pitzer database was developed from existing published data, adding chemical species such as nitrate and silica, and extending the temperature range of applicability to 95°C (203°F). Details are provided in supporting documentation (CRWMS M&O 2000cl, Section 5.3). It is a conservative, approximate model that is used for predicting the composition of water in the emplacement drifts for a time interval during the thermal period when seepage is strongly concentrated by evaporation.

Three sources of experimental data were used for validation of the model (but not for model development or calibration; CRWMS M&O 2000cl, Section 4.1.2). All three studies involved evaporation of synthetic J-13 well water in a beaker open to the atmosphere and maintained at constant elevated temperature. In one study, 30 L (7.9 gal) of synthetic average J-13 water were evaporated to 30 mL and the precipitated solids analyzed. In a second study, the pH of the water was monitored during evaporation, and, in a third, 100-times concentrated average J-13 well water was dripped through a column of heated tuff and final solution composition compared to the initial composition (CRWMS M&O 2000cl, Section 4.1.2).

Results from the high-relative-humidity salts model show that sodium, potassium, chloride, sulfate, and carbonate species simply concentrate

without much precipitation. As J-13 water is concentrated to a total ionic content of 10 molal, the pH approaches 10. Species containing silicon, aluminum, calcium, magnesium, iron, and fluoride tend to precipitate in significant amounts relative to their aqueous concentrations. Among the precipitates included in the model, calcite and chalcedony are produced in greatest quantity; magnesium-bearing clay (represented in the model by sepiolite) and fluorite are the next most abundant.

**Model for Microbial Activity in the Emplacement Drifts**—The approach to assessing the potential effects from microbial activity has two parts: (1) a threshold model for environmental conditions that permit microbial growth and activity and (2) a quantitative model to bound the quantity of biomass, including microbes, that could develop in the emplacement drifts.

Relative humidity, temperature, and radiation dose conditions are combined to formulate threshold environmental conditions for microbial activity. Published results based on extreme behaviors of known organisms are used as a guide where site-specific data are sparse. More precise estimates based on characterization of organisms at Yucca Mountain are unwarranted because of the uncertainty about which types of organisms will be present and the potential for biological adaptation.

Microbial growth and activity does not occur until the local temperature decreases to less than 120°C (248°F) and relative humidity increases to 90 percent. Microbially influenced corrosion of the waste package is conservatively assumed to begin when the relative humidity reaches 90 percent.

The microbial communities model quantifies the abundance and metabolic activity of microorganisms in the engineered barrier system environment. It is based on models used in the Swiss and Canadian nuclear waste programs (CRWMS M&O 2000cp, Section 6). An idealized elemental composition for microbial biomass is used, consisting of carbon, nitrogen, sulfur, and phosphorous in fixed proportions, plus water. The rates of supply for these constituents are input as constant release rates for each natural and engineered material present in the drifts. The other major constraint is

the chemical energy available for microbes to grow, which is maximized from possible oxidation/reduction reactions.

The presence of water, nutrients, and energy sources is required for microbial growth and activity. There are three main categories of introduced materials that could furnish nutrients and energy: steels/alloys, cementitious materials, and organic substances (CRWMS M&O 2000as, Section 3.1.2.4.2.1).

Three basic approaches to modeling microbial nutrient and energy balances are possible, based on nutrient balance, thermodynamic energy balance, and chemical kinetics. The microbial communities model (CRWMS M&O 2000cp, Section 6) combines the nutrient and thermodynamic approaches. The available materials are decomposed into their basic elements and combined with the constituents available from groundwater and gas fluxes through the repository. Release of chemical constituents is controlled by estimating the degradation lifetime of each material. The model assumes that all available nutrients and redox energy sources are used for microbial processes and is therefore bounding.

Application of the microbial communities model to the potential repository design shows that approximately 10 grams of biomass would be produced per lineal meter of emplacement drift per year, during the first 10,000 years. Based on this small generation rate, effects on the bulk chemical environment are considered negligible for the TSPA-SR analyses (CRWMS M&O 2000as, Section 5.3.2.4). Localized effects of microbial activity could nevertheless alter the longevity of materials and the transport of radionuclides. For that reason, microbially influenced corrosion of the waste packages was included in TSPA-SR calculations (CRWMS M&O 2000a, Section 3.4.1.6).

#### 4.2.3.3.3 Modeling the Effects of Engineered Materials on the Chemical Environment

**Modeling the Effects from Corrosion of Steel and Alloys**—Steels and alloys introduced to the potential repository as ground support and other

structural materials will degrade with time. The important effects of metal corrosion on the bulk chemical environment, and the approaches used to represent those effects, are summarized as follows.

Oxygen in the drift environment will be consumed, decreasing the partial pressure of oxygen while corrosion is active. This effect is modeled by converting rates of metal corrosion to rates of oxygen consumption and comparing the results with estimates of the available oxygen flux (CRWMS M&O 2000as, Section 3.1.2.3.4).

A corrosion-rate model for structural steel was used to develop estimates of oxygen availability. The potential consumption of oxygen from corrosion of other alloys is also discussed briefly. Corrosion rates for A516 carbon steel have been measured for representative vapor-phase conditions (not immersion), elevated temperature, and proximity to synthetic groundwater with a composition similar to evaporatively concentrated J-13 water. These data are used to represent corrosion of structural steel in the drifts, as there is a paucity of equivalent data for other steels. The rate can vary with temperature, pH, and water composition. In addition, laboratory data for a similar carbon steel composition (CRWMS M&O 2000cg, Section 6.4) suggest an approximate sixfold increase in the corrosion rate once moisture returns to the drifts because of microbial activity. Steel corrosion will be insignificant until the relative humidity exceeds 70 percent (CRWMS M&O 2000cg, Section 6.3.2.2).

Applying measured corrosion rates for structural steel and using environmental conditions representing the potential repository environment yields the following results (CRWMS M&O 2000cg, Section 6.3):

- Steel present in the drifts will completely corrode within a few hundred years, starting at times from approximately 300 to 2,000 years after waste emplacement. (Timing will depend on the duration of preclosure operations and location in the repository layout; steel corrosion can begin at 300 years after emplacement if the preclosure period is

50 years, and corrosion first occurs near the repository edge, which cools fastest.)

- The calculated rate of steady-state oxygen consumption will be replenished by the flux of oxygen that is transported to the drifts by buoyant gas-phase convection.

Results indicate that oxygen partial pressure in the drifts would be decreased but that the flux of oxygen would probably be sufficient to maintain oxic (i.e., corrosive) conditions. In the potential repository, the corrosion rate for structural steel will tend to decrease as the oxygen partial pressure decreases, prolonging the degradation process but moderating the impact on oxygen partial pressure. This model is therefore conservative because the laboratory corrosion data on which the rate model is based were acquired for oxic conditions (CRWMS M&O 2000as, Section 3.1.2.3.4).

The drip shield, waste package, and waste package supports in the design described in this report would be made from titanium, Alloy 22, and stainless steel. Corrosion of these materials will be much slower than for carbon steel and therefore slower to consume oxygen. Consumption of oxygen by corrosion of Grade 7 titanium or Alloy 22 could contribute slightly to depletion of oxygen in the engineered barrier system. However, the potential rate of consumption is a small fraction of the oxygen availability (CRWMS M&O 2000cg, Section 6.3).

**Modeling the Effects from Cementitious Materials**—The model for the effects of cement grout used in rock bolts is based on dissolution of cement mineral phases and subsequent interaction of cement leachate with carbon dioxide in the drift environment. The results indicate that the potential contribution of cement leachate to the bulk chemical environment will be minor (CRWMS M&O 2000cg, Sections 6.3 and 6.7).

Chemical equilibrium calculations for cement are performed using a mineral assemblage that includes constituents of young cement as a bound on the potential to produce alkaline leachate (CRWMS M&O 2000cg, Section 6.3). Mineral assemblages representing alteration of Portland

cement by aging and carbonation are available but tend to produce less alkaline leachate.

The initial composition of water that interacts with cement is assumed to be that of J-13 water, but the potential contribution of influent water chemistry to the leachate is minor because leachate composition (before reaction with carbon dioxide) will be dominated by the cement. Reaction of groundwater with the grout is assumed to be closed (i.e., it does not include reactions with gas-phase carbon dioxide), which maximizes the leachate pH. Biotic processes are also assumed to have a negligible effect on leachate composition because the organic content of the plasticizer admixture probably has very low biological reaction rates (CRWMS M&O 2000cg, Section 6.3).

Once the leachate flows into the drift opening or the surrounding rock, it will be exposed to carbon dioxide in the emplacement drifts, which will moderate the pH. Because of the small amount of leachate compared to the total percolation through the host rock, open-system conditions are used for evaluating this interaction. In addition, contact with silica, such as the cristobalite present in the host rock, will also moderate leachate pH.

The grout permeability is small, which limits chemical interaction with the drift environment while increasing the longevity of the grout to dissolution. Very small flow rates (a few milliliters per year per rock bolt) are obtained using the saturated hydraulic conductivity of the grout. A more conservative bounding approach is used to account for the possibility of grout cracks, allowing higher water contact rates. This approach is based on the ratio of the rock bolt grout cross-sectional area to the drift diameter. This method produces flow rates on the order of a few percent of the total seepage inflow to the drifts.

Results from this model show that prior to contact with carbon dioxide or siliceous minerals, the leachate will be highly alkaline, with a pH value of 11 or greater. This is caused primarily by dissolution of portlandite, which has retrograde solubility (higher solubility at lower temperatures). Buffering on contact with carbon dioxide and near-field rock in the drift environment will result in substantial

decrease in leachate pH. Accordingly, elevated pH values from the leachate are unlikely to be present at the drip shield or waste package.

The model does not consider the possibility that grout could break up into fragments, some of which may fall and come to rest on the drip shield. A transient pulse of alkaline leachate could result from such failure, and the current model does not explicitly address rapid leaching. However, the analysis shows that if such leaching occurs during the thermal pulse, the chemical composition of the leachate will be similar to evaporatively concentrated waters that will form in the drift. During and after cooldown, the concentration of carbon dioxide will increase in the drift environment, and cement fragments will be exposed to increased carbon dioxide levels. The potential for strongly alkaline conditions will then be moderated by reaction of leachate with the drift environment. Also, carbon dioxide gas will diffuse into the grout and react directly with the cement. This process is not considered in the current model but will be more important for fragmented grout. Finally, the current model indicates that the quantities of leachate produced are likely to be small, whether or not the grout is fragmented.

**Modeling the Effects of Colloids Produced from Engineered Materials—Ferric-oxide colloids with strong affinity for plutonium and americium will be produced from corrosion of steel in the emplacement drifts. The size and concentration distributions of natural colloids observed in local groundwaters are used to represent the behavior of ferric-oxide colloids. This is justified because these waters are similar in composition to seepage waters that are likely in the potential repository (CRWMS M&O 2000a, Section 3.3.2.4). It is conservative because the effect of ionic strength in evaporatively concentrated waters, and the behavior of ferric-oxide at near-neutral pH, will decrease the stability of ferric-oxide colloids. Colloids are discussed further in Section 4.2.7 in the context of the radionuclide transport model.**

#### **4.2.3.3.4 Modeling the Environment on the Surfaces of the Drip Shield and Waste Package**

**Conditions for Aqueous Corrosion and Humidity Corrosion—**At permanent closure, the surfaces of the drip shield and waste package will be dry, with relative humidity less than 50 percent, and no humidity corrosion or aqueous corrosion processes active. This condition will continue through the period of peak temperatures. During cooldown, the relative humidity on the barrier surfaces will gradually increase (CRWMS M&O 2000n, Section 3.1.3).

Figure 4-75 shows that aqueous salt solutions on the drip shield and waste package can exist for relative humidity less than 100 percent but greater than the deliquescence point. Analysis of salts formed from laboratory evaporation tests shows that the salt with the lowest deliquescence point is sodium nitrate (CRWMS M&O 2000n, Section 3.1.3.1).

For modeling purposes, it is assumed that sodium nitrate—the salt with the lowest deliquescence point among all the salts likely to be present—will determine the minimum relative humidity at which aqueous conditions can occur (50 percent). Another value of relative humidity is selected to represent the condition at which all salts, including chlorides, sulfates, and carbonates, are dissolved as brine (85 percent). This value is greater than the deliquescence points for all salts that are likely to be present. The low-relative-humidity salts model is used to predict the composition of brines present on the drip shield and waste package surfaces as the relative humidity increases from 50 to 85 percent. This is a conservative approach because waste packages under intact drip shields will be affected only by dust and aerosols, which may be more benign than the brine conditions considered in the model.

The high-relative-humidity salts model is used to calculate the composition of brines as they undergo further dilution at relative humidity greater than 85 percent. If seepage occurs during the thermal pulse, the waters that contact the drip shield and waste package surfaces will be evaporatively

concentrated because the relative humidity on the surfaces will be less than in the surroundings. The high-relative-humidity salts model is used to calculate the composition of evaporatively concentrated seepage waters. The degree of evaporative concentration will decrease with time as the relative humidity increases.

The high-relative-humidity submodel of the in-drift precipitates and salts analysis was implemented for relative humidity greater than 85 percent. In this regime, the steady-state water composition is controlled by the ratio of the evaporation rate to the seepage rate; this ratio is always less than one. The submodel calculates water composition, pH, chloride molality, and ionic strength in the repository for several temperatures, relative humidities, relative evaporation rates, and carbon dioxide gas fugacity values (CRWMS M&O 2000cl, Section 6.4.2).

**Composition of Aqueous Solutions Used for Corrosion Testing**—The exact chemistry of the water that contacts the drip shield and waste package surfaces cannot be known precisely. However, several test solutions have been developed for laboratory corrosion testing of titanium, Alloy 22, and other materials. These solutions were selected to represent a range of dilute and concentrated conditions, pH, and temperatures that could result from evaporative concentration in the repository. The test solutions are described in Section 4.2.4.2.

The chemistry of the waters that contact drip shield and waste package surfaces would vary in a repository, and the test solutions described previously represent a range of possible conditions. Results from corrosion testing with these solutions are discussed in Section 4.2.4.

#### 4.2.3.3.5 Model for Rockfall onto the Drip Shield

The effect of rockfall on the emplaced drip shield was screened from the TSPA-SR model based on the following analysis. *Drift Degradation Analysis* summarizes the analysis of key blocks, including block failure due to seismic and thermal effects (CRWMS M&O 2000e, Section 6), using the prob-

abilistic Discrete Region Key Block Analysis method (CRWMS M&O 2000a, Section 3.3.1; CRWMS M&O 2000e, Attachments VIII through XI).

Based on mapping data and results from key block analysis, the orientation of the emplacement drifts, as discussed in Section 2.1.2, was selected to maximize drift stability (CRWMS M&O 2000e, Sections 1.4 and 6.4). Considering static plus seismic loads, rockfalls were estimated using the probabilistic key-block analysis. The results include probability distributions for the size of fallen key blocks and the number of such blocks per length of emplacement drifts.

Heating and subsequent cooling of the repository host rock would impose stresses, deposit minerals, and shift rock joints. This was represented in the analysis as reduction in joint cohesion from the time of closure until about 2,000 years after closure and thereafter. The resulting changes in estimated rockfall are provided in supporting documentation (CRWMS M&O 2000e, Section 6). Results for combined thermal and static loads are similar to those for combined seismic and static loads.

Given the distribution of key block size, a structural calculation was performed to determine the stresses in the titanium drip shield (BSC 20011). The analysis considered a range of rock sizes falling onto a 3-m (10-ft) length of drip shield. This length is half that of a drip shield segment and was chosen to take advantage of symmetry and thereby reduce computational effort. A range of rock sizes up to 10 metric tons (approximately 4.15 m<sup>3</sup> [147 ft<sup>3</sup>]) is the design basis for the drip shield. For rock sizes up to 4 metric tons, the entire volume of a rock can be located above a 3-m (10-ft) partial-length drip shield. An analysis of the joint geometry suggests that an increase in rock size must occur by an increase in length of the rock block along the drift, rather than an increase in block height (CRWMS M&O 2000e, Attachment IX). The probabilistic key-block analysis showed that the maximum block size could be greater than 10 metric tons, but such large blocks would be relatively unlikely. Probabilistic key-block analysis was performed for the middle nonlithophysal, lower lithophysal, and lower nonlithophysal host

rock units. For these units, the proportion of rock blocks simulated that exceeded 10 metric tons ranged from 0 to 5.8 percent (CRWMS M&O 2000e, Figures 27 to 29 and Attachment II). Also, because of their large dimensions, each block would be distributed over more than one 6-m (20-ft) drip shield segment, so the loads would be shared. Using the concept of effective rock mass over a 3-m (10-ft) partial-length drip shield, the maximum rock mass is determined to be 10 metric tons per 3-m (10-ft) partial-length drip shield. In other words, any rock mass greater than 10 metric tons will load a 3-m (10-ft) partial-length drip shield the same as a 10-metric-ton rock. Calculations for the effective rock mass for different size blocks were calculated using finite element techniques and are documented in *Rock Fall on Drip Shield* (BSC 2001I, Section 5.2 and Table 7-1). Preliminary results from the analysis indicated that the impact would not dent the drip shield in such a way that it would contact the waste package. (Design criteria are presented in *Emplacement Drift System Description Document* [CRWMS M&O 2000ab].) The impact from a 10-metric-ton block was estimated to produce one 13-cm (5-in.) long crack in a 3-m (10-ft) long portion of a drip shield segment because of stress corrosion cracking that could occur after the rockfall (BSC 2001I, Table 6-1). Smaller rocks, such as a 2-metric-ton rock, were estimated not to produce enough residual stress to initiate stress corrosion cracking. It is expected that such stress corrosion cracks would be narrow and would not conduct much water flow (see Section 4.2.4). The calculation is conservative because it does not take credit for energy expended by fracturing of the rock or dislocation of the drip shield.

Effects from rockfall events involving multiple rock blocks have not been analyzed explicitly. However, because the dimensions of the maximum expected block size are of the order of the dimensions of the waste packages, it is reasonable to assume that multiple falls of blocks of the maximum size would have to act independently. The effects from multiple, smaller-size block falls would be bounded by the analyses of the effects of the maximum block size.

#### 4.2.3.3.6 Limitations and Uncertainties

As discussed in Section 4.4.1.2 of this report, uncertainties are an inherent component of the TSPA method. Uncertainty is introduced through the conceptual model selected to characterize a process, as well as the mathematical, numerical, and computational approaches used to implement the model. Uncertainty is also introduced from imperfect knowledge of important parameters used for input to the models (e.g., physical properties). This section emphasizes limitations and uncertainties relative to the in-drift physical and chemical environment: (1) the thermal-hydrologic-chemical model used to characterize seepage water chemistry that enters the drift, (2) the in-drift chemical environment model and supporting analyses, and (3) the rockfall model and supporting analyses.

Since the TSPA-SR model, the DOE has performed several supplemental activities to address uncertainties and limitations in the TSPA-SR model. Additionally, as noted in Section 4.1.4, the DOE is evaluating the possibility for mitigating uncertainties in modeling long-term repository performance by operating the design described in this report at lower temperatures. Consequently, some of the models describing the thermal-hydrologic-chemical model, precipitates salts model, and the drift degradation model have undergone further evaluation since the TSPA-SR model. Some alternative models have been implemented and sensitivity analyses conducted to address parameter and model uncertainties. These supplemental analyses are summarized in *FY01 Supplemental Science and Performance Analyses* (BSC 2001a, Sections 4, 5 and 6). The sensitivity of TSPA model results to alternative process models is discussed in Volume 2, Sections 3.2 and 4.2 of *FY01 Supplemental Science and Performance Analyses* (BSC 2001b) and is summarized in Section 4.4.5.5 of this report.

**Thermal-Hydrologic-Chemical Seepage Model Limitations and Uncertainties—Uncertainties exist in the thermodynamic and kinetic input data used in the model. For example, as the concentrations of dissolved solutes increase during evaporation, the theoretical limitations of the chemical activity model may be exceeded. Rapid boiling can lead to mineral precipitation that is**

controlled by nucleation kinetics and other surface-related phenomena. The specific conditions for which the model becomes invalid, however, may not be important for the overall dynamics of the system. Geochemical reactions are a strong function of temperature and the presence of water, both of which are better constrained than the rates of reaction and may control the spatial distribution even if the exact quantities of the phases at a given time are uncertain (CRWMS M&O 2000a1, Section 3.3.4).

The model is based on information obtained from thermal testing in the middle nonlithophysal unit of the Topopah Spring Tuff, which may exhibit somewhat different thermal-hydrologic behavior or mineralogy than lower lithophysal units, in which most of the repository emplacement drifts would be located. Although this could change the system response, it is noted that the bulk chemistry is similar for all the welded host rock units (CRWMS M&O 2000a1, Section 3.3.4). Thermal testing that is planned for the lower lithophysal unit will evaluate the applicability of the current model over the repository footprint.

Another aspect of thermal-hydrologic response that will affect aqueous and gas-phase chemistry in the host rock is buoyant gas-phase convection (CRWMS M&O 2000cm), controlled by the large-scale permeability. As discussed previously, gas-phase convection will be an important source of carbon dioxide and oxygen as chemical reactants to the in-drift chemical environment. Buoyant gas-phase convection is not evident from the Drift Scale Test, probably because the rock bulk permeability at this location does not support it. However, results from the unsaturated zone flow model (Section 4.2.1) indicate that permeability of the host rock increases with scale, and current thermal-hydrologic models do not incorporate mass transfer along the axes of the drift openings. Therefore, it is likely that further investigation will show that gas-phase convection in the potential repository will exceed that observed in the Drift Scale Test. It is anticipated that the magnitude of gas phase convection will be great enough to supply sufficient amounts of gas through drift openings to preclude depletion of gas components

through chemical reactions with drift components (CRWMS M&O 2000cg, Sections 6.3.2 and 6.3.3).

Section 4.2.2.3.5 summarized supplemental studies to the TSPA-SR model related to physical changes in permeability and seepage resulting from thermal-hydrologic-chemical processes. These studies also addressed thermal-hydrologic-chemical model uncertainties related to the chemistry of potential seepage water. Specific studies included:

- Supplemental sensitivity studies of different initial water and gas boundary conditions (BSC 2001a, Section 4.3.6.5)
- Simulated evolution of water and gas compositions in the Tptpmn and Tptpll units (BSC 2001a, Section 6.3.1.4.3)
- Modified base-case and extended case geochemical systems (BSC 2001a, Sections 4.3.5.3.2, 4.3.6.4, and 6.3.1.5).

These activities included a range of different input data and assumptions, including thermodynamic and kinetic data input data (BSC 2001a, Sections 4.3.6.4 and 6.3.1.4).

**Precipitates and Salts Model Limitations and Uncertainties**—This modeling approach is based on literature data that describe the minerals and salts produced by evaporative concentration and the relations between solution composition and relative humidity. In certain aspects, the thermal-chemical data support is incomplete. Therefore, the accuracy of this model was tested using independent collected laboratory data for the evolution of solids and water composition during evaporation. As described in *In-Drift Precipitates/Salts Analysis* (CRWMS M&O 2000cl, Section 7.3), the precipitates and salts model is expected to provide results that are within an order of magnitude for chloride concentrations and ionic strength and within a pH unit for pH predictions. This degree of accuracy is acceptable because it greatly reduces the potential ranges of these variables, thereby considerably reducing uncertainty.

Data were not available to directly evaluate the accuracy of the low-relative-humidity salts model.

The model did, however, produce reasonable trends and results in chloride and ionic strength outputs in its applied relative humidity range and produces consistent results at 85 percent relative humidity, where the high-relative-humidity salts model takes over (CRWMS M&O 2000cl, Section 7.3).

Simplifying assumptions were required to reduce the complexity of the precipitates and salts analysis and to avoid sophisticated approaches where data were lacking, although these assumptions tended to be conservative. The greatest uncertainties in the analysis are likely the thermal-hydrologic and thermal-hydrologic-chemical predictions and other predicted inputs to the analysis (CRWMS M&O 2000cl, Section 7.3). Therefore, the models were applied for a variety of these conditions.

The precipitates/salts model has been modified in several ways since the TSPA-SR model analyses. Each modification involved the high relative humidity submodel. The Pitzer database was improved by the addition of several minerals and thermodynamic data, and the amount of output data reported in lookup tables was increased (BSC 2001a, Section 6.3.3.4).

Additional discussion of uncertainties related to the precipitate and salts model is described in supplemental studies (BSC 2001a, Sections 6.3.3.3, 6.3.3.4, and 6.3.3.5). Supplemental studies emphasized selected uncertainties, including the sensitivity of starting water composition on evaporative chemical evolution and effects of mineral suppression (BSC 2001a, Section 6.3.3.5.1). Sensitivity studies show in-drift chemistry to be sensitive to starting water composition and that thermodynamic and kinetic data are secondary in importance or negligible (BSC 2001a, Section 6.3.3.5). These studies also show that using the water composition obtained from the thermal-hydrologic-chemical model is reasonable, as implemented in the TSPA-SR model and supplemental TSPA model analyses.

**Microbial Communities Model Limitations and Uncertainties**—This model is not intended to quantify localized microbial activity or its consequences but bounds overall microbial growth and

activity in the engineered barrier system. It has been validated by testing against laboratory data, natural system observations, and other modeling efforts, as described in Section 6.6 of *In-Drift Microbial Communities* (CRWMS M&O 2000cp). Comparison with these independent data sets indicates that the estimates are within an order of magnitude of the actual values.

The approach uses a well-mixed reaction system to represent the emplacement drift and provides estimates of total biomass production that can be used to bound the extent of microbially influenced corrosion of the waste package. In this approach, one of the primary uncertainties is in the degradation rates that supply nutrients and energy for microbial growth. This is evaluated by varying the rates over large ranges and using bounding results (CRWMS M&O 2000cp, Section 6).

**Engineered Materials Effects Modeling Limitations and Uncertainties**—The rate of steel corrosion for sub-oxic conditions, including the effects of microbial activity, is an important factor in predicting the oxygen budget in the emplacement drifts. Current estimates for steel corrosion are based on (1) abiotic test results obtained for similar steel under oxic conditions and (2) preliminary data for microbially influenced corrosion of similar steel at water-saturated and nutrient-augmented culture conditions. The results for oxic conditions overestimate the rate of oxygen consumption for conditions of decreased oxygen availability, which could occur for a few hundred years in the repository during peak thermal conditions. Applicability of the available microbial testing data to environmental conditions in the repository is more uncertain (CRWMS M&O 2000cg, Section 6.3).

Boiling of water during the thermal event will produce water vapor that will displace much of the air from the drift, with the result that oxygen will be depleted. This may lead to decreased corrosion rates, but the extent of such decreases is uncertain for steel and corrosion-resistant materials such as titanium and Alloy 22. In any case, the effect of decreased oxygen availability will be of limited duration.

Supporting analyses to the TSPA model has previously demonstrated that including these uncertainties would increase the potential for reduced corrosion and solubility, which would have a beneficial impact on performance (BSC 2001a, Section 6.3.2.3.1).

Conceptualization of leachate that could be contributed from degradation of cement grout is adapted from simplifying assumptions and studies of concrete reported in the literature (CRWMS M&O 2000cg, Section 6.3.1; CRWMS M&O 2000as, Section 3.1.2.3.5). Confirmatory testing of rock bolt longevity, carbonation of the grout, microbial attack of organic superplasticizers, and other aspects of grouted rock bolt performance has not been undertaken. The final design of ground support in the emplacement drifts is under development, and analysis of ground support function is preliminary. Accordingly, the longevity of grouted rock bolts in response to thermal loading and environmental conditions remains somewhat uncertain. Rock-mass deformation could lead to failure of the rock bolts (not necessarily associated with failure of the drift openings).

Supporting the TSPA-SR model analyses, supplemental analyses have provided additional confirmation indicating cement leachate-influenced seepage water would have a negligible affect on in-drift chemistry (BSC 2001a, Section 6.3.2.3.2).

**Limitations and Uncertainties on Conditions Used to Model Barrier Corrosion—Microbial activity on the waste package surface under an intact drip shield may be negligible, even above 90 percent relative humidity, as long as water has not leaked through the drip shield onto the waste package and the waste package has not directly contacted the invert. Thus, significant corrosion would not commence until the drip shield fails and water contacts the waste package. Similarly, if salt-tolerant organisms are present, the relative humidity threshold for microbially influenced corrosion may decrease to 75 percent, which would mean that the onset of microbially influenced corrosion could shift to an earlier time. Such a shift represents only a small fraction of the time that microbial processes are modeled to be present.**

Furthermore, uncertainty as to the timing for the onset of general corrosion or microbially influenced corrosion is of low importance for performance assessment because the expected corrosion rate for the waste package, even with microbes present, is low enough that a shift in the timing of the onset of corrosion is insignificant to the overall performance of the potential repository. Further discussion of corrosion rates for the drip shield and waste package is provided in Section 4.2.4.

Common scale minerals that are produced from natural waters include calcite, gypsum, and silica (CRWMS M&O 2000ck, Section 6.1.1). If seepage occurs, the chemical components of these minerals will be present in waters that contact the drip shield and waste package. The tendency for scale formation is enhanced by evaporative concentration and changes in pH. Scale can protect the underlying material if it forms a dense adherent layer, but it may have a deleterious effect if it forms a porous layer or a crevice with the underlying material. Interfaces between scale-covered and bare regions of the surfaces might be subject to corrosion. Few data on the effects of scale are presently available, but related laboratory tests have been performed to evaluate the potential for crevice corrosion. The results show that crevice corrosion is insignificant for titanium and Alloy 22 at the expected repository temperature and humidity. By inference, the effects of scale are also thought to be insignificant.

Another potentially important aspect of scale formation is the production of decomposition products, such as lime, from scale minerals at elevated temperatures. Subsequent dissolution of such products by seepage water or deliquescence could produce highly alkaline solutions. Decomposition temperatures for potential scale minerals are known, and some are within the operating temperature limits for the waste package (CRWMS M&O 2000ck, Sections 4.1.11 and 6.11). However, as discussed previously, the presence of gaseous carbon dioxide in the drift environment implies that the formation of highly alkaline hydroxide species is unlikely.

**Rockfall Model Limitations and Uncertainties—The usefulness of the rockfall model is**

affected by how well the data inputs describe the actual fracture conditions. The natural variability of fractures within a rock mass always represents uncertainty in the design of structures in rock. The extensive fracture data collected at Yucca Mountain provide a good representation of fracturing at the emplacement drift horizon. The range of fracture variability from tunnel mapping has been captured in the rockfall model through multiple Monte Carlo simulations of the rock mass. To account for uncertainties associated with seismic, thermal, and time-dependent effects on rockfall, a conservative reduction of joint strength parameters has been included in the approach (CRWMS M&O 2000e, Section 5).

Sensitivity analyses supplemental to the TSPA-SR model did not change the results of the rockfall model analyses (BSC 2001a, Section 6.3.4.9). Consequently, the process remains insignificant to performance and remains screened from TSPA analyses (BSC 2001a, Section 6.3.4.6).

#### 4.2.3.3.7 Alternative Conceptual Processes

As with limitations and uncertainties, some of the following alternative conceptual models have been addressed in supplemental analyses and summarized in *FY01 Supplemental Science and Performance Analyses* (BSC 2001a, Section 1; BSC 2001b, Section 1).

**Alternative Concepts for Thermal-Hydrologic-Chemical Seepage Model**—Alternative approaches for modeling the compositions of the gas-phase and liquid seepage have been evaluated in *Engineered Barrier System: Physical and Chemical Environment Model* (CRWMS M&O 2000cg, Sections 6.2 and 6.7). Both the bicarbonate-type and chloride-sulfate-type waters were evaluated for a range of carbon dioxide conditions. The results were used to evaluate the carbon dioxide budget, taking into account processes in the host rock and within the drifts, as discussed previously. The liquid and gas compositions obtained are comparable to results from the thermal-hydrologic-chemical seepage model, which were abstracted for the TSPA-SR model.

As noted in Section 4.2.2.3.5, supplemental studies have evaluated a number of additional alternative starting water compositions in sensitivity analyses. Additional water compositions included water perched on top of the Calico Hills formation, water collected from the Drift Scale and Single Heater Tests, and water predicted by the thermal-hydrologic-chemical model, as well as other seepage water compositions discussed in this section (BSC 2001a, Section 6.3.3.5). Alternative conceptual models described in Sections 4.2.2.3.5 and 4.2.3.3.6 include alternative initial water and gas compositions, alternative host rock assumptions, and modified base-case and extended case geochemical systems (BSC 2001a, Sections 4.3.5.3.2, 4.3.6.4, 4.3.6.5, 6.3.1.4.3, and 6.3.1.5). In general, the sensitivity studies suggest that the models incorporated in the TSPA-SR are reasonable or conservative.

**Alternative Concepts for Precipitates and Salts Model**—An alternative approach for representing the composition of waters contacting the drip shield and waste package would be a bounding concept. Considering that some dripping of water onto the drip shields may occur throughout the repository in small quantities because of condensation, small accumulations of minerals and salts, on the scale of individual droplets, could occur in locations where seepage will never occur. Microscopic quantities of salts would interact with changes in the relative humidity but would not be mobilized by flow or diluted by seepage. In this alternative bounding approach, the environment on the drip shield surface would be represented by the permanent presence of minerals and soluble salts or the solutions obtained when they equilibrate with water vapor in the air (CRWMS M&O 2000cg). Although simpler than the current precipitates and salts model used for TSPA-SR, this approach would not yield very different corrosion conditions. Current estimates of corrosion rates are small, with limited sensitivity to the presence of soluble salts (see Section 4.2.4).

An alternative model for seepage/invert interactions has been developed but has not yet been implemented in its entirety (BSC 2001a, Section 6.3.3.4.2.1). This alternative model abstracts in-drift mixed solutions using ionic strength, pH, and

an acid neutralizing capacity parameter (which is an indication of the resistance of a solution to pH changes). The abstracted solutions are mixtures of seepage fluxes from the crown above the drift, the water wicked through the rock and corroded metals in the invert, and the diffusion film or flux from a waste package after failure.

**Alternative Concepts for Microbial Communities Model**—As stated previously, the implemented model bounds the overall production of biomass in the emplacement drifts. Two approaches, while not precisely alternatives to the microbial communities model, could be used to extend the model from estimation of biomass to estimation of bounding rates for microbially influenced corrosion. The first approach is an empirical approach based directly on microbial corrosion laboratory test data. The second approach, which is the principal alternative concept for predicting microbial effects on the bulk chemical environment, is the chemical kinetics approach mentioned previously. In this concept, biotic and abiotic chemical reactions are treated similarly, as quantitatively explicit reactions distinguished by different reaction rates. Reaction pathways would include organic species and compounds produced by microbial activity. This approach has long been recognized as an alternative but has not been used because reasonable data support is not available. The advantages of the approach would include quantitative predictions involving specified chemical systems. Pathways for microbially mediated reactions can be complex, and extensive laboratory testing could be required to represent conditions in the repository. Process models for these approaches have not been developed.

**Alternative Concepts for Engineered Materials Effects Modeling**—An alternative concept for the possible effect of steel on the performance of the titanium drip shield was analyzed. Specifically, the potential for hydrogen embrittlement and cracking of the titanium was evaluated. It is likely that steel ground support members will eventually fail from corrosion, possibly augmented by rock support loads, and fall onto the drip shields so that steel would come to rest on the titanium. This concept is neglected in the TSPA-SR model because (1) at the time of failure the steel will probably be coated

with oxides that have no deleterious effect on titanium and (2) fine cracks in the drip shields will not transmit significant amounts of water (CRWMS M&O 2001c, Section 6.1), similar to stress corrosion cracks in the waste package (see Section 4.2.4).

**Alternative Approaches for Modeling Rockfall**—An alternative approach that was considered for modeling rockfall involved the use of multidimensional distinct-element analysis (CRWMS M&O 2000e). The approach has the benefit of directly applying dynamic loading to the rock mass. However, the approach is deterministic and cannot readily accommodate the available data on variability of fracturing in the potential host rock units. Accordingly, distinct element modeling was used only to confirm results obtained with the probabilistic key-block analysis and to assess thermal effects on host rock permeability (see Section 4.2.2.3.4).

#### 4.2.3.3.8 Model Calibration and Validation

**Thermal-Hydrologic-Chemical Seepage Model Calibration and Validation**—The goal of model validation is to determine reasonable bounds on the system behavior over 10,000 years or longer, based on relatively short-term tests. The thermal-hydrologic-chemical Drift Scale Test model is an implementation of the repository-scale thermal-hydrologic-chemical seepage model for the situation of the Drift Scale Test. The results were compared to gas and water samples, representing potential seepage collected during the Drift Scale Test (CRWMS M&O 2000a, Section 3.6.3.2) as a means to validate the repository scale model. These comparisons include gas-phase carbon dioxide concentrations as a function of time and space, the pH of waters collected in boreholes, and general observations on changes in concentrations of chloride and other aqueous species.

Gas-phase carbon dioxide concentrations in the model results and in the measured values showed a similar halo of strongly elevated values (approximately 2 orders magnitude greater than the air in the observation drift) around the Drift Scale Test heaters that grew outward over time. Modeled pH values of fracture waters in the drainage zones of

around 6.5 to 7.5 (calcite-silica-gypsum system) are within one pH unit of waters collected from boreholes during the Drift Scale Test. Increases in the modeled pH of the waters as the rock around the boreholes heated further and began to dry out were also similar to the measured values where multiple samples were collected over time. This indicates that the model also captured the time-dependence of thermal-hydrologic-chemical processes. Simulations employing a more complex set of minerals and aqueous species estimate pH values about 0.5 to 1 pH unit higher than for the calcite-silica system. Such behavior may be more characteristic of longer time-scale water-rock interaction, which can be validated as the Drift Scale Test produces data that reflect conditions of more stable isotherms, as opposed to the data that were collected during the more transient first two years of the heating phase.

Concomitant increases (with pH and temperature) in measured silica concentrations and depletions in calcium suggest silicate mineral dissolution and calcite precipitation, trends that were also predicted by the model. Ongoing studies (by sidewall sampling and overcoring) of the actual minerals precipitated in fractures and their effect on hydrologic properties will allow for further comparisons to model results.

Measured chloride concentrations (a conservative species that shows the effects of dilution, boiling, and fracture-matrix interaction) are 5 to 10 times lower than in the pore water, a characteristic that was also captured by the model in the drainage zones. This validates that the model approximates fairly well the overall effects of dilution through condensate formation and fracture-matrix interaction (diffusive equilibration).

**Precipitates and Salts Model Calibration and Validation**—The normative precipitates and salts model approach (CRWMS M&O 2000cg, Section 6.5) was applied to the laboratory test results on a qualitative basis, and the results were in reasonable agreement for the bicarbonate-type water. There evidently is some sensitivity to the relative availability of calcium and sodium to form sulfate salts, which is not accounted for in the model. Minor species such as sylvite were identified by the

normative model but were not detected in the laboratory tests because they were scarce and because of interference from ambient humidity. Additional testing with the chloride-sulfate-type water produced similar agreement between the normative assemblage and the minerals observed on complete evaporation. From these results, the normative model is determined to provide a valid approximation to the major minerals and salts formed on complete evaporation of waters with composition similar to either J-13 water or matrix pore water.

The low- and high-relative-humidity salts models were independently developed and validated with laboratory data (CRWMS M&O 2000cl, Section 4.1.2). The low-relative-humidity salts model approach is conservative because it tends to shorten the dry period by not allowing dry conditions for relative humidity greater than 50 percent in the presence of nitrate salts. Also, it predicts elevated chloride concentrations at low relative humidity (CRWMS M&O 2000cl, Section 7.1). The model is valid because it reproduces trends in the known behavior of salts and provides results that are within an order of magnitude of independently developed data. Such accuracy reduces uncertainty associated with the processes that control water composition at low relative humidity. The low-relative-humidity salts model results that are important for TSPA modeling are a decrease in ionic strength (due to the thicker water film) and an increase in chloride concentration as the relative humidity rises from 50 to 85 percent.

Validation of the high-relative-humidity salts model is approached using results from laboratory tests, including those described previously in which bicarbonate-type and chloride-sulfate-type waters were evaporated, and handbook solubility values for pure salts. Reasonable agreement is obtained between measured and modeled values for pH and the concentrations of sodium, carbonate species, fluoride, chloride, and sulfate (CRWMS M&O 2000cl, Section 6.5.1). Agreement to within an order of magnitude is obtained for other constituents, which is acceptable for use in abstracted models for the TSPA. As an additional check, the model is also used to calculate the solubilities of several sodium and potassium salts that are potentially important products of evaporating J-13 water.

Calculated values are within a factor of 2 of the handbook values, up to 10 molal (the limit of the Pitzer model).

**Microbial Communities Model Calibration and Validation**—This is a bounding model that has been validated by comparison to laboratory and field data. Both model validation and code verification are described in Section 6.6 of *In-Drift Microbial Communities* (CRWMS M&O 2000cp). In these applications, agreement was obtained with observed microbial abundances within the order-of-magnitude tolerance level identified for the use of this model. Three comparisons were used:

- Replication of model results originally calculated for the Swiss repository program demonstrates that the code used for the microbial model (MING) functions correctly where natural materials are combined with engineered materials.
- Modeling of microbial conditions investigated underground at Yucca Mountain and at an analogue site at Rainier Mesa replicated the ambient microbial abundance to within an order of magnitude and confirmed that water and phosphorous availability are limiting factors to microbial growth.
- Modeling of the laboratory tests shows that the numbers of organisms calculated by MING can agree to within an order of magnitude with independently measured data from both energy-limited and nutrient-limited tests.

**Engineered Materials Effects Model Calibration and Validation**—Models for oxygen consumption by steel corrosion, the effects of cementitious materials, and the impact of ferric-oxide colloids on radionuclide transport are based on bounding approaches, and the best available supporting data are used. Key uncertainties and approaches to confirmation of these bounding arguments have been identified (CRWMS M&O 2000cg, Sections 6.3 and 6.6).

**Rockfall Model Calibration and Validation**—The rockfall model involved the use of probabi-

listic key block theory, which is an accepted approach for analyzing this type of geotechnical problem. The static key block results are in agreement with observed key block occurrence in the Exploratory Studies Facility main drift and cross-drift (CRWMS M&O 2000e, Section 7.2). The results from the rockfall model have shown that key blocks are most predominant in the Tptm unit, which agrees with field observations. The size of key blocks observed in the field is generally less than one cubic meter, which agrees with the simulated distribution of block sizes.

The seismic component of the rockfall model involves a quasi-static method of reducing the joint strength parameters. This method was verified based on the test runs using the dynamic functions of the distinct element code UDEC. Comparison between results from the dynamic and quasi-static analyses shows a consistent prediction of block failure at the opening roof (CRWMS M&O 2000e, Attachment V).

#### 4.2.3.4 Total System Performance Assessment Abstraction

This section describes abstraction of only those models selected for inclusion in the TSPA. The microbial communities model and the models used to bound the effects of engineered materials are determined to have minor impacts on calculated waste isolation performance (although it is acknowledged that microbially influenced corrosion may affect the longevity of Alloy 22 locally) and are excluded from the base case. Also, design analysis has shown that rockfall will not degrade the functionality of the drip shield or waste packages, so the rockfall model is also not included in TSPA-SR.

**Abstraction of the Thermal-Hydrologic-Chemical Seepage Model for the Total System Performance Assessment**—The thermal-hydrologic-chemical abstraction using the mean distribution of infiltration rate (CRWMS M&O 2000a, Section 3.3.3.4.2), including climate change, is calculated for both geochemical systems discussed above. The abstracted results for both the less complex and more complex chemical systems are shown in Table 4-17 (CRWMS M&O 2000al,

Table 4-17. Thermal-Hydrologic-Chemical Abstraction for the Mean Infiltration Rate Case with Climate Change

Parameter	Preclosure (Period 1) 0 to 50 years Abstracted Values 80°C	Boiling (Period 2) 50 to 1,000 years Abstracted Values 95°C	Transitional Cooldown (Period 3) 1,000 to 2,000 years Abstracted Values 90°C	Extended Cooldown (Period 4) <sup>a</sup> 2,000 to 100,000 years Abstracted Values 50°C
<b>Constituents from the Limited Chemical System (calcite-silica-gypsum)</b>				
log CO <sub>2</sub> , vfrac	-2.8	-6.5	-3.0	-2.0
pH	8.2	8.1	7.8	7.3
Ca <sup>2+</sup> , molal	1.7 × 10 <sup>-3</sup>	6.4 × 10 <sup>-4</sup>	1.0 × 10 <sup>-3</sup>	1.8 × 10 <sup>-3</sup>
Na <sup>+</sup> , molal	3.0 × 10 <sup>-3</sup>	1.4 × 10 <sup>-3</sup>	2.6 × 10 <sup>-3</sup>	2.6 × 10 <sup>-3</sup>
SiO <sub>2</sub> , molal	1.5 × 10 <sup>-3</sup>	1.5 × 10 <sup>-3</sup>	2.1 × 10 <sup>-3</sup>	1.2 × 10 <sup>-3</sup>
Cl <sup>-</sup> , molal	3.7 × 10 <sup>-3</sup>	1.8 × 10 <sup>-3</sup>	3.2 × 10 <sup>-3</sup>	3.3 × 10 <sup>-3</sup>
HCO <sub>3</sub> <sup>-</sup> , molal	1.3 × 10 <sup>-3</sup>	1.9 × 10 <sup>-4</sup>	3.0 × 10 <sup>-4</sup>	2.1 × 10 <sup>-3</sup>
SO <sub>4</sub> <sup>2-</sup> , molal	1.3 × 10 <sup>-3</sup>	6.6 × 10 <sup>-4</sup>	1.2 × 10 <sup>-3</sup>	1.2 × 10 <sup>-3</sup>
<b>Constituents from the More Complete Chemical System (including aluminosilicates)</b>				
Mg <sup>2+</sup> , molal	4.0 × 10 <sup>-6</sup>	3.2 × 10 <sup>-7</sup>	1.6 × 10 <sup>-6</sup>	7.8 × 10 <sup>-6</sup>
K <sup>+</sup> , molal	5.5 × 10 <sup>-6</sup>	8.5 × 10 <sup>-6</sup>	3.1 × 10 <sup>-4</sup>	1.0 × 10 <sup>-4</sup>
AlO <sub>2</sub> <sup>-</sup> , molal	1.0 × 10 <sup>-10</sup>	2.7 × 10 <sup>-7</sup>	6.8 × 10 <sup>-8</sup>	2.0 × 10 <sup>-9</sup>
HFeO <sub>2</sub> <sup>+</sup> , molal	1.1 × 10 <sup>-10</sup>	7.9 × 10 <sup>-10</sup>	4.1 × 10 <sup>-10</sup>	2.4 × 10 <sup>-11</sup>
F <sup>-</sup> , molal	5.0 × 10 <sup>-6</sup>	2.5 × 10 <sup>-6</sup>	4.5 × 10 <sup>-5</sup>	4.5 × 10 <sup>-6</sup>

NOTES: <sup>a</sup>Thermal-hydrologic-chemical calculations have been carried out to 100,000 years, while TSPA calculations have been carried out to 1 million years. Source: CRWMS M&O 2000c, Table 3.10-3.

Section 3.3.1). The evolution of chemical conditions at the drift wall is presented as a series of four discrete time periods for the TSPA-SR calculations: (1) preclosure, (2) boiling, (3) transitional cooldown, and (4) extended cooldown. The log carbon dioxide value represents the composition of gas at the drift wall. These time periods are selected so that relatively constant concentrations can be defined for constituents of interest. After the extended cooling period, the system is considered to have returned to the ambient conditions before thermal perturbation. For both chemical systems considered, major differences in concentrations for key constituents (factor of 10) are limited to calcium, sodium, and bicarbonate ions.

**Abstraction of the Precipitates and Salts Model for the Total System Performance Assessment—**For the TSPA-SR model, the evolution of water in the repository drifts as temperature decreases and relative humidity increases over time is generalized as an evolution from brine to increasingly dilute water. This evolution is modeled as a succession of time intervals. In each interval, the incoming seepage flow and its composition, as well as temperature, are assigned constant values; the

evaporation rate varies, and the in-drift chemical environment is determined from the evolution of thermal-hydrologic conditions at the particular location evaluated (CRWMS M&O 2000a, Section 3.3.4).

Below 50 percent relative humidity, any salts present in the drift environment will exist in crystalline form and will not form brines. At relative humidities between 50 and 85 percent, salts in the environment will deliquesce and form brines; compositions are provided by the low-relative-humidity salts model. Above 85 percent relative humidity, all of the salts are considered dissolved, and the composition is estimated by the high-relative-humidity salts model using a quasi-steady-state approximation of the degree of evaporative concentration (CRWMS M&O 2000a, Section 3.3.4.5.1).

For each time interval, values of the temperature, carbon dioxide partial pressure, seepage, and evaporation rate are obtained from other models. Lookup tables are then developed for the in-drift water composition to be used in the TSPA, based on a set of calculations using the low-relative-

humidity salts model and the high-relative-humidity salts model. The lookup tables are developed for the following conditions: temperature at 95°, 75°, 45°, and 25°C (203°, 167°, 113°, and 77°F); carbon dioxide partial pressure at  $10^{-1}$ ,  $10^{-3}$ , and  $10^{-6}$  atmospheres; and evaporative concentration ranges up to a thousandfold (CRWMS M&O 2000a, Section 3.3.4.5.1).

Inputs to and outputs from the precipitates and salts model were abstracted for use in the TSPA-SR model (CRWMS M&O 2001b, Section 1; CRWMS M&O 2000cg, Section 6.7.4). The abstracted results used in the TSPA-SR model were based on the thermal-hydrologic-chemical model as follows:

- Incoming seepage composition represented by the thermal-hydrologic-chemical abstraction
- Carbon dioxide fugacity and temperature fixed at thermal-hydrologic-chemical abstracted values.

The supplemental TSPA model used a modified abstraction of the thermal-hydrologic-chemical model. Modifications included the effects of operating temperature, the effects of different carbon dioxide partial pressures, and the effects of different initial pore water (and infiltration) compositions (BSC 2001a, Sections 6.3.1.6.3 and 6.3.1.9).

Likewise, the precipitates and salts model abstraction has been updated in supplemental TSPA modeling to include the effect of the concentrations of a revised suite of elements and a select number of aqueous species used to estimate alkalinity (BSC 2001a, Section 6.3.3.6). Another improvement to the precipitates and salts model is consideration of condensation. The combined effect of improvements to the near-field geochemical model shows differences at the subsystem level composition (BSC 2001a). However, supplemental analyses do not show a significant impact at the TSPA level for either higher- or lower-temperature operating modes (BSC 2001b, Sections 3.2.4.2 and 4.2.4).

#### 4.2.4 Waste Package and Drip Shield Degradation

The roles of the waste package and drip shield are discussed in detail in Section 3. This section addresses the expected performance of these components in the potential repository and, along with Sections 4.2.1 through 4.2.6, provides an explanation of the relationship of the waste package and the geologic environment at Yucca Mountain.

The degradation process models and the abstracted models discussed in this section serve as feeds to the WAPDEG code, which integrates the various models to address the overall performance (degradation rates) of the waste package and the drip shield. WAPDEG results, in turn, are used as feeds to the overall TSPA-SR. Specifically, the integrated model included in the WAPDEG performance assessment code used repository environmental conditions as a function of time from other process models to estimate the performance of the waste package and drip shield in terms of time to failure.

As noted in Section 4.1.4, the DOE is evaluating operation of the repository at lower temperatures. The conceptual basis and model abstractions presented in this section reflect the effects of higher-temperature operating modes, specifically those implemented in *Total System Performance Assessment for the Site Recommendation* (CRWMS M&O 2000a, Section 3.4). Alternative thermal operating modes and/or conservatisms and conceptual uncertainties have been reevaluated since the TSPA-SR model and are reported or summarized in *FY01 Supplemental Science and Performance Analyses* (BSC 2001a, Section 9; BSC 2001b, Sections 3 and 4).

##### 4.2.4.1 Conceptual Basis

Lifetimes of the drip shield and waste package depend on the environmental conditions to which they are exposed and the degradation processes that occur in that environment. Section 4.2.3 describes the conceptual understanding of the evolution of physical and chemical conditions in the repository emplacement drifts, the models used to represent those conditions, and the experimental

data that support and contribute to the validation of the models. Environmental conditions within the drifts that influence the degradation of the waste package and drip shield are tightly coupled to the thermal-hydrologic and geochemical processes occurring in the rock surrounding the drifts. These processes involve the vaporization and condensation of water under changing thermal conditions, redistribution and precipitation of dissolved salts, and the effects of gaseous species on solution chemistry. Included in the conceptualization are the contributions of construction material degradation processes (i.e., rock structural support materials and cementitious grout) and the effects of microbial action.

Once the exposure environments have been established, the most important and relevant degradation processes can be identified, which in turn can be used for selecting engineered materials for the drip shield and the waste package. This section discusses the degradation modes of the waste package and drip shield materials under the changing environmental conditions. Corrosion is the degradation process most relevant and important to the selection of the materials for the waste package and drip shield. Mechanical deformation of the waste package and drip shield are estimated to be less significant to the waste package containment time than corrosion (CRWMS M&O 2000n, Section 1.5). A number of corrosion processes have been investigated in detail and the results used to support the selection of materials and the design of these components.

**Waste Package and Drip Shield Materials—**Degradation modes for the drip shield and waste package are dependent on the materials used in these components and as mentioned earlier, on the environment in which they function. Performance of these materials are reviewed in *General Corrosion and Localized Corrosion of Waste Package Outer Barrier* (CRWMS M&O 2000cq) and *General Corrosion and Localized Corrosion of the Drip Shield* (CRWMS M&O 2000cr). Titanium alloys were selected for construction of the drip shield because of their high resistance to corrosion. This corrosion resistance is due to the formation of a passive oxide film, which is stable over a relatively wide range of environments. The rates of

general corrosion and dry oxidation (or dry-air oxidation) of this material have been shown to be very low (CRWMS M&O 2000n, Sections 3.1.1.1, 3.1.5.1, and 3.1.5.4).

Alloy 22 (UNS N06022) was selected for construction of the waste package outer barrier. The main alloying elements of this material are nickel, chromium, molybdenum, iron, tungsten, and cobalt. Alloy 22 is less susceptible to localized corrosion in environments that contain chloride ions than Alloys 825 and 625, materials of choice in earlier waste package designs (CRWMS M&O 2000n, Section 3.1.1.2). This material is one of the most corrosion-resistant nickel alloys for the expected range of repository environments (Gdowski 1991, Section 1.2.5). Alloy 22 and its predecessor alloys have been in use for the past 50 years in a variety of environments and have performed extremely well. Figure 4-79 shows the appearance of a test coupon made from Alloy C, which is a predecessor of Alloy 22, after almost 60 years of exposure to a marine environment. Its shiny, mirror-like appearance was restored by rinsing the dirt and sand from the surface. In comparison to Alloy C and C-4, Alloy 22 has greater corrosion resistance. This is based on the fact that Alloy C-4 and Alloy C-276 have a comparable corrosion resistance (Gdowski 1991, Section 1.2.4), and resistance of Alloy 22 to crevice corrosion is greater than Alloy C-276 (Gdowski 1991, Tables 22 and 25).

Stainless Steel Type 316NG will be used for construction of the structural support container inside the waste package outer barrier to increase the overall strength of the waste package. This material is less susceptible to localized corrosion in environments that contain chloride ions than stainless steel 304, but it is more susceptible than other corrosion-resistant materials such as Alloys 22, 625 and 825, which were considered in various waste package designs (CRWMS M&O 2000n, Section 3.1.1.3). However, the stainless steel layer is used primarily for structural support for the outer barrier and not as a corrosion barrier to the ingress of water into the waste package. The key factor in placing the structural material on the inside is that its strength does not begin to degrade until the outer shell is breached by corrosion or other degradation modes. This is in contrast to the VA design



000500C, ATP, 21942, Fig. 27

**Figure 4-79. Alloy C Test Coupon after Almost 60 Years of Exposure to a Marine Environment**  
This test coupon has maintained its mirror finish even after 58 years of exposure to a saltwater atmosphere at the Kure Beach (North Carolina) Marine Atmosphere Test Lot. The coupon was cleaned by simply rinsing it with water.

in which the structural carbon steel was the outer shell, with degradation of strength beginning soon after repository closure.

Figures 4-80 and 4-81 provide a visual perspective to illustrate the physical arrangement of the waste packages and the drip shield within the drift. Figure 4-80 shows schematically the arrangement of different types of waste packages and drip shield. Figure 4-81 shows a schematic sketch of a typical waste package designed for 21 pressurized water reactor fuel assemblies, along with the materials used for the various components.

The dual-barrier design of the waste package and the number of options for the thermal design of the potential repository required a comprehensive testing program to evaluate how materials would perform under the wide range of possible conditions in the potential repository.

Degradation processes evaluated for the drip shield and the waste package include general and localized corrosion under humid air and aqueous conditions, stress corrosion cracking, and hydrogen-induced cracking. The effects of microbially influenced corrosion and aging of the waste package outer barrier were also included in the modeling. An integrated model was developed to evaluate the combined effects of the various degradation modes and was used to estimate the range of lifetimes of the drip shields and the waste packages, including an evaluation of uncertainties.

#### 4.2.4.2 Summary State of Knowledge

**Surface Environment**—The starting waters present at Yucca Mountain are classified into two types: (1) bicarbonate-type water (e.g., J-13 water) and (2) unsaturated zone pore water (chloride-sulfate water). Chemical modeling and laboratory testing of these water compositions have shown that the bicarbonate-type water evolves by evapo-

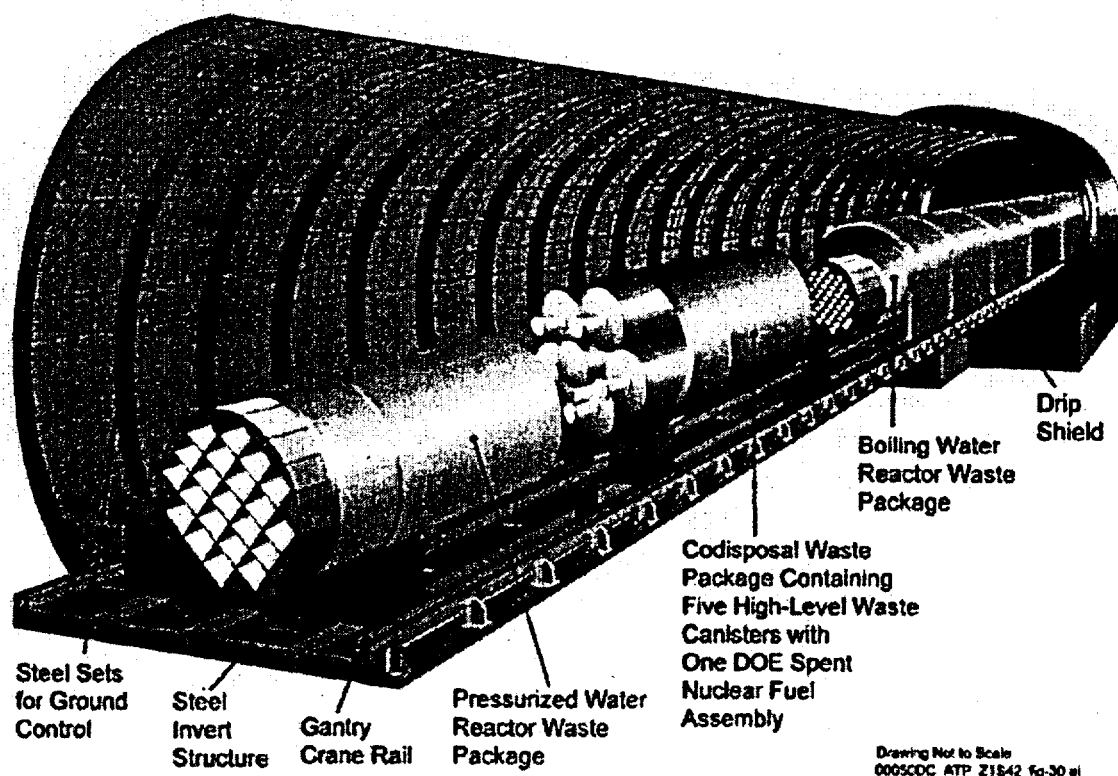


Figure 4-80. Schematic Illustration of the Arrangement of Waste Packages and Drip Shield  
Waste packages are shown in cutaway view to illustrate different waste streams, such as commercial spent nuclear fuel and high-level radioactive waste. Source: CRWMS M&O 2000n, Figure 1-2.

rative concentration to a high-pH brine, whereas the chloride-sulfate-type water evolves to a brine with nearly neutral pH (CRWMS M&O 2000ck, Section 6.1).

In the model used, hygroscopic salts on the drip shield or waste package formed due to evaporation of the dripping water will be limited to sodium or potassium salts. As a bounding condition, it is assumed that sodium nitrate—the salt with the lowest deliquescence point at elevated temperature—will determine the minimum relative humidity at which aqueous conditions can occur (CRWMS M&O 2000ck, Section 6.4.2).

The exact chemistry of the water that contacts the drip shield and waste package surfaces cannot be known precisely. However, the range of potential types of aqueous solutions has been estimated from the range of potential starting water compositions, from knowledge of near-field and in-drift

processes that can alter these compositions, and from laboratory experiments and natural analogue observations. From these results, a range of water compositions was developed and is being used for corrosion testing; the range also includes the potentially important effects of processes at the engineered component surfaces.

**Composition of Aqueous Solutions Used for Corrosion Testing**—Test solutions developed for laboratory corrosion testing of titanium, Alloy 22, and other materials were selected to represent a range of dilute and concentrated conditions, pH, and temperatures that could result from evaporative concentration in the potential repository (CRWMS M&O 2000ck, Section 6.12). The test solutions include the following:

- **Simulated Concentrated Water**—Formulated to simulate evaporative concentration of J-13 water by a factor of 1,000. The resulting

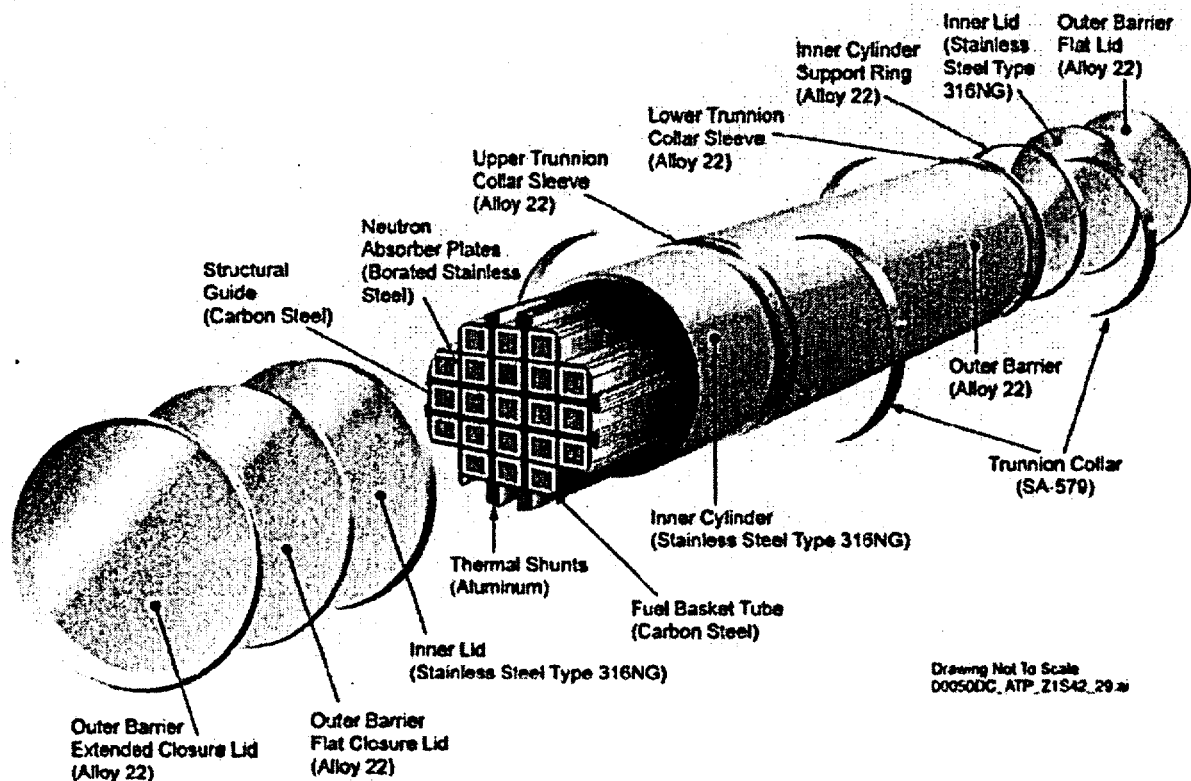


Figure 4-31. Schematic Illustration of a Typical Waste Package Designed for 21 Pressurized Water Reactor Fuel Assemblies, and the Materials Used for the Various Components

This figure shows the arrangement of the two cylinders and the location of trunnions used for lifting and handling of the waste packages. The internal parts of the waste package include basket tubes, a structural guide, and neutron absorber plates. Source: CRWMS M&O 2000n, Figure 1-1.

solution has a moderately high pH (9 to 10) (CRWMS M&O 2000ck, Section 6.12.1).

- **Simulated Dilute Water**—Formulated to simulate evaporative concentration of J-13 water by a factor of 10. This type of water might exist on the drip shield or waste package when the temperature difference between these components and the surrounding drift environment is small and evaporation is slow (CRWMS M&O 2000ck, Section 6.12.2).
- **Simulated Acidic Water**—Similar to the simulated concentrated water solutions but acidified to pH 2.7. This solution is intended to simulate acidification of J-13 water, or pore water from the tuff matrix, by surface

processes on the engineered components (CRWMS M&O 2000ck, Section 6.12.3).

- **Simulated Saturated Water**—Simulates solutions that can become concentrated in the most soluble constituents, namely nitrate and chloride salts. In the host rock around the emplacement drifts, soluble salts can become separated from other constituents of the starting water and concentrated. This test solution is therefore a concentrated solution of sodium nitrate with some additional potassium chloride and with the concentrations adjusted to promote oxygen solubility (CRWMS M&O 2000ck, Section 6.12.4).
- **Basic Saturated Water**—Formulated to simulate extreme evaporative concentration of a bicarbonate-type water such as J-13

water. In addition, three values of pH are used (controlled by addition of sodium hydroxide) to simulate different values of carbon dioxide partial pressure (CRWMS M&O 2000ck, Section 6.12.5).

Corrosion tests were conducted at Lawrence Livermore National Laboratory on specimens of waste package and drip shield materials, including titanium and Alloy 22, exposed to the above environments. The tests were comprehensive and examined many forms of corrosion: pitting, stress corrosion cracking, galvanic corrosion, corrosion in crevices, and general corrosion. In addition, some long-term tests had counterpart shorter-term tests for stress corrosion cracking and galvanic corrosion. The results of the tests were used for developing various corrosion models to predict the long-term behavior of the materials in the repository.

**Long-Term Corrosion Testing**—Test environments for long-term corrosion testing were structured to simulate concentrated solution conditions. The samples were exposed in the aqueous phase, in the vapor phase above the solutions, and at the waterline (DOE 1998, Volume 2, Section 5.1.4.1). To date, some 13,000 specimens, including welded samples, have been tested in water for periods from 6 months to 2 years in duration. The first materials tested were arranged in three categories: corrosion-allowance materials, intermediate corrosion-resistance alloys, and corrosion-resistant alloys (DOE 1998, Volume 2, pp. 5-44 to 5-45). The specimen designs and test procedures were based on specifications developed by the American Society for Testing and Materials, including specifications ASTM G 1-90, *Standard Practice for Preparing, Cleaning, and Evaluating Corrosion Test Specimens*, ASTM G 30-94, *Standard Practice for Making and Using U-Bend Stress-Corrosion Test Specimens*, and ASTM G 46-94, *Standard Guide for Examination and Evaluation of Pitting Corrosion*. Figure 4-82 shows the arrangement of the test specimens in the racks, and Figure 4-83 shows the typical appearance of the specimens after 12 months of exposure in the corrosion test facility.

**Complementary Short-Term Tests**—The long-term corrosion tests were a key component for evaluating waste package materials. They were complemented by short-term tests designed to develop mechanistic understanding. For example, short-term tests measured the relative susceptibilities of the candidate materials to general, localized, and microbially influenced corrosion. The short-term tests were important for developing models of corrosion behavior.

**Field Test Assessment**—Field tests provide an independent confirmation of the performance of materials in the Yucca Mountain environment. Specimens included in the accelerated thermal field tests were characterized to determine how candidate materials degrade with exposure to actual field environments at Yucca Mountain under repository temperature conditions. The specimens are subjected to changing environmental conditions, including temperature, relative humidity, and possible intermittent water contact. In comparison, laboratory experiments are being run at fixed and constant environmental conditions (DOE 1998, Volume 2, Section 5.1.4.1), and the laboratory experiments also include bounding or conservative aggressive environments.

In each field study, test specimens were placed in drifts and boreholes that were well characterized with respect to temperature and relative humidity (DOE 1998, Volume 2, Section 5.1.4.1). The data on corrosion generated from the field tests were used in activities related to performance assessment, materials selection, model development, and potential repository design.

The materials selected for the drip shield (titanium) and the waste package outer barrier (Alloy 22) are highly corrosion-resistant. Based on literature and prior industrial experience, these materials are not expected under repository exposure conditions to be subject to degradation processes that could lead to failure in a short time period (Gdowski 1991, pp. 1 to 3; Gdowski 1997, pp. 38 to 39). Those degradation modes are localized corrosion (pitting and crevice corrosion), stress corrosion cracking, and hydrogen-induced cracking (applicable only to the drip shield). Both the drip shield and waste package degrade by general corrosion at very low

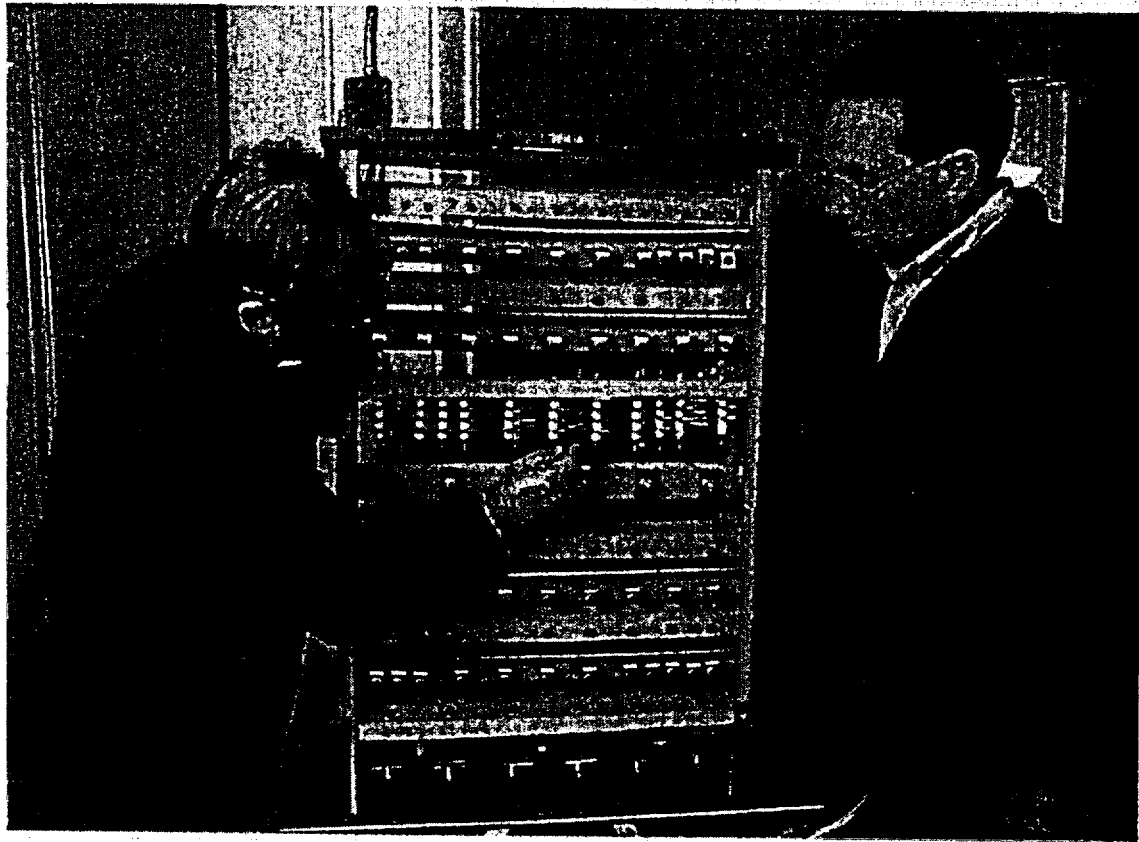


Figure 4-82. Arrangement of the Test Specimens in the Racks

000500C\_ATP\_Z1542\_fig 28.cdr

rates. The current experimental data and detailed process-level analyses also indicate that the candidate materials would not be subject to rapidly penetrating corrosion modes under the expected repository conditions. The exception to this is the closure-lid welds of the waste package, where unmitigated residual stresses could potentially lead to stress corrosion cracking. To preclude this occurrence, weld residual stress mitigation processes will be implemented on each of the dual-lid Alloy 22 waste package closure welds. As a result, the estimated long lifetime of the waste packages in the current analyses is attributed mostly to two factors: (1) stress mitigation in the dual closure lid weld area and (2) the low general-corrosion rate, which will very slowly remove the beneficial compressive stress zones at each weld surface, thereby providing a long delay before stress corrosion cracking can potentially initiate and grow to penetrate the weld thickness.

Models were created to predict the performance of the various materials in the expected repository environment. The modeling effort served the following two major purposes:

1. It supported the selection of materials for which a key selection criterion was the predictability of the component material performance.
2. It furnished information about how the selected materials would perform in the repository environment. Consistent with ASTM C 1174-97, *Standard Practice for Prediction of the Long-Term Behavior of Materials, Including Waste Forms, Used in Engineered Barrier Systems (EBS) for Geological Disposal of High-Level Radioactive Waste*, relevant data from testing activities were interpreted with a mechanistic understanding of how materials behave.



000000C\_ATP\_21542\_0g 23 out

**Figure 4-83. Typical Appearance of an Alloy 22 Specimen after 12 Months of Exposure to an Aqueous Environment in the Long-Term Corrosion Test Facility**

The "scratched" appearance of the surface finish is the same as that observed before the start of testing. The small, faint circular area of discoloration in the center is caused by a Teflon washer used to create a creviced area.

#### 4.2.4.3 Process Model Development and Integration

This section addresses waste package and drip shield material degradation models and their abstractions and alternative models considered for the waste package and drip shield lifetimes. Degradation modes for the components are discussed and the dominant modes determined. Available test data are summarized. The section concludes that the modes of waste package and drip shield degra-

ation (i.e., corrosion) and their dependence on expected thermal-hydrologic and geochemical conditions are sufficiently understood and conservatively captured in the model abstractions to support evaluation of postclosure performance.

**Waste Package Material Degradation Modes—** The degradation processes were selected for modeling on the basis of an extensive review of available information on the candidate materials for the waste package and drip shield. These

processes have been documented in a number of degradation mode surveys (Gdowski 1991; Gdowski 1997). In addition, a review and analysis of features, events, and processes relevant to the degradation of the waste package and drip shield was recently completed and is described in Section 4.3. The degradation models provided a quantitative analysis of early failure of waste packages. The degradation models also calculated the range of expected degradation histories of both waste packages and drip shields. These models consisted of several individual process models or analyses and associated abstraction models. Figure 4-84 shows the elements of each process model, associated abstraction models, and the interrelationships among the various process and abstraction models (CRWMS M&O 2000n, Figure 1-4). The process models for general and localized corrosion of the waste package outer barrier include dry oxidation, humid-air corrosion, and the expected environment

on the surface. In addition, the figure also shows how the process models feed the integrated model for waste package and drip shield degradation (WAPDEG), which is used to predict the lifetimes of these two components. Details of the process models and abstraction models are presented in the following analysis model reports and calculations (which also document evaluation of the applicable modes of degradation of the waste package and the drip shield and their models):

- *Environment on the Surfaces of the Drip Shield and Waste Package Outer Barrier* (CRWMS M&O 2000ck)
- *Analysis of Mechanisms for Early Waste Package Failure* (CRWMS M&O 2000cs)
- *Aging and Phase Stability of Waste Package Outer Barrier* (CRWMS M&O 2000ct)

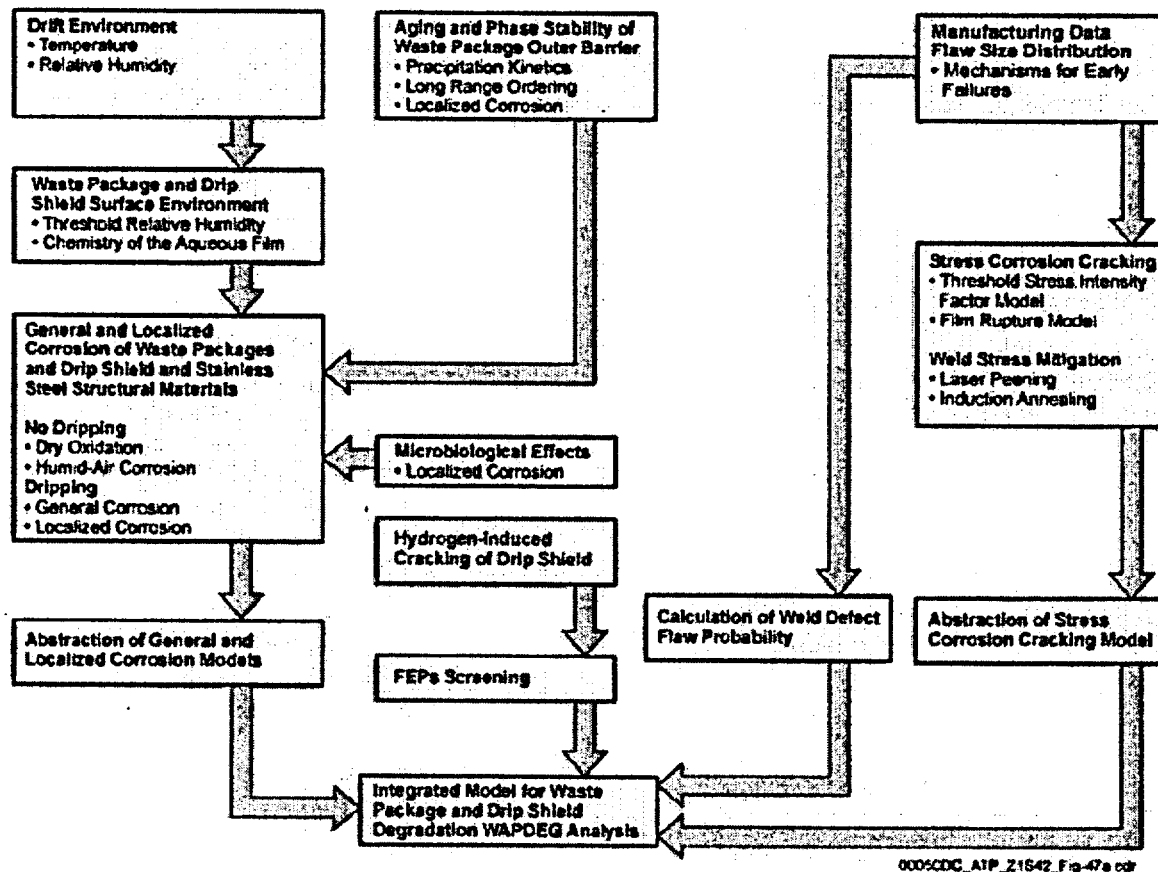


Figure 4-84. Schematic Representation of the Elements of Process Models and the Interrelationships among the Process Models

- *General Corrosion and Localized Corrosion of Waste Package Outer Barrier (CRWMS M&O 2000cq)*
- *General Corrosion and Localized Corrosion of the Drip Shield (CRWMS M&O 2000cr)*
- *Stress Corrosion Cracking of the Drip Shield, the Waste Package Outer Barrier and the Stainless Steel Structural Material (CRWMS M&O 2000cu)*
- *Hydrogen Induced Cracking of Drip Shield (CRWMS M&O 2000cv)*
- *Degradation of Stainless Steel Structural Material (CRWMS M&O 2000cw)*
- *FEPs Screening of Processes and Issues in Drip Shield and Waste Package Degradation (CRWMS M&O 2000cx)*
- *Calculation of Probability and Size of Defect Flaws in Waste Package Closure Welds to Support WAPDEG Analysis (CRWMS M&O 2000cy)*
- *Calculation of General Corrosion Rate of Drip Shield and Waste Package Outer Barrier to Support WAPDEG Analysis (CRWMS M&O 2000cz)*
- *Abstraction of Models for Pitting and Crevice Corrosion of Drip Shield and Waste Package Outer Barrier (CRWMS M&O 2000da)*
- *Abstraction of Models of Stress Corrosion Cracking of Drip Shield and Waste Package Outer Barrier and Hydrogen Induced Corrosion of Drip Shield (CRWMS M&O 2000db)*
- *WAPDEG Analysis of Waste Package and Drip Shield Degradation (CRWMS M&O 2000dc)*

Figure 4-85 shows the model confidence foundation, along with the inputs and outputs for the various degradation process models. This figure

shows the critical input parameters for the degradation mechanisms and data inputs and sources, which provide lifetimes for the components. Confidence in the overall model is based on the comprehensive nature of the input parameters, data, and degradation mechanisms considered in the overall performance assessment. Highlights of the waste package degradation process models are addressed in the following subsections.

#### 4.2.4.3.1 Mechanisms for Early Failures

There is a potential for early failures of the waste package due to material defects and waste package fabrication processes, including welding. The probability of waste package fabrication defects, the uncertainty and variability of those defects, and the consequences of the defects on waste package failure times (e.g., number of potential failure sites and flaw-size distribution) were assessed.

A literature review was performed to determine the rate of failure from manufacturing defects for various types of welded metallic containers. Types of components examined included boilers and pressure vessels, nuclear fuel rods, underground storage tanks, radioactive cesium capsules, dry-storage casks for spent nuclear fuel, and tin-plate cans. In addition to providing examples of the rate at which defective containers occur, this information provided insight into the various types of defects that can occur, and the mechanisms that cause defects to propagate to failure (CRWMS M&O 2000cs, Section 6.1).

The fraction of the total population that failed due to defect-related causes during the intended lifetime of the component was generally in the range of  $10^{-3}$  to  $10^{-6}$  per waste package (equivalent to 1 component in 1,000 to 1,000,000 components). In most cases, defects that led to failure of the component required an additional stimulus to cause failure (i.e., the component did not fail immediately when it was placed into service). In fact, there were several examples that indicated that even commercial standards of quality control could reduce the rate of initially failed components well below  $10^{-4}$  per package (or 1 out of 10,000 components) (CRWMS M&O 2000cs, Section 7).

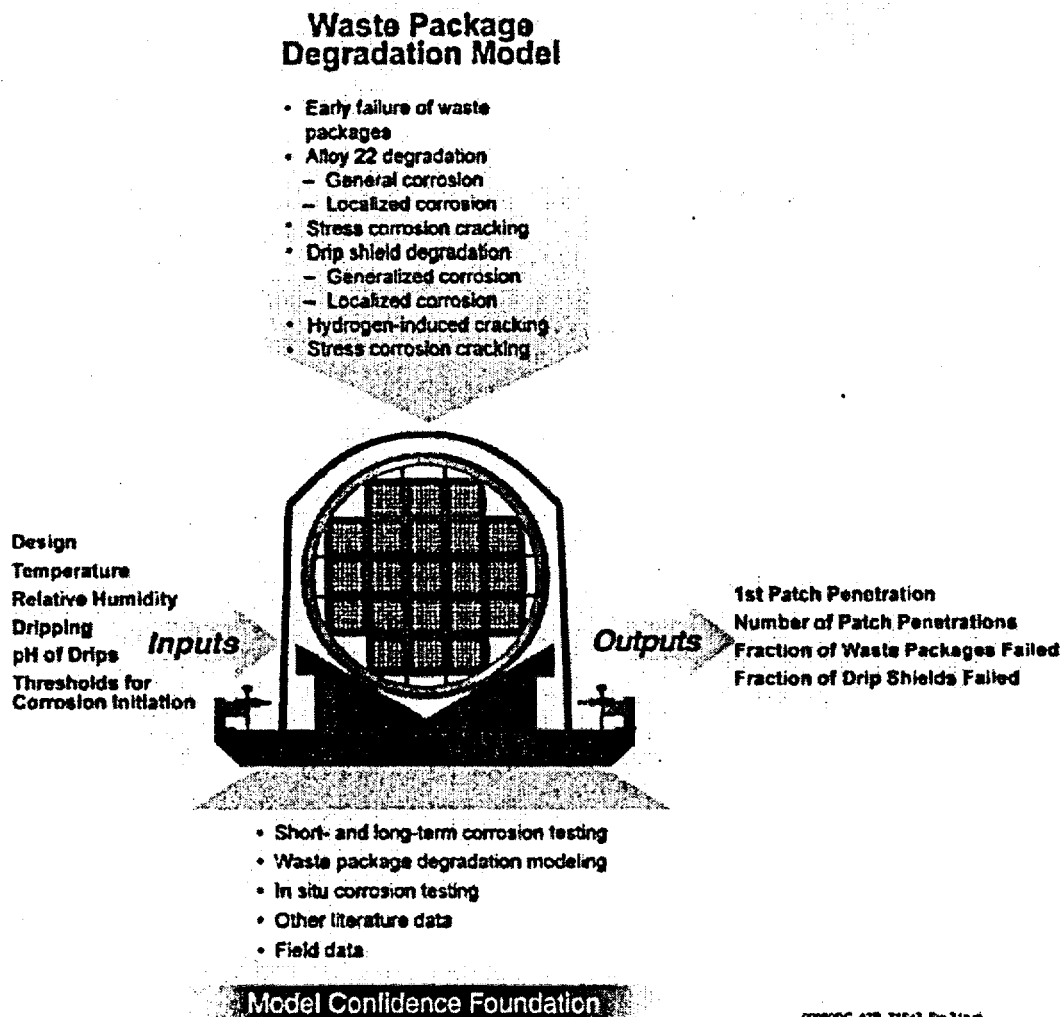


Figure 4-85. Foundation for Model Confidence, including Inputs and Outputs for the Various Degradation Process Models

Confidence in the outputs of the degradation model is influenced by the accuracy of the inputs, such as design parameters and repository environments. These inputs are used in combination with testing data and descriptions of predictive models. It is therefore important to have reliable data and models that address all credible degradation mechanisms. Source: CRWMS M&O 2000n, Figure 1-3.

The literature review identified 11 generic types of defects that could cause early failures in the components examined (CRWMS M&O 2000cs, Section 6.1.7). These were:

- |                                                                                                                                                                                                                                                |                                                                                                                                                                                                                                                     |
|------------------------------------------------------------------------------------------------------------------------------------------------------------------------------------------------------------------------------------------------|-----------------------------------------------------------------------------------------------------------------------------------------------------------------------------------------------------------------------------------------------------|
| <ol style="list-style-type: none"> <li>1. Weld flaws</li> <li>2. Base metal flaws</li> <li>3. Improper weld material</li> <li>4. Improper heat treatment</li> <li>5. Improper weld flux material</li> <li>6. Poor weld joint design</li> </ol> | <ol style="list-style-type: none"> <li>7. Contaminants</li> <li>8. Mislocated welds</li> <li>9. Missing welds</li> <li>10. Handling and installation damage</li> <li>11. Administrative error resulting in an unanticipated environment.</li> </ol> |
|------------------------------------------------------------------------------------------------------------------------------------------------------------------------------------------------------------------------------------------------|-----------------------------------------------------------------------------------------------------------------------------------------------------------------------------------------------------------------------------------------------------|

Four of these defect types were not considered applicable to the waste package: improper weld flux material, poor joint design, missing welds, and mislocated welds. This conclusion was based on

the processes to be used for welding and the process qualification and weld inspection programs that will be implemented (CRWMS M&O 2000cs, Section 7).

The analysis also estimated the probability that specific defect types would occur on a given waste package, considering the expected preventive quality controls. The analysis applies to those defects for which probabilities are estimated using event sequence trees, namely: drip shield emplacement error, waste package handling error, waste package surface contamination, thermal misload, and improper heat treatment. The method used to establish an upper bound value for event sequences combines the human error rates probabilistically. Uncertainties are considered only for human error probabilities related to failures. Probability components for success are treated at their nominal level (i.e., without uncertainty), which produces conservative results. No upper bounds were estimated for other failure probabilities related to mechanical failure or based on historical data. Accordingly, the upper bound for an event sequence probability is adjusted for only human error probability uncertainties. This analysis is much more rigorous and mathematically defensible in comparison to the prior analyses conducted for the Viability Assessment.

Results of the analysis for the remaining seven types of defects showed that, with the exception of the administrative error category, all the defect probabilities were less than  $10^{-4}$  per waste package. This is equivalent to less than one waste package failure out of 10,000 in the entire repository. The administrative error defect rate will be reduced through implementation of stringent administrative controls (CRWMS M&O 2000cs, Section 7).

Subsequently, in reevaluating the potential of early failure mechanisms and their potential consequences, a more conservative approach resulted in the inclusion of improper heat treatment and subsequent failure of a few waste packages in the supplemental TSPA analysis. To ensure that the potential consequence of early waste package failures is treated conservatively, it is included in the nominal scenario, not as a sensitivity analysis (BSC 2001a, Section 7.3.6).

#### 4.2.4.3.2 Aging and Phase Stability of the Waste Package Outer Barrier

Alloy 22, a nickel-based alloy, has excellent corrosion resistance and good strength and ductility. Under certain conditions, changes in the internal structure of the material can degrade its corrosion resistance and/or ductility. Three general areas were addressed in the models: complex phases, ordering, and welds.

Complex phases are known to form in Alloy 22 at temperatures above approximately 600°C (1,100°F). They can presumably form at lower temperatures, but it would take much longer than is typically observed in the laboratory because these types of changes require thermal energy and occur more slowly at lower temperatures. The rate at which these phases form in Alloy 22 was measured at temperatures above 600°C (1,100°F) as a function of temperature. Extrapolation of this rate relation to 300°C (570°F), the expected peak temperature in the emplacement drift, indicates that the rate of complex phase formation would be very slow under potential repository conditions and would have an insignificant contribution to corrosion. To bound this effect, however, a worst case was defined for the fully aged material with complete coverage of the grain boundaries with precipitates (CRWMS M&O 2000n, Section 3.1.4.2). Figure 4-86 shows the effects of aging on precipitation in the grain boundaries.

Samples with this worst-case structure were created and provided for corrosion testing. Samples of Alloy 22 were aged at 700°C (1,292°F) for either 10 or 173 hours. The corrosion resistance of these aged samples is compared to that of base metal in several standardized test media using cyclic polarization technique. The results of this testing showed that the fully aged material exhibited a slightly higher corrosion rate than the unaged material. The maximum increase in corrosion rate was by a factor of 2.5 over the unaged sample. The results are described in greater detail in *General Corrosion and Localized Corrosion of Waste Package Outer Barrier* (CRWMS M&O 2000cq, Section 6).

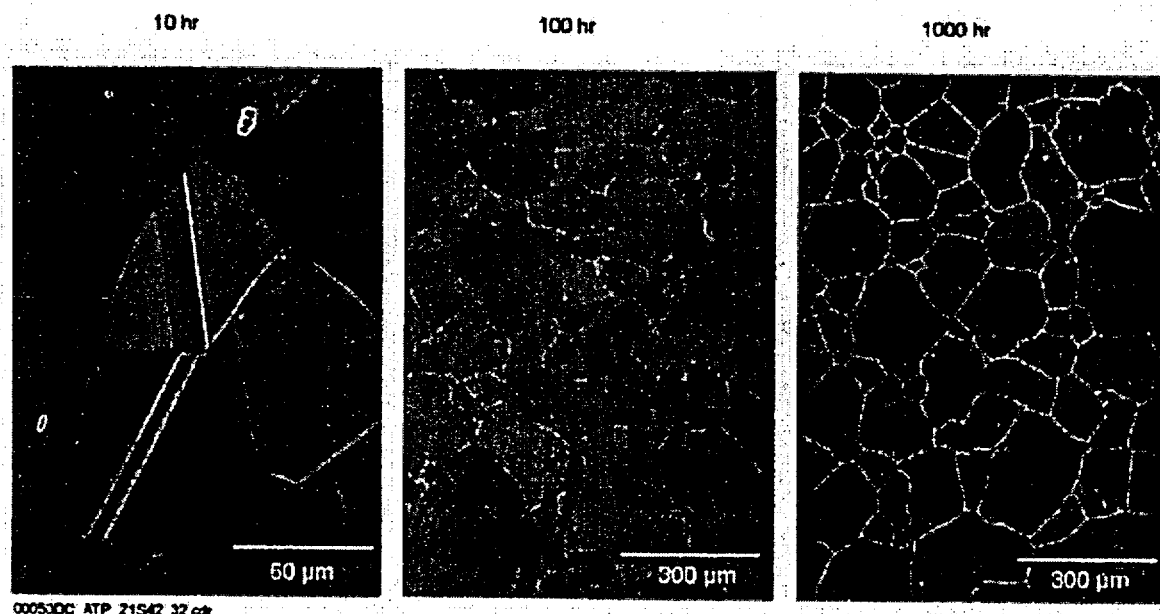


Figure 4-86. Effects of Aging on Precipitation at Alloy 22 Grain Boundaries

The figure shows the amount of precipitation of complex phases in the boundaries of grains due to aging at high temperatures. After 10 hours of aging at 649°C (1,200°F), few or no precipitates are seen in the left photomicrograph. After 100 hours, as shown in the center, parts of the grain boundaries are decorated (covered) with white precipitates. After 1,000 hours, the grain boundaries are completely covered with precipitates, as seen in the photo on the right. Source: CRWMS M&O 2000n, Figure 3-5.

The second general area is ordering. Commercially available Alloy 22 is a single-phase alloy. At temperatures below approximately 600°C (1,100°F), the atoms slowly transform from a somewhat random arrangement into an ordered pattern, with the highest rates of transformation at higher temperatures below the 600°C (1,100°F) temperature limit. This process results in the rearrangement and segregation of alloying elements into specific locations in the crystal structure. This is a slow process, occurring over a long period of time. Ordering may affect the mechanical properties of alloy systems. For example, ordering can increase the strength of the alloy and reduce its ductility, which also decreases its resistance to stress corrosion cracking and hydrogen embrittlement. Because ordering occurs only at lower temperatures and because these reactions are slow, the data for the rate of ordering in Alloy 22 are limited. However, based on the available data, ordering will not become a problem, provided the temperature does not go above about 260°C (500°F) for significant periods of time (CRWMS

M&O 2000n, Section 3.1.4.4). Testing will continue into the performance confirmation period to more accurately predict the performance of this alloy in the potential repository environment.

The third general area is welds. Complex phases form during welding of Alloy 22 and are present in the as-welded condition. These phases and segregation in the weld cause the welds to have lower corrosion resistance than the base metal. Work to determine the effects that long-term exposures to repository-relevant temperatures have on the properties of Alloy 22 welds is ongoing (CRWMS M&O 2000n, Section 3.1.4.3).

The aging times for the various stages of intermetallic precipitation in Alloy 22 base metal as a function of temperature were obtained from the examination of aged samples after approximately 1, 10, 100, 1,000, and in some cases 16,000 hours (CRWMS M&O 2000n, Section 3.1.4.2). These measurements are only intended as an initial estimate of the precipitation kinetics. These obser-

variations were used to generate the isothermal time-temperature transformation diagram for Alloy 22 base metal shown in Figure 4-87.

The long-term aging of Alloy 22 at elevated temperatures can cause the precipitation of undesirable intermetallic phases if the temperature is sufficiently high. The data shown in Figure 4-87 do not indicate that the phase stability of Alloy 22 base metal will be a problem at less than about 300°C (572°F). It is expected that the waste package surface temperature will stay below 300°C (572°F) in the emplacement drift (CRWMS M&O 2000n, Section 3.1.4). While this estimate is bounding, it is based on limited data. The analysis will be further refined and improved as additional data and analysis become available.

For comparison, estimated temperature of the waste package surface as a function of time in the repository is shown in Figure 4-88 for repository designs with and without backfill. This figure shows that even for the hottest waste package containing design basis spent fuel waste the peak temperature does not exceed 250°C (482°F) for the design with no backfill. The sharp increase in surface temperature seen in both curves is due to the assumed (for this analysis only) termination of ventilation at 25 years after emplacement. Based on this comparison, the impact of aging and phase instability on the corrosion of Alloy 22 is not expected to be a problem for the repository design without backfill (CRWMS M&O 2000n, Section 3.1.4.2). The significance of the uncertainties in this data is discussed in Section 3.

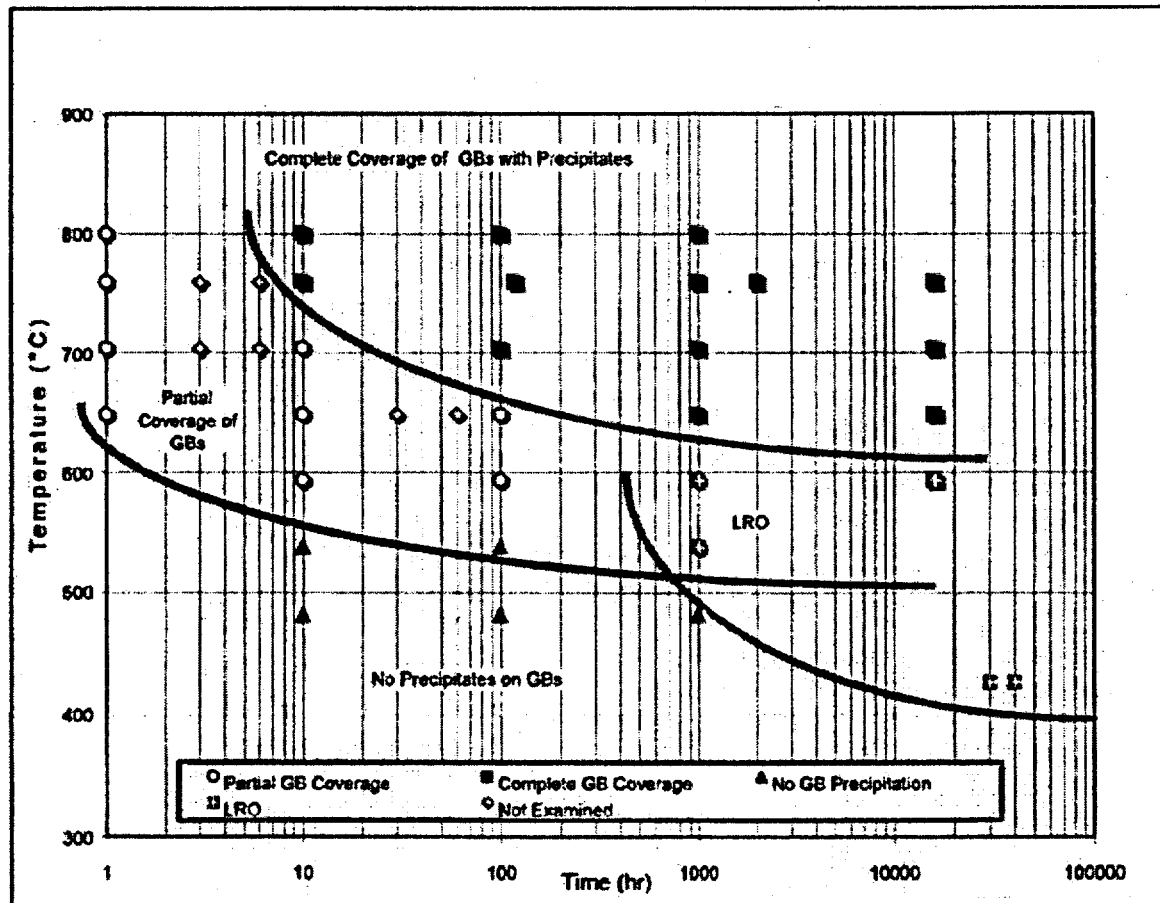


Figure 4-87. Isothermal Time-Temperature Transformation Diagram for Alloy 22 Base Metal  
GB = grain boundary; LRO = long-range ordering. Source: CRWMS M&O 2000n, Figure 3-4.

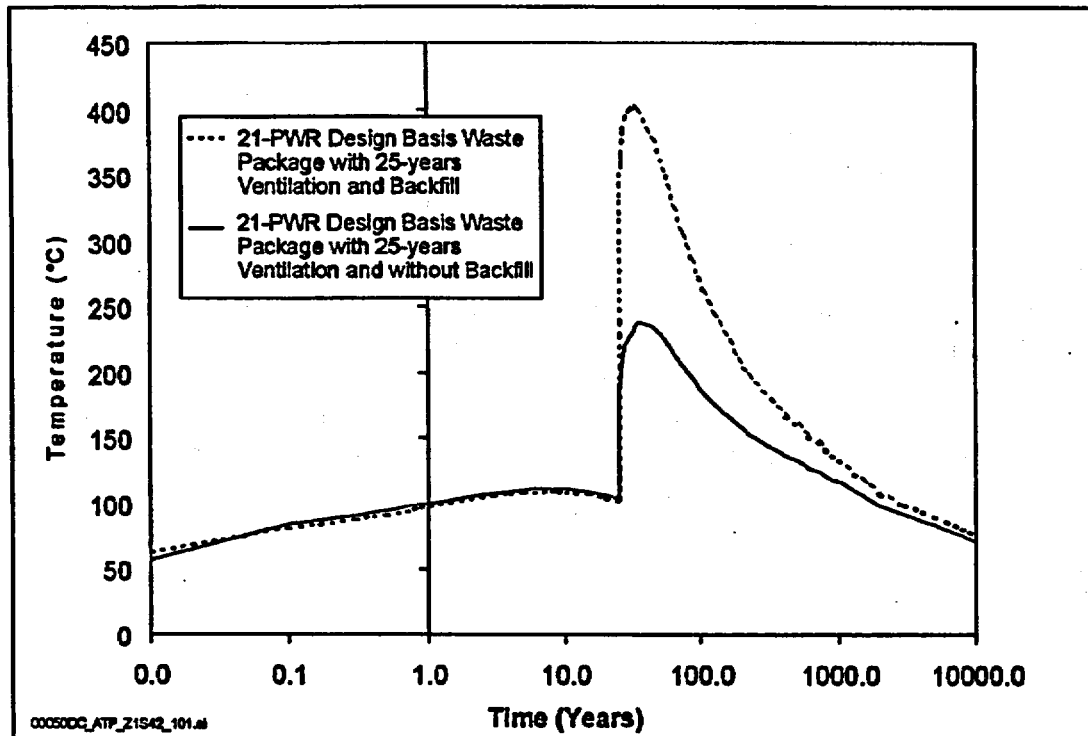


Figure 4-88. Temperature of the Waste Package Outer Barrier Surface as a Function of Time for the Hottest Waste Package

The sharp rise in temperature for both cases is due to the termination of ventilation which in this analysis is assumed to occur after 25 years. The use of backfill results in much higher waste package surface temperature because the backfill acts as an insulator against heat dissipation. Source: CRWMS M&O 2000n, Figure 3-7a.

Since the completion of the TSPA-SR model, aging and phase stability of Alloy 22 was reevaluated using new data and analyses. These analyses confirm the conclusion of the TSPA-SR model that aging of the Alloy 22 barrier is not a concern (BSC 2001a, Section 7.2.1).

#### 4.2.4.3.3 General and Localized Corrosion

Three separate process models were developed to address general and localized (including microbial) corrosion of the drip shield, waste package outer barrier, and stainless steel structural material. The design described in this report uses Grade 7 titanium for the drip shield, Alloy 22 for the waste package outer barrier, and Stainless Steel Type 316NG as stainless steel structural material. While the stainless steel structural material is not specifically intended to be a corrosion barrier, it may affect the chemistry and the rate of water entering

the waste package and retard the rate of radionuclide release from the breached waste package. Given the limited availability of corrosion data for Stainless Steel Type 316NG, data for Stainless Steel Type 316L were used as representative class of materials. This is appropriate since the compositions of the two materials are similar, and aqueous corrosion characteristics are expected to be similar (CRWMS M&O 2000n, Section 1.5.4).

The process model for general and localized corrosion includes submodels for dry oxidation, humid-air and vapor-phase corrosion, and aqueous phase corrosion.

**Dry Oxidation**—The dry oxidation submodel assumes that dry oxidation could be treated as a single mode of attack, that is, as general corrosion. Corrosion rates were estimated as a function of

temperature (CRWMS M&O 2000n, Section 1.5.4.1).

**Humid-Air and Vapor-Phase Corrosion—**Humid-air and vapor-phase corrosion are treated as a single mode of attack, that is, as general corrosion. Corrosion rates were estimated as a function of temperature (CRWMS M&O 2000n, Section 1.5.4.2).

**Aqueous-Phase Corrosion—**The process model for aqueous-phase corrosion of the drip shield and waste package accounts for both general and localized corrosion. Two different modeling methods were used to model this process. The first method determined the threshold corrosion potential for localized attack of the material from short term experiments that used relevant test media. Test environments covered the range from the least aggressive environment of J-13 water to the most aggressive environment of concentrated J-13 water, and the temperature range was between 30° and 90°C (86° and 194°F). Using data from published literature and tests at elevated temperature and pressure, the second method determined the threshold temperature for localized attack. The aqueous-phase corrosion model was applied independently to a large number of small regions (patches) on each waste package (CRWMS M&O 2000n, Section 1.5.4.3).

Abstracted models were developed to account for general and localized corrosion of the drip shield and waste package materials. The abstracted models were input to the TSPA analysis using the WAPDEG code. The abstracted models included thresholds for initiation of various modes of corrosion, as well as the corresponding penetration rates. The relative humidity and temperature thresholds for initiation of humid-air and aqueous-phase corrosion were included, as well as the electrochemical potential for initiation of localized corrosion during aqueous-phase corrosion.

In the case of the drip shield and waste package outer barrier, distributions of general corrosion rates were based upon data from the Long-Term Corrosion Test Facility, while project and published data were used as the basis of estimating localized corrosion rates. For the Stainless Steel

Type 316NG inner barrier, both general and localized corrosion rates were based upon data presented in *Degradation of Stainless Steel Structural Material* (CRWMS M&O 2000cw, Section 6). These general and localized corrosion rates included estimates of the uncertainty and variability. Sufficient information was also provided to determine expected failure mode characteristics (e.g., number of failure sites and opening size).

**General and Localized Corrosion of Alloy 22—**Based on a detailed analysis of the test data, the mean value of the general corrosion rate of Alloy 22 after 24 months of exposure was 10 nm/yr (0.0000004 in./yr). The mean is the average over the number of duplicate samples in the range of test temperatures and the chemical environments summarized earlier. The general corrosion rates determined thus far are so low that the depth of penetration is not deep enough to accurately determine the sensitivity to the temperature and chemical composition of the water. The low general corrosion rates at all test temperatures and chemical environments indicate that the sensitivity is not large. Extrapolation of the mean corrosion rate to 10,000 years implies an average penetration of the Alloy 22 of only 0.1 mm (0.004 in.) of the waste package outer barrier. Even at the highest corrosion rate measured in this data set, the maximum penetration would be less than 1 mm (0.04 in.) over a 10,000-year time period, far less than the package thickness. The TSPA-SR uses the entire range of measured values from the long-term tests using a stochastic approach.

At planned times, some of the samples were withdrawn from the tests for examination. No evidence of localized corrosion was observed on the surfaces of the exposed Alloy 22 specimens for the three exposure times—6, 12, and 24 months (CRWMS M&O 2000n, Section 3.1.5.4). The tests are continuing with the remaining samples. Because of the low general-corrosion rate and the absence of localized corrosion and stress corrosion crack initiation, Alloy 22 is expected to be extremely long-lived as a waste package shell.

**General and Localized Corrosion of Titanium—**General corrosion rates for the titanium drip shield material were based on Long-Term Corrosion Test

Facility weight-loss samples. These rates appeared to be independent of temperatures between 60° and 90°C (140° and 194°F) and the chemistry of the test medium. The median rate was approximately zero, with most measurements for uncreviced samples lying between -200 and +200 nm/yr.

Crevice corrosion rates also appeared to be independent of temperature and test medium. As with the uncreviced samples, the median rate was approximately zero, with most of the corrosion rates between -350 and +350 nm/yr. The largest measured rate was less than +0.35 µm/yr and would not lead to failure of the drip shield during the first 10,000 years of its lifetime. Based upon these data, the life of the drip shield does not appear to be limited by crevice corrosion of titanium at temperatures less than those involved in the test (90°C [194°F]). Testing and model results indicate that the highest probable corrosion rate for titanium is approximately 25 nm/yr and the maximum rate is less than 350 nm/yr.

**Microbially Influenced Corrosion of Alloy 22 and Stainless Steel**—It has been observed that nickel-based materials such as Alloy 22 are relatively resistant to microbially influenced corrosion (CRWMS M&O 2000cq, Section 6.8). Corrosion rates of Alloy 22 are enhanced by microbially influenced corrosion by only a factor of approximately two (CRWMS M&O 2000cq, Table 25). The augmentation of corrosion rates due to microbially influenced corrosion is accounted for in the model documented in *General Corrosion and Localized Corrosion of Waste Package Outer Barrier* (CRWMS M&O 2000cq, Section 6.8). Corrosion studies have shown that microbes can enhance corrosion rates of 304 stainless steel by a factor of approximately ten (CRWMS M&O 2000cq, Table 25). It is assumed that microbially influenced corrosion will have the same effect on Stainless Steel Type 316NG.

The principal nutrient-limiting factor to microbial growth in situ at Yucca Mountain has been determined to be low levels of phosphate. Yucca Mountain bacteria grown in the presence of Yucca Mountain tuff are apparently able to dissolve phosphate contained in the tuff to support growth to levels of 10<sup>6</sup> cells per milliliter of groundwater.

When exogenous phosphate is added (10 mM), then levels of bacterial growth increase to 10<sup>7</sup> to 10<sup>8</sup> cells per milliliter. It may be noted, however, that the two-fold enhancement of corrosion included in the model was in the presence of sufficient phosphate to sustain higher levels of bacterial growth (in an effort to achieve accelerated Alloy 22 attack).

Other environmental factors that could affect levels of bacterial growth include temperature and radiation. However, these factors are closely coupled to relative humidity. As temperature and radiation decrease in the repository, relative humidity is predicted to increase. There are some types of microorganisms that can survive elevated temperatures (up to 120°C [248°F]) and high radiation doses; if there is no available water, then bacterial activity is completely prevented. Thus, because water availability is the primary limiting factor, and this factor is coupled to other less critical limiting factors, water availability (as expressed by relative humidity) was used as the primary gauge of microbial activity.

It has been assumed that a critical mass of bacteria exists for microbially influenced corrosion. Bacterial densities in Yucca Mountain rock have been determined to be on the order of 10<sup>4</sup> to 10<sup>5</sup> cells per gram of rock. In absolute terms, this is almost certainly above the threshold required to cause microbially influenced corrosion. Further, bacterial densities were shown above to increase 1 to 2 orders of magnitude when water was available. More germane concerns are the types of bacteria present, their abundance, and how their relative numbers are affected when water is available for growth. Corrosion rates will be affected (at least on some waste package materials), for example, if organic acid producers outcompete sulfate reducers or inorganic acid producers for available nutrients when water is sufficient to support growth. No data are currently available regarding the composition of the bacterial community over the changing environmental conditions anticipated during repository evolution. As described previously, this issue has been addressed for Alloy 22 in the current model with a corrosion enhancement factor that was determined from the ratio of measured corrosion current densities for inoculated and abiotic

samples. The enhancement factor has an upper bound of 2 (for the inoculated condition) and a lower bound of 1 (for the sterile condition). The enhancement factor is applied to the entire surface of the waste package outer barrier when the relative humidity at the surface is greater than a threshold value (i.e., 90 percent relative humidity).

**Effect of Gamma Radiolysis on Corrosion Potential**—Anodic shifts in the open circuit corrosion potential of stainless steel in irradiated aqueous environments have been experimentally observed (CRWMS M&O 2000cq, Section 6.4.4). Experiments performed at ambient-temperature cyclic polarization of Stainless Steel Type 316L samples in 0.018 M NaCl solution during exposure to 3.5 Mrad/hr gamma radiation showed that the corrosion potential shifted in the anodic direction by approximately 200 mV. This shift in corrosion potential was shown to be due to the formation of hydrogen peroxide. This finding was subsequently confirmed by another cyclic polarization experiment at ambient-temperature with 316 stainless steel in acidic (pH~2) 1.5 M NaCl during exposure to 0.15 Mrad/hr gamma radiation which showed a 100 mV anodic shift in the corrosion potential, with very little effect on the corrosion current. Note that these experiments were performed on stainless steels, not Alloy 22.

To determine the maximum impact that gamma radiolysis could have on the corrosion potential, hydrogen peroxide was added to the test media used for testing Alloy 22. As the concentration of hydrogen peroxide in simulated acidic concentrated water approaches 72 ppm (calculated from number of added drops of hydrogen peroxide), the corrosion potential asymptotically approaches 150 mV, well below the potentials where localized attack would be expected. Similarly, as the concentration of hydrogen peroxide in simulated concentrated water approaches 72 ppm, the corrosion potential asymptotically approaches -25 mV, well below any threshold where localized corrosion would be expected. Therefore, gamma radiolysis is not expected to result in the localized corrosion of Alloy 22 since the maximum shift in corrosion potential (induced by hydrogen peroxide additions) is less than that required for initiation of localized corrosion.

**Pitting and Crevice Corrosion of Alloy 22 and Titanium**—Short-term tests evaluating the susceptibility of Alloy 22 and titanium to pitting and crevice corrosion were conducted in accordance with ASTM G 61-86, *Standard Test Method for Conducting Cyclic Potentiodynamic Polarization Measurements for Localized Corrosion Susceptibility of Iron-, Nickel-, or Cobalt-Based Alloys*, to determine relative susceptibility to these types of localized corrosion. The results of these tests do not indicate a susceptibility to localized corrosion in plausible repository environments.

Since the completion of *Total System Performance Assessment for the Site Recommendation* (CRWMS M&O 2000a), the DOE has performed further research and analysis utilizing available project data to develop a temperature-dependent general corrosion rate and calculated the change in performance of the waste package over a range of operating modes. The inclusion of a temperature-dependent corrosion rate was included as a supplemental sensitivity analysis (BSC 2001b, Section 3.2.5.3). In the revised supplemental TSPA model discussed in *Total System Performance Assessment—Analyses for Disposal of Commercial and DOE Waste Inventories at Yucca Mountain—Input to Final Environmental Impact Statement and Site Suitability Evaluation* (Williams 2001a, Section 5.2.4.1), the general corrosion model was independent of temperature. Results of both supplemental analyses are consistent with the conclusions drawn from the results of the TSPA-SR model analyses and also provide additional insights into the behavior of the disposal system.

#### 4.2.4.3.4 Stress Corrosion Cracking Models

Stress corrosion cracking is a mechanism of cracking in some materials caused by tensile stresses in an aggressive environment (CRWMS M&O 2000cu). This mechanism requires a combination of three elements: material susceptibility, tensile stresses, and an appropriate environment. Unique aspects of the stress corrosion cracking mechanism include brittle-type cracking in ductile materials, crack initiation and propagation under constant load without a need for cyclic load, and occurrence of cracking at lower stresses than would be expected without the presence of an

aggressive environment. This process model accounted for the possibility of stress corrosion cracking of the drip shield, the waste package outer barrier, and the stainless steel structural material. The model for stress corrosion cracking evaluated two alternative methods. The first method was based on the stress-intensity threshold criterion; the second method was based on a mechanistic film-rupture model yielding a finite rate of stress corrosion crack propagation. The modeled rate of stress corrosion crack propagation was dependent upon both the local environment and the stress intensity factor at the crack tip. The stresses for initiation and propagation of stress corrosion cracking in the models were due to unannealed closure welds, deformation caused by rockfall, and the weight of the waste package.

**Stress Corrosion Cracking of the Stainless Steel Waste Package Inner Shell**—The stainless steel structural material may or may not be susceptible to stress corrosion cracking. However, because the corrosion rate of stainless steel is expected to be much higher than that of Alloy 22, the TSPA is using a simplified model in which the stainless steel is assumed to fail immediately after the Alloy 22 outer barrier. Potential performance contribution of the stainless steel structural material will be evaluated as additional data and analyses become available.

**Stress Corrosion Cracking of the Titanium Drip Shield**—Stress corrosion cracking of the titanium drip shield is not expected in a design that uses backfill, because drip shield stresses that are relevant to stress corrosion cracking are insignificant in this case. The major source of drip shield stress is loading due to earthquakes.

For designs without backfill, rockfall directly on the titanium drip shields could result in localized areas of high residual stresses which could lead to stress corrosion cracking and through-wall penetration of the drip shields. While this is possible, it is expected that, because of their size, these penetrations will not prevent the drip shields from performing their intended function of diverting seepage water away from the waste package surface.

Stress corrosion cracks in passive alloys, such as Titanium Grade 7 and Alloy 22, tend to be very tight (small crack opening displacement) by nature (CRWMS M&O 2000cu). Stress analyses that consider rockfall have estimated the local residual titanium stresses following a large (i.e., greater than 4 metric tons) rock impact. The subsequent stress corrosion crack is expected to be approximately 100  $\mu\text{m}$  (0.1 mm, or 0.004 in.) wide. The crack faces are expected to corrode slowly and eventually fill the crack space with corrosion products. While the crack faces are corroding slowly, there may be a small amount of water transported by surface diffusion into the crack and through the drip shield. However, the small temperature gradient present across the drip shield wall will result in evaporation of the slowly flowing water, and a resultant scale deposit will form over and within the crack on the upper drip shield surface. This formation of scale deposits is well documented in seawater environments and in heat exchangers. Such deposits form rapidly under flowing conditions and must be regularly removed to avoid loss of heat exchanger efficiency. In the case of J-13 water concentrated by evaporation, calcium carbonate precipitation is the first stage of the concentration process. Consequently, evaporation of J-13 water slowly flowing through an approximately 100- $\mu\text{m}$  crack opening would lead to rapid scale deposition. The rate of plugging would be inversely proportional to the volume flow rate through the crack. For a 100- $\mu\text{m}$  wide crack through a 15-mm (15,000- $\mu\text{m}$ ) thick drip shield, scale deposition would be an efficient process involving the need for only a small volume flow through the crack. In addition, because of the expected high density of the deposits and lack of a pressure gradient to drive water through the crack, the probability of solution flow through the plugged crack would approach zero. It is therefore concluded that the function of the drip shield will not be compromised even in the event of stress corrosion cracking (CRWMS M&O 2000cu).

**Stress Corrosion Cracking of the Alloy 22 Waste Package Outer Shell**—For Alloy 22, the stress corrosion cracking film rupture model (the second model) assumes crack growth could begin at any surface defect that could generate a stress intensity, regardless of size and surface tensile

stress level. However, examination of the relevant literature indicated that there is a threshold stress below which stress corrosion cracking would not initiate on a "smooth" surface. In the case of the waste package closure weld, the range of threshold stress was conservatively estimated at 10 to 40 percent of the material yield stress (CRWMS M&O 2000cu, Section 6.5.2). This threshold stress range was based on literature reporting stress corrosion cracking-initiation test results for stainless steels and nickel alloys (with known susceptibility to stress corrosion cracking) with comparable surfaces exposed to very aggressive environments.

**Mitigation of the Alloy 22 Closure Weld Residual Stress**—Examination of the weld residual stress profiles for the initial waste package outer barrier closure design revealed that tensile stresses exceeding 20 percent of Alloy 22 yield stress existed in the vicinity of the closure weld surface in both the radial and circumferential directions. This indicated stress corrosion cracking initiation in unacceptably short times could not be precluded for that design. Further, the stress intensity plot indicated that, at least for radially oriented stress corrosion cracks, through-wall crack propagation was possible once a crack initiated.

To reduce weld residual tensile stresses below the stress corrosion cracking-initiation threshold, improved waste package closure designs were evaluated. These included low residual-stress welding techniques and postweld residual tensile-stress-reduction techniques such as induction annealing (heating of the weld) and laser peening (subjecting the weld to laser-generated compressive stresses). Based on these evaluations and a review of the relevant literature (CRWMS M&O 2000cu, Section 6), the Alloy 22 closure design was improved to add a second flat closure lid on the top end of the waste package. This lid will be placed between the extended Alloy 22 closure lid and the stainless steel inner lid (see Figure 3-2 in Section 3). In the improved design, the inner lid closure weld is relieved of its tensile stress using laser peening. Then the outer lid closure weld is completed and its residual tensile stresses are relieved using postweld induction annealing.

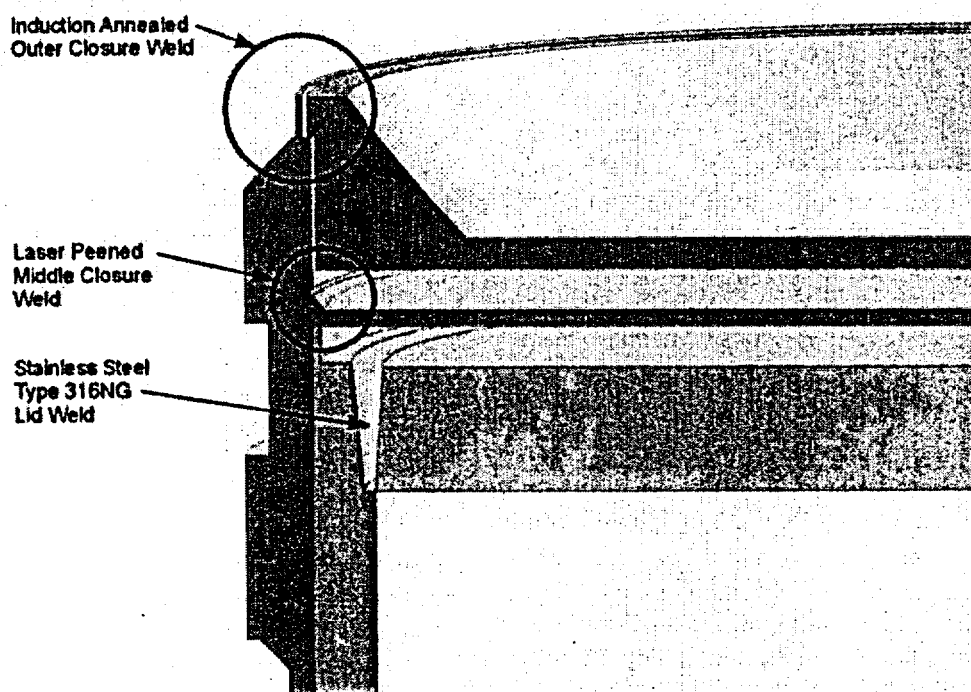
To optimize the new Alloy 22 closure design, experimental measurements were made to quantify the expected stress reduction benefit resulting from laser peening. In addition, extensive ANSYS finite element model calculations were performed to determine the expected stress and stress intensity reduction benefits resulting from the application of both processes. The results of these calculations show that both processes reduced the surface residual tensile stresses below 20 percent of the yield stress (the threshold value for initiation of stress corrosion cracking). These stress reductions persist to depths of about 2 to 3 mm (0.08 to 0.12 in.) for laser peening and at least 6.5 mm (0.25 in.) for postweld induction annealing.

As the waste package outer surface corrodes away, the beneficial low-tensile-stress surface layers resulting from either process are removed. Use of the dual Alloy 22 closure lids in the design improved the longevity of the overall closure, since the flat closure lid does not begin to corrode until the extended closure lid is breached. Figure 4-89 shows the schematic of the dual closure lid design, and Figure 4-90 shows conceptual details of remote welding, annealing, and laser peening for the closure weld area of the waste package.

The closure lid design, as mentioned earlier, helps extend the life of the waste package. The closure weld area of the extended lid is subjected to localized induction annealing to mitigate the weld residual stresses. Stress corrosion cracking of this lid is delayed until the stress-mitigated layer is removed by corrosion. The closure weld area of the flat closure lid is subjected to residual stress mitigation by laser peening. This lid is exposed to the repository environment only after the extended lid is breached, and the stress corrosion cracking of this lid is delayed until after the mitigation layer corrodes away.

Figure 4-90 shows how welding, inspection, laser peening, and induction annealing can be performed at a single work station in the transfer cell facility. This conceptual arrangement will continue to evolve during the next few years.

Additional analyses and quantification of uncertainties performed since the completion of the



Drawing Not To Scale  
006900C\_ATP\_Z1542\_Fig-25.cdr

Figure 4-89. Schematic Illustration of the Dual Alloy 22 Lid Waste Package Design  
The use of two lids for the outer barrier extends the waste package lifetime.

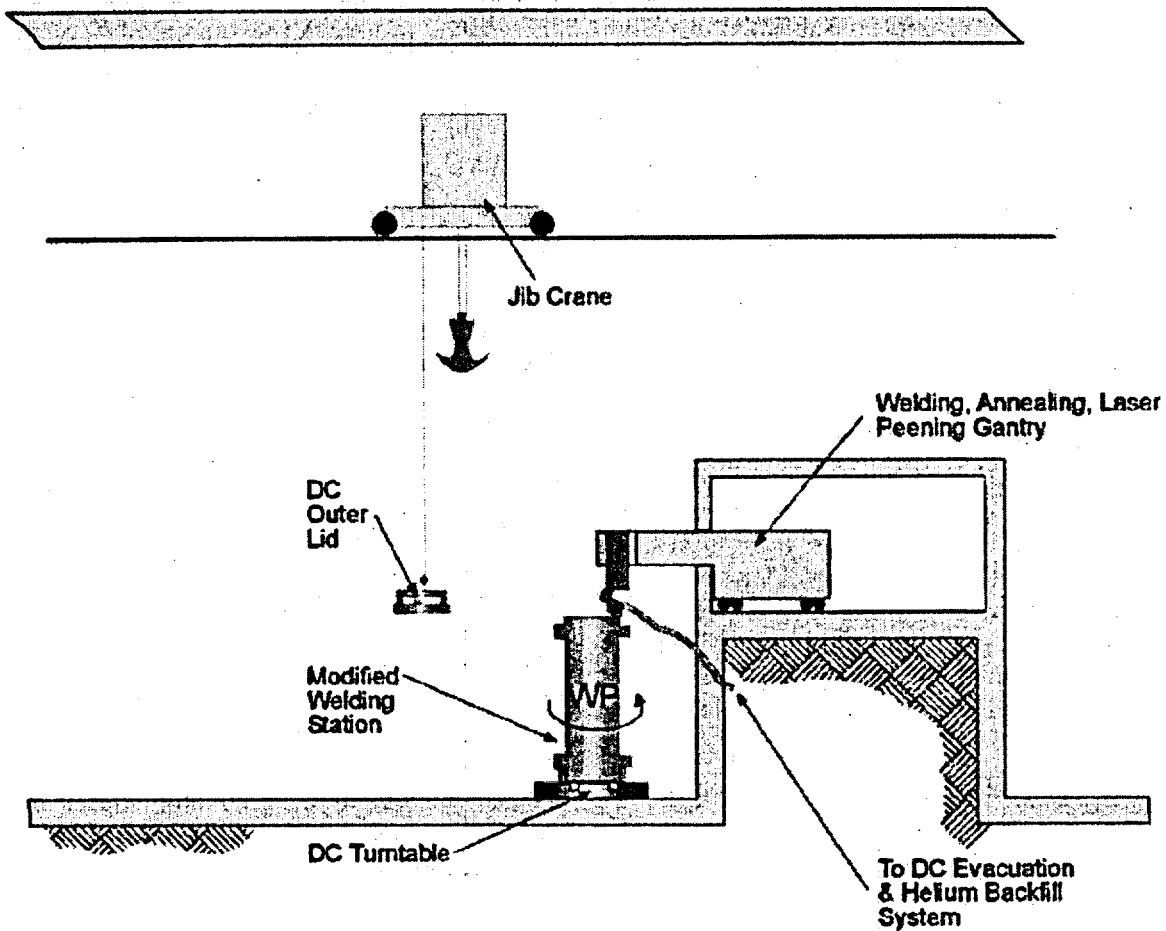
TSPA-SR model provide additional confidence that the stress corrosion cracking model used in the TSPA-SR model is conservative and that the likelihood of stress corrosion cracking of the waste package in the repository environment will be less than predicted by the TSPA-SR model (BSC 2001a, Sections 7.2.5 and 7.3.3).

#### 4.2.4.3.5 Hydrogen-Induced Cracking of the Titanium Drip Shield

Another potential failure mechanism for titanium and its alloys under waste disposal conditions is hydrogen absorption leading to hydrogen-induced cracking. Hydrogen-induced cracking is also called "hydrogen embrittlement," which is a process resulting in a decrease of fracture toughness or ductility of a metal due to the presence of atomic hydrogen. The usual failure mode for a ductile material is the ductile tearing observed during slow crack growth. In this case, the material will fail as the stress intensity factor reaches a threshold value.

The decrease of fracture toughness can also cause fast crack growth (brittle fracture) of a normally ductile material under a sustained load. During fast crack growth, the same material will fail as the stress intensity factor reaches another threshold value, which is less than threshold value for slow crack growth. The process model developed for this degradation mode established the conditions under which the drip shield would experience hydrogen uptake, potentially leading to hydrogen embrittlement and hydrogen-induced cracking.

Generally, the passive oxide film on titanium acts as an excellent barrier to the transport of hydrogen, and hydrogen absorption under natural corrosion conditions would not be expected and is generally not observed over normal operating periods (up to tens of years). In a repository situation, even very slow hydrogen absorption may be significant over thousands of years, leading to a significant accumulation of hydrogen and the danger of hydrogen-



Drawing Not To Scale  
00050DC\_ATP\_Z1542\_Rg-29.CDR

Figure 4-90. Conceptual Design of Remote Welding, Annealing, and Laser Peening for the Closure Welding of the Waste Package

This design allows remote welding, induction annealing, and laser peening to be conducted at a single station. DC = disposal container; WP = waste package.

induced cracking. The model addressed these considerations, which are summarized below:

1. The passive oxide is assumed to be permeable to atomic hydrogen.
2. Atomic hydrogen is generated at the surface of the titanium alloy. This is described by a hydrogen generation rate, which is taken to be proportional to the general passive corrosion rate.
3. A fraction of the hydrogen is absorbed into the oxide and assumed to directly enter the alloy. The remainder combines to yield hydrogen gas, which is lost to the surroundings. The rate of absorption is taken to be directly proportional to the hydrogen generation rate multiplied by an absorption efficiency coefficient.
4. Once in the alloy, the hydrogen is distributed uniformly throughout the entire thickness of the material. That is,

transport processes within the alloy are rapid compared to the rate of absorption.

5. The hydrogen content of the alloy is allowed to increase until a critical level is reached. The material then is assumed to fail immediately. The model allows for the calculation of hydrogen content and for comparison with the critical concentration.

The hydrogen-induced cracking model was presented in *Hydrogen Induced Cracking of Drip Shield* (CRWMS M&O 2000cv, Section 6). In that report, extensive evidence supported a qualitative assessment of titanium alloys as an excellent choice of material for the drip shield with regard to degradation caused by hydrogen-induced cracking, where the hydrogen source is from general corrosion of the titanium. Quantitative evaluation based on this model indicated that the drip shield material was able to sustain the effects of hydrogen-induced cracking. Using available general corrosion test data, the model calculated a hydrogen concentration below 120  $\mu\text{g}$  per gram, which is less than the critical hydrogen concentration of 400  $\mu\text{g}$  per gram for the titanium grade that was tested.

The source of the hydrogen for embrittlement can also be through galvanic coupling of the titanium drip shield with less corrosion-resistant materials, such as carbon steel. At the bottom of the drip shield, this galvanic coupling is precluded by the use of a small Alloy 22 "foot" separating the drip shield and the carbon steel invert structure (CRWMS M&O 2000cv).

In a design without backfill, steel components such as rock bolts, wire mesh, and steel liners used in the drift may fall on the drip shield and undergo active corrosion. This could potentially lead to generation of hydrogen on the surface of the drip shield, leading in turn to hydrogen pickup levels higher than the critical levels needed for cracking. Preliminary evaluation shows that these embrittled titanium regions are likely to be self-limiting "hotspots" from the point of view of hydrogen absorption and embrittlement of the drip shield. The buildup of carbon steel corrosion products at

the contact site would be expected to eventually break the contact. The drip shield is expected to be unaffected by contact with iron corrosion products, since the galvanic connection would be poor (CRWMS M&O 2000cv).

#### 4.2.4.3.6 Limitations and Uncertainties

Uncertainties in each of the process models were identified in the discussion of the models in the previous sections and in the individual analysis model reports. The approach generally used in dealing with these uncertainties is to be conservative and bound the uncertainties. In several cases combinations of approaches were used. For example, in the case of Alloy 22 thermal aging, accelerated testing (i.e., higher-temperature aging) was used to predict long-term behavior based on short-term data, in accordance with ASTM C 1174-97. The data were then used with conservative bounding estimates. In the case of general corrosion, aggressive test media were used to represent potential concentrating effects in the repository. Features, events, and processes were evaluated to screen out degradation processes that have very low probability of occurrence (less than  $10^{-4}/\text{yr}$ ) or that have very low consequences. Examples of screened-out processes include radiolysis-enhanced corrosion and inside-out corrosion of waste package barrier materials.

As noted in Section 4.1.1.2, the DOE has performed several activities to improve the treatment of uncertainty in current models. Additionally, as noted in Section 4.1.4, the DOE has evaluated the effect that operating the repository at lower temperatures would have on repository performance models. Uncertainty about the waste package corrosion rate may be reduced by avoiding the conservatively defined window of corrosion susceptibility for Alloy 22, which can be accomplished by keeping waste package temperatures at or below 85°C (185°F) or maintaining the relative humidity in emplacement drifts below 50 percent. The results of the analyses of lower-temperature operating modes are described in *FY01 Supplemental Science and Performance Analyses* (BSC 2001a; BSC 2001b).

A review of the uncertainties in the various models is presented below.

**Thermal Aging**—A graphical approach to bounding the uncertainty in the aging model is used. In Figure 4-91, the line representing a “best fit” to the data for “complete grain boundary coverage” predicts that more than 10,000 years at 300°C (572°F) will be required to completely cover the grain boundaries of Alloy 22 with inter-metallic precipitates. However, the line with the “minimum slope possible within the error bars” shows that complete grain boundary coverage might occur in as few as 100 years (very unlikely bounding case). The “best fit” line is the most likely scenario. In the case of bulk precipitation, none is predicted with the line representing the minimum possible slope. Thus, it can be concluded with reasonable certainty that no bulk precipitation will occur before 10,000 years at 300°C (572°F).

From the corrosion tests conducted, it appears that a fully aged sample of Alloy 22 could change the observed corrosion potential. For example, corrosion potential was shifted in a less noble (negative) direction by a small value (less than 100 mV) in simulated acidic concentrated water and simulated concentrated water at 90°C (194°F). The shift was not considered significant, and it was concluded that full aging of Alloy 22 (complete coverage of the grain boundaries) does not significantly alter passive film stability and result in significantly enhanced corrosion.

Thermal aging of Titanium Grade 7 at 300°C (572°F) is expected to have little impact on the corrosion resistance of this material. Since no credit is claimed for the corrosion resistance of Stainless Steel Type 316NG, all TSPA calculations are insensitive to the uncertainty associated with the corrosion of Stainless Steel Type 316NG.

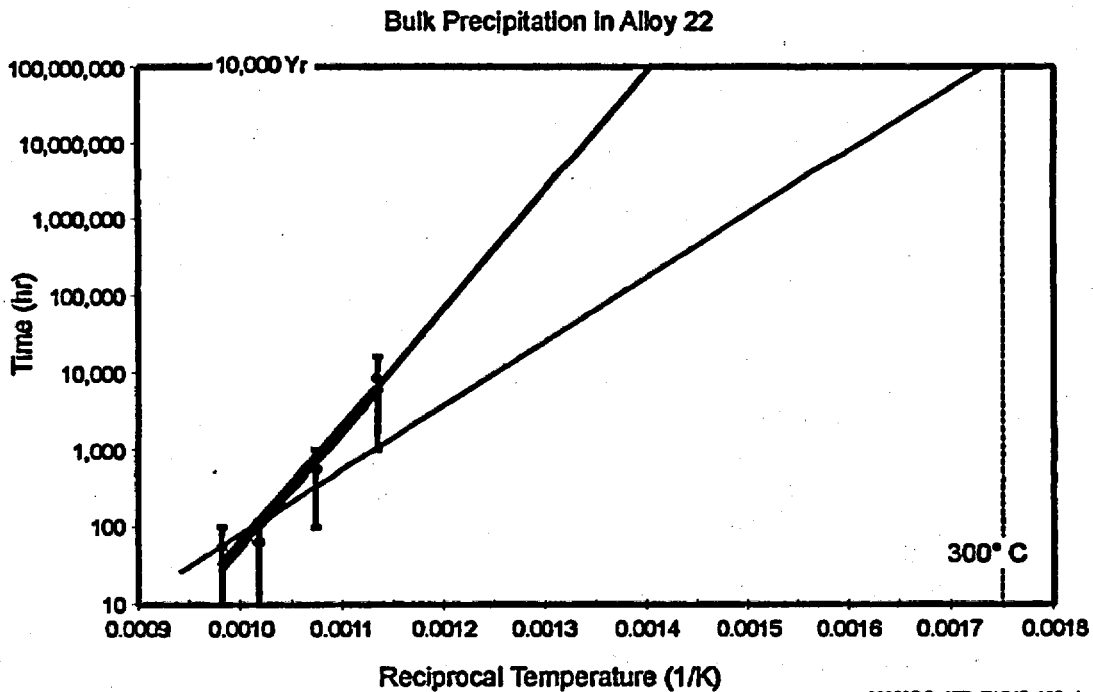
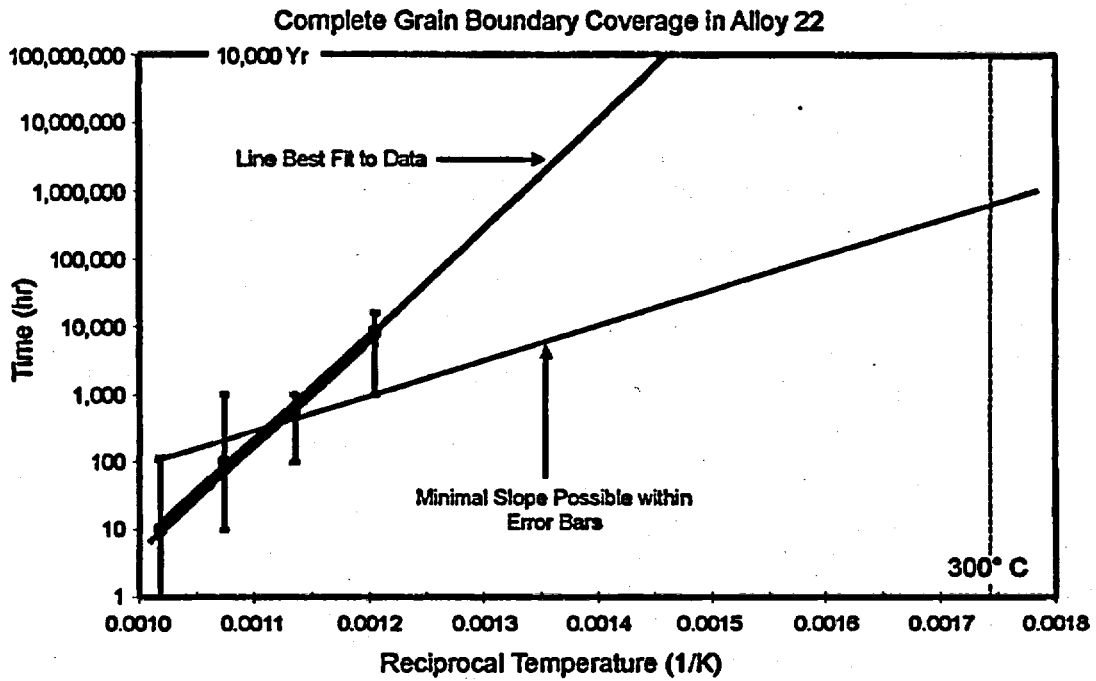
**Dry Oxidation**—In the case of Alloy 22 and Stainless Steel Type 316NG, the rates of dry oxidation are negligible even over hundreds of years and the expected repository temperature. Therefore, uncertainty in the dry oxidation rate is not expected to have any significant impact on the performance of these materials. The current model is based upon

published data and does not include estimates of uncertainty.

**Humid-Air and Aqueous-Phase Corrosion**—Uncertainty in the threshold relative humidity for these corrosion modes is primarily due to the composition of the salt film. The waste package and drip shield would always experience some combination of humid-air and aqueous-phase corrosion. The uncertainty in this parameter is discussed in more detail in *Degradation of Stainless Steel Structural Material* (CRWMS M&O 2000cw, Section 6), *General Corrosion and Localized Corrosion of the Drip Shield* (CRWMS M&O 2000cr, Section 6), and *General Corrosion and Localized Corrosion of Waste Package Outer Barrier* (CRWMS M&O 2000cq, Section 6).

The distribution of general corrosion rates for either humid air corrosion or aqueous phase corrosion is represented by the curves given in Section 3.1.5.4 of the *Waste Package Degradation Process Model Report* (CRWMS M&O 2000n, Figures 3-14 through 3-26). Distributions for Stainless Steel Type 316NG are represented by distributions formed from published data. The distribution of rates for Alloy 22 and the distribution for Titanium Grade 7 rates are based upon data from the Long-Term Corrosion Test Facility. The dispersion in these curves is assumed to be entirely due to uncertainty. A detailed analysis of the error in general corrosion rate was given in each supporting report (CRWMS M&O 2000cw, Section 6; CRWMS M&O 2000cr, Section 6; CRWMS M&O 2000cq, Section 6).

Determinations of corrosion and threshold potential are based upon three replicate cyclic polarization measurements at each combination of environment and temperature. The results are tabulated in *General Corrosion and Localized Corrosion of Waste Package Outer Barrier* (CRWMS M&O 2000cq, Section 6). The uncertainty in the corrosion potential due to gamma radiolysis (i.e., a maximum positive shift in error of about 250 mV) is also addressed in *General Corrosion and Localized Corrosion of Waste Package Outer Barrier* (CRWMS M&O 2000cq, Section 6.4.4) and *Waste Package Degradation Process Model Report* (CRWMS M&O 2000n,



000500C\_ATP\_Z1S42\_100.ai

Figure 4-91. Graphical Extrapolation of the Curves to Repository-Relevant Temperatures  
Source: CRWMS M&O 2000ct, Figure 98.

Section 3.1.6). Estimates of uncertainty in the selection of corrosion and threshold potential have been made and are embedded in WAPDEG analyses.

The rates of localized corrosion have been bounded with the range of values found in the published literature.

**Stress Corrosion Cracking**—Two alternative stress corrosion cracking models have been considered, one based upon a threshold stress intensity factor (Method A) and another based upon a threshold stress for a smooth surface (Method B) (CRWMS M&O 2000cu). In the second approach, cracks are assumed to propagate by the slip-dissolution mechanism after initiation. Method B is used as the basis of the performance assessment. The slip-dissolution model, Method B, predicts that crack propagation is a function of the local stress intensity at the crack tip. Thus, the uncertainty in this driving force must be estimated.

Local stress intensity is calculated from the local stress and the crack penetration. The uncertainties in the stress distribution (stress versus depth) are based upon analyses of measured residual stresses in welds, before and after mitigation, as well as finite element modeling with the ANSYS code. These uncertainties are abstracted for WAPDEG. Aside from the stress intensity, the parameters in the slip-dissolution model for stress corrosion cracking propagation are based upon measurements for stainless steel from the boiling water reactor industry. Since stainless steels are much more prone to stress corrosion cracking than Alloy 22, these parameter estimates are conservative for Alloy 22.

The threshold stress for initiation of stress corrosion cracking on a smooth surface is conservatively estimated to be approximately 10 to 40 percent of the yield stress, based upon the determination of such thresholds for related but more susceptible alloy systems exposed to very aggressive environments, such as boiling magnesium chloride.

Since completion of the TSPA-SR model, the DOE has continued to explore uncertainties associated with the model. Volume 1, Section 7 of *FY01*

*Supplemental Science and Performance Analyses* (BSC 2001a) describes in detail the additional work performed to further defend, model, and understand uncertainties associated with the waste package degradation models. It further discusses uncertainties related to mechanisms for early failures, aging and phase stability of the waste package outer barrier, general and localized corrosion, and stress corrosion cracking. In order to assess the performance consequences of early waste package failures, the supplemental TSPA model described in Volume 2 of *FY01 Supplemental Science and Performance Analyses* (BSC 2001b) included a model that assumed that improper heat treatment of welds could lead to cracks forming in a small fraction of waste packages. The formation of cracks in a few waste packages (up to three) resulted in the calculation of small doses (approximately  $2 \times 10^{-4}$  mrem/yr) in the supplemental TSPA model (compared to zero dose in the TSPA-SR model). The inclusion of a thermally-dependent corrosion rate in the waste package performance model resulted in significantly improved long-term performance of the waste packages. In summary, the results of the additional analysis provide added confidence that the TSPA-SR model is conservative and that the behavior of the waste package in the repository environment is likely to be better than predicted by the TSPA-SR model.

#### 4.2.4.3.7 Alternative Approaches or Models

Alternative models have been considered for oxidation, localized corrosion thresholds, stress corrosion thresholds, stress corrosion cracking, stress mitigation, and hydrogen-induced cracking. These alternatives are summarized below.

As with limitations and uncertainties, alternative conceptual models for corrosion, early waste package failure, and stress corrosion cracking have been updated in supplemental analyses as summarized in *FY01 Supplemental Science and Performance Analyses* (BSC 2001a, Section 7; BSC 2001b, Sections 3.2.5 and 4.2.5). These analyses generally tend to confirm the results of the TSPA-SR. These analyses are also summarized in Section 4.4.5.5 of this report.

**Dry Oxidation**—This process can be represented by two different methods: the parabolic growth law and the logarithmic growth law. In the parabolic growth law, the oxide film is assumed to grow continuously with the rate of film growth controlled by the diffusion of oxygen through the film. The thickness of the oxide is proportional to the square root of the exposure time. In the case of the logarithmic growth law, the oxide film asymptotically approaches a small maximum thickness. In the case of dry oxidation, parabolic growth law is used for Alloy 22 and Stainless Steel Type 316NG, while logarithmic growth law is used for Titanium Grade 7. These model selections were based upon the published literature for these types of corrosion-resistant materials (CRWMS M&O 2000n, Section 3.1.5.1).

**Localized Corrosion Threshold**—Localized corrosion process can be expressed in terms of the threshold electrochemical potential or threshold temperature for the initiation of the localized corrosion. For the highly corrosion resistant materials under consideration, the threshold potential model is used because it is more solidly rooted in the theoretical concepts underlying passive film stability. Furthermore, it is expected that a good correlation of threshold and corrosion potential can be used to deduce a threshold temperature. The threshold temperature would be the temperature at which the corrosion and threshold potentials are equivalent.

**Stress Corrosion Cracking**—The stress corrosion cracking model includes two separate models, one based on the threshold stress intensity factor at the tip of a preexisting flaw and the second based on the threshold stress for propagation by slip-dissolution mechanism. The second method is used in the abstraction for TSPA because it is the more conservative model and because it has been used for predicting the performance of boiling water reactors. The method is considered to be conservative because it is based upon data for stainless steel, a material more prone to stress corrosion cracking than Alloy 22 (CRWMS M&O 2000cu). Predictions based upon a correlation for stainless steel would yield a conservative prediction for Alloy 22.

**Weld Stress Mitigation**—Two methods will be used for mitigation of the weld residual stresses: localized induction annealing and laser peening. Induction annealing will be used for the outer lid, and laser peening will be used for the inner lid on the Alloy 22 outer barrier of the waste package. This selection is based upon the ability of the induction annealing process to place compressive stress deeper into the weld. Laser peening is more compatible with the design of the inner lid weld, due to the occluded nature of such a weld.

**Hydrogen-Induced Cracking of Titanium**—Two methods are available to address hydrogen induced cracking: threshold electrochemical potential and threshold hydrogen concentration. The first method is applicable primarily for conditions that would lead to galvanic coupling of titanium. As this will be avoided by design, this method has not been used in the model. Therefore, hydrogen-induced cracking evaluation is based upon a threshold hydrogen concentration. Also, since such concentrations are possible to be measured with secondary iron mass spectrometry, this method is preferred.

The threshold concentration model is a simple and conservative model. The basic premise of the model is that failure will occur once the hydrogen content exceeds a certain limit or critical value. This model is conservative because it assumes that, once the environmental and material conditions can support that particular corrosion process, failure will be effectively instantaneous. Quantitative evaluation based on the hydrogen-induced cracking model described in *Hydrogen Induced Cracking of Drip Shield* (CRWMS M&O 2000cv, Section 6) indicates that the drip shield material (Titanium Grade 7) is able to sustain the effects of hydrogen-induced cracking. Available test data show that the hydrogen concentration is below 180  $\mu\text{g}$  per gram, which is less than the critical hydrogen concentration of 400  $\mu\text{g}$  per gram for Titanium Grade 7.

With the removal of backfill from the repository design, the potential for that galvanic interaction between carbon steel ground support and the drip shield is increased. The impact of this on the potential hydrogen pickup has been evaluated using the

threshold concentration model. Preliminary results show that hydrogen-induced cracking is not a problem (CRWMS M&O 2000cv).

#### 4.2.4.3.8 Model Calibration and Validation

According to ASTM C 1174-97, *Standard Practice for Prediction of the Long-Term Behavior of Materials, Including Waste Forms, Used in Engineered Barrier Systems (EBS) for Geological Disposal of High-Level Radioactive Waste*, model validation is the process through which independent measurements are used to ensure that a model accurately predicts an alteration behavior of waste package materials under a given set of environmental conditions (e.g., in the repository environment over 10,000 years). Obviously, models cannot be tested for 10,000 years. Therefore, validation relies on accelerated testing. According to the same standard, an accelerated test is a test that results in an increase in the rate of an alteration mode, when compared with the rates for service condition. Changes in alteration mechanism, if any, must be accounted for in the use of the accelerated test data.

The thermal aging model assumes Arrhenius-type kinetics (CRWMS M&O 2000ct, Sections 6.2 and 6.5). Precipitation and long-range ordering can be accelerated by increasing the temperature above those levels expected in the repository. If the model can accurately predict the kinetics of these phenomena at combinations of time and elevated temperature, it will be considered valid for making predictions at lower temperature and longer time.

Since all available data has been used to establish these correlations, the correlations are considered valid for their intended use. Additional data that are being collected will help to reduce uncertainties and improve the level of confidence in the model.

The effects of precipitation and long-range ordering on corrosion are determined with electrochemical techniques. Through application of electrochemical potentials more anodic than the open circuit corrosion potential, corrosion phenomena can be accelerated (CRWMS M&O 2000cq, Section 6.7). Variations in corrosion and threshold potential can be correlated with the extent of thermal aging. Similarly, variations in

rates of dissolution through the stable passive film can also be correlated with the extent of thermal aging. These rates of dissolution are accelerated by application of a potential between the corrosion and threshold potentials and are proportional to the passive current density (CRWMS M&O 2000cq, Section 6.7.1). The corrosion rate enhancement factor is determined by calculating the ratio of measured passive current densities for aged and unaged samples (CRWMS M&O 2000cq, Section 6.7.3). Since all available electrochemical data has been used to establish the corrosion model for thermally aged samples, this model is considered valid for its intended use.

The models for dry oxidation of Alloy 22 (CRWMS M&O 2000cq, Section 6.1), Titanium Grade 7 (CRWMS M&O 2000cr, Section 6.1), and Stainless Steel Type 316NG (CRWMS M&O 2000cw, Section 6.1) are based upon published data found in the scientific literature. More specifically, the model for dry oxidation of Alloy 22 is based upon the parabolic growth of the oxide film at elevated temperature (CRWMS M&O 2000cq, Section 6.1). However, in the absence of any such low-temperature data, the parabolic rate constant for high temperature is applied at low temperature. Given the extremely small magnitudes of these rates, dry oxidation is expected to have no significant impact on waste package performance (CRWMS M&O 2000cq, Section 6.1).

The threshold relative humidity for humid-air corrosion is based on the deliquescence point of sodium nitrate (CRWMS M&O 2000ck, Section 7; CRWMS M&O 2000cq, Section 4.1.2). The threshold for salt films deposited in the repository may be slightly different. However, salt deposits produced by evaporating simulated J-13 water to dryness support this basis.

Rates of humid air corrosion are expected to follow general distributions based upon weight-loss data from the Long-Term Corrosion Test Facility (CRWMS M&O 2000cq, Section 6.5.2; CRWMS M&O 2000cr, Section 6.5.2). The distributions are for Alloy 22 data for 6, 12, and 24 months of exposure to a variety of test media. Corroborative measurements made with the atomic force microscope and other surface analytical techniques have

also been used as further means of model validation (CRWMS M&O 2000cq, Section 6.5.5). The test program will continue, ultimately providing data for 60 months of exposure. Future data will be considered independent and corroborative, and will be used to reduce uncertainties and conservatism in the model.

The threshold relative humidity for aqueous phase corrosion is the same as that used for humid air corrosion (CRWMS M&O 2000ck, Section 6.3; CRWMS M&O 2000cq, Section 6.3). The same approach has been used for validation. Rates of general corrosion in the aqueous phase also obey the general distributions based upon weight-loss data from the Long-Term Corrosion Test Facility. The same approach described for validation of the rate model for humid air corrosion has been employed for validation of the rate model for general corrosion in the aqueous phase.

Comparisons of corrosion and threshold potentials are used to determine whether rates for general or localized corrosion are applicable. The initial correlations given in the *Waste Package Degradation Process Model Report* (CRWMS M&O 2000n, Sections 3.1.5 and 3.1.6) are based upon standard cyclic polarization measurements in simulated dilute water, simulated concentrated water, simulated acidic concentrated water, and simulated saturated water, covering a broad range of temperature.

The stress corrosion model is primarily based on published data. Limited data have been obtained under repository-relevant conditions. The data obtained under the Yucca Mountain project include precracked specimens tested under very aggressive environments (CRWMS M&O 2000cu, Sections 4.1.3 and 6.3.2). Thus, the model uses a conservative approach. Future data will serve to reduce the level of conservatism and improve the confidence in the model.

#### 4.2.4.4 Total System Performance Assessment Abstraction

An integrated model was developed from the process and abstraction models for the various degradation modes. The integrated model included

in the WAPDEG performance assessment code used repository environmental conditions as a function of time from other process models to estimate the performance of the waste package and drip shield. The WAPDEG model uses a stochastic approach to sample model parameters over the ranges including uncertainties. The following sections discuss model abstractions for the TSPA-SR. Details of the abstraction of individual process models and the development of the integrated model parameters are provided in Section 3.2 of the *Waste Package Degradation Process Model Report* (CRWMS M&O 2000n).

**Abstraction of General Corrosion Models**—The model abstractions are to develop two cumulative distribution functions to represent the general corrosion rate distribution for Alloy 22 outer barrier and the titanium drip shield. For each material, the weight loss and crevice sample penetration rate data were combined to yield one general corrosion rate data set. For Alloy 22, the general corrosion rate data with 6-month, 1-year, and 2-year exposure were considered. Since the variance in the corrosion rate data is reduced with the exposure time, and the median rate also decreases with the exposure time, it was concluded that the 2-year data are sufficiently conservative to represent the long-term general corrosion rate. Therefore, only the 2-year data were used in the model abstraction. For the drip shield, only the 12-month data were used in the model abstraction. The cleaning method employed with the 6-month titanium samples caused significant metal loss, thereby yielding inaccurate corrosion rates. Assumptions shown below were employed in the model abstraction.

- For both alloys considered (Alloy 22 and Titanium Grade 7), corrosion penetration rate data from the weight loss of both plain and creviced geometry test coupons were considered to represent general corrosion penetration rate.
- The maximum general corrosion rate for Alloy 22 was set to  $7.30 \times 10^{-5}$  mm/yr (0.073  $\mu\text{m}/\text{yr}$ ). This assumed upper bound is greater than the maximum penetration rate of  $7.25 \times 10^{-5}$  mm/yr (0.0725  $\mu\text{m}/\text{yr}$ ) observed.

- The maximum general corrosion rate of Titanium Grade 7 was set to  $3.25 \times 10^{-4}$  mm/yr (0.325  $\mu\text{m}/\text{yr}$ ). This assumed upper bound is greater than the maximum penetration rate of  $3.19 \times 10^{-4}$  mm/yr (0.319  $\mu\text{m}/\text{yr}$ ) observed.

As discussed in Section 6.5.5 of *General Corrosion and Localized Corrosion of Waste Package Outer Barrier* (CRWMS M&O 2000cq), the formation of silica scale deposit on the surface of the Alloy 22 sample coupons could bias the estimated general corrosion rate. The potential measurement bias for the weight loss sample coupons was estimated to be 0.063  $\mu\text{m}/\text{yr}$ , and the Alloy 22 general corrosion rate was corrected for the maximum bias by adding a constant value of 0.063  $\mu\text{m}/\text{yr}$  to the estimated value of the general corrosion rate. The same data treatment was used for the Titanium Grade 7 drip shield general corrosion rate data. As a result, the corrosion rate correction increased the median rate (50<sup>th</sup> percentile value) by about 50 percent.

**Abstraction of Localized Corrosion Models—**This section discusses the approaches and assumptions used in the abstraction of localized corrosion models for the waste package outer barrier and drip shield, as well as the abstraction results.

The model abstractions are to develop two localized corrosion initiation criteria: one representing the localized corrosion initiation criterion for the waste package outer barrier (Alloy 22) and the other for the localized corrosion initiation criterion for the drip shield (Titanium Grade 7). Cyclic polarization measurements were made in several synthetic concentrated J-13 waters. For each curve obtained, the critical potential for localized corrosion initiation and the corrosion potential were determined. The potential difference between these two was then fit to a function of relevant exposure parameters. According to the model, localized corrosion should initiate if the corrosion potential exceeds the critical potential. The abstraction results showed that localized corrosion of Alloy 22 and titanium do not initiate under repository conditions, based on extrapolation of the repository-relevant experimental data used in the analysis.

**Abstraction of Stress Corrosion Cracking Model—**In the current waste package degradation analysis, two alternative stress corrosion cracking models, the slip dissolution (or film rupture) model and the threshold stress intensity factor model, are considered (CRWMS M&O 2000cu, Section 6). In the threshold stress intensity factor model, this factor is used to determine when stress corrosion cracking will occur. Provided that an initial flaw and corrosive environment are present, a stress corrosion cracking failure will occur when the applied stress intensity factor is greater than or equal to the threshold stress intensity factor. The slip dissolution model also assumes that incipient cracks or defects grow continuously when the oxidation reaction that occurs at the crack tip ruptures the protective film via an applied strain in the underlying matrix. The rate at which the crack grows is a function of the crack tip strain rate and environmental and material chemistries.

In the waste package degradation analysis (WAPDEG), the slip dissolution model is employed to calculate the growth rate of cracks initiated by stress corrosion cracking. The waste package degradation analysis employs a stochastic approach to model the initiation and propagation of cracks from stress corrosion. The major efforts in the abstraction are to develop an approach to represent the uncertainty and variability associated with the stress corrosion cracking initiation and crack propagation processes. The associated parameters in the model include two model parameters ( $A$  and  $n$ ), stress intensity factor, threshold stress, and incipient crack density and size. The analysis also includes preexisting manufacturing defects in the closure lid welds. The manufacturing defect sizes are sampled for the closure lid weld patches, and the sampled flaws are included in the analysis. Because manufacturing defects are much larger than the incipient cracks, the closure lid weld patches with manufacturing defects are likely to fail initially because of stress corrosion cracking.

**Abstraction of Stress and Stress Intensity Factor Profile—**The Alloy 22 barrier has dual closure lids, referred to as outer and inner lids. The process model analyses calculated the stress and stress intensity factor profiles along the circumference of the welds for each of the closure lids

(CRWMS M&O 2000cu, Section 6), and the results were analyzed to develop abstracted models to represent the uncertainty and variability of the profiles in the closure lid welds.

Assumptions employed in the abstraction are:

- The hoop stress (and the corresponding stress intensity factor for radial cracks) is the prevailing stress in the closure lid welds that could lead to stress corrosion cracking through wall cracks in the closure lid weld of waste packages.
- The hoop stress and corresponding stress intensity factor profiles as a function of depth in the closure lid welds from the process model analyses represent the mean profiles.
- The hoop stress and stress intensity factor profiles vary along the circumference of the closure lid welds, and those represent the variability in the profiles on a given waste package.
- As a crack propagates in the closure lid welds or the weld is thinned by general corrosion, the residual stresses in the welds may redistribute in such a way that the stress corrosion cracking initiation and crack growth are mitigated. Such stress redistribution or relaxation is not considered in the current abstraction. This is a conservative approach.

Three cases have been evaluated: "optimum," "realistic," and "most conservative." The uncertainty range in the hoop stress (and corresponding stress intensity factor profiles based on the hoop stress) is bounded between  $\pm 5$ ,  $\pm 10$ , and  $\pm 30$  percent, respectively, of the yield strength and centered around the mean hoop stress profile. The technical basis for the three uncertainty ranges is discussed in Section 6.2.2.5 of *Stress Corrosion Cracking of the Drip Shield, the Waste Package Outer Barrier and the Stainless Steel Structural Material* (CRWMS M&O 2000cu).

**Abstraction for Manufacturing Defects in Waste Package Closure Welds**—Abstracted models were developed for the probability and size

of manufacturing defects in the waste package closure lid welds. The flaw density is used as the parameter to represent the frequency of occurrence of flaws in a given length of closure weld. The flaw sizes are given as a probability density function on each closure lid weld.

Further details of the assumptions used in the abstraction analyses are discussed in Section 3.2 of *Waste Package Degradation Process Model Report* (CRWMS M&O 2000n). Major assumptions employed in the abstraction are:

- For the cases analyzed, both surface-breaking flaws and embedded flaws are considered.
- Flaws occur randomly.
- The fraction of surface breaking flaws is uniformly distributed. The use of the uniform distribution is a reasonable representation of the uncertainty in expressing this value.

The number of flaws that appear on a waste package patch is sampled stochastically as a Poisson random variable. For each flaw that occurs, a flaw size is randomly assigned to it by sampling from the calculated flaw size cumulative distribution function. This flaw's location and size are then used in the stress corrosion cracking analysis.

Because embedded defects can become surface breaking defects as general corrosion proceeds, the consideration only of preexisting surface breaking defects may not be appropriate. As an alternative conservative abstraction, both surface breaking defects and embedded defects within the outer quarter region of the weld surface are considered. Three observations for the sum of the fraction of surface breaking flaws and the fraction of flaws embedded within the outer quarter region of the surface are used in the alternative conservative abstraction. This, however, may be overly conservative because most embedded defects would be oriented in the radial direction that would not lead to stress corrosion cracking. The stress corrosion cracking analysis considers that hoop stress is the dominant stress in the closure lid welds and drives radial crack propagation.

**Integrated Analyses for Drip Shield and Waste Package Degradation**—This section reports WAPDEG analysis results for drip shield and waste package degradation. The section includes the discussion of results for the three cases (optimum, realistic, and most conservative) that are likely to represent the potential range of major corrosion model parameter values that could affect the long-term performance of the waste package and the drip shield in the repository. The optimum case represents the parameters achievable through stringent control of such processes as stress mitigation, material variability, welding, and other fabrication steps. The realistic case represents what is achievable through appropriate levels of process controls. The most conservative case represents the combination of the worst case parameters that might result from inadequate control of the processes. In the WAPDEG analyses for the three cases, the potential performance credit of the stainless steel structural material is not considered.

The WAPDEG model, an integrated model used for waste package and drip shield degradation analysis, is based on a stochastic simulation approach. It describes waste package degradation, which occurs as a function of time and repository location for specific design and thermal hydrologic modeling assumptions. The corrosion modes that were included in the analyses are:

- Humid-air phase general corrosion of the drip shield
- Aqueous phase general corrosion of the drip shield
- Localized (pitting and crevice) corrosion of the drip shield
- Humid-air phase general corrosion of the waste package outer barrier
- Aqueous phase general corrosion of the waste package outer barrier
- Localized (pitting and crevice) corrosion of the waste package outer barrier

- Stress corrosion cracking of closure lid welds of the waste package outer barrier.

The following corrosion parameters were abstracted and included in the analyses:

- Relative humidity threshold for corrosion initiation of the drip shield and waste package outer barrier
- Corrosion potential-based threshold for localized corrosion initiation of the drip shield and waste package outer barrier
- Probability of the occurrence and size of manufacturing defects in closure lid welds of the waste package outer barrier
- Stress and stress intensity factor profiles in the closure lid welds of the waste package outer barrier (incorporating stress mitigation techniques)
- Threshold stress intensity factor for the waste package outer barrier (used with the threshold stress intensity factor model)
- Threshold stress for the initiation of stress corrosion cracking crack growth for the waste package outer barrier (used with the slip dissolution model)
- Corrosion enhancement factor for aging and phase instability of the waste package outer barrier
- Corrosion enhancement factor for microbologically influenced corrosion of the waste package outer barrier.

For the stress corrosion cracking analysis of the waste package closure lid welds in the WAPDEG analysis, the slip dissolution model has been adopted over the threshold stress intensity factor model. For the analysis with the slip dissolution model, the following should be met before initiating a stress corrosion cracking crack propagation in a patch: (1) the stress intensity factor ( $K_I$ ) should be positive, and (2) the stress state must be greater than or equal to the threshold stress. In the

WAPDEG analysis, for those patches with a compressive stress zone (or layer) in the outer surface, the compressive stress zone is removed by general corrosion, and this delays the application of the slip dissolution model for the crack propagation rate. The delay time depends on the compressive zone thickness and the general corrosion rate sampled for the patch.

In addition, preexisting manufacturing defects in a patch are all assumed to be surface breaking for the optimum case. For the most conservative and the realistic cases, all flaws within the outer quarter thickness were included. All of the surface breaking flaws grow at the same general corrosion rate as each sampled patch. Growth of the defects at the general corrosion rate of the patch is a conservative assumption. Therefore, patches with preexisting defects would be subject to stress corrosion cracking earlier than patches without defects.

Corrosion enhancement factors for microbially influenced corrosion and aging and for phase instability are applied to the general corrosion rate of the waste package outer barrier. No microbially influenced corrosion and aging or phase instability factor is applied to the localized corrosion rate because no localized corrosion occurs.

Because temperature and relative humidity do not significantly affect waste package and drip shield degradation, except in the case of relative humidity threshold for corrosion initiation, a representative set of histories for these parameters were used in the current analysis. In addition, the threshold for localized corrosion initiation for the drip shield and waste package outer barrier, which requires the presence of drips, is much higher than the conditions expected in the repository. The stainless steel inner layer of the waste package was not considered in the analysis.

Additional waste package degradation model improvements were implemented after completion of the TSPA-SR analyses. After incorporation of new analyses, models, and data, the predicted performance against general and localized corrosion of the waste package was shown to improve. The TSPA-SR model shows no waste

package failures before 10,000 years (CRWMS M&O 2000a, Section 5.3). The supplemental TSPA model conservatively included a small number of waste package failures (up to three) due to improper heat treatment of welds. These failures lead to small calculated doses before 10,000 years. Excluding those early failures, the supplemental TSPA models show significant improvement in waste package lifetime (BSC 2001a, Section 7.5; Williams 2001a, Figure 6-1). The results of the additional analyses provide added confidence that the TSPA-SR model is conservative and that the behavior of the waste package in the repository environment is likely to be better than that predicted by the TSPA-SR model.

The various cases analyzed for waste package and drip shield degradation constitute 100 realizations of WAPDEG simulation (or 100 WAPDEG runs) that used 100 inputs for uncertain corrosion model parameters sampled from their respective range. The parameters used in the analysis are:

- Temperature, relative humidity, and contacting solution pH histories in the presence of backfill
- 400 waste package and drip shield pairs
- Thickness of the waste package outer barrier (Alloy 22)
- 15-mm (0.6-in.) thick drip shield (titanium)
- 1,000 patches per waste package
- 500 patches per drip shield.

The DOE codisposal waste package and the naval spent nuclear fuel waste package have a thicker outer barrier than commercial spent nuclear fuel packages. Therefore, the calculation of patch penetration times by general corrosion of those waste packages is conservative (i.e., the model calculates faster corrosion than is expected). However, radionuclides that contribute most to the peak dose (technetium-99, iodine-129, neptunium-237, and plutonium-239; see Section 4.4.2.2) from DOE spent nuclear fuel and high-level radioactive waste in the codisposal waste packages represent only

about 10 percent of the total inventory of radionuclides in the repository (CRWMS M&O 2000bm, Table 3.1-4). Therefore, the delayed patch penetrations of the codisposal waste packages by general corrosion would not affect the peak dose significantly. In addition, because stress corrosion cracks, once initiated, propagate very rapidly, the crack penetration times by stress corrosion cracking in the closure lid welds would not be affected significantly for the codisposal and naval spent nuclear fuel waste packages with the thicker outer barrier. The WAPDEG analysis results (i.e., waste package and drip shield failure time and number of crack, pit, and patch penetrations) are reported as a group of degradation profile curves that represent the potential range of the output parameters.

The optimum case (the upper bound profile, which is the upper extreme of the probable range of the failure time) indicates that the earliest possible waste package failure time is about 51,000 years. An extremely low probability is associated with the estimated earliest possible failure time. The failure time of the median profile is about 80,000 years. The time to fail 10 percent of waste packages for the two profiles is about 80,000 and 97,000 years, respectively.

Because conditions for localized corrosion do not develop, degradation of the drip shield occurs primarily because of general corrosion. Stress corrosion cracking of the drip shield due to rockfall is not expected to affect drip shield functions (CRWMS M&O 2000cu, Section 6.5.5). Both the top and under sides of the drip shield are exposed to emplacement drift conditions and subject to corrosion. In addition, both sides are assumed to experience the same exposure conditions, regardless of whether the drip shields are dripped on or not. Results of the WAPDEG analysis show that for the optimum case (i.e., the upper bound profile), the drip shield failure starts at about 24,000 years, and 50 percent of the drip shields fail within several thousand years after the initial failure.

The most conservative case analysis was to evaluate the effects of the alternative conservative model abstractions of several key corrosion model parameters. Those parameters are stress corrosion

cracking-related parameters and general corrosion parameters, along with corrosion rate bias to account for silicate deposits. This case represents the worst case combination of those parameters from the perspective of first waste package failure time. As shown in Figure 4-92, the results of this case indicate that in the TSPA-SR model the earliest possible failure time of a waste package for the upper bound profile is about 12,000 years, much earlier than the realistic case (about 50,000 years) (see Section 4.4.2.2 for the analysis result summary). This estimated earliest possible failure time has a very low probability. The results also show that the initial failure comes from a stress corrosion crack penetration. The failure time of the median profile is about 50,000 years. The time to fail 10 percent of waste packages for the upper bound profile is about 22,000 years. These results do not include the possibility of small releases resulting from early failures described in *FY01 Supplemental Science and Performance Analysis* (BSC 2001a).

For the most conservative case, the failure profiles of drip shields are not significantly affected because the failures occur only by general corrosion. The difference between the conservative and optimum cases consists only of bias correction for the silicate deposits. As with the optimum case analysis, both the outer and inner sides of the drip shield are exposed to the same conditions in the emplacement drift and subject to general corrosion. The results show that for the upper bound profile, drip shield failure starts at about 20,000 years, and 50 percent of the drip shields fail within a thousand years after the initial failure.

The realistic case represents what is achievable for fabrication and material parameters under present-day processes. The results for this case fall between those of the optimum and most conservative cases.

**Analysis Summary**—The candidate materials for the drip shield (Titanium Grade 7) and the waste package outer barrier (Alloy 22) are highly corrosion resistant. Under the expected repository exposure conditions, these materials are not expected to be subject to degradation modes that, if initiated, could lead to failure in a short time.

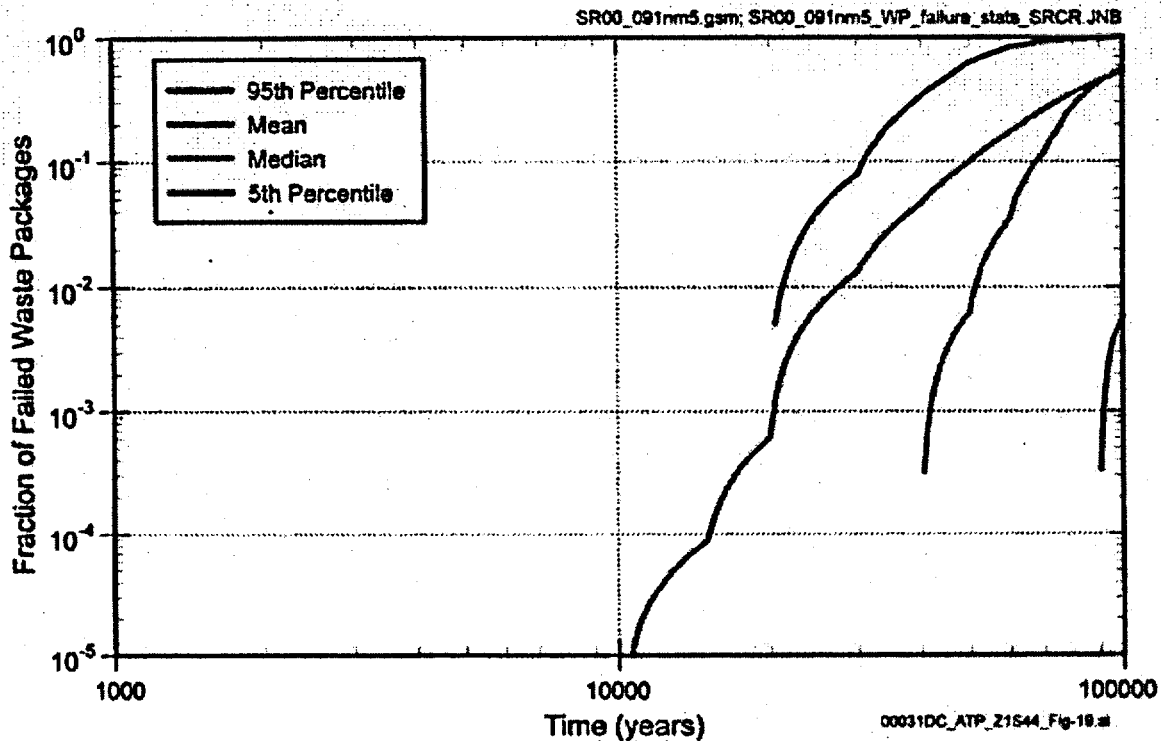


Figure 4-92. TSPA-SR Performance Assessment Results for Waste Package Degradation (Nominal Scenario)  
Source: Modified from CRWMS M&O 2000a, Figure 4.1-9.

Those degradation modes are localized corrosion (pitting and crevice corrosion), stress corrosion cracking, and hydrogen-induced cracking (applicable to drip shield only). Both drip shield and waste package degrade by general corrosion at a very low passive dissolution rate. The current experimental data and detailed process-level analyses, upon which the model abstractions that have been incorporated in the WAPDEG analysis are based, indicate that, except for the closure lid welds of the waste package, the candidate materials would not be subject to those rapidly penetrating corrosion modes under the expected repository conditions. The waste package and drip shield degradation analyses for the two "end-member" cases (i.e., the optimum case and the most conservative case) have shown that, based on the TSPA-SR corrosion model abstractions and assumptions, both the drip shields and waste packages do not fail within 10,000 years. From the perspective of first waste package failure, the analysis results are encouraging because the most

conservative case represents the worst case combination of key corrosion model parameters that significantly affect the long-term performance of waste packages in the repository. The most conservative case accounts for potential uncertainties in the fabrication and process control steps, such as stress mitigation. However, the estimated long lifetime of the waste packages in the TSPA-SR model analysis is attributed primarily to two factors: (1) stress mitigation to substantial depths in the dual closure lid welds and (2) the very low general corrosion rate applied to the closure lid welds to corrode the compressive stress zones. Complete stress mitigation as proposed may not be possible for the closure lid welds, and because of the potential residual stresses, the closure lid welds may be subject to stress corrosion cracking. Once a stress corrosion crack begins, it penetrates the closure lid thickness in a very short time. Thus, stress mitigation in the closure lid welds is a key design element to avoid premature waste package failures from stress corrosion cracking.

**Movement of Water into Breached Waste Packages to Contact Waste**—The temperature conditions in the waste package over time (before and after waste package breach) are used to calculate the number of spent nuclear fuel rods that develop pinholes due to creep rupture, in addition to those that have pinholes prior to being delivered to the repository. If waste package breaches occur while temperatures are high, oxygen can enter the waste package, and thermally-driven oxidation of the spent fuel pellets exposed through the pinholes can cause large length cracks (unzipping) in a significant number of fuel rods. The amount of cracking is very small if the waste package breaches occur after temperatures fall, which is the more likely situation. In the TSPA-SR, the amount of water that is calculated to have access to the waste package interior is based on the degraded areas of both the drip shield and the waste package. The distribution of water within the waste package is modeled using a conservative mixing cell approach. Resident water within the cell is based on the water fraction in saturated corrosion products of the spent nuclear fuel of the high-level radioactive waste glass. No credit is taken in this model for the potential for water to not fully wet the large surface area available in the waste package interior or the possibility that residual heat in the waste package could evaporate the water before it contacts the waste. The mobilization of radionuclides by the water from the exposed waste (through the cladding pinholes and cracks) is described in Section 4.2.6.

Once radionuclides are mobilized, they are transported to the exterior of the waste package by a simple one-dimensional diffusion model. No credit is taken in this model for the time it could take for the radionuclides to reach the inner surface of the waste package breach location or for sorption by corrosion products within the waste package. The diffusion model uses the crack width to determine the cross-sectional area, the thickness of the closure weld for the diffusion distance, the mixing-cell concentration as the source concentration, and a zero sink concentration (by assuming advection of the contaminated effluent from the outer surface of the crack). The output of this diffusion model is the source term for the sequential engineered barrier system, unsaturated zone, and saturated

zone transport calculations described in Sections 4.2.7, 4.2.8, and 4.2.9.

#### 4.2.5 Water Diversion Performance of the Engineered Barriers

The water diversion functions of the engineered barrier system are to limit or delay the amount of water contacting waste packages for at least 10,000 years (CRWMS M&O 2000ab, Section 1.2.1.8) and to increase the predictability of environmental conditions at the waste package surface. The engineered barrier system components that will perform these functions include the drip shield, the invert (consisting of a steel support structure with crushed rock ballast), the waste package pallet, and the steel ground support. Engineered barriers are described in Section 2.4.

This section describes how the engineered barriers in the potential repository will function together with the natural barriers to minimize water contact with waste packages. Over time, the drip shields and waste packages will become susceptible to corrosion, as discussed in Section 4.2.4. Once these processes result in breaches in the drip shield and the waste package, water can contact the waste form and mobilize radionuclides. The water diversion model described in *Total System Performance Assessment for the Site Recommendation* (CRWMS M&O 2000a, Sections 3.6.1 and 3.6.2) identifies flow pathways and calculates, among other things, leakage through a breached drip shield as well as leakage from a breached waste package. Another aspect of engineered barrier system performance is to moderate the transport of released radionuclides from breached waste packages to the host rock at the drift wall. This will be accomplished for the case of a breached waste package under an intact drip shield using a diffusion barrier concept (see Section 4.2.7). For the case of a breached drip shield, transport will be moderated through partial performance of the drip shield by reducing the amount of water that contacts the waste package.

Finally, free drainage from the drifts is important for engineered barrier system performance. Sufficient drainage capacity will prevent partial

inundation of waste packages or their supports, promote diffusion-barrier performance of the invert, and prevent saturated flow conditions that could lead to faster transport for released radionuclides through the engineered barrier system and the host rock. Complete saturation of the invert is possible if seepage inflow exceeds the drainage capacity of the floor.

As noted in Section 4.1.4, the DOE has conducted sensitivity studies of the operation of the repository at lower temperatures. The conceptual basis and model abstractions presented in this section reflect the effects of higher-temperature operating conditions, specifically those implemented in *Total System Performance Assessment for the Site Recommendation* (CRWMS M&O 2000a, Section 3.6). Alternative thermal operating modes and/or conservatisms and conceptual uncertainties in the model have been reevaluated since the TSPA-SR model and are reported or summarized in *FY01 Supplemental Science and Performance Analyses* (BSC 2001a, Sections 8 and 15; BSC 2001b, Sections 3.2.6 and 4.2.6).

The issues reevaluated since the TSPA-SR model include evaporative reduction of seepage, condensation under the drip shield, geometric constraints on advective flux into the waste package, and the effect of allowing accumulation of water within the waste package (i.e., the "bathtub effect").

#### 4.2.5.1 Conceptual Basis

Initially, preclosure ventilation will remove heat and moisture from the emplacement drifts. Ventilation at ambient temperature in the Exploratory Studies Facility has been observed to dry the surrounding rock (Section 4.2.2), and even more drying of the rock will occur during preclosure operations because of the duration and the elevated temperature. After permanent closure, the emplacement drifts and the surrounding rock will heat up, and depending on the thermal loading, the dryout zone will extend around the drifts. Eventually, within approximately 1,000 years (for the mean and upper infiltration distributions, see Section 4.2.2), moisture will return to the

surrounding rock. At a few locations in the potential repository, seepage of liquid water into the drifts may occur. The drip shield will prevent such seepage from contacting waste packages.

Seepage in the future may increase because of altered climate conditions or episodic fluctuations in infiltration at the ground surface. In addition, at a limited number of locations in the potential repository, faults or fractures may focus percolation into an emplacement drift. Drainage capacity will ensure water diversion performance for extreme seepage conditions.

**Conceptual Basis for Types of Flow on the Drip Shield and Waste Package**—Water that enters the emplacement drifts as seepage can flow along three types of pathways: (1) water flow directly to the invert; (2) water flow that contacts the drip shield, but is diverted to the invert; and (3) water flow through breaches in the drip shield or waste package. Breaches in the drip shield or waste package can take different forms, ranging from fine cracks caused by stress corrosion cracking of the waste package to patches where general corrosion has penetrated a larger area of the drip shield or waste package (Section 4.2.4). Conceptual features related to film flow and droplet formation are discussed in this section, some aspects of which are not directly modeled (CRWMS M&O 2001c, Section 6.1). As outlined in the process model and abstraction sections 4.2.5.3 and 4.2.5.4, the TSPA-SR conceptual model for fluid flux through the drip shield and waste package bounds many of the discussed conceptual processes using simplified and conservative approaches (CRWMS M&O 2000a, Sections 3.6.1 and 3.6.2).

Thin films can be predicted to form on any wetting or partially wetting surface that is exposed to humidity (Middleman 1995, Chapter 9). Films may then flow because of gravity or possibly because of other differences in water potential on the surface. Film flow capacity is limited by viscosity, the extent of the flow area, surface roughness, and other factors. Film flow on the engineered barriers can deliver liquid water at significant flow rates and could be significant to waste isolation performance. However, film flow through breaches in the drip shield is likely to continue as film flow on the

underside of the drip shield and thus will tend to be diverted from the waste package. Also, film flow through fine cracks into the waste package will be limited by heat generation within the waste package, which will cause water to be rejected as vapor (CRWMS M&O 2000as, Section 3.1.1).

Depending on the aperture of a breach, capillary flow and droplet flow modes can occur. For fine cracks, flow will be dominated by capillarity. In capillary flow, water will be either strongly imbibed or excluded in a crack, depending on whether the surfaces are wetting or nonwetting, respectively. If the local environment has low relative humidity, which would occur mainly during the thermal pulse, a fine crack may dry out. Molecular films of water could then form on the crack surfaces, but the flow capacity would be negligible because the films would be very thin. As the relative humidity increases during cooldown, water films will thicken, and fine cracks will become increasingly water-saturated (CRWMS M&O 2001c, Section 6.1).

As saturation increases and water bridges a fine crack or pore, it will be held there at a negative potential by capillarity. It will not flow unless the adjacent downstream flow pathway is at a more negative potential, or unless sufficient water pressure is applied upstream to overcome the negative potential. For the case of water flowing through the drip shield or through the waste package under the impetus of gravity, neither of these conditions is likely unless the water evaporates at the downstream end (CRWMS M&O 2001c, Section 6.1). Thus, the movement of water through fine cracks is limited to very thin water films that can form in the crack and, when humidity conditions permit, to evaporation of water from the downstream end.

Wetting behavior of the crack surfaces is required for capillary effects to occur, and the assumption of wetting behavior is conservative because it increases the liquid pathways available for radionuclide transport (CRWMS M&O 2000as, Section 3.1.1). If the crack surface is nonwetting, water cannot enter and bridge the crack except if pushed by greater water pressure, which is unlikely in the emplacement drifts.

As breaches in the drip shield or waste package increase in size, capillary flow will be more important. As the relative humidity increases during cooldown, and especially when seepage water is present, wider aperture cracks and other types of flow channels will become partially or fully water-saturated. As the relative humidity approaches 100 percent, the saturation and flow capacity of cracks and pores in the drip shield or waste package will increase. Water droplets can form at the downstream end of such channels, and depending on the relative humidity and the channel aperture, they may be released. Once released, droplets can flow on the surface (e.g., the underside of the drip shield) or fall (e.g., onto the waste package). If the crack or channel aperture is fine enough, droplet release will not occur. There is a limit to the aperture above which drops can form and fall from the lower end of the channel. This limit will depend in a complex manner on the geometry of breaches, the wetting properties of the surfaces, and relative humidity (CRWMS M&O 2001c, Section 6.1).

The foregoing discussion applies to an equilibrium situation in which drop size and relative humidity are related (CRWMS M&O 2001c, Section 6.1), so that for a given relative humidity there is an associated equilibrium drop size. If the equilibrium drop size is greater than or equal to the aperture of a potential flow channel, then the channel can be considered fully saturated and flow will depend on the conditions described previously. This is the basis for the capillary flow concept, which can be used to establish a lower threshold of aperture below which flow does not occur for given relative humidity conditions.

A different mode of flow may result when drops fall from the roof of the emplacement drift at locations where seepage contacts the drip shield or waste package. The kinetic energy at impact can produce smaller droplets that are not at equilibrium with the relative humidity and can travel through smaller channels without forming films or causing the channels to become saturated. For breaches due to general corrosion, even equilibrium droplets could do this. Thus, there is another mode of flow that is dynamic and not limited by capillary retention.

The dynamic droplet mode of flow will be limited by several factors (CRWMS M&O 2001c, Section 6.1). Firstly, production of smaller drops will increase the surface energy, and the increase must be less than the kinetic energy of impact, which constrains the distribution of drop sizes produced by the impact. Secondly, as debris accumulates in the drifts, falling drops may dissipate their kinetic energy before contacting the drip shield or waste package. Thirdly, the breaches may fill with corrosion products or debris, so that the resulting flow channels are smaller than the droplets produced. The interlocking drip shield joint design will obstruct and prevent dynamic penetration by water droplets. Finally, multiple breaches will tend to interfere, whereby an upper breach intercepts the flow to a lower breach.

In summary, for fine cracks and pores the flow of water because of gravity will be negligible, especially at low relative humidity, compared with the potential diffusion of radionuclides through such channels. There is an aperture threshold above which flow through cracks or other channels can occur, depending on the relative humidity conditions. Dripping behavior is complex and depends on the channel geometry, material surface characteristics, and relative humidity. This aperture threshold concept does not apply to droplets that are smaller than the channel aperture, which can penetrate dynamically. The dynamic droplet mode is limited by several factors but is taken into account in the interlocking joint of the drip shield design described in this report.

**Conceptual Basis for the Environment Under the Drip Shield**—During the thermal pulse, the relative humidity at the waste package surface will be less than in the drift environment, primarily because the temperature will be greater. Several studies supporting the TSPA-SR model evaluated the potential for water vapor emanating from the invert to condense on the underside of the drip shield (CRWMS M&O 2001c, Section 6.4; CRWMS M&O 2000dd, Section 6.3.3). As a minimum, this would require very wet conditions in the invert, corresponding to high rates of seepage inflow to the drifts during the thermal pulse. Without such seepage, moisture conditions in the invert material will be too dry to produce

water vapor partial pressures that can condense on the underside of the drip shield. An important reason for this is that the vapor pressure in unsaturated porous media, such as the invert, is lowered by capillarity (CRWMS M&O 2001c, Section 6.4).

The drip shield must also be cooler than the invert for condensation to occur. As the thermal output of the waste decays, the driving force for condensation under the drip shield will be greatly diminished, so the potential condensation rate will be diminished even if condensation is still possible. Differences in temperature and relative humidity between the waste package and the drift environment will gradually decay and become insignificant after a few thousand years. The timing will depend on location within the potential repository and hydrologic factors, as discussed in Section 4.2.2.

The chemical environment under the drip shields will be protected from liquid or solid-phase mass transport, and thermally driven coupled chemical processes taking place outside the drip shields, for as long as the drip shields are intact and functional. Gas-phase composition, including humidity and the partial pressures of oxygen and carbon dioxide, will be similar to the drift environment and is readily predicted (see Section 4.2.3). There will be dust present on the waste package, derived mainly from the host rock and construction materials and also including particles that may be contributed by the preclosure ventilation air.

Finally, condensate under the drip shield would be pure water that interacts with carbon dioxide in the gas phase, dust on the surfaces, and the metal oxide corrosion products. The resulting bulk composition of condensate would be dilute and well within the range of corrosion resistance for the waste package and drip shield materials (discussed in Section 4.2.4). Condensate would tend to moderate chemical conditions by dilution and flushing of dust and salts. The thickness of water films that form on the surfaces of the waste package or drip shield will increase with time as the relative humidity increases. However, the potential rate of condensation will decrease with time, as the thermal output of the waste package decays.

In summary, the physical and chemical environment under the drip shields will be protected from potential seepage and thermally driven chemical coupled processes taking place outside the drip shields.

**Conceptual Basis for Drainage**—Free drainage is an important attribute of the potential repository host rock at the Yucca Mountain site. Drainage from the emplacement drifts will be facilitated by the permeability of the rock immediately below the drift floor. If drainage capacity is exceeded locally, water will flow from less permeable to more permeable regions. Thus, the spatial distribution of seepage and drainage capacity could be used to develop greater estimates of drainage capacity.

Excess drainage capacity is desirable because the permeability of the rock below the emplacement drifts may be decreased by thermal-hydrologic-chemical-mechanical coupled processes occurring early in the thermal period. The possibility for fracture plugging increases from migration of fines from the drift into fractures and from thermally driven reaction of those fines to form clays or other products, particularly on contact with water. Fracture plugging may also be associated with thermal-mechanical loading of the host rock (Hardin and Chesnut 1997, Section 3.2.2).

#### 4.2.5.2 Summary State of Knowledge

**Results from Laboratory Testing of Drip Shield Concepts**—A series of drip shield tests was conducted in a mockup of an emplacement drift to investigate drip shield performance. Results from the tests demonstrated the capillary flow mode and showed, for a set of thermal conditions similar to those of the design and operating mode described in this report, that condensation does not form on the underside of the drip shield. The following description, summarized from *Water Distribution and Removal Model* (CRWMS M&O 2001c), pertains to one of the tests in the series, which involved water injection onto a simulated drip shield, without backfill, at elevated temperature.

The drip shield test configuration shown in Figure 4-93 consists of an outer steel canister, simulated drip shield, invert structure, and simulated waste

package. At one-fourth scale, the outer canister represented a 5.5-m (18-ft) diameter emplacement drift. The canister was thermally insulated on the outside, and the total weight was monitored to measure bulk water content. The scale-model drip shield was fabricated from stainless steel and was similar to the design concept described in this report (see Section 2.4), except that simple overlap joints were used between sections rather than the interlocking design. Drift seepage was simulated using an array of drippers at the top of the canister, which injected water at a rate of 1 L/hr (0.26 gal/hr). The water contained a blue dye to facilitate tracing of water movement. Temperature and humidity measurements were made in the canister and under the drip shield. Moisture content and temperature were measured in the invert material. The dripper locations, measurement locations, and other details are shown in Figure 4-94.

The temperature of the simulated waste package was maintained at 80°C (176°F) and that of the outer canister wall at 60°C (140°F). The volume of water recovered from the test as a function of time is shown in Figure 4-95. Of the 760 L (200 gal) introduced, approximately 650 L (170 gal) were recovered; the difference was retained in the granular invert material. The water injection rate represented localized seepage conditions extreme, that might be encountered in the potential repository. Relative humidity above the drip shield typically remained around 85 percent, while under the drip shield the relative humidity was typically 65 percent (Figure 4-96). Condensation under the drip shield can occur only if the relative humidity approaches 100 percent. Observation with remote television cameras indicated no condensation under the drip shield or on the waste package.

**Observations of Drainage from Exploratory Tunnels**—Water use is limited in exploratory excavation and scientific testing in tunnels at Yucca Mountain. The amount of water used during excavation was monitored and was typically in the range of 1,900 to 2,700 L (500 to 700 gal) per meter of drift. Ponded water on the tunnel floor evaporated and drained into the rock and did not persist. Drainage was difficult to quantify because construction water was removed along with the waste rock and because ventilation also removed

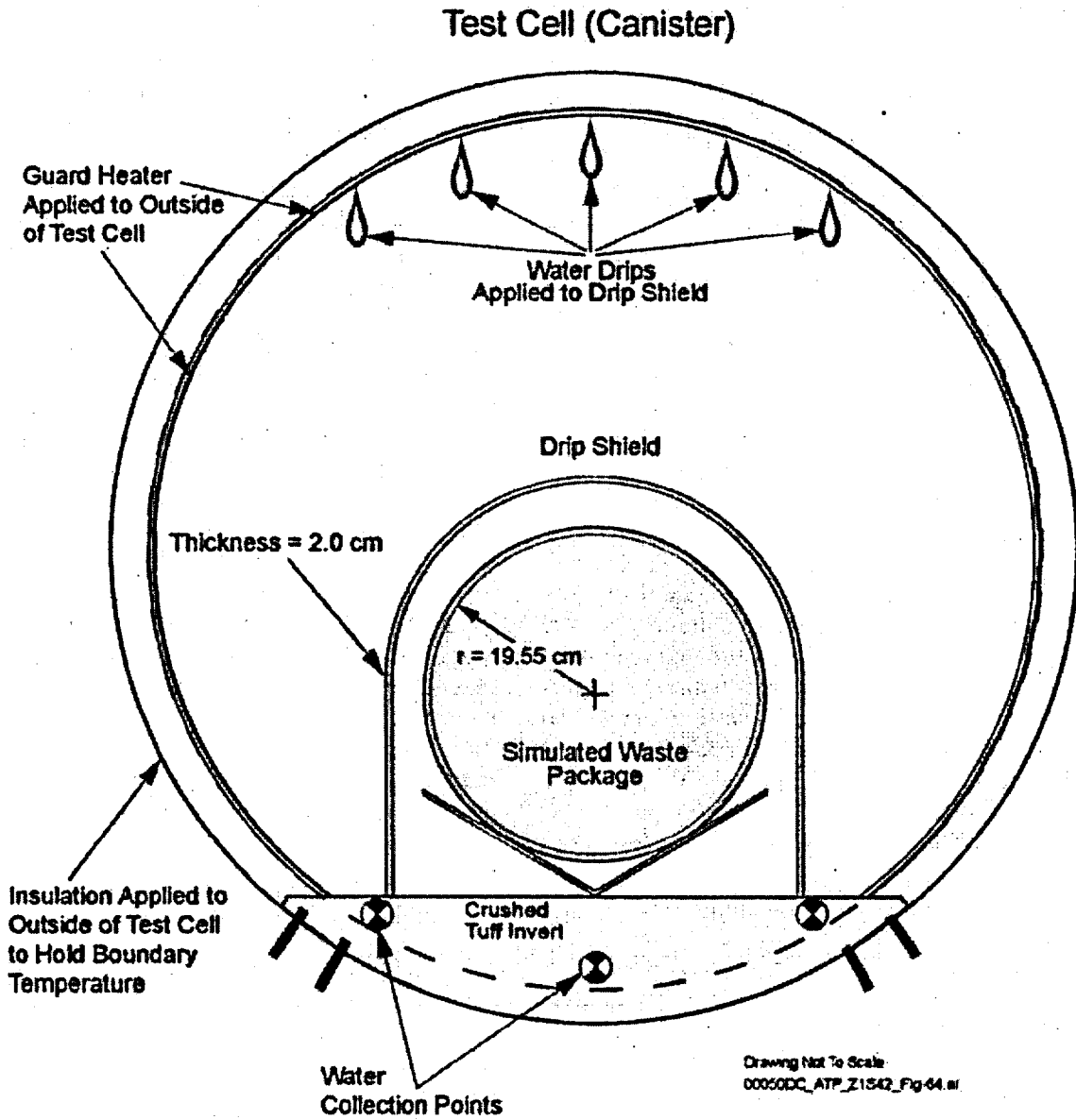


Figure 4-93. Schematic of Drip Shield Test

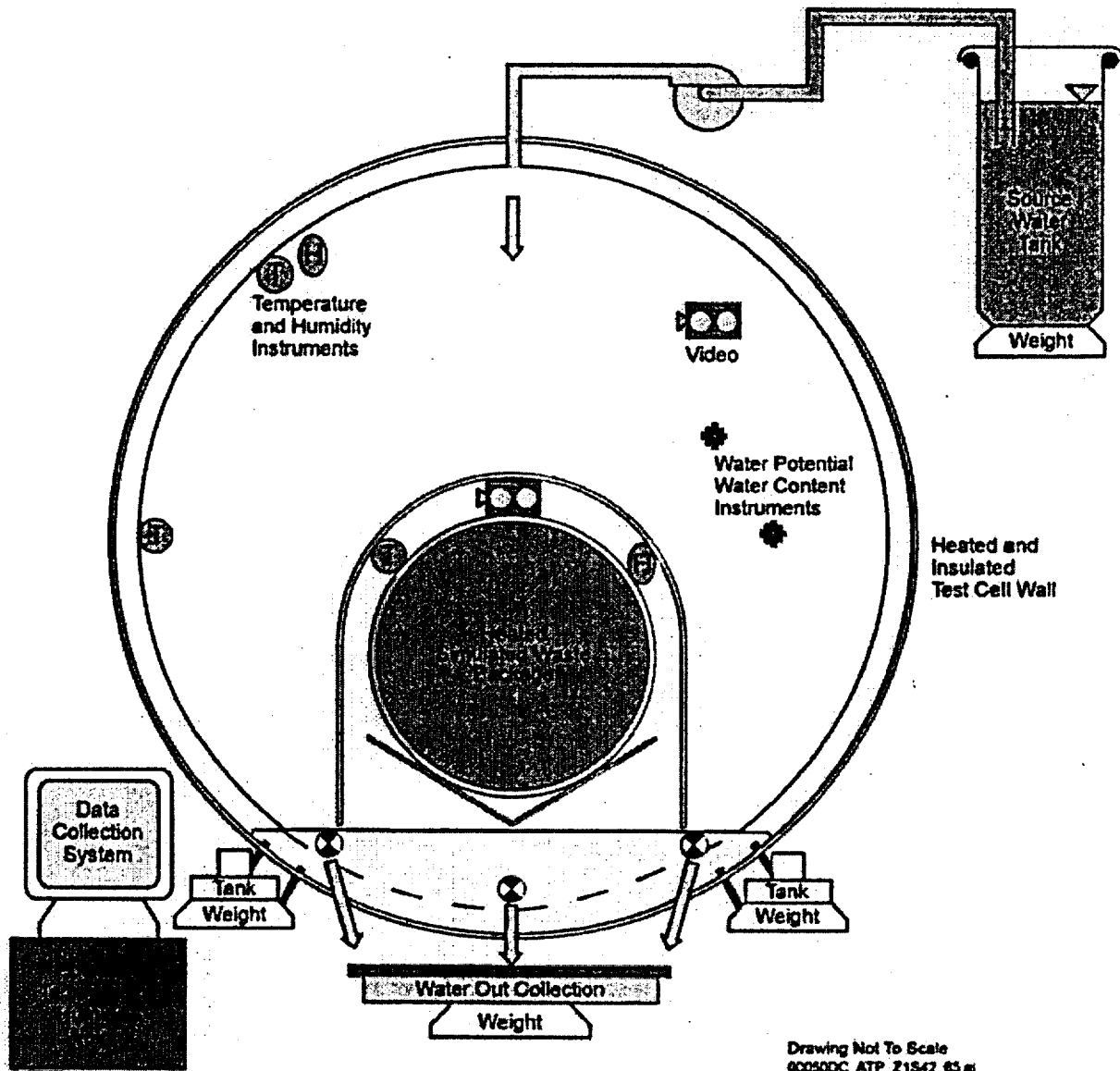
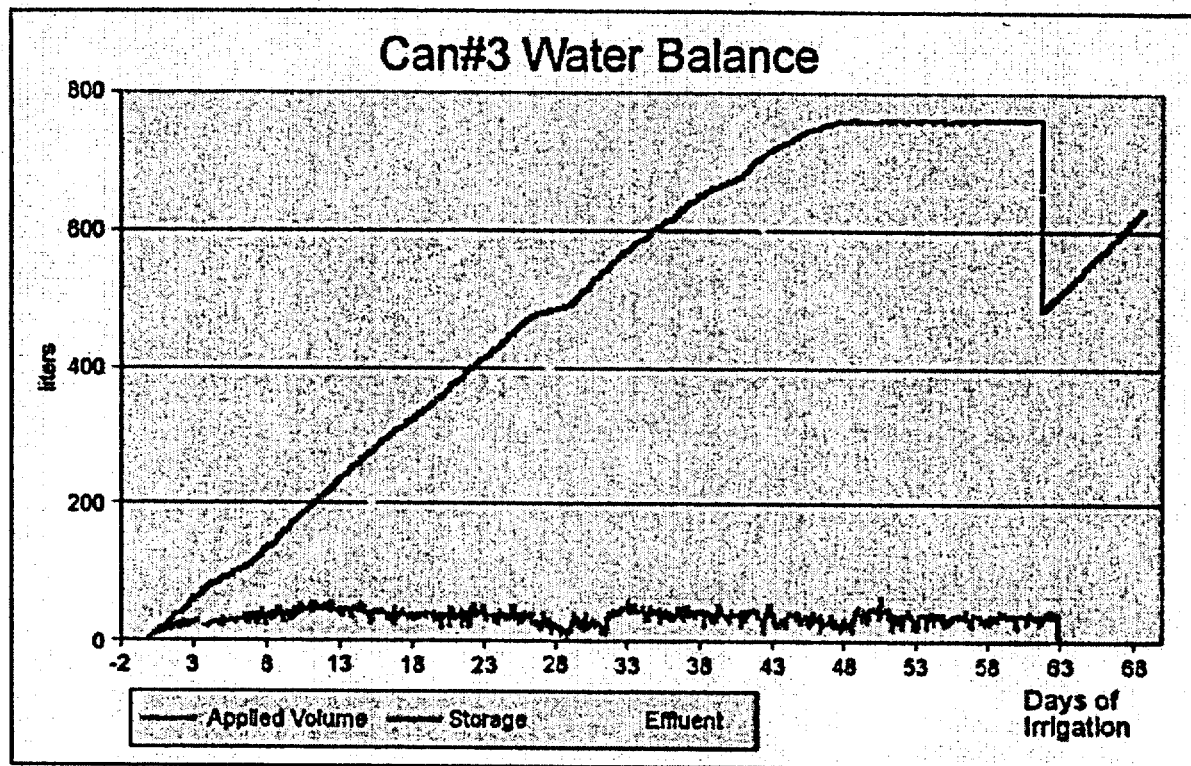


Figure 4-94. Schematic of Drip Shield Test Measurements



00050DC\_ATP\_Z1S42\_Fig-08.ai

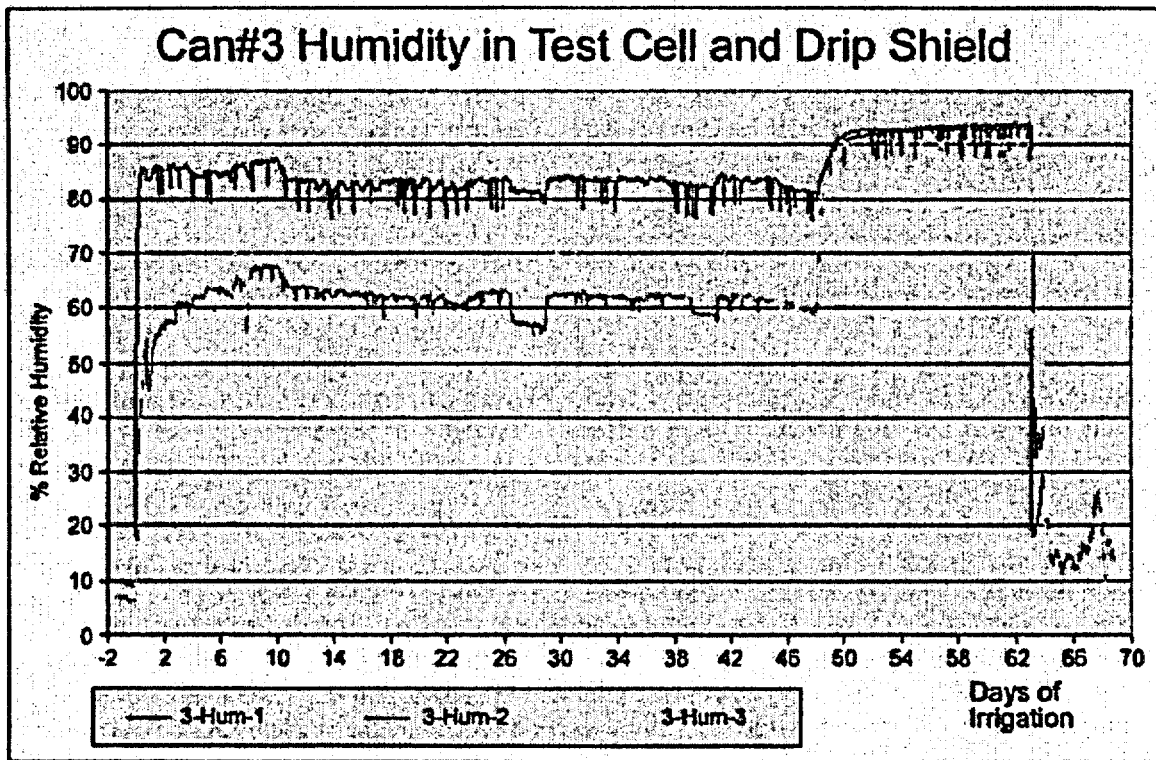
Figure 4-95. Water Balance for the Pilot-Scale Drip Shield Test without Backfill  
This figure shows the total water injected into Canister Test #3 (blue curve), the total collected (yellow curve), and the difference, representing water stored in the test (magenta curve). The test was terminated at approximately 62 days.  
Source: Modified from Howard et al. 2001, Figure 58.

water. Temporary ponding of construction water on the floor did not occur uniformly, so drainage capacity was apparently heterogeneous.

Measurements from the Yucca Mountain site have shown that the ambient, in situ bulk permeability of the rock exceeds the necessary drainage capacity by orders of magnitude, on average. Hydrologic properties developed for the welded tuff host rock units, constrained by air injection testing in boreholes, indicate that bulk permeability is 1 darcy or more (CRWMS M&O 2000cj, Tables 13, 14, and 15). This permeability corresponds to water drainage capacity of more than 300 m/yr (1,000 ft/yr), which exceeds the drainage capacity requirement for the most extreme seepage criterion (CRWMS M&O 2000ab, System Performance Criterion 1.2.1.8) by at least an order of magnitude.

#### 4.2.5.3 Process Model Development and Integration

**Drip Shield Design Features for Water Diversion, Rockfall, and Seismic Stability**—The interlocking drip shield joint will maintain a functional configuration capable of diverting water, mitigating impact loads from rockfall, and resisting the effects of seismic motion. A description of the drip shield concept is provided in Section 2.4.4. Design requirements are presented in *Emplacement Drift System Description Document* (CRWMS M&O 2000ab). Drip shield design requirements include corrosion resistance and structural strength. Corrosion resistance is required so that drip shields can function with high reliability as water diversion barriers for at least 10,000 years. Structural strength is needed so they can withstand rockfall (see Section 4.2.3). Drip shield degrada-



000500C\_ATP\_Z1542\_Fig 47.a

Figure 4-96. Relative Humidity in the Pilot-Scale Drip Shield Test without Backfill

This figure shows relative humidity measured at three locations in Canister Test #3. The blue curve shows relative humidity in the test cell outside the drip shield. The yellow and magenta curves show relative humidity at two locations in the air space between the drip shield and the simulated waste package. The relative humidity under the drip shield was substantially lower, and condensation was not observed there. The period of heating was terminated at approximately 48 days, and temperature returned to ambient values. Source: Modified from Howard et al. 2001, Figures 48 and 49.

tion from dislocation, deformation, and corrosion processes is the focus of ongoing analyses.

In the design described in this report, the drip shield sections will interlock to prevent separation between adjacent segments (see Figure 2-74 in Section 2.4.4.1). Interlocking will be accomplished by overlapping the specially designed ends of adjacent segments. Each segment will be lowered into place over the end of its predecessor. This will engage interlocking channels located on the top and sides of each segment. To separate the segments will require relative movement of approximately 1 m (3.3 ft) in the vertical direction, which is more than seismic ground motion or rockfall are likely to produce.

The interlocking design of the joint will include water diversion channels to capture and divert dripping water that may penetrate the joints between drip shield segments, so that the water runs downward to the invert rather than to the underside of the drip shield. The water diversion channels will also provide capillary breaks between adjacent diversion rings (Figure 2-74) so that water cannot wick into the joint as observed in the pilot-scale test. The interlocking joint design will prevent droplet flow and capillary flow for as long as the joints remain intact. The joints are designed to accommodate thermal expansion and seismic displacement (Figure 2-74). Joint stability under rockfall is currently being analyzed.

Significant structural strength is required so the drip shield can protect the waste package from

damage by rockfall. The drip shield will be designed to withstand damage from rocks up to several tons in size (CRWMS M&O 2000ap, Section 4.2.1.1, Table 3). The drip shield must also withstand static loads from rock debris due to collapse of the emplacement drift. Titanium Grade 7 will provide superior corrosion resistance for the drip skin, while Titanium Grade 24 will be used for internal bracing because of its greater strength (see Section 2.4.4).

The drip shield legs will rest on transverse steel support beams in the drift invert and will be set alongside longitudinal steel guide beams (see Section 2.4.4, Figures 2-71 and 2-72). These longitudinal guide beams will maintain the geometry of the pallet that supports the waste package and the drip shield, even when they are exposed to seismic shaking. The pallet will also be designed to restrain the waste package and prevent dislocation relative to the drip shield, when exposed to seismic shaking. The invert ballast will support and constrain the drip shield and waste package after the steel beams have failed from corrosion.

**Water Diversion by the Drip Shield and Waste Package**—Film flow will not provide a significant advective pathway for release of radionuclides, particularly through fine cracks or when the waste packages are warm. However, transport of radionuclides may occur by molecular diffusion in water films. Capillary flow and droplet flow will be negligible in fine cracks. The most likely cause of fine cracks is stress corrosion cracking, particularly around the waste package closure welds, but these cracks will probably be protected from dripping water by a skirt on the waste package. Capillary flow and droplet flow in the joint between drip shield segments has been considered in the drip shield joint design.

The drip shields are not expected to be penetrated by rockfall and will remain in place for 10,000 years. When drip shields or waste packages are eventually penetrated by general corrosion, capillary or droplet flow (where there is seepage) could transport water through breaches.

Conceptually, if seepage water leaks through the drip shield, only a portion of the water would actu-

ally contact the waste package, and it would be distributed over only a portion of the waste package area. Realistically, breaches in the waste package would capture water emanating from a co-located breach in the drip shield above. In other words the capture area should depend on the relative location of the breaches. Where multiple breaches occur in the drip shield or waste package, there would also be interference between them, limiting the total leakage.

**Flux Through the Drip Shield and Waste Package**—In the process model for water diversion by the drip shield, all seepage into the drift falls onto the crown of the drip shield (CRWMS M&O 2000a, Sections 3.6.1 and 3.6.2). Breaches in the drip shield intercept this flow and permit a fraction of the incoming seepage to flow through the drip shield (CRWMS M&O 2000a, Section 3.6.2.1). Fluid flux only occurs through drip shield patches, as pitting of the titanium drip shield does not occur in the modeled near-field geochemical environment. The remainder of the water flows directly down to the invert and then drains into the host rock.

The process model for water diversion by the waste package in the TSPA-SR model specifies that all water transmitted through the drip shield contacts the waste package (CRWMS M&O 2000a, Sections 3.6.1 and 3.6.2). Breaches in the waste package intercept this flow and permit a fraction of the incident water to flow into the waste package. Conceptually, continuous flow paths are assumed through breaches penetrating the waste package (i.e., patches and stress corrosion cracks). The fraction of water flowing into a waste package is the ratio of the summed axial length of the patch breaches in the waste package to the total length of the waste package. The remainder flows off the waste package, down to the invert, and then into the host rock.

The TSPA-SR model conservatively assumes no resistance to flow in the waste package. The model conservatively ignores a fundamental physical requirement for leakage to occur: breaches in the upper and lower areas of the waste package. This means through-flow is assumed possible through the waste package even with only penetration(s) on

the upper surface (CRWMS M&O 2000dd, Section 6.3.3).

Advection is modeled as the dominant transport process through any patches that form in the drip shield or waste package whenever there is an appreciable amount of water dripping (CRWMS M&O 2000a, Section 3.6.1.2). Diffusion will be the dominant transport process through fine cracks in the waste package so long as the drip shield remains functional. In both cases:

- WAPDEG output (i.e., timing and location of breaches) is used by the engineered barrier system flow abstraction to define the time-dependent fluxes that flow through (or are diverted around) the drip shield and the waste package (CRWMS M&O 2000a, Section 3.6.1.1)
- All of the seepage entering the drift falls on the crown of the drip shield. Conservatively, a patch at any axial location on the drip shield or waste package will collect fluid, even if the axial location of the drip and breach area do not coincide (CRWMS M&O 2000a, Section 3.6.2.1).

**Environment Under the Drip Shield**—Heat transfer between the waste package and drip shield and humidity under the drip shield are simulated using the multiscale thermal-hydrologic model (Section 4.2.2). Predicted relative humidity is less than 100 percent for most conditions that control the thermal-hydrologic response (rock properties, infiltration flux, thermal loading, and location). For certain conditions, some studies suggest that condensation under the drip shield may be possible (CRWMS M&O 2001c, Sections 6.3.3 and 6.4). Such conditions are limited to many thousands of years after closure, when cooldown has progressed and the temperature differences between engineered barrier system components (e.g., invert and drip shield) approach only a few degrees. At such late time, the thermal output of the waste and the potential for thermally driven condensation would be greatly reduced. In summary, the potential for condensate to drip from the underside of the drip shield is not included in the TSPA-SR model. This is based on TSPA-SR supporting calculations indi-

cating that either condensation would not occur or the effect would be inconsequential (CRWMS M&O 2000dd, Section 6.3.3; CRWMS M&O 2001c, Section 6.4; CRWMS M&O 2000cc, Section 6.4.6).

The chemical environment at the waste package surface will be slowly varying and predictable while the drip shields are intact. Dust derived from repository operations will be present on the waste package surface. Humidity conditions in the presence of dust may support microbially influenced corrosion activity, so for TSPA-SR the corrosion rate is conservatively increased to account for possible microbial activity (see Section 4.2.3). Once drip shield breach occurs, the chemical environment at the waste package surface will be similar to the environment on the drip shield surface.

**Water Drainage from the Emplacement Drifts**—Numerical modeling of drainage from the emplacement drifts, using extreme seepage, was performed to confirm the conditions that could lead to complete saturation of the invert. The hydrologic simulations were similar to the thermal-hydrologic models described in Section 4.2.2, except that heating was not applied for many of the calculations, and a sand backfill was included in the drift (CRWMS M&O 2001c, Section 6.2). These calculations are applicable to the design without backfill described in this report because drainage through the invert must occur in either case. The same hydrologic properties used in the unsaturated zone flow model for the host rock (as described in Section 4.2.1) were used, along with the same boundary conditions, except that the infiltration boundary condition was manipulated to simulate different values of extreme seepage (CRWMS M&O 2001c, Section 6.2).

The approach to drainage is to establish that there is sufficient drainage capacity throughout the potential repository to handle extreme seepage. The value of seepage flow used for this purpose is approximately 2,000 L (528 gal) per meter of drift, recurring once per year (CRWMS M&O 2000ab, System Performance Criterion 1.2.1.8). Such seepage can occur in only a small portion of the potential repository because the estimated future

infiltration flux will be less, even for the wettest conditions anticipated (see Section 4.2.1). This seepage value is several times greater than the maximum average percolation flux that is estimated to occur anywhere in the host rock for the glacial-transition climate state (CRWMS M&O 2000cf, Figure 6-48). In addition, the numerical simulations were two-dimensional, without provision for diversion of seepage inflow axially along the emplacement drifts to more permeable locations. Accordingly, the approach for evaluating drainage is conservative. The results nevertheless lead to a conclusion that sufficient drainage capacity exists or can be accommodated in design and construction of the emplacement drifts.

The effects of fracture plugging were investigated in the numerical models by setting fracture permeability to zero below the drift for a distance of 3 m (10 ft) from the opening. The most important result was further increase in liquid saturation in the invert and complete saturation given sufficient seepage flux. Drainage was still possible even with fractures plugged, such that the invert remained unsaturated up to a limiting value of the seepage flux.

In summary, model calculations show that the invert could become completely saturated only if the fracture permeability in the host rock is plugged, and seepage exceeds a threshold value. Complete saturation of the invert did not occur in the simulations, even with very high seepage rates, if the fracture permeability was unmodified.

#### **4.2.5.3.1 Limitations and Uncertainties**

As noted in Section 4.1.1.2, the DOE performed several activities to improve the treatment of uncertainty in certain TSPA-SR models. The following limitations and uncertainties have been assessed in supplemental TSPA model results as summarized in *FY01 Supplemental Science and Performance Analyses* (BSC 2001a, Section 15; BSC 2001b, Section 3.2.6). These include the following:

- **Evaporative Reduction of Seepage on the Drip Shield and Waste Package**—Evaporative reduction of the amount of water

contacting the drip shield and waste package is ignored in the TSPA-SR model. When accounted for in the model, supplemental TSPA model studies suggest a negligible effect (BSC 2001b, Section 3.2.6.1).

- **Geometrical Constraint in Flux into Waste Package**—In the TSPA-SR model, geometrical constraints on flux through the waste package (such as the coincidence of the axial locations of the breaches and the assumption that any breach is located so that it collects dripping fluid) are ignored. Supporting the conservatism of the TSPA-SR model, supplemental TSPA model studies implemented alternative assumptions and the representation of the fraction of water flowing through the waste package (BSC 2001b, Section 3.2.6.3).
- **Condensation under the Drip Shield**—Condensation under the drip shield as a source for additional water on the waste package is reevaluated in supplemental TSPA model studies. The results corroborate the approach used in the TSPA-SR model (BSC 2001b, Section 3.2.6.2).
- **Bathtub Model for the Waste Package**—Inundation of the waste package, caused by considering the timing of breaches on the top and bottom of the container, result in short-term releases and a negligible, short-term effect on performance (BSC 2001b, Section 3.2.6.4).

**Water Diversion Performance of the Drip Shield**—Water diversion performance of the drip shield design, and resistance to dislocation by rockfall and seismic motion, are based on design criteria (CRWMS M&O 2000ab, Section 1.2). Consistency with many of these criteria has been evaluated, and some confirmatory testing has been performed (Section 4.2.5.2).

**Environment Under the Drip Shield**—As stated above, supplemental studies have addressed uncertainties pertaining to the potential for condensation under the drip shield. The reevaluation supports the TSPA-SR approach. Fundamentally, the effect

remains negligible in the nominal scenario because the waste packages do not fail in the period when evaporation might be important (BSC 2001b, Section 3.2.6.2).

**Water Drainage from the Emplacement Drifts**—The uncertainties in the calculation of seepage entering drifts is addressed in Section 4.2.1.4.2 and Table 4-14. However, 2,000 liters per meter of drift assumed in this analysis exceeds the maximum value in Table 4-14. Site characterization data, such as permeability testing in boreholes, does indicate that the drainage capacity of the drift floor is sufficient to ensure free drainage from the drifts.

#### 4.2.5.3.2 Alternative Conceptual Processes

**Water Diversion Performance of the Drip Shield**—The rate of seepage inflow may vary with time and location, driven by episodic hydrologic conditions or changes in properties of the host rock (CRWMS M&O 2000by, Section 6.3). At locations where seepage occurs, dripping could occur at a point, then move around to other points as time passes. If there is a breach in the drip shield at such a location, seepage may flow through directly or may be diverted to another part of the drip shield. Such behavior will be random and is accommodated by associating the model results with the average response of multiple breached drip shields to seepage. The maximum and minimum rates of flow through a single breach are not represented, but the average behavior overall is represented. A similar argument applies to modeling of flow through breaches in the waste package. Such an approach has been implemented in supplemental TSPA model studies to quantify conservatism (BSC 2001b, Section 3.2.6.3).

**Environment Under the Drip Shield**—The chemical environment on the surface of the waste package under an intact drip shield may not support microbially influenced corrosion, as conservatively assumed. The overall rate of microbial activity is known to be limited by the availability of water, nutrients, and energy sources (CRWMS M&O 2000cg, Section 6.4). Water could be provided by humidity on the waste package surface, and energy could be provided by the waste

package outer barrier material, but nutrients will be very scarce under intact drip shields. The available phosphorus and other nutrients will be limited to what may accumulate in the form of dust on the waste package surface during preclosure operations.

**Water Drainage from the Emplacement Drifts**—Modeling described in Section 4.2.3 has shown that fracture plugging in the host rock from thermal-hydrologic-chemical processes (i.e., chemical precipitation) is unlikely to significantly affect host rock hydrologic properties. However, those results did not include the potential effects of fines migration within the engineered barrier system and thermal-mechanical loading of the host rock. Also, if there is seepage during the thermal pulse and the invert is the last part of the engineered barrier system to cool (as indicated by models described in Section 4.2.2), then precipitates and salts could accumulate near the drift floor. As stated previously (Section 4.2.5.3), the combination of excess drainage capacity in the host rock, plus the possibility of axial flow in the drifts in response to localized extreme seepage, support a conclusion that complete saturation of the invert in the emplacement drifts will not be important to waste isolation performance.

#### 4.2.5.3.3 Model Calibration and Validation

Modeling has been conducted to evaluate water diversion by the drip shield and the potential for condensation under the drip shield (CRWMS M&O 2001c, Section 6.3.3; CRWMS M&O 2000dd, Section 6.4; CRWMS M&O 2000cc, Section 6.4.6). Bounding models are useful where complex phenomena limit modeling approaches, for example, in assuming that all seepage falls as drops and that all water which flows through breached drip shields contacts the underlying waste packages. Model validation for water diversion models is addressed using a combination of bounding approaches and preliminary results from pilot-scale testing. When engineered barrier system pilot-scale testing results become available, this quantitative test data can be compared to predicted model results using NUFT to provide full validation of the model (CRWMS M&O 2001c, Section 6.2.7).

#### 4.2.5.4 Total System Performance Assessment Abstraction

The water diversion model described in the TSPA-SR model identifies eight key flow pathways used in the TSPA-SR abstraction for water diversion for use in engineered barrier system transport models (CRWMS M&O 2000a, Section 3.6.2.1):

- **Seepage Flux Entering the Drift**—This water may be flowing or dripping slowly through the engineered barrier system. Alternatively, this water may form a continuous film of stationary liquid.
- **Flow through the Drip Shield**—Fluid flux through the drip shield begins once patches form due to general corrosion.
- **Flow Diversion around the Drip Shield**—The portion of the flux that does not flow through the drip shield is assumed to bypass the invert and flow directly into the unsaturated zone.
- **Flow through the Waste Package**—Fluid flow through the waste package does not occur until the drip shield failures begin and patch breaches occur in the waste package. Leakage of liquid water through stress corrosion cracks in the waste package is considered negligible because these cracks will be so fine that leakage will not occur by capillary flow or droplet flow. Diffusion of radionuclides through such cracks is included in transport models. There is no assumed locational correspondence between breaches in the drip shield and waste package because corrosion of the different barriers is initiated under different environmental conditions. Microbially influenced corrosion of waste packages is initiated when humidity conditions permit, even under intact drip shields (CRWMS M&O 2000cg, Section 6.4).
- **Flow Diversion around the Waste Package**—The portion of the flux that does not flow into the waste package is assumed to

bypass the waste form and flow directly to the invert.

- **Evaporation from the Invert**—The magnitude of the evaporative flux from the invert is based on the thermal-hydraulic abstraction (CRWMS M&O 2000cc). Condensation as a source for dripping on the waste package is neglected based on supporting studies (see Section 4.2.5.3).
- **Flow from the Waste Package to the Invert**—All flux from the waste package flows to the invert, independent of the breach location on the waste package. The presence of the emplacement pallet is ignored, and the waste package is assumed to be lying on the invert so that a continuous liquid pathway for diffusive transport exists at all times.
- **Flow through the Invert into the Unsaturated Zone**—All fluid and mass flux into the invert is immediately released into the unsaturated zone.

Uncertainties in abstraction inputs were accommodated in general by using bounding values and building conservatism into the models. In this way, it is believed that significant uncertainties have been adequately accounted for in the TSPA calculations in *Total System Performance Assessment for the Site Recommendation* (CRWMS M&O 2000a). This has been confirmed in supplemental work (see Section 4.2.5).

**Exclusion of Drainage Effects from the Total System Performance Assessment**—From the foregoing discussion, the invert will not be completely saturated unless there is extreme seepage and fracture plugging. Extreme seepage on the order of 1,000 mm/yr (39 in./yr) is extremely unlikely, and although useful for design criteria, such seepage is not included in the performance assessment. The calculations described above have shown that complete saturation of the invert will not occur unless both extreme seepage and fracture plugging occur. Therefore, complete saturation of the invert is screened out as a process that requires explicit representation in the TSPA-SR due to its low probability. In conjunction with this approach,



each of the modeled processes, limitations and uncertainties of using the developed models, alternative conceptual processes, and model calibration and validation are discussed. The TSPA abstractions are presented in Section 4.2.6.4.

As noted in Section 4.1.4, the DOE has evaluated operation of the repository at lower temperatures. The conceptual basis and model abstractions presented in this section primarily reflect the effects of higher-temperature operating modes, specifically those implemented in *Total System Performance Assessment for the Site Recommendation* (CRWMS M&O 2000a, Section 3.5). Alternative thermal operating modes and/or conservatisms and conceptual uncertainties have been reevaluated since the TSPA-SR model and are reported or summarized in *FY01 Supplemental Science and Performance Analyses* (BSC 2001a, Section 9; BSC 2001b, Sections 3 and 4).

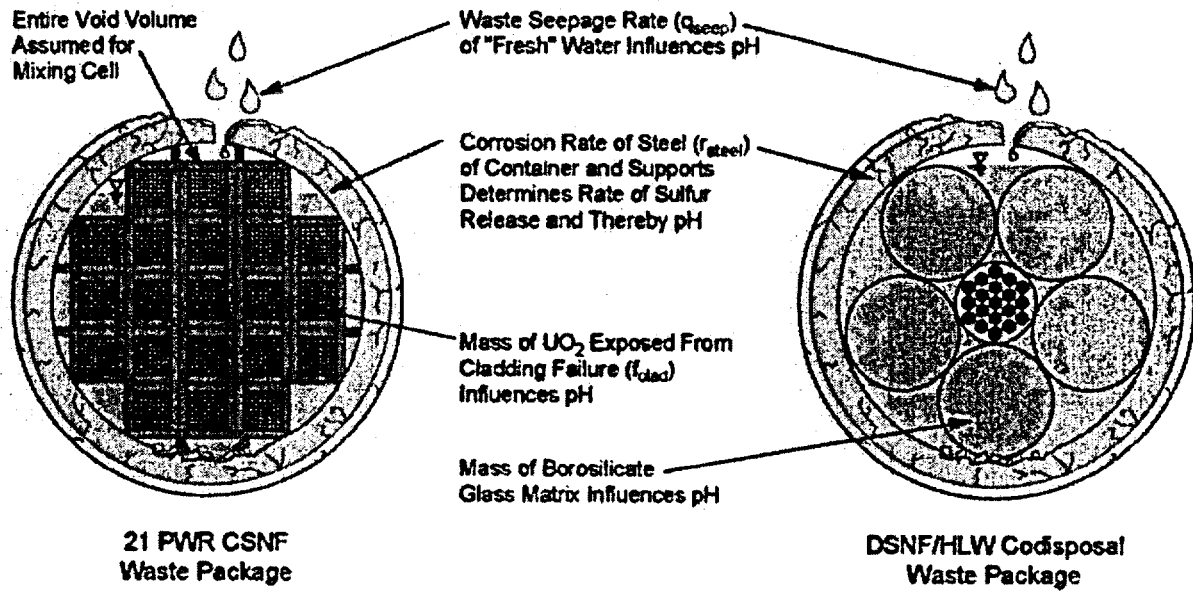
#### 4.2.6.1 Conceptual Basis

Radionuclide release from the waste forms is a three-step process requiring (1) degradation of the waste forms, (2) mobilization of the radionuclides from the degraded waste forms, and (3) transport of the radionuclides away from the waste forms. Water strongly influences all three processes. The release of specific isotopes may be limited in any step. The release of insoluble elements such as plutonium is usually limited by the mobilization step. The solubility and colloid stability of plutonium is so low that it remains with the waste form degradation products unless large flow rates flush it away. The opposite is true for technetium, which is quite soluble in an oxidizing environment. Technetium release is usually limited only when the waste form degradation rate or technetium inventory is very low, or when there is not enough water for effective diffusive transport. Water flow and radionuclide transport are discussed in Sections 4.2.5 and 4.2.7. This section focuses on the degradation and mobilization processes, their interactions, and the controls they exert on radionuclide release.

Waste form degradation and radionuclide mobilization are part of a highly coupled thermal-hydrologic-chemical system that may follow many

scenarios. An overall description of the processes that may occur is provided here, followed by a summary of the testing that has led to this conceptualization in Section 4.2.6.2.

**Water Contact and Chemistry**—Radionuclide release begins after breach of the waste package and the ingress of air. If the breach is early, the waste may still be highly radioactive and physically hot. The thermal output of hot waste packages, particularly from commercial spent nuclear fuel, will limit groundwater access at early times. When water enters the package, the rate of water inflow and evaporation will determine when and if water accumulates. During this period, gamma radiolysis of the humid air within the package may cause production of nitric acid, which could condense into any accumulated water. If the breach is late, radiation levels and heat will be much lower, and evaporation and radiolytic acid production will be less important. During either period, water may enter the package either as water vapor or as flowing groundwater. The groundwater species entering the package may have a significant effect on in-package chemistry only if evaporation has concentrated them by orders of magnitude. This is unlikely to occur unless the waste package is breached only at the top, and large amounts of water enter and evaporate within the package (Figure 4-98). During this period, there is no water transport of groundwater species or radionuclides out of the package. If the package overflows, or if holes in the bottom allow flow-through, fresh groundwater will dilute the groundwater components, and water-based radionuclide releases may begin. Chemistry within the package is important because it influences the rate of degradation of the package and waste forms (including cladding), and it determines the mobility of radionuclides as dissolved or colloidal species. Films of stagnant, concentrated, acidified groundwater are considered the worst possible scenario for degradation because they do not inhibit oxygen and carbon dioxide transport and may support localized corrosion of the cladding and waste. Such films, however, do not support significant mobilization and transport of radionuclides, and are only possible at times when there is an exact balance of water inflow and evaporation.



Drawing Not To Scale  
000500C-ATP-21642-171 a

Figure 4-98. Conceptual Model of In-Package Chemistry

DSNF = DOE spent nuclear fuel; HLW = high-level radioactive waste; CSNF = commercial spent nuclear fuel.  
Source: CRWMS M&O 2000bm, Figure 3.2-1.

**Cladding Degradation**—The release of radionuclides does not begin until after the breach of the cladding (for spent fuel). Stainless steel cladding is expected to be susceptible to stress corrosion cracking and therefore cannot be relied upon for long term protection. Some spent fuels, such as N Reactor, have high fractions of damaged cladding, so little protection is expected. Most commercial spent fuel, however, will have intact Zircaloy cladding at the time of emplacement. Zircaloy is a highly corrosion resistant material that is expected to provide significant protection of the waste. The mechanisms that may initially fail Zircaloy produce small flaws such as pinholes or cracks. These mechanisms include ones that are expected only in-reactor (fretting, baffle-jetting) and those that may occur after reactor operation (creep, hydride reorientation, earthquake damage). Under some circumstances, the initial flaw may propagate, splitting open the cladding. This has been rarely observed in reactors, due to hydride effects, and during exposure to hot air due to oxidation and swelling of the fuel.

**Waste Form Degradation**—There are many waste form types that may be emplaced within a repository, but most of them are thermodynamically unstable under moist, oxidizing conditions. Uranium dioxide fuels will oxidize and hydrate; glass waste forms will react with water and form clays, zeolites, and oxides; and all but a few of the over 250 DOE spent fuel types will undergo similar reactions. The rate of these reactions, however, will in most cases be quite slow and may be limited by the rate that reactants such as oxygen and water can be transported to the waste form surface. Although a few radionuclides such as cesium and iodine may concentrate between the fuel and cladding during reactor operation, most of the radionuclides will be tied up within the various waste forms and cannot be released from the waste package until the waste forms degrade.

**Radionuclide Mobilization**—Once the waste form degrades, radionuclides may be mobilized in flowing or diffusing water. Water-mobilized radionuclides include dissolved species and suspended particles (Figure 4-99). Larger suspended particles

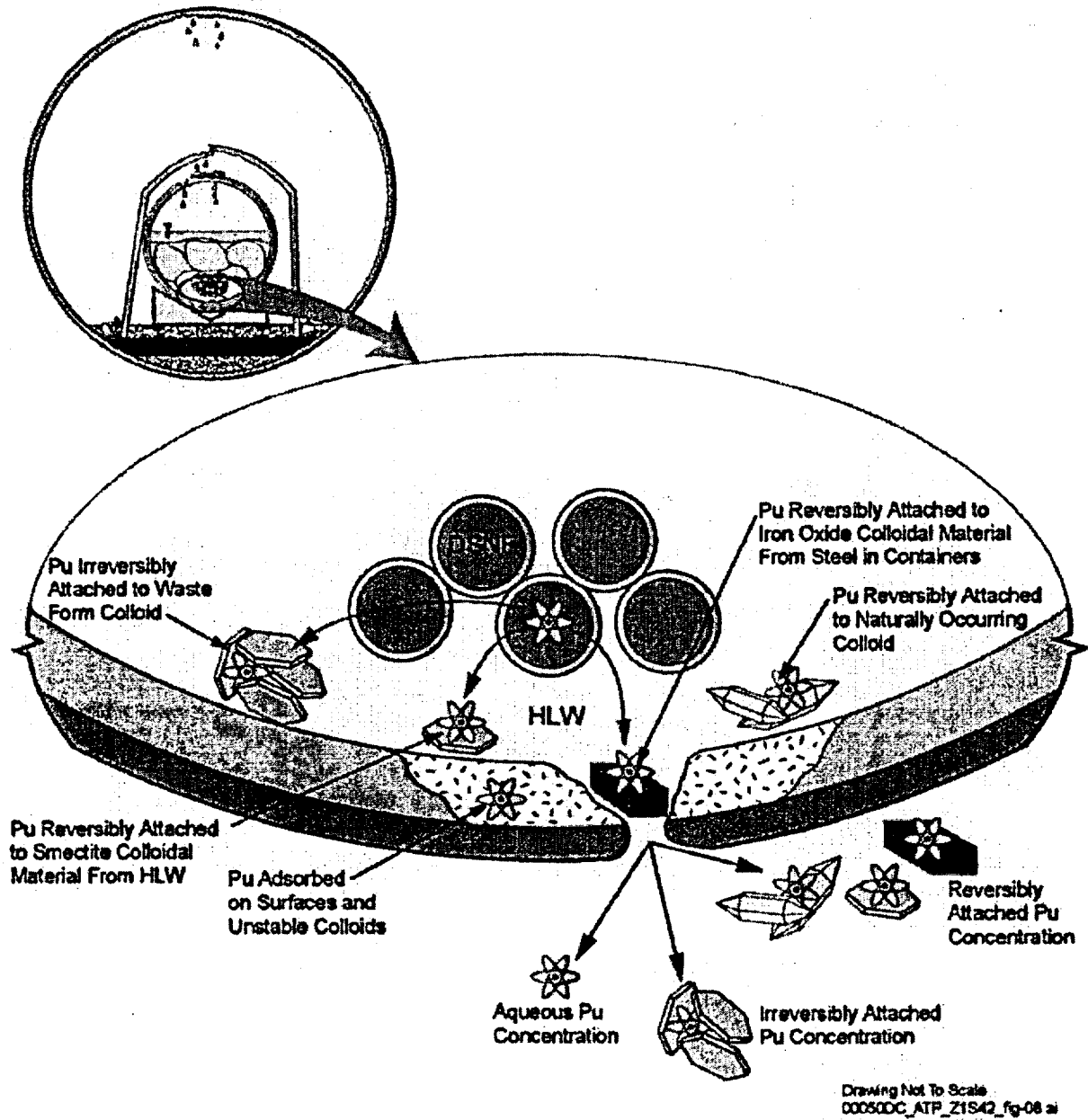


Figure 4-99. Conceptual Model of the Formation of Reversibly and Irreversibly Attached Radionuclides on Colloids

DSNF = DOE spent nuclear fuel; HLW = high-level radioactive waste. Source: CRWMS M&O 2000bm, Figure 3.8-1.

quickly settle out of solution or are trapped in small openings. Only after gross failure of the package would these larger particles fall or wash out of the package. Particles in the colloid size range, however, can remain suspended by Brownian forces and may travel significant distances. The concentration of radionuclides associated with colloids is limited by the colloid concentration and radionuclide carrying capacity of the colloids. The concentration of dissolved species is limited by the elemental solubility of the radionuclide within the local environment.

#### 4.2.6.2 Summary State of Knowledge

This section discusses the testing done to elucidate the degradation and mobilization processes for commercial light water reactor spent nuclear fuel, DOE spent nuclear fuel, and other high-level radioactive waste encased in borosilicate glass or ceramics. The work briefly summarized below is presented in more detail in *Waste Form Degradation Process Model Report* (CRWMS M&O 2000bm) and fully discussed in the analyses and models reports referenced therein. The tests identify degradation and mobilization mechanisms, as well as inputs for predictive models as described in Section 4.2.6.3.

##### 4.2.6.2.1 Inventory Characterization Tests

The radionuclide inventory of commercial spent nuclear fuel depends upon the initial enrichment of uranium-235 and burnup. Burnup is determined by the total neutron fluence to which the fuel was subjected and thus depends on both the total time the fuel is in the reactor and the location of the fuel within the core during its irradiation history. The burnup of a given rod varies both axially and radially, with the highest burnup at the central height and at the fuel pellet periphery. Modern core management techniques allow for a fairly uniform axial burnup profile, the exception being at the ends of the rods.

The fuels used in waste form tests have been extensively characterized prior to testing (Guenther, Blahnik, Jenquin et al. 1991; Guenther, Blahnik, Campbell, Jenquin, Mendel, and Thornhill 1988; Guenther, Blahnik, Campbell, Jenquin, Mendel,

Thomas, and Thornhill 1988, 1991). This characterization includes electron and optical microscopy (scanning electron microscopy, transmission electron microscopy, ceramography), X-ray diffraction, and, most importantly, radionuclide inventory determination. The burnup and inventory determination procedures follow the approved radiochemical and analytical methods in appropriate American Society for Testing and Materials standards. These procedures are well developed and have validated the codes used to predict burnup and inventory.

##### 4.2.6.2.2 In-Package Chemistry Tests

Most testing relevant to in-package chemistry has considered the role of heat and the interaction of water chemistry and waste form degradation, although recent testing has also included interaction of water with drift gases, waste package materials, and engineered barrier system materials (see Sections 4.2.2 through 4.2.4). The tests with waste forms and radionuclides are summarized in Sections 4.2.6.2.3 through 4.2.6.2.7.

##### 4.2.6.2.3 Cladding Degradation Tests

Zirconium was initially used in the chemical industry to handle extremely corrosive liquids and gasses. The experimental bases for this are discussed by Yau and Webster (1987). Zirconium alloy (Zircaloy) was introduced as a nuclear fuel cladding material in the late 1950s because of its corrosion resistance and neutron absorption characteristics. Extensive research has been continuous since that time as the nuclear industry has been driven to limit fuel defects and increase fuel longevity. Cladding degradation tests are published at regular intervals in publications such as *Zirconium in the Nuclear Industry* (published by the American Society for Testing and Materials every two and a half years), *Proceedings of the International Topical Meeting on Light Water Reactor Fuel Performance* (published by the American Nuclear Society every 3 years), and *Journal of Nuclear Materials* (published monthly by Elsevier Science), as well as in many other publications. As an example of the extent of data available, an International Atomic Energy Agency document summarizing waterside corrosion cites 538 sources

on corrosion (IAEA 1998, pp. 281 to 309). The TSPA-SR cladding degradation model is based on cladding tests reported in the open literature, as well as data collected specifically for the Yucca Mountain Project. These include tests used to generate the cladding characteristics as it is received at Yucca Mountain (CRWMS M&O 2000de), corrosion tests (CRWMS M&O 2000df), experiments on hydride effects in cladding (CRWMS M&O 2000dg), tests on wet and dry splitting of cladding (CRWMS M&O 2000dh; CRWMS M&O 2000di), and experiments on creep failures (CRWMS M&O 2000dj). In addition, there is an active dry storage testing program in Europe that is generating additional data on cladding behavior under conditions very similar to the early phases of repository placement.

#### 4.2.6.2.4 Commercial Spent Nuclear Fuel Degradation Tests

Many tests have been performed to evaluate the mechanism and rate of degradation of commercial spent nuclear fuel under various conditions. These tests are summarized in *CSNF Waste Form Degradation: Summary Abstraction* (CRWMS M&O 2000dk). These include: oxidation tests, batch tests, unsaturated drip tests, vapor phase tests, electrochemical tests, and flow-through tests.

**Oxidation Tests**—Hot oxidation testing of spent fuel and uranium dioxide fragments has been done for over 40 years and is summarized in *Clad Degradation—Dry Unzipping* (CRWMS M&O 2000di). Tests have been conducted from about 200° to 360°C (390° to 680°F) using either dry baths or thermogravimetric apparatus. These tests demonstrate the influence of fuel characteristics (e.g., fission gas release, burnup, fuel type) and atmospheric variables (e.g., moisture content or radiation field) on oxidation rates and mechanisms. Results obtained by the project and those from outside laboratories are very similar, which has permitted the development of oxidation models for spent fuel and uranium dioxide. Results indicate that the oxidation rate is very temperature-dependent and too slow to be significant at temperatures expected when waste packages breach.

**Batch Tests**—Immersion tests were performed on segments of spent fuel rods, as well as unclad fuel particles, in both deionized water and J-13 well water. The fuel rod segments were fitted with watertight end fittings. Small holes were laser-drilled through the cladding of one, a slit was machined in one, and another was tested intact. In a fourth experiment, unclad fuel particles removed from the cladding plus the cladding hull sections were immersed. The tests were semi-static in that they were run for several months, solutions removed and analyzed, and the vessel walls were acid stripped to recover any deposited radionuclides. Tests were performed at both 25° and 85°C (77° and 185°F). These tests showed that secondary phases form on the surface of the reacting fuel, colloidal sized particles form in solution, the concentration of most dissolved actinides remained quite low, and the release rate of actinides is much higher from unclad fuel than from defected clad fuel.

**Unsaturated Drip Tests**—To simulate dripping under repository conditions, small samples of spent nuclear fuel fragments were held within Zircaloy or stainless steel cups with screens on both ends. The cups were held within the top of a sealed stainless steel autoclave-like vessel, and water was dripped over the samples at controlled rates and collected in a catch basin below. The tests were performed at 90°C (194°F) to maximize the reaction rates, and J-13 water was equilibrated with tuff rock at 90°C (194°F) prior to use. Both low and high drip rate tests were conducted to cover a range of possible repository dripping rates. Solutions from the bottom of the test vessels were collected and analyzed about every six months for both dissolved and colloidal materials. In addition, small samples of the reacted fuel were removed for detailed analysis. Tests on several different fuels, as well as uranium dioxide fragments, have been ongoing since 1992. These tests have provided information on the forward dissolution rates, chemistry of water interacting with fuel, the sequence of alteration products, and concentrations of dissolved and colloidal species under dripping conditions. The alteration phases are similar to those observed in the corrosion of natural uraninite deposits, indicating that the experimental results are indeed relevant to long-term behavior.

**Vapor Phase Tests**—The configuration for the vapor phase tests was similar to the unsaturated drip tests and was designed to study the degradation of fuel that is not directly contacted by flowing water but exposed to 100 percent relative humidity. Small amounts of water were introduced into the collection basin of the vessels, which were placed in ovens and heated to the test temperatures, usually around 200°C (390°F) to accelerate the reactions. The water evaporated from the collection basin and condensed on the waste forms. Alteration of the test samples and transport of radionuclides to the collection basin was observed, although much less than in the drip tests. It is believed that thin-film flow and waste form and secondary product spallation were the mechanisms of transport.

**Electrochemical Tests**—Electrochemical tests with spent nuclear fuel are similar in concept to tests performed with metallic materials. An electrochemical cell is established between a corroding electrode (a spent fuel or uranium dioxide pellet) and a noncorroding (e.g., platinum) electrode in an electrolyte, under an impressed voltage. The current passed between the electrodes is measured over time. This information can then be utilized to establish the oxidation state of the spent fuel or uranium dioxide surface and the dissolution rate as a function of the voltage and water chemistry in relatively short-term experiments. These tests shed light on the dissolution process and provide the basis for understanding aqueous attack of these materials.

**Flow-Through Tests**—Flow-through tests were designed to measure the fundamental spent fuel dissolution/oxidation rates. Under the stagnant or slow flowing conditions of the other tests, secondary phases precipitate on the surface of the reacting fuel, which complicates the interpretation of results. In flow-through tests, the water is flowed over the reacting surfaces fast enough to prevent saturation and precipitation of secondary minerals. These tests provide the fundamental forward dissolution rate at the given tests conditions. These tests were performed on many fuel types (burnup 0 through 70 GWd/MTHM), at many laboratories, under many conditions (21° to 75°C [70° to 167°F], pH of 3 to 10, various carbon

dioxide and oxygen pressures). These tests have provided the mechanistic and empirical basis for the fuel dissolution rate model.

From the many experiments performed (CRWMS M&O 2000dk), an understanding of the mechanisms of spent nuclear fuel dissolution has emerged. Commercial nuclear fuel is composed primarily of uranium dioxide which, when exposed to mildly oxidizing solutions, is oxidatively dissolved to uranyl ion,  $UO_2^{2+}$ . The rate of uranium dioxide oxidation depends on the interaction of specific surface species that control the rate-determining dissolution step. The increase in commercial spent nuclear fuel degradation rates with decreasing pH (at low pH), and with increasing carbonate levels (at high pH), suggests that adsorbed protons and/or carbonate ions control the dissolution reaction under flow-through conditions. Important aqueous species that might also affect dissolution rates are calcium and silicon ions, which can form stable corrosion products possessing low solubilities.

#### 4.2.6.2.5 Tests on Vitrified High-Level Radioactive Waste

High-level waste glass currently being tested includes mock and real radioactive glasses from the Savannah River (South Carolina) Technology Center and the West Valley (New York) Demonstration Program. Glass compositions corresponding to those expected from the Hanford Site high-level waste glass program will be tested when they become available. Because glass degradation is quite slow, various methods have been used to elucidate mechanisms and rates under fully saturated conditions:

- Testing at elevated temperatures, which accelerates reaction rates
- Testing at high surface-area-to-volume ratios, which accelerate rates proportionally to the exposed surface area of the glass
- Flow-through tests and closed-system tests.

Like the flow-through tests of spent nuclear fuel, the glass flow-through tests were designed to

prevent secondary phase formation and measure the forward dissolution rate over a range of conditions that bounded anticipated repository conditions (CRWMS M&O 2000dl).

Parallel efforts have also been undertaken to better calibrate glass dissolution mechanisms. The results of standard static leaching tests based on ASTM C 1220-98, *Standard Test Method for Static Leaching of Monolithic Waste Forms for Disposal of Radioactive Waste*, have been compared to the measurements of glass surface chemistry to link glass surface chemistry and dissolution mechanisms. Measured dissolution rates have been compared against long-term glass degradation rates measured on geologic samples. Lastly, two types of nonsaturated glass degradation experiments were done to examine degradation under conditions that might exist upon waste package breach: drip tests and vapor hydration degradation.

#### 4.2.6.2.6 Tests on U.S. Department of Energy Spent Nuclear Fuel and Other Waste Forms

The National Spent Nuclear Fuel Program has been conducting degradation testing on several of the DOE spent fuel types. To date partial test results are available only on N Reactor and uranium-aluminum spent nuclear fuel, but testing on mixed-oxide spent nuclear fuel is also underway. The preliminary N Reactor spent nuclear fuel results indicated that dissolution rates were significantly faster than that of commercial spent nuclear fuel and high-level waste glass, whereas the uranium-aluminum spent nuclear fuel showed dissolution rates lower than for the commercial spent nuclear fuel and high-level radioactive waste glass. Differences could also exist in neptunium solubility, colloid formation, and radionuclide transport through and out of the engineered barrier system. However, for the TSPA-SR, bounding values have been used. Details of this analysis are provided in Section 4.2.6.3.

#### 4.2.6.2.7 Solubility Tests

The solubilities of a number of radionuclide-bearing solids were measured as a function of fluid composition and temperature. These measurements

were used to update thermodynamic databases describing radionuclide stabilities. This in turn involved performing critical reviews of the thermochemical literature and reliance on international efforts (e.g., the Nuclear Energy Agency of the Organization for Economic Cooperation and Development) to develop internally consistent thermodynamic databases.

**Uranium**—Uranyl ( $\text{UO}_2^{2+}$ ) minerals are expected to precipitate under the oxidizing conditions likely to prevail when breached waste packages are initially altered by incoming fluids. Laboratory experiments and field observations suggest that the most common secondary uranyl minerals to form at low temperatures are schoepite, soddyite, uranophane, and/or sodium boltwoodite.

**Neptunium**—Neptunium solubilities in Yucca Mountain waters as a function of pH and temperature have been described by Nitsche et al. (1993). Efurd et al. (1998) measured neptunium solubilities up to approximately pH 8 in carbonate-containing media and up to approximately pH 12 in carbonate-free systems. Results of the neptunium solubility experiments from both over- and under-saturation were found to converge to approximately the same steady-state concentrations. With increasing temperature, a slight decrease in solubility is observed at pH 7 and 8.5, while at pH 6 the neptunium solubility remains approximately constant. The soluble neptunium concentrations are similar at pH 7 and 8.5, while at pH 6 the solubility is about one to two orders higher depending on the temperature. Note that although neptunium dioxide is expected to be the most stable neptunium-bearing phase, it has only rarely been observed to precipitate in laboratory experiments, presumably because kinetic obstacles prevent its nucleation and growth over short periods of time.

**Plutonium**—Plutonium solubility was studied by Efurd et al. (1998) only from oversaturation. In general, plutonium is about three orders of magnitude less soluble than neptunium, and pH does not affect the soluble concentration as much as seen in the neptunium solubility studies. Increasing temperature decreases the plutonium solubility below  $10^{-8}$  mol/L. The plutonium concentrations at 60°C (140°F) and 90°C (194°F) are pH indepen-

dent, while at 25°C (77°F) they show higher variability. The plutonium precipitates were dark green in color, which is characteristic of plutonium (IV) solid phases, and plutonium hydroxides and/or plutonium colloids, aging toward  $\text{PuO}_2 \cdot x\text{H}_2\text{O}$ , are interpreted to be the solubility-controlling solids. Since the crystalline phase forms within the laboratory time scale, it is reasonable to assume that over geological time, plutonium hydroxides will convert to plutonium dioxide. However,  $\alpha$ -decay of plutonium isotopes has been observed to decrease the crystallinity of plutonium dioxide, while at the same time plutonium hydroxide can gradually convert to anhydrous, though poorly crystalline, material.

**Americium, Actinium, Curium, Samarium**—Nitsche et al. (1993) showed that  $\text{AmOHCO}_3$  precipitates from J-13 water at a pH range from 5.9 to 8.4, and temperatures from 25° to 90°C (77° to 194°F), and is therefore the most likely phase to control americium solubility. Additional americium thermodynamic data has been developed by the Nuclear Energy Agency.

**Technetium, Carbon, Chlorine, Iodine, Cesium, and Strontium**—Under the conservative assumption of oxidizing repository conditions, laboratory measurements and thermodynamic analysis indicate that no insoluble salts of technetium, chlorine, iodine, or cesium form. Each forms relatively large monovalent ions in solution that are exceedingly soluble. Therefore, the solubility of each is set to 1.0 mol/L, which will let the waste inventory control their respective release. Carbon and strontium both form less soluble metal carbonate minerals—either pure-phase or solid solution. An involved prediction of carbon and strontium solubility was not done. Instead, the solubility for each was set to 1.0 mol/L, which will let the waste inventory control release.

#### 4.2.6.2.8 Colloid Tests

Colloid testing has focused on spallation (i.e., flaking) of colloids from glass, the stability and abundance of smectite colloids, and sorptive uptake and release of actinides from colloidal material. Long-term tests done with high-level waste glass (CRWMS M&O 2000dl) indicate that

colloids are produced through spallation of altered glass at the glass-water interface. The colloids are primarily smectite clay that contain discrete radionuclide-bearing phases incorporated (“entrained”) into the clay. Some iron silicate colloids are also observed. Several entrained actinide and rare earth-containing phases were identified, including brockite (thorium calcium orthophosphate) and an amorphous thorium-titanium-iron silicate similar to thorutite. Uranium was detected within the clays and iron silicates in some samples.

The entrained phases are often engulfed in a smectite clay substrate, and the properties of the latter are such that the entrained phases are expected to destabilize only at pH of about 2. Since a pH this low is not anticipated in the repository, smectite colloids are expected to remain stable under repository conditions. Smectite colloids become increasingly sensitive to ionic strength as pH drops below about 8 (Tombacz et al. 1990).

During static glass dissolution tests, colloids developed and increased in concentration with time up to a point where the colloid concentration reached a maximum and then became unstable. This was attributed to the ionic strength increasing to a threshold above which the colloids precipitated and agglomerated. These data provide an experimental basis for evaluating the ionic strength regimes in which the waste form colloids are stable or unstable.

Sorption of plutonium (IV) and plutonium (V) onto colloidal dispersions of hematite, goethite, montmorillonite, and silica was measured over time periods of 4 to 10 days. Information on americium (III) was also collected for the same minerals—except goethite. The observed ranges of the adsorption coefficients ( $K_d$ ) are generally consistent with those found in the literature. Experimental evidence from plutonium sorption experiments (CRWMS M&O 2000cn, Section 6.1.3) with colloidal hematite and goethite show that the rate of desorption (backward rate) of plutonium is significantly slower than the rate of sorption (forward rate). More importantly, over a significant time period (up to 150 days in some experiments), the extents of desorption is somewhat less than the extent of sorption.

Groundwater colloids may include those already present in the geosphere, such as microbes, organic macromolecules (humic substances, including humic and fulvic acids), and mineral colloids (primarily clay minerals, silica, and iron-oxide or iron-hydroxide minerals). Microbe-facilitated radionuclide transport is disregarded because the relatively large size of microbes makes them susceptible to filtration. Experimental studies indicate that Yucca Mountain humics possess a very low complexation capability. Mineral colloids present at the site are assumed to consist of smectite clays, which are fairly strong sorbers.

#### 4.2.6.3 Process Models

This section provides a description of the individual process models and the interfaces between them. It builds upon the overall concepts described in Section 4.2.6.1 and the summary state of knowledge given in Section 4.2.6.2. The components of the waste form degradation model are shown in Figure 4-97. The inputs to the waste form degradation models include the waste package design and the drift environment as a function of time.

##### 4.2.6.3.1 Inventory Modeling

In TSPA modeling of repository performance, it is important to have good estimates of the initial inventory for all radioisotopes important to human dose. These estimates are provided by the fuel and waste generators using records of reactor and reprocessing operations, burnup calculations and experimental validation of calculations.

Fuel burnup at any location along a fuel rod can be accurately calculated using complex, multidimensional neutronics codes. Simpler and more general calculations of burnup and inventory are performed using the ORIGEN (ORIGEN, ORIGEN-2, and ORIGEN-S) code, which uses experimental data to develop burnup-dependent neutron cross sections. ORIGEN is used to compute time-dependent concentrations of numerous radionuclides that are both generated and depleted through neutronic transmutation, fission, and radioactive decay. ORIGEN is a point depletion (i.e., no spatial dependence) model where the neutron cross section data and spectral parameters are averaged

over the spatial region of interest, making these codes valuable for rod- or assembly-average inventory calculations.

Validation of the ORIGEN codes within the limiting conditions (burnup, enrichment, etc.) of each neutron cross section library has been performed by comparing the code output with both project-generated and literature data. Results are usually well within 10 percent for measured fuel actinide and fission product data; some of the higher-order actinides have predicted results that differ by 15 to 25 percent with measured results (Parks 1992). Larger discrepancies for the radionuclides of importance to the repository are most often explained by large analytic uncertainties or sample preparation. ORIGEN has been shown to predict radionuclide inventories with reasonable accuracy. Continuing verification of additional approved test materials with predictions is performed whenever a new fuel is subjected to testing.

##### 4.2.6.3.2 In-Package Chemistry Model

Outputs of the in-package chemistry model, such as pH and ionic strength, are used as inputs by several other models (see Figure 4-97) that describe processes that depend on the chemistry of in-package fluids. The latter include the degradation of cladding, the degradation of the matrix of the waste forms, the dissolved concentration of radioisotopes, and the stability of colloids. The in-package chemistry model is summarized in *Waste Form Degradation Process Model Report* (CRWMS M&O 2000bm) and described in detail in *Summary of In-Package Chemistry for Waste Forms* (CRWMS M&O 2000dm).

The in-package chemistry model component estimates over time the fluid chemistry inside the waste package after the initial breach of the waste package. In-drift solutions seeping into breached waste packages would contact several materials whose reaction rates and effective reaction surface areas are imprecisely known (see Figure 4-98). These materials include waste forms and waste package internal structures, such as canisters, baskets, and heat conductors. Waste forms include uranium dioxide fuel within Zircaloy cladding;

DOE spent nuclear fuels, such as graphite, mixed plutonium-uranium oxides, uranium metal, and thorium oxides; and high-level radioactive waste glass or ceramic. Waste package internals include aluminum alloy, Type 316L and 304L stainless steels (with and without neutron absorbers, such as boron or gadolinium phosphate), A516 low-carbon steel, and Alloy 22. Other uncertainties affecting the in-package chemistry modeling include flow rates and chemical composition of water and drift gases entering the package. To encompass the accumulated uncertainties, many of the input parameters used in the model were sampled from broad ranges or conservatively bounded. In particular, clad coverage and water flow rates were varied orders of magnitude. Partial pressures of carbon dioxide and oxygen were conservatively set to  $10^{-3}$  and  $10^{-0.7}$  bar respectively.

As described in *Summary of In-Package Chemistry for Waste Forms* (CRWMS M&O 2000dm), simulations of waste package and waste form alteration by ambient groundwater were done using the qualified reaction path code EQ3/6 (CRWMS M&O 1998h; CRWMS M&O 1999n), which titrates masses of waste package and waste form components at a rate determined by input reaction rates and fluid influxes into the breached waste package. EQ3/6 estimates the elemental composition of the reacting fluid for the duration of the reaction path calculation while at the same time providing estimates of the nature and masses of secondary phases that are predicted to form. The code cannot predict kinetic inhibitions, which must instead be done on the basis of expert judgment. Moreover, the code cannot account for local nonequilibrium effects such as galvanic coupling or radiolysis.

Table 4-18 summarizes the range of in-package fluid compositions predicted to occur for both the waste package types.

Table 4-18. Range of In-Package Fluid Compositions

Variable	Commercial Package	Codisposal Package
pH	3.6 to 8.1	4.8 to 10.0
Ionic Strength	0.003 to 1.7	0.003 to 5.8
Carbon	$2.8 \times 10^{-5}$ to 0.002	$3.5 \times 10^{-5}$ to 0.5

NOTES: Measurements given in mol/L for all except pH.  
Source: CRWMS M&O 2000dm, Table 3.

For the waste packages containing spent nuclear fuel, the in-package chemistry model predicts a decrease in pH, caused by dissolution of low-carbon steel, followed by a subsequent rise in pH due to the dissolution of commercial spent nuclear fuel, the oxidation of aluminum alloy, and the inflow of additional water. The lowest predicted pH levels are those calculated for the least amount of clad failure, as shown in Figure 4-100. Yet the bulk pH is not expected to go low enough to cause significant increases in clad failure rates. Under the bounded fixed carbon dioxide conditions assumed for the simulations, carbonate levels are relatively high at high pH and low at low pH. Because both uranium and plutonium form soluble complexes with carbonate, the dissolved levels of each tend to increase at high pH and decrease at neutral pH. However, the lowest pH levels occur in the early stages of the reaction paths, before appreciable amounts of uranium or plutonium have been dissolved from the commercial spent nuclear fuel matrix.

In the codisposal simulations (Figure 4-101), the moderately alkaline pH of the input solution prevails initially, then progresses towards a minimum, primarily due to the oxidation of the A516 carbon steel (degradation of fast flux test facility waste packages was modeled to bound degradation of codisposal waste packages). The high specific rate and relatively high surface area of the latter mean that its dissolution tends to dominate the whole reaction path, at least as long as it remains (oxidation of sulfur in the steel to sulfate is the primary proton-producing reaction). After the steel is exhausted, dissolution of base cation-containing high-level radioactive waste glass leads to increased pHs. pHs as high as 10 and ionic strengths as high as about 5.8 mol/L were predicted for codisposal waste packages under conditions of high glass dissolution and low flow rates. At ionic strengths greater than about 0.7 mol/L, the calculations are less accurate than for dilute systems. Because the solubilities of many minerals do not appear to depend strongly on ionic strength at and above this range, the lack of exactness does not prevent the results from providing useful bounding ranges of fluid chemistry (CRWMS M&O 2000dm).

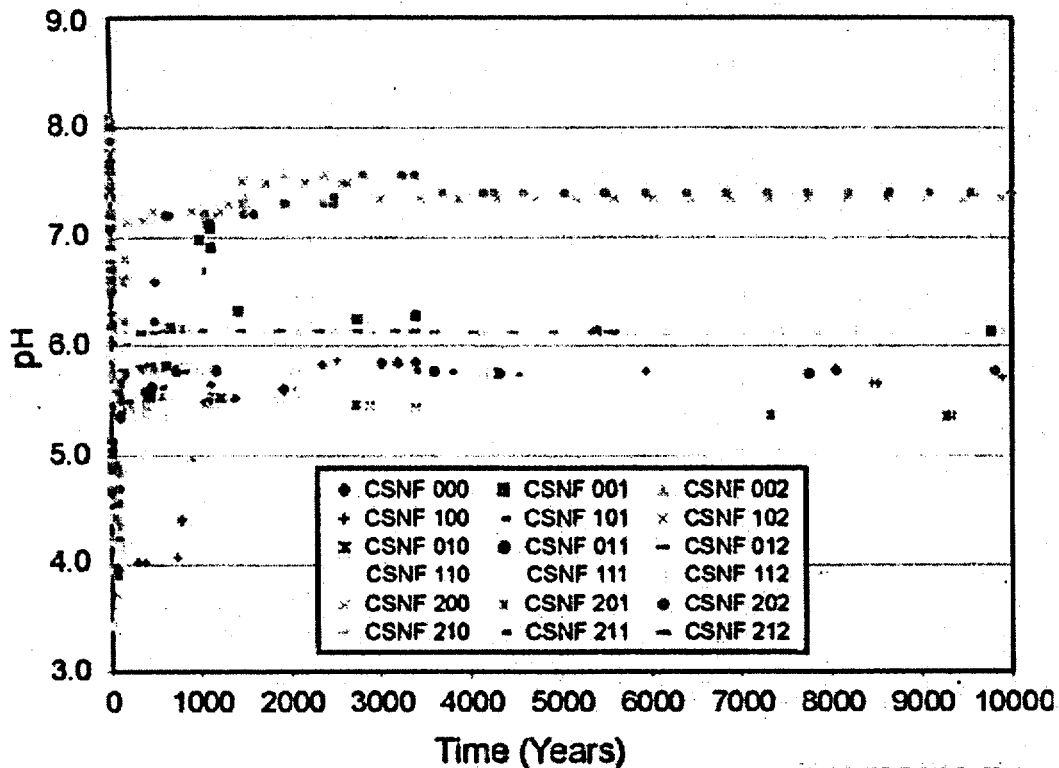


Figure 4-100. pH History for Commercial Spent Nuclear Fuel Process Model Calculations  
The numbers in the legend indicate individual calculation runs. For details, see *In-Package Chemistry Abstraction* (CRWMS M&O 2000dn). Source: CRWMS M&O 2000bm, Figure 3.2-3.

Since the completion of the TSPA-SR models, the DOE has developed additional information to further understand and quantify uncertainties associated with the in-package chemistry models. Uncertainties in the in-package chemistry models include those associated with steel and glass degradation rates, oxygen fugacity, in-package sorption, and choice of solubility limiting phase. In the TSPA-SR models, the DOE utilized bounding approximations or conservative inputs for these processes. Since completion of the TSPA-SR analyses, a series of sensitivity studies were performed to assess the impact of uncertainty with these processes on repository performance. Volume 1, Section 9.3.1 of *FY01 Supplemental Science and Performance Analyses* (BSC 2001a) provides detailed discussions of the additional studies, specifically the investigation of the impact on pH-time trajectories from lower degradation rates of

glass and steel. The lower-temperature operating mode is reflected in the model because the degradation rates and thermodynamic data were developed for ambient temperature conditions (25°C [77°F]).

Since the completion of the TSPA-SR models, an updated in-package chemistry model was developed to provide a sensitivity study on the effect of input fluid chemistry on calculated reaction paths (i.e., the likely variation in major-element composition of in-package fluids), to provide a sensitivity study on the effect of different partial pressures of oxygen and carbon dioxide on reaction paths, and to provide a formal examination of the potential for radiolysis-induced corrosion on spent fuel rod cladding. Results of these sensitivity studies are discussed in detail in *In-Package Chemistry for Waste Forms* (BSC 2001p) and are included in

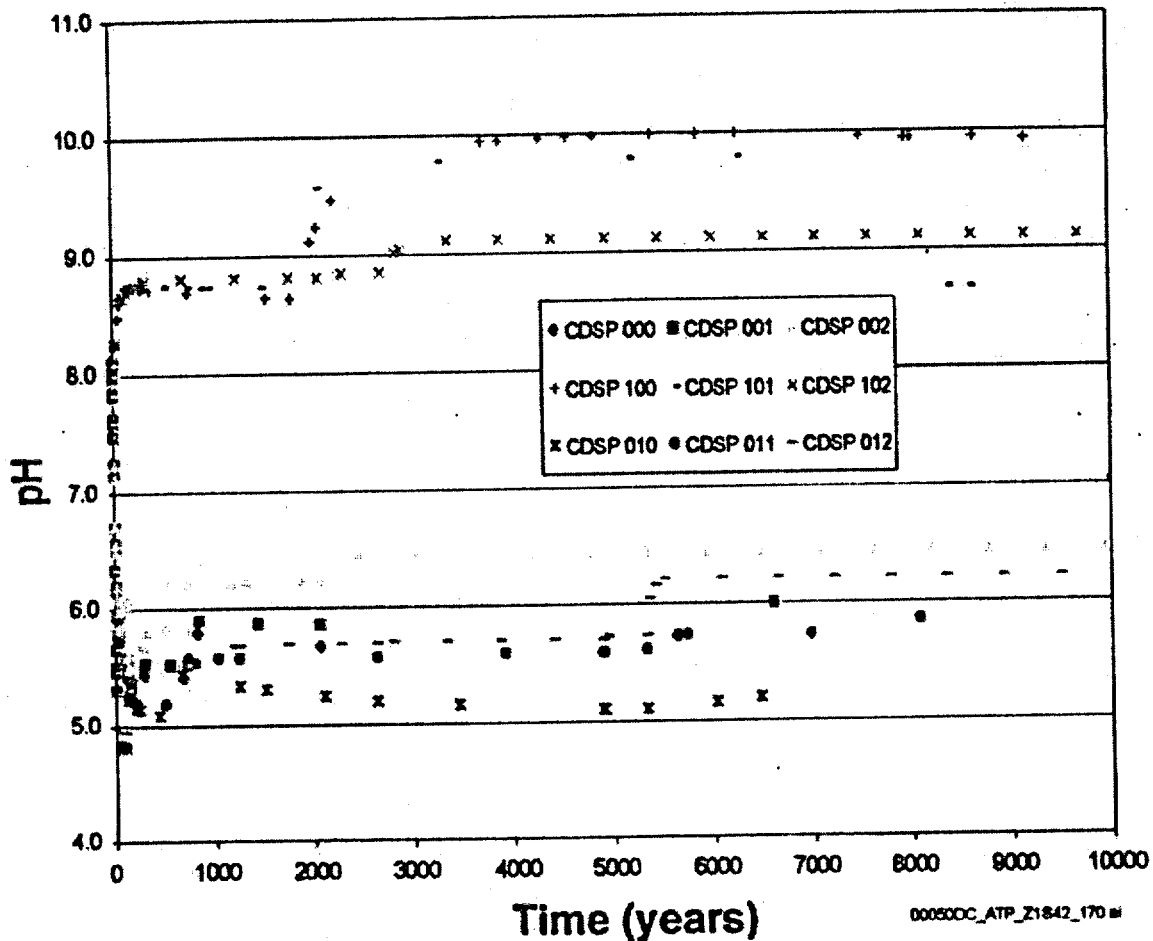


Figure 4-101. pH History for Codisposal Process Model Calculations  
The numbers in the legend indicate individual calculation runs. For details, see *In-Package Chemistry Abstraction* (CRWMS M&O 2000dn). Source: CRWMS M&O 2000bm, Figure 3.2-4.

Volume 1, Section 9 of *FY01 Supplemental Science and Performance Analyses* (BSC 2001a). This additional work has provided additional confidence that the models used in the TSPA-SR analyses are reasonable.

#### 4.2.6.3.3 Cladding Degradation Model

Since the 1950s, most commercial spent nuclear fuel has been clad with less than 1 mm (0.04 in.)—usually between 600 through 900  $\mu\text{m}$  (0.024 through 0.035 in.)—of Zircaloy, an alloy that is about 98 percent zirconium with small amounts of tin, iron, nickel, and chromium. The Zircaloy cladding is not a designed engineered barrier of the

Yucca Mountain disposal system; rather it is an existing characteristic of the commercial spent nuclear fuel important to determining the rate of release of radionuclides once engineered barriers such as the waste package have breached. Zircaloy is very resistant to corrosion, and cladding failure is expected to be minimal in the first 10,000 years. However, while Zircaloy provides excellent protective properties, characterization of the uncertainty in its performance is important. This characterization is possible because data has been collected on its performance over the past 40 years by the nuclear industry and by others in several different harsh environments.

The cladding degradation model predicts the rate at which the commercial spent nuclear fuel matrix is exposed and altered based on the number of rods with perforated cladding at any one time. The technical basis for the model is summarized in *Waste Form Degradation Process Model Report* (CRWMS M&O 2000bm) and described in more detail in the following analysis and modeling reports:

- *Clad Degradation—Summary and Abstraction* (CRWMS M&O 2000dj)
- *Initial Cladding Condition* (CRWMS M&O 2000de)
- *Clad Degradation—Dry Unzipping* (CRWMS M&O 2000di)
- *Hydride-Related Degradation of SNF Cladding Under Repository Conditions* (CRWMS M&O 2000dg)
- *Clad Degradation—FEPs Screening Arguments* (CRWMS M&O 2000do)
- *Clad Degradation—Wet Unzipping* (CRWMS M&O 2000dh)
- *Clad Degradation—Local Corrosion of Zirconium and Its Alloys Under Repository Conditions* (CRWMS M&O 2000df).

The conceptual model for the degradation of commercial spent nuclear fuel cladding is shown in Figure 4-102. Cladding degradation is assumed to proceed through two distinct steps: (1) rod failure (perforation of the cladding) and (2) progressive exposure of uranium dioxide spent fuel matrix from tearing of the cladding.

In the TSPA-SR model, perforation of the cladding may occur because (1) the cladding initially fails within the reactor or during storage, (2) the cladding fails from creep or stress-corrosion cracking, (3) an earthquake severely shakes and severs the rods, or (4) the cladding fails from localized corrosion. Other mechanisms of initiating cladding perforations, such as diffusion controlled cavity growth or delayed hydride cracking, were specifi-

cally evaluated using features, events, and processes screening analyses and were screened out based on either low consequence or low probability (CRWMS M&O 2000do).

Local corrosion was included because corrosion of zirconium has been observed in concentrated fluoride or chloride solutions at very low pHs or very high oxidation potential (CRWMS M&O 2000df, Section 4.1). These conditions are not predicted to occur in the bulk solution (see Section 4.2.6.3.2) but have not yet been ruled out for localized or nonequilibrium effects such as microbially influenced corrosion, galvanic coupling, radiolysis in a humid environment, and extreme concentration by evaporation. Each of these mechanisms may locally depress the pH or increase the concentration of corrosive species such as fluoride or chloride, at least temporarily. None of these conditions is expected to impact cladding performance under repository conditions. However, until they can be ruled out or shown to be too transitory to have negative consequences on cladding, a conservative model that includes local corrosion mechanisms will be used to bound the uncertainty associated with cladding corrosion.

The localized corrosion model is just one example of the conservative models included in TSPA to bound the uncertainty of cladding performance (CRWMS M&O 2000dj). For each of the cladding perforation mechanisms assumed in the TSPA-SR, conservative bounding estimates were generated for the number of cladding failures, their timing, and their character. These estimates were based upon one or more of the following: analyses of data from decades of reactor operations for fuel handling and wet and dry storage; fuel performance reports; analytical methods and assumptions previously used in licensing of storage or transportation designs; interim guidance from the NRC; corrosion studies; and experiments reported in the literature.

The release of radionuclides does not occur until after the waste package fails and air and water can enter the waste package. The release occurs in two stages, fast release of immediately accessible radionuclides followed by slower release as the matrix degrades.

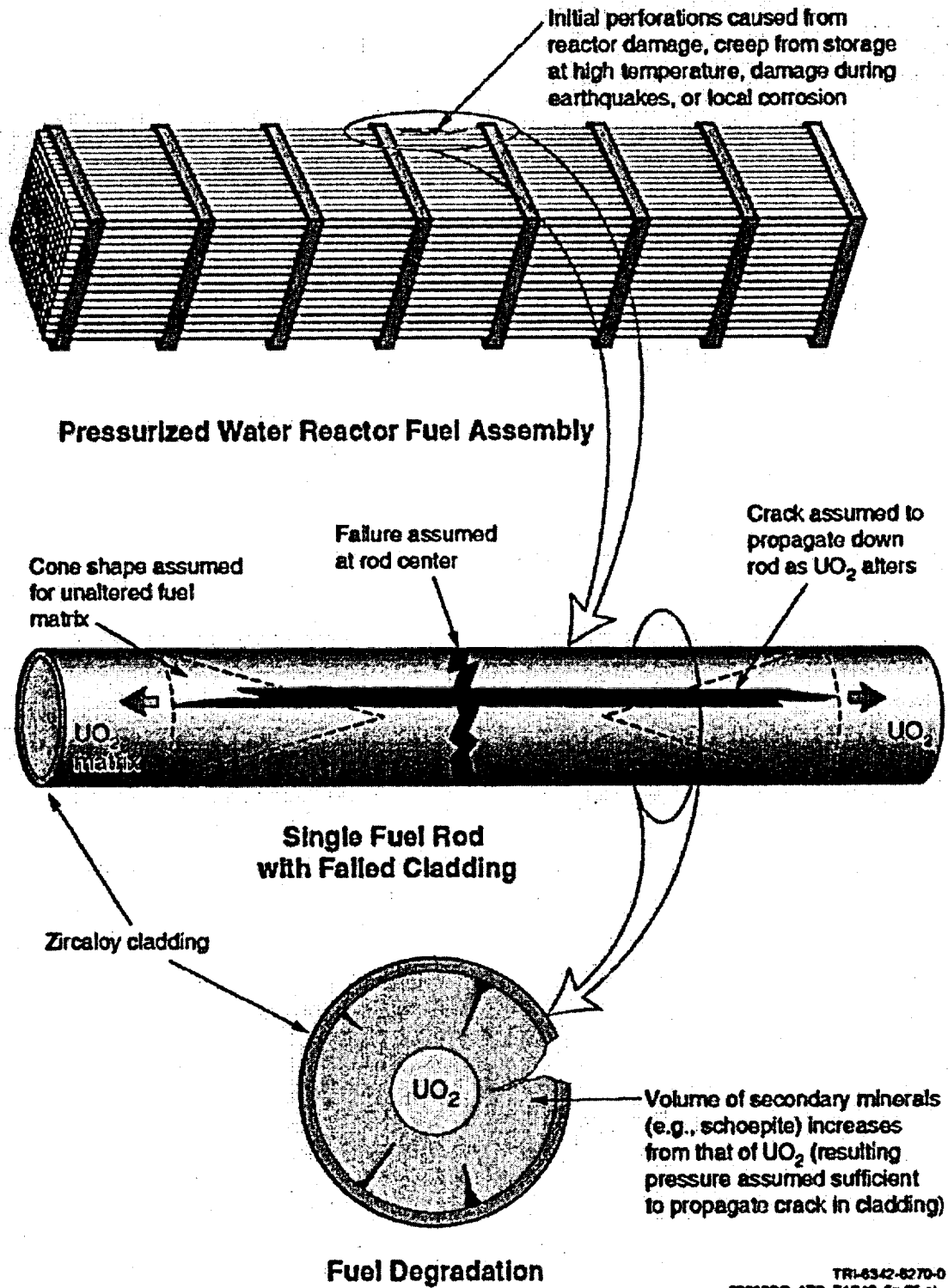


Figure 4-102. Conceptual Model of Commercial Spent Nuclear Fuel Cladding Degradation  
Source: CRWMS M&O 2000bm, Figure 3.8-2.

TR1-8342-8270-0  
000500C\_ATP\_Z1542\_fig-05.m

Fast release refers to the inventory of radionuclides that are in the gap between the fuel pellets and the cladding (gap inventory) and the radionuclides at the grain boundaries of the spent nuclear fuel matrix. A small percentage of the inventory of iodine, cesium, and a few other radionuclides resides in the gap between the cladding and waste matrix. For the TSPA-SR, the release of the gap inventory is conservatively assumed to be instantaneous when the cladding is perforated and, thus, independent of the cladding tearing. Cladding that was initially perforated releases the gap inventory when the waste package is breached. The inventory of the radionuclides in the grain boundaries is also released quickly.

As water and air enter the fuel rods, they slowly react with any available exposed spent fuel surfaces. This may include a gap between the fuel and cladding and cracks through the fuel pellets. Under slow flow or unsaturated conditions, secondary phases precipitate at the reaction front. The phases that precipitate depend on the water chemistry, but metaschoepite has been used as representative phase. As these phases precipitate, they will fill the void spaces within the fuel and may exert force outward force on the fuel cladding. If there is sufficient force, the cladding may tear open in a process called "unzipping." Unzipping has been observed under dry, high-temperature, oxidizing conditions but has not been observed in failed fuel rods under wet conditions outside of the reactor. A wet unzipping model has been developed based on analogy to dry unzipping (CRWMS M&O 2000dh). This model predicts that hundreds of years are required for the void spaces to be filled and for unzipping to start. During this time, a small fraction of the matrix is predicted to react, and the radionuclides contained within this matrix are assumed to be released instantly along with the other fast releases.

Wet unzipping is modeled to start at waste package failure for rods perforated prior to waste package failure or to start when rod perforation occurs if after waste package failure. The fuel matrix is modeled to dissolve at the intrinsic dissolution rate for the predicted temperature and in-package chemistry and precipitate as metaschoepite. The volume increase is modeled to split the cladding,

exposing more of the spent nuclear fuel matrix as the cladding unzips along its length. The reaction region is conservatively assumed to be cone-shaped based on experimental observations of dry unzipping, and it is assumed that the perforation is in the center of the rod. The unzipping is modeled to propagate along the rod at a rate approximately 40 times (range 1 to 240 times) as fast as the intrinsic dissolution rate discussed in Section 4.2.6.3.4. This results in most sampled unzipping times greater than 10,000 years. The long time periods associated with unzipping mean that cladding contributes to a significant delay in radionuclide release from the commercial spent nuclear fuel waste form.

The anticipated temperature of the fuel matrix is not high enough, nor do the high temperatures occur for a long enough period, to cause unzipping in a dry environment, so dry unzipping is not included in the TSPA-SR. Based on observed behavior within storage pools at reactors, unzipping in a wet environment does not occur in observed time periods of 40 years once the Zircaloy cladding has been perforated. However, these observations are not sufficient to entirely rule out the possibility of a wet environment unzipping process. By including in the TSPA-SR the possibility of the clad unzipping in a wet environment, the assumed complete exposure of the fuel matrix conservatively bounds diffusive releases of radionuclides through the perforations. Exposure of the spent nuclear fuel is evaluated through a hypothetical but bounding rate of unzipping of the cladding such that the entire inventory of radionuclides can eventually be exposed over sufficient time.

Since the completion of the TSPA-SR analysis, the DOE has developed additional information to further understand and quantify uncertainties associated with the cladding model. Uncertainties exist related to the fraction of cladding perforated because of creep rupture and stress corrosion cracking, the localized corrosion rate, the potential for mechanical damage (seismic and rock overburden), and the unzipping velocity of the cladding. In the TSPA-SR models, the DOE utilized bounding approximations or conservative inputs for these processes. Volume 1, Section 9.3.3 of *FY01 Supplemental Science and Performance*

*Analyses* (BSC 2001a) provides detailed discussions on how the sensitivity model reduced uncertainties by utilizing the more realistic approach for many aspects of the cladding model. The behavior of cladding within the repository is not expected to differ significantly between a lower- and higher-temperature operating mode as long as the cladding temperature limit of 350°C (660°F) is not exceeded (BSC 2001a, Section 9.3.3).

#### 4.2.6.3.4 Commercial Spent Nuclear Fuel Degradation Model

The commercial spent nuclear fuel degradation model is important to TSPA because it predicts the rate at which soluble isotopes important to humans dose (e.g., technetium-99) become available for transport and release. *CSNF Waste Form Degradation: Summary Abstraction* (CRWMS M&O 2000dk) documents the development of this semi-empirical model from flow through test data, and the validation of the model by comparison to other test data and natural analogues. Because it directly relies upon only the flow through tests, which give upper limits to the actual dissolution rates, this model is a bounding one, and has been validated as such.

Figure 4-103 shows the predicted rate of degradation of the fuel rate in  $\text{mg}/(\text{m}^2\text{-day})$  as a function of temperature and pH for the oxygen and carbon

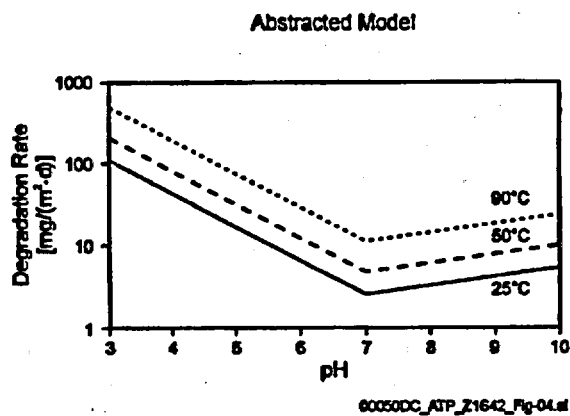


Figure 4-103. Abstracted Degradation Rates for Commercial Spent Nuclear Fuel  
Source: CRWMS M&O 2000dk, Figure 2.

dioxide partial pressures used in the TSPA calculations. This model uses two linear regression equations based on pH, the partial pressures of oxygen and carbon dioxide, and temperature. One equation is applicable for pH less than or equal to 7 and another for pH greater than 7. Considering the uncertainty of the applicability of data from young spent nuclear fuel (less than 30 years out of reactor) and unburned uranium dioxide toward the prediction of long-term (greater than 1,000 years) performance of spent fuel, the dissolution model was estimated to be valid to within 1.5 orders of magnitude. Comparisons of the abstracted dissolution model for commercial spent nuclear fuel with long-term unsaturated drip tests, batch tests, and literature results provide confidence that the model adequately accounts for all dissolution rates and provides conservative overestimates of dissolution rates for use in the TSPA-SR. In addition, a comparison of the phases produced in the unsaturated drip tests compare well with that of the natural analogue at Nopal I, a uranium mining site at Peña Blanca, Mexico (CRWMS M&O 2000dk, Section 6.6). This site is one of the best natural analogues for spent fuel degradation in Yucca Mountain because it contains substantial quantities of uraninite in a geologic, geochemical, and hydrogeologic setting similar to Yucca Mountain. Overall, the phase assemblage observed at Nopal I is similar to that derived experimentally in the commercial spent nuclear fuel alteration drip tests. The general agreement between the observed alteration products in the various tests, the natural analogues, and the geochemical modeling provide confidence that the mechanisms of spent nuclear fuel corrosion are well understood and that the forward dissolution model is bounding for long-term prediction of commercial spent nuclear fuel degradation rates.

#### 4.2.6.3.5 High-Level Radioactive Waste Glass Degradation Model

The high-level radioactive waste degradation model is used to predict conservative borosilicate glass degradation rates over the range of conditions (i.e., immersion, humid air, and dripping water) expected after waste package failure. The rate of radionuclide release from high-level radioactive waste is calculated by multiplying the glass degra-

dition rate by the mass fraction of the radionuclide in the glass. Although much of the glass will be exposed only to humid air or dripping water conditions, a conservative bounding scenario of complete saturation is used in modeling dissolution.

The area of the glass surface available for corrosion in the disposal environment is difficult to estimate precisely. The logs of waste glass will crack within the pour canister due to thermal and mechanical stresses generated as the glass cools and as the waste form is handled, ultimately increasing the total surface area available for contact with water. The key differences between the dissolution rates of the glass within cracks and at the outer surface are the transport rates of reactant and products, respectively, into and out of the crack. Surface-area-normalized dissolution of fractured glass is therefore sometimes found to be slower than that of nonfractured glass. The conservative, bounding approach that has been followed assumes they are equal (CRWMS M&O 2000dl, Section 6.1.2).

The rate expression for high-level waste glass degradation contains two main parts: a forward reaction rate term, which represents the dissolution rate in the absence of feedback effects of dissolved silica (and other aqueous species), and a reaction affinity term ( $1-Q/K$ ), which quantifies the feedback effects.  $Q$  represents the concentration of dissolved silica in the solution, in units of mass/volume, while  $K$  represents the quasi-thermodynamic fitting parameter equal to the apparent silica saturation concentration for the glass, in units of mass/volume. The dissolution rate will decrease as the value of the affinity term decreases (i.e., as the value of  $Q$  approaches  $K$ ) until a minimum rate is reached (CRWMS M&O 2000dl, Section 6.1.1).

Corrosion proceeds in three stages:

- Stage I—The value of the affinity term is one, and glass dissolves at the forward rate for the specific temperature and pH conditions involved. Stage I will not occur when glass is contacted by groundwater containing high levels of dissolved silica (from the dis-

solution of minerals present in the tuff rock and from the dissolution of the glass itself).

- Stage II—The value of the affinity term approaches zero due to the accumulation of glass components in solution. The value of the affinity term cannot become zero because glass is thermodynamically unstable; therefore, it cannot equilibrate with the solution.
- Stage III—The dissolution rate increases concurrently with the formation of alteration phases. The formation of alteration phases is believed to cause a decrease in the value of  $Q$  due to the consumption of dissolved silica as silica-bearing phases form.

Dissolution rates were independent of the glass composition within the limits prescribed by the high-level radioactive waste glass waste acceptance product specification (CRWMS M&O 2000dl, Section 6.2), but high-level waste glass degradation rates do depend on pH and temperature. Abstracted degradation rates are shown in Figure 4-104.

Since the completion of the TSPA-SR models, the DOE has performed additional sensitivity studies on high-level waste glass degradation rates. In the TSPA-SR models, conservative estimates of important model parameters were used to calculate degradation rates. In Volume 1 of *FY01 Supplement Science and Performance Analyses* (BSC 2001a, Section 9), the DOE utilized a more realistic treatment of glass degradation rates that resulted in slower calculated degradation. These analyses indicated that dose calculations are not highly sensitive to glass degradation rates.

#### 4.2.6.3.6 U.S. Department of Energy Spent Nuclear Fuel and Other Waste Form Degradation Modeling

The degradation rates of all waste forms other than commercial spent nuclear fuel and high-level radioactive waste are summarized in *Waste Form Degradation Process Model Report* (CRWMS M&O 2000bm, Section 3.5). Over 250 distinct types of DOE spent nuclear fuel may be disposed in the potential repository at Yucca Mountain. The

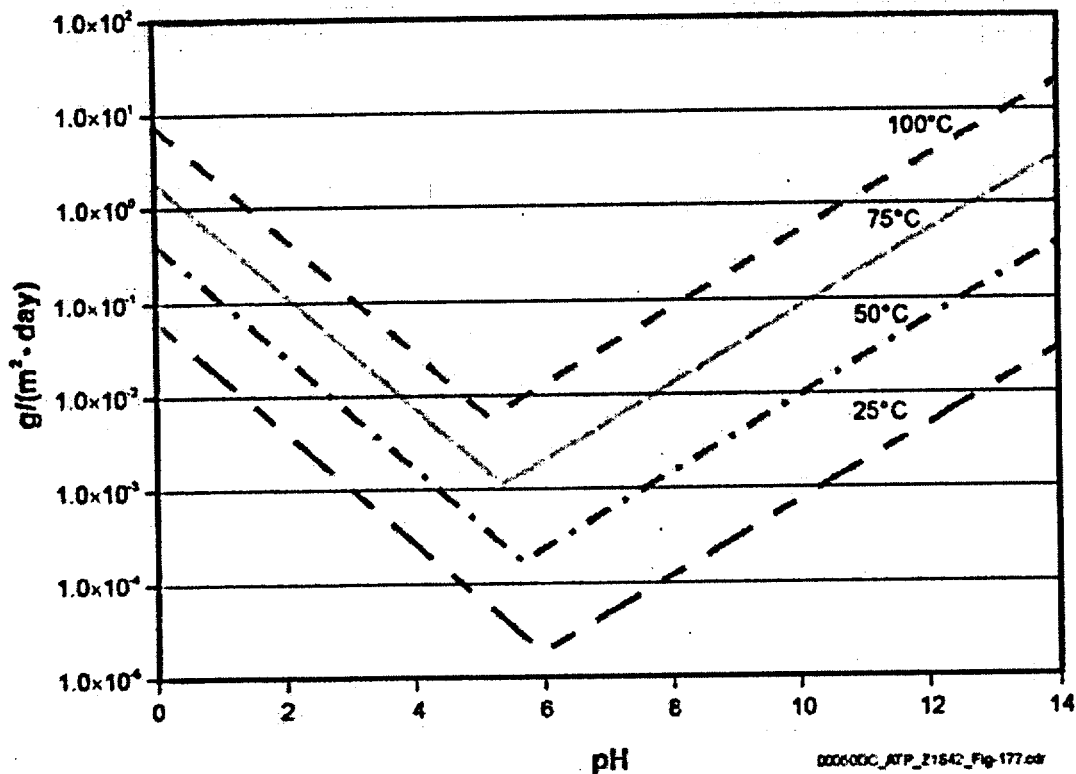


Figure 4-104. Abstracted Degradation Rates for High-Level Radioactive Waste Glass  
Source: Modified from CRWMS M&O 2000bm, Figure 3.6-2.

Office of Civilian Radioactive Waste Management and the National Spent Nuclear Fuel Program have collaborated in the identification of spent nuclear fuel "groups" (CRWMS M&O 2000bm, Section 3.5) to simplify the analysis of their effects on repository preclosure safety analyses or for post-closure TSPA.

The DOE spent nuclear fuel groups are:

- Group 1—Naval spent nuclear fuel
- Group 2—Plutonium/uranium alloy
- Group 3—Plutonium/uranium carbide
- Group 4—Mixed oxide and plutonium oxide fuels
- Group 5—Thorium/uranium carbide
- Group 6—Thorium/uranium oxide
- Group 7—Uranium metal
- Group 8—Uranium oxide
- Group 9—Aluminum-based spent nuclear fuel
- Group 10—Unknown
- Group 11—Uranium-zirconium-hydride.

In addition, the immobilized ceramic plutonium waste form was also evaluated. This waste form will consist of disks of a plutonium-containing, titanium-dioxide-based ceramic that will be enclosed in stainless steel cans, which in turn will be encased in a borosilicate glass matrix within the high-level radioactive waste canisters.

*Waste Form Degradation Process Model Report* (CRWMS M&O 2000bm, Section 3.5) summarized three types of degradation models for the DOE spent nuclear fuel and plutonium-ceramic waste forms: upper-limit, conservative, and best-estimate, to provide the user of the models appropriate flexibility in their application to any particular postclosure performance scenario. An upper-limit model predicts release rates always well in excess of actual dissolution rate data. The conservative degradation model provides an estimate of dissolution rate that reflects the higher rate end of available dissolution data on the spent nuclear fuel groups or similar materials. A best-estimate model is appropriate only when sufficient

dissolution data exist and the characteristics of the waste form can be shown to correspond to the characteristics of the materials that provided the dissolution database. For the conservative and best-estimate models, various surrogate spent nuclear fuels were evaluated for degradation behavior. In general, the degradation rates of the oxide fuels are much lower than the metallic uranium or carbide fuels. Because the metallic uranium and carbide fuels degrade very rapidly compared to repository time scales, the TSPA results have been very insensitive to these rates. In addition, TSPA analyses have shown that the overall performance of the potential repository is driven primarily by the commercial spent nuclear fuel and high-level radioactive waste inventories. For these reasons, the conservative Hanford N Reactor fuel model (1.75 kg/m<sup>2</sup>-day) was recommended as the surrogate to bound all the DOE spent nuclear fuel groups 2 through 11.

The best-estimate for the degradation of the immobilized ceramic plutonium is given by a titanate ceramic model, with an exposed surface area corresponding to the geometric surface area of the plutonium-containing ceramic disks. For the TSPA-SR, however, the immobilized plutonium inventory was averaged into the high-level radioactive waste inventory, and the higher rates for high-level radioactive waste degradation were used.

The application of the DOE spent nuclear fuel and other waste degradation models involves the extrapolation of the models over long periods of time, which are orders of magnitude greater than the experimental test periods used to generate the data used to derive the models. The general lack of qualified experimental dissolution and degradation data for many of the DOE spent nuclear fuel waste forms was addressed by the use of conservative degradation models for the TSPA.

One of the types of DOE-owned spent nuclear fuel to be disposed in the potential repository is naval spent nuclear fuel. There are 65 MTHM of naval spent nuclear fuel included in the base case repository design. The Naval Nuclear Propulsion Program modeled the performance of naval spent nuclear fuel with the same environmental condi-

tions used in the commercial spent nuclear fuel degradation model (Mowbray 2000).

#### 4.2.6.3.7 Solubility Model

Doses calculated for groundwater pathways from the repository to the environment depend significantly on the concentrations of radionuclides in fluids issuing from breached waste packages. While dissolution of the waste forms is the primary source of radionuclides, formation of secondary phases often limits available levels of radionuclides for subsequent groundwater transport. The primary report supporting the radioisotope concentration model component is *Summary of Dissolved Concentration Limits* (CRWMS M&O 2000dp).

The dissolved concentration calculation builds upon three primary feeds: (1) estimates of in-package fluid major element composition (i.e., pH, Eh, ionic strength, carbonate levels); (2) measured (and estimated) thermodynamic parameters describing the stabilities of aqueous species and solid radioisotope phases; and (3) determination/estimation of solubility-controlling phases. The thermodynamic databases that were used are described in *Summary of Dissolved Concentration Limits* (CRWMS M&O 2000dp) and *Pure Phase Solubility Limits—LANL* (CRWMS M&O 2000dq).

Modeling was based on EQ3NR (a component of EQ3/6) analyses and a recently revised thermodynamic database incorporating experimental solubility data and critical reviews of parameterizations used internationally. Important components of this effort included the measurement and critical analysis of neptunium and plutonium solubility in J-13 groundwater and an analysis of technetium and uranium silicate thermodynamic data. The chosen solubility-controlling phase can affect the calculated radionuclide concentrations by orders of magnitude and is one of the sources for uncertainty in the predicted concentration. For the TSPA-SR analysis, the pure phases were chosen because in general they yield higher dissolved concentrations. See *Secondary Uranium-Phase Paragenesis and Incorporation of Radionuclides into Secondary Phases* (CRWMS M&O 2000dr) for discussion of the effects of secondary phases on radionuclide

concentration. The phases were chosen based upon geologic and/or experimental observations or crystallochemical arguments. These issues are discussed in *Summary of Dissolved Concentration Limits* (CRWMS M&O 2000dp) for each radionuclide. Schoepite was assumed to be the solubility-controlling mineral for uranium because (1) schoepite is the first mineral to be formed during spent fuel corrosion; (2) field observations and modeling study indicate that schoepite can persist for more than 10,000 years; (3) schoepite is the most soluble of the common secondary phases; and (4) the temperature dependence of schoepite solubility is known. Relatively soluble  $\text{Np}_2\text{O}_5$  (or  $\text{Np}(\text{OH})_4(\text{am})$  under reducing conditions) are assumed to be the solubility-controlling minerals for neptunium.  $\text{Pu}(\text{OH})_4(\text{am})$  was chosen as the solubility-controlling phase for plutonium, though less soluble plutonium dioxide might form instead.  $\text{AmOHCO}_3$  was chosen as the conservative solubility-controlling phase for americium. Because of chemical similarities, the solubility functions for actinium, curium, and samarium were set identical to that of americium.

Three radioisotope solubilities were abstracted as a direct function of in-package chemistry (neptunium, uranium, americium); three solubilities were set equal to that used for americium (actinium, curium, samarium); four were defined by probability distributions (plutonium, lead, protactinium, nickel); and bounding values were used for the remainder. Figure 4-105 shows the neptunium solubility as a function of pH abstraction and the neptunium solubility data (CRWMS M&O 2000bm).

Since the completion of the TSPA-SR models, the DOE has performed additional uncertainty analyses on the solubility model. The radionuclides considered most important to dose and which are conservatively modeled in the TSPA-SR models are thorium, neptunium, plutonium, and technetium. Volume 1, Section 9 of *FY01 Supplemental Science and Performance Analyses* (BSC 2001a) describes the uncertainties associated with these radionuclides and how these uncertainties were modeled in supplemental analysis. Utilizing more realistic solubility models for key radionuclides has a significant effect on peak dose calculations

(reducing calculated doses) although doses during the first 10,000 years are not affected.

#### 4.2.6.3.8 Colloid Model

Critical to repository performance are the availability and the stability of three types of colloids: (1) existing colloids in the groundwater, (2) colloids generated by degradation of the waste, and (3) colloids generated during degradation of the disposal container (ferric iron-oxide and iron-hydroxide minerals). Figure 4-99 illustrates this conceptually, and Figure 4-106 shows how these concepts are reflected in colloid modeling.

Colloid transport is potentially most important for low solubility, highly sorbing radionuclides. Plutonium and americium are the most likely such radionuclides to affect dose in the regulatory time period (CRWMS M&O 2000ds, Table 11).

The colloid abstraction (CRWMS M&O 2000cn) builds on waste form corrosion testing and measurements of plutonium and americium adsorption and desorption from clay and iron-(hydr)oxide colloids. A model was developed to calculate the colloid radioisotope concentration for each of the three colloid types. The model for the waste form colloids includes the contributions of the engulfed (irreversibly attached) plutonium observed in waste glass tests. The models for all three colloid types include reversibly attached radionuclides. These models are based on the population of each colloid type (expressed in terms of mass of colloids per volume of fluid) and experimental data for the sorption of radionuclides onto the colloid substrate materials involved. The effects of pH and ionic strength on the stability of dispersions of each colloid type are considered. Specifically, the location of the boundaries between pH and ionic strength regimes in which each type of colloid substrate is stable or unstable are defined, together with the colloid mass concentration in each regime.

The mobile colloidal radionuclide source term is the sum of the radionuclide contribution from waste form colloids (reversibly and irreversibly attached), corrosion product colloids, and groundwater colloids. The total colloid mass

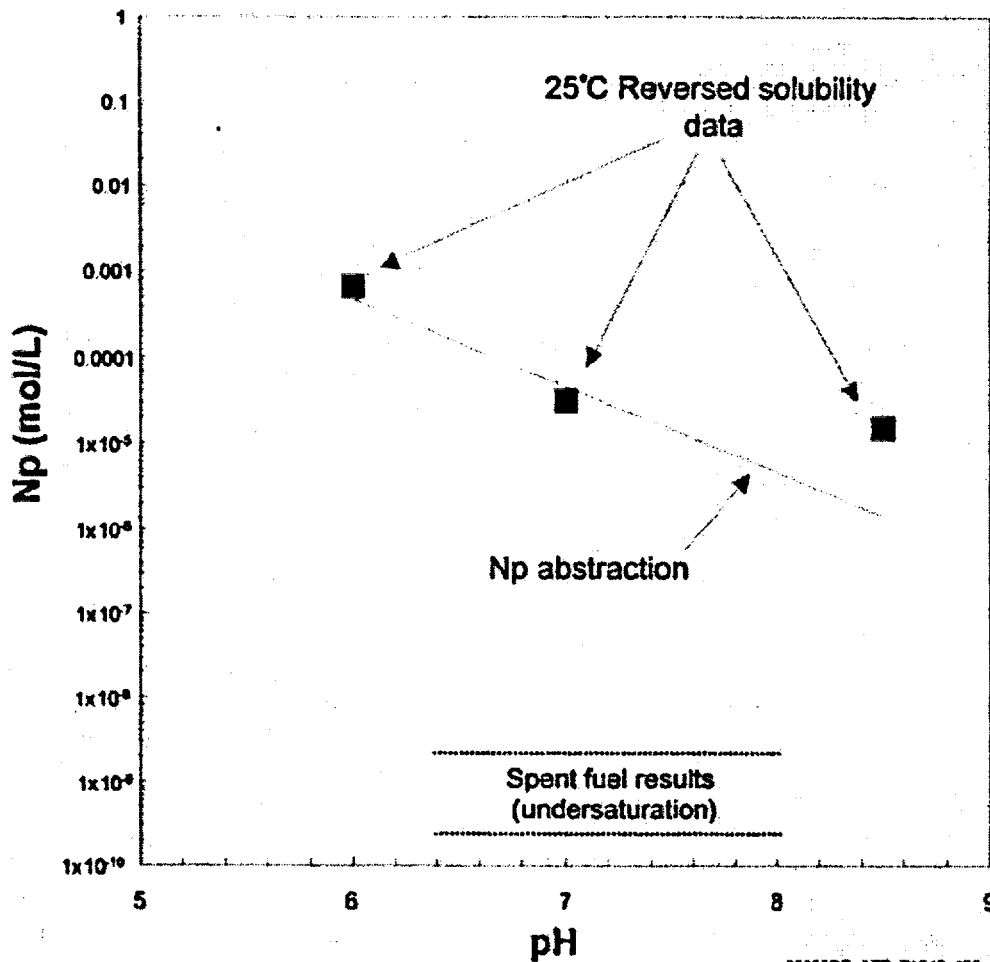


Figure 4-105. Neptunium Solubility Abstraction and Neptunium Solubility Data  
Source: CRWMS M&O 2000bm, Figure 3.7-3.

concentration is also used to estimate reversibly attached radionuclide concentrations as dissolved concentrations change during transport. Reversibly attached actinides can subsequently re-equilibrate with adjacent fluids, whereas engulfed radionuclide-bearing phases cannot.

The sorption processes controlling the attachment and detachment of soluble materials to colloidal substrates are complex but are similar to sorption of dissolved materials to rock surfaces. The most common approach used in assessing such interactions is the linear isotherm, as described in *Waste Form Colloid-Associated Concentrations Limits*:

*Abstraction and Summary* (CRWMS M&O 2000cn).

**Waste Form Colloid Concentration Model and Abstraction**—The waste form concentration model includes contributions from colloids with reversibly and irreversibly attached radionuclides. The concentration of irreversibly attached colloidal plutonium is calculated in part from the ionic strength conditions adjacent to the waste form. The details of these calculations are described more fully in *Colloid-Associated Radionuclide Concentration Limits: ANL* (CRWMS M&O 2000dt). The concentration of reversibly sorbed radionuclides is

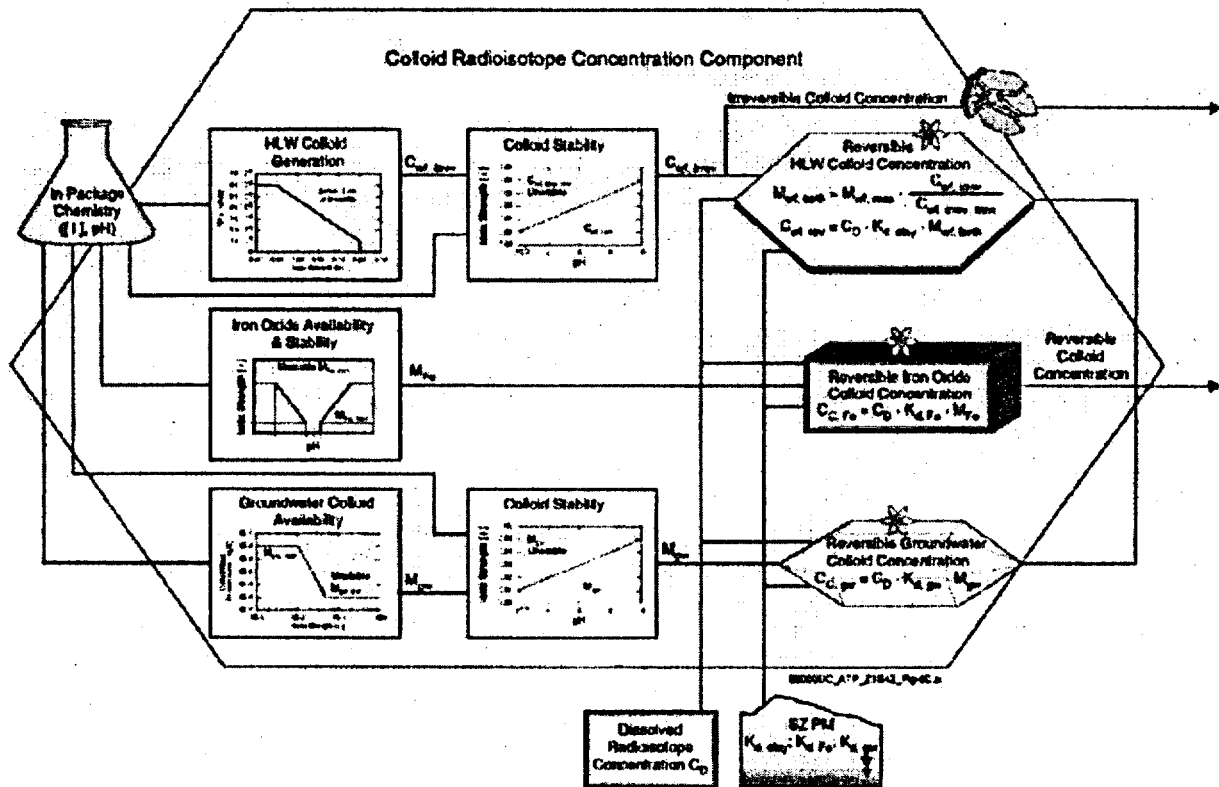


Figure 4-106. Linkage of Subcomponents of the Waste Form Degradation Process Model Colloidal Radionuclide Component  
HLW = high-level radioactive waste; SZ PM = saturated zone process model. Source: CRWMS M&O 2000bm, Figure 3.8-2.

determined using technically applicable sorption coefficients and a mobile mass determined by scaling from the predicted mass of irreversibly attached colloidal plutonium.

**Groundwater Colloid Model and Abstraction—**McCarthy and Zachara (1989) and McCarthy and Degueldre (1993) studied and compiled the characteristics of colloids in groundwaters from crystalline and sedimentary rocks in saturated and unsaturated hydrologic regimes. The data show a general inverse correlation above an ionic strength of about 0.01 M and provide a predictive tool for estimating groundwater colloid mass concentration. For TSPA-SR analysis calculations, these data were converted to mass or surface area per unit volume. It is assumed that sorption for groundwater colloids is similar to clay minerals (CRWMS

M&O 2000cn, Section 6.2.3), and the same sorption coefficients that were used for waste form colloids were used for groundwater colloids. The concentration of reversibly sorbed radionuclides is determined using technically applicable sorption coefficients.

**Corrosion Product Colloid Concentration Model and Abstraction—**It is assumed that corrosion product colloid concentrations will be similar to the concentration of iron-hydroxide colloids found adjacent to the iron-rich rock at the Morro de Ferro natural analogue site (CRWMS M&O 2000bm, Section 3.8.2.3.1). The stability behavior of iron-oxide and iron-hydroxide colloids was abstracted as a function of ionic strength and pH. Given the mass concentration of the corrosion product colloids, the concentration of reversibly

sorbed radionuclides is determined using appropriate sorption coefficients.

Since the completion of the TSPA-SR models, the DOE has performed additional uncertainty analyses on the colloid model. Uncertainties can be roughly grouped as pertaining to amounts of colloids available, nature and extent of sorption to colloids, and colloid retardation. Generally, in the TSPA-SR models, uncertainties were addressed by following bounding approaches and choosing conservative inputs and/or conceptual models. In Volume 1, Section 9 of *FY01 Supplemental Science and Performance Analyses* (BSC 2001a), the DOE further defines these uncertainties and describes how these uncertainties were modeled in supplemental analyses. These analyses indicate that colloidal transport can have a significant impact on dose calculations in some cases. The supplemental analyses also suggest that the assumptions used in the TSPA-SR model were reasonable or conservative (BSC 2001a, Section 10.3.5).

#### 4.2.6.3.9 Limitations and Uncertainties

Because models are imperfect representations of complex processes, it is important to identify their limitations and associated uncertainties, to outline alternative models that might describe the respective process, and, where possible, to fully validate the chosen process model. For most waste form models, process uncertainties are addressed by using bounding approximations or by using conservative inputs.

As noted in Section 4.1.1.2, the DOE has initiated several activities to improve the treatment of uncertainty in current models. Additionally, as noted in Section 4.1.4, the DOE has evaluated the possibility of mitigating uncertainties in modeling long-term repository performance by operating the design described in this report at lower temperatures. Some of the models that evaluate the performance of the waste form, particularly those that have used bounding approximations or conservative inputs, may be updated as a result of those activities. The model updates and evaluation results will be documented in future reports. The limitations of each waste form model described in this report are discussed below.

**Radionuclide Inventory**—The representative TSPA inventories (see Section 4.2.6.4.1) were derived from projections of future waste streams. The actual waste streams will be known only at the time of actual repository loading. The projected waste streams could differ from the actual waste streams in their fuel burnups, fuel ages, fuel enrichments, and utility efficiencies. As discussed in *Waste Form Degradation Process Model Report* (CRWMS M&O 2000bm, Section 3.1.1.4), the numbers of waste packages were specified for this analysis. As described in Section 1.2.1, these numbers are subject to change if a second repository is available or if the Nuclear Waste Policy Act is amended. However, changes that might be expected in the waste stream would produce only minimal changes in the average per-package radionuclide activities for commercial spent nuclear fuel used in TSPA modeling. The total curies of isotopes important to TSPA were between  $1 \times 10^4$  and  $1 \times 10^5$  for over 99 percent of the commercial fuel assemblies modeled in the TSPA-SR, with totals between  $1 \times 10^3$  and  $1 \times 10^4$  for the rest, as summarized from *Waste Packages and Source Terms for the Commercial 1999 Design Basis Waste Streams* (CRWMS M&O 2000bb). The inventory within the codisposal packages is more variable than the commercial spent fuel packages but on average is much lower. The range of total curies of isotopes important to TSPA for high-level glass waste canisters is  $1 \times 10^3$  to  $1 \times 10^5$ , as summarized in *Source Terms for HLW Glass Canisters* (CRWMS M&O 1999o), and the range for DOE spent nuclear fuel canisters is  $1 \times 10^1$  to  $1 \times 10^6$ , as summarized from *Per Canister Inventories of DOE SNF for TSPA-SR* (CRWMS M&O 2000du). Changes in waste stream are more likely to change the average per-package inventory of codisposal packages, but because these packages have significantly lower total activity, these changes are less likely to affect the TSPA results. The calculated average initial inventories in commercial spent nuclear fuel and codisposal waste packages are valid for the waste stream, as described in *Inventory Abstraction* (CRWMS M&O 2000ds).

**In-Package Chemistry**—The in-package chemistry model is limited by its reliance on reaction paths calculated at 25°C (77°F), by uncertainties in

the kinetic and thermodynamic database, and by uncertainties in the mode of water contact with the breached waste package (CRWMS M&O 2000dm). The difference between 25°C (77°F) reaction paths and those expected in reality should not be great after the thermal pulse has passed and temperatures approach ambient. At ionic strengths greater than about 0.7 mol/L, the calculations are less accurate than for dilute systems. Because the solubilities of many minerals do not appear to depend strongly on ionic strength at and above this range, the lack of exactness does not prevent the results from providing useful bounding ranges of fluid chemistry. To address thermokinetic uncertainties, where possible, conservative reaction parameters have been assumed. Specifically, rates tend to be overestimated, and solubility-limiting phases that tend to be the most soluble are chosen. Other parameter uncertainties, such as estimated extents of clad failure and fluid influxes, have been addressed by considering a range of values as inputs.

**Cladding Degradation**—There are limitations to the cladding model. The model is strictly applicable only to commercial pressurized water reactor fuel with Zircaloy cladding, but it is used for boiling water reactor fuel and fuel with advanced zirconium-base cladding as well. Such application is conservative because boiling water reactor fuel is less heavily stressed and advanced cladding alloys have better performance than Zircaloy. The model is also limited to fuel exposed to normal operation and anticipated operational events; it is not applicable to fuel that has been exposed to severe accidents. Fuel burnup projections have been limited to the current licensing environment with restrictions on fuel enrichment, oxide coating thickness, and rod plenum pressures. Cladding degradation from surface facility handling and operation was not considered. Ranges of uncertainties have been established and conservatism was used in developing this analysis.

**Commercial Spent Nuclear Fuel**—The dissolution model is appropriate for repository conditions, as discussed in Section 4.2.6.3.11. From an analysis of the fit of the model to the data, and from further consideration of the uncertainty of application of data from young spent fuel (less than 30

years out of reactor) and unburned uranium dioxide toward the prediction of long-term (greater than 1,000-year) performance of spent fuel, the model was estimated to be valid to about one order of magnitude (a factor of ten). The model and uncertainty range adequately accounted for, or overestimated, all dissolution rate data.

**High-Level Radioactive Waste Glass Degradation**—The primary uncertainties in the long-term corrosion rate of high-level radioactive waste glass are associated with the value of the  $k_{eff}$  (i.e.,  $k_{eff} = k_0 \cdot [1 - Q/K]$ , where  $k_0$  is the intrinsic dissolution rate and  $Q$  and  $K$  are as defined in Section 4.2.6.3.5) term in the model. The value of  $k_{eff}$  is mathematically constrained to the range  $k_0 > k_{eff} > 0$ , but the appropriate value to use for  $k_{eff}$  is uncertain. The available data show that the dissolution rate decreases monotonically over time in static or nearly static systems. However, for some compositions, after initially decreasing, the dissolution rate has been observed to increase to an apparently constant value. Because the factors that trigger this increase in the glass corrosion rate are not well understood, the abstracted model conservatively assumes that an increase in the rate will occur for all waste glass compositions.

**DOE Spent Nuclear Fuel**—Because of their robust design (see Section 3.3.1), releases from naval spent nuclear fuel waste packages are very small (Mowbray 2000). Releases from naval spent nuclear fuel are significantly less than releases from commercial spent nuclear fuel (CRWMS M&O 1998g, Chapter 6, Appendix A-2.1.14). This comparison shows that it is very conservative to represent releases from naval spent nuclear fuel waste packages with releases from commercial spent nuclear fuel waste packages.

The application of models for the remaining DOE spent nuclear fuel and immobilized ceramic plutonium involves the extrapolation of the models over long periods of time. The sparseness of directly relevant experimental dissolution/degradation data precludes the development of a mechanistic model. In addition, uncertainties in the data—such as in the surface area measurements used to calculate normalized dissolution rates—produce significant uncertainties even in the short-term application of

the models. For this reason and because preliminary TSPA analyses have shown that the overall performance of the repository is very insensitive to the degradation rate of DOE spent nuclear fuel, upper-limit or bounding degradation models were used.

**Solubility**—The limitations of the in-package chemistry model also apply to the solubility model. Inherent limitations within the databases can lead to an uncertainty, up to a factor of 2, when the ionic strength exceeds about 0.7 M. Uncertainties in the kinetic and thermodynamic databases are bounded by suppressing many of the more insoluble actinide solids and using experimentally confirmed solids as the solubility limiting phases. For example, a recent study on the reaction of  $\text{PuO}_2$  with water has found that in the presence of water and oxygen,  $\text{PuO}_2$  may be metastable and can be converted into  $\text{PuO}_{2+x}$  (Haschke et al. 2000). This new finding has raised the concern that plutonium may be more soluble than previously believed. This concern, however, is mitigated by the use of the much more soluble  $\text{Pu}(\text{OH})_2(\text{am})$  instead of  $\text{PuO}_2(\text{c})$  as the solubility controlling solid. While  $\text{PuO}_{2+x}$  may be more soluble than  $\text{PuO}_2(\text{c})$ , it is not clear that  $\text{PuO}_{2+x}$  is more soluble than  $\text{Pu}(\text{OH})_2(\text{am})$ . Because  $\text{Pu}(\text{OH})_2(\text{am})$  solubility is quite high relative to dissolved plutonium concentrations observed in spent fuel tests, this model is believed to be conservative.

**Colloids**—Uncertainty was captured directly in distribution functions for the adsorption coefficients, and bounding values or bounding estimates from experimental results were used for mass concentrations of groundwater and waste-form colloids. Another large uncertainty comes from the limited available information describing formation of colloids from degradation of N Reactor fuel and its potential contribution to repository performance. In the absence of useful data, it is assumed that, due to the small quantity of N Reactor fuel, any colloids generated from degradation of the fuel will have little or no effect on repository performance.

A less significant uncertainty is the mass of colloids produced by commercial spent nuclear fuel degradation. Little colloidal material was

observed experimentally. Colloids formed were smectites, some apparently possessing adsorbed plutonium, and uranium silicates. However, no embedded radionuclide phases were observed in the few clay colloids produced during degradation testing. If any contain embedded (irreversibly attached) radionuclides, the consequences for waste package releases would be minimal, since it is assumed that all colloid-associated radionuclides leave a breached waste package.

Since completion of the TSPA-SR models, the DOE has continued to explore uncertainties associated with these models. Volume 1, Section 9 of *FY01 Supplemental Science and Performance Analyses* (BSC 2001a) describes in detail the additional work performed to further define, model, and understand uncertainties associated with the waste form degradation models. In general, Volume 1 of *FY01 Supplemental Science and Performance Analyses* (BSC 2001a) further discusses uncertainties related to the in-package chemistry model, the dissolved concentration abstraction (solubilities), the high-level waste glass degradation model, the cladding model, and the colloid model. Detailed descriptions and analyses performed since the TSPA-SR model are available in Volume 2 of *FY01 Supplemental Science and Performance Analyses* (BSC 2001b).

In general, these analyses indicate that uncertainty in the relevant processes did not significantly affect performance (e.g., high-level radioactive waste glass dissolution rates, cladding degradation) or that the assumptions used in the TSPA-SR models were conservative (e.g., radionuclide solubilities). In addition, several improved process model representations (e.g., neptunium solubility) were developed and implemented in the supplemental TSPA model. Results of the supplemental analyses support the conclusions drawn from the TSPA-SR analyses in the evaluation of the site's long-term performance.

#### 4.2.6.3.10 Alternative Conceptual Models

Alternate conceptual models were considered in the development of all waste form models. The model chosen for the TSPA-SR was either the one with the most mechanistic and experimental basis

or one that is most easily demonstrated to be bounding. Some model alternatives are discussed below.

As with limitations and uncertainties, alternative conceptual models for engineered barrier system transport processes have also been updated in supplemental analyses, summarized in *FY01 Supplemental Science and Performance Analyses* (BSC 2001a, Section 1; BSC 2001b, Section 1).

**Radionuclide Inventory**—Although the radionuclide inventory is not a model, the use of alternative approaches is nevertheless of interest. In previous TSPAs (e.g., TSPA for viability assessment), radionuclide activities for commercial spent nuclear fuel were developed by assuming an average set of fuel characteristics (enrichment, burnup, and age of the waste) and calculating the radionuclide inventory for that type of fuel having the specified characteristics (CRWMS M&O 2000bm, Section 3.1.3). Radionuclide inventories for high-level radioactive waste were similarly based on an average waste glass. Radionuclide activities for DOE spent nuclear fuel were developed by combining these fuels into a few representative groups and calculating the inventory for a representative fuel from each group.

The current inventory analysis is more detailed and flexible than previous analyses and is tied to the waste stream. Changes in waste package configuration or waste stream are more easily reflected in the per-package inventory of representative waste packages.

**In-Package Chemistry**—The in-package chemistry model provides an average composition for the water in a waste package. Local variations in composition (e.g., crevice chemistries) are possible, but it would be difficult to validate and defend such models.

The in-package chemistry will have some dependence on the composition of the incoming groundwater. Ongoing sensitivity studies are addressing this subject.

**Cladding Degradation**—In the TSPA-VA model, the fuel in rods that were failed before emplace-

ment was assumed to be completely exposed for dissolution. The fuel in an area below an impacting rock or a failed corrosion patch was available for dissolution, but the remaining ends of the rods were not. This model was not necessarily conservative.

Creep rupture of cladding by diffusion-controlled cavity growth has been accepted by the NRC as the predominant mechanism for failure of cladding during dry storage (NRC 2000a, p. 8-5). Dry storage conditions are similar to repository conditions for the period before the waste packages are breached. However, more recent guidance from the NRC (NRC 2000b) allows the use of other models for creep rupture and admits a lack of experimental evidence for diffusion-controlled cavity growth in Zircaloy (NRC 1999a, p. 56).

Other performance assessments have assumed no credit for cladding protection of the fuel. No cladding credit is easily defended as the worst case for repository performance during the regulatory period. However, this alternative is extremely conservative and gives unrealistically high releases at early times.

**Commercial Spent Nuclear Fuel**—This semi-empirical model was based on an understanding of the chemistry of uranium dioxide dissolution. This understanding was used to choose the functional form of the equation for dissolution rate. More complex empirical functions were also considered, but the current form was chosen for its simplicity.

The spent fuel dissolution model was based on results from flow-through experiments in which dissolved material is washed away rapidly. As a result, the model does not reflect the effects of saturation or formation of secondary phases. More realistic models might be constructed to include these effects, but they would necessarily be much more complex, require more data, and be more difficult to validate.

**High-Level Radioactive Waste Glass Degradation**—An alternative model of waste glass degradation envisions corrosion under humid air and dripping water conditions. Water vapor will continually condense in the film of saline water on

the exposed waste glass as the glass corrodes. Continuous exposure to water-saturated air will result in a process of vapor condensation, flow across the sample, and dripping, wherein dissolved species can be transported away from the glass as solution drips from the glass, and fresh water vapor condenses. The corrosion rate of the glass under these conditions will be affected by the rates at which water vapor condenses in the film and solution drips from the sample. These processes will affect the glass dissolution rate through their effects on the solution chemistry of the film. The fully saturated model described elsewhere results in a more rapid dissolution rate and was therefore used instead.

**DOE Spent Nuclear Fuel**—As discussed in Section 4.2.6.3.6, upper-limit, conservative, and best-estimate models have been proposed for each of the groups of DOE spent nuclear fuel, other than naval spent nuclear fuel. The Naval Nuclear Propulsion Program modeled the performance of naval spent nuclear fuel with the same environmental conditions used in the commercial spent nuclear fuel degradation model (Mowbray 2000).

**Solubility**—An alternative approach to estimating dissolved levels of radionuclides is to use dissolved levels measured in contact with experimentally altered fuels. Figure 4-105 shows neptunium concentrations measured in contact with spent fuels in long-term degradation experiments. In general, reliance on values derived from long-term degradation measurements would result in estimated radionuclide concentrations several orders of magnitude below those estimated from solubility measurements.

**Colloids**—An alternative model for waste-form colloid generation was proposed in *Waste Form Colloid-Associated Concentrations Limits: Abstraction and Summary* (CRWMS M&O 2000cn) and *Colloid-Associated Radionuclide Concentration Limits: ANL* (CRWMS M&O 2000dt), in which the rate of colloid formation was based on the rate of release of a tracer ion (boron and technetium), high-level radioactive waste glass and spent nuclear fuel corrosion, and plutonium concentrations. This model was not recommended

for implementation because it is based on limited laboratory data, but it may be useful in the future.

The use of a mass-based adsorption coefficient ( $K_d$ ) or a surface-area-based adsorption coefficient ( $K_a$ ) may be significant in some colloid systems because the effectiveness of colloids at facilitating contaminant transport is largely due to their very large mobile surface area available for sorption. The greatest variability exists in situations in which an inordinately large number of very small colloids exist, which have a high surface-area-to-mass ratio. Based on experimental measurements and observations of colloid characteristics in Yucca Mountain groundwater, this situation does not exist at Yucca Mountain, and the use of a mass-based  $K_d$  is believed to be satisfactory.

In the approach used in the TSPA for the viability assessment, a constant steady-state mass concentration of colloids in groundwater was assumed. The steady-state mass concentration was embedded in a sorption term referred to as  $K_c$ . The approach used in the TSPA-SR is more comprehensive, in that by not assuming a uniform colloid mass concentration, the effect of ionic strength and pH on mass concentration is included, and mass concentration is used in conjunction with  $K_d$  values. This approach provides more realism by accounting for the destabilizing effect of high ionic strength conditions and some pH conditions. The  $K_c$  approach, however, is well suited for far-field transport, where transients in aqueous chemical conditions are not expected.

#### 4.2.6.3.11 Model Validation

In all waste form models, some model validation has been performed. In most cases this has been done by comparing model outputs against experimental observations or geologic occurrences. A number of these comparisons are summarized below.

**Radionuclide Inventory**—Since the radionuclide inventory is simply an accounting analysis, rather than a model, it is not subject to model validation. However, see Section 4.2.6.3.10 for a discussion of other approaches and their effects on inventory.

**In-Package Chemistry**—EQ3/EQ6, the reaction-path code used to model waste package degradation, has been used over the past 20 years to successfully model such complex natural processes/features as seawater speciation and evaporation, hydrothermal ore formation, granite weathering, and high temperature alteration of mid-ocean ridge basalts by seawater. A degree of confidence in the model is also implied by the successful validation of model inputs—thermodynamic data and rate constants.

**Cladding Degradation**—The cladding degradation model is based on over 40 years of experiments and observations of cladding behavior. The analysis of initial cladding conditions is based on reactor fuel performance reports that have been published since the start of the industry. Creep, stress corrosion cracking, and delayed hydride cracking analyses are supported by extensive experimental data. Zirconium alloys were originally developed for use in the chemical industry to handle very corrosive fluids such as hydrochloric acid. In water environments, continuous corrosion experiments have been performed for 27.5 years. Fuel has been exposed in spent fuel pools for over 25 years and in dry storage research programs. The models, including ranges and uncertainties, developed for TSPA are based primarily on experimental observations.

**Commercial Spent Nuclear Fuel**—The dissolution model was based on a large set of qualified flow-through experiments under a wide range of environmental conditions. It is valid from pH 3 to 10, oxygen pressure from 0.002 to 0.2 atmospheres, and total carbon concentrations from  $2 \times 10^{-4}$  to  $2 \times 10^{-2}$  molar. At pHs less than or equal to 7, this model is valid at carbon dioxide pressures of  $10^{-3}$  atmospheres. To provide additional confidence, the model was compared to unsaturated drip tests, batch tests, and a range of literature results.

**High-Level Radioactive Waste Glass Degradation**—To show that the model provides a conservative upper bound to the long-term rate under basic conditions, calculated rates were compared with the Stage III rates measured with long-term product consistency tests (CRWMS

M&O 2000dl, Section 6.2.3). This was done by first estimating the pH at the reaction temperature of 90°C (194°F) and then using the mean values for the model parameters. The calculated rates are plotted against the experimentally measured rates in Figure 4-107. A diagonal line is drawn to indicate where the calculated and measured rates are equal. All of the points lie above the diagonal line, which indicates that the model provides an upper bound estimate of the long-term rates for these glasses. Note also that model rates have been compared against long-term alteration of submarine basalt glass and been shown to be conservative.

**DOE Spent Nuclear Fuel**—The initial results of TSPA sensitivity analyses for DOE spent nuclear fuel (CRWMS M&O 2000dv, Section 7) indicate that the performance of the repository is very insensitive to its degradation kinetics. Even if all radionuclides are released instantaneously, the calculated boundary dose is well within requirements. Use of a less conservative model would not significantly lower the calculated boundary dose, because even with the upper-limit model, releases due to DOE spent nuclear fuel are significantly lower than those due to high-level waste and commercial spent nuclear fuel.

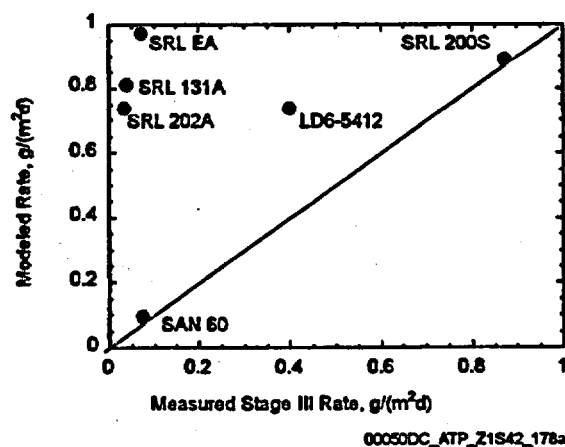


Figure 4-107. Plot of Long-Term Estimated Glass Dissolution Rates vs. Stage III Measured Product Consistency Test Rates

Source: Derived from data in CRWMS M&O 2000dl, Table 3.

The conservative and best estimate models for DOE spent nuclear fuel waste forms are primarily impacted by the validity of the uranium metal-based DOE spent nuclear fuel dissolution models.

**Solubility**—The solubility model is based on well-established chemical principles, so model validation is primarily validation of the thermodynamic data used in the model. A systematic review of thermodynamic data and controlling phases has been performed for a large range of chemical conditions. When uncertainties were encountered, choices were made that would result in higher predicted solubilities. Inherent limitations within the databases can lead to an uncertainty up to a factor of 2 when the ionic strength exceeds about 0.7 mol/L. However, this uncertainty is small relative to other uncertainties within the system. Figure 4-105 shows neptunium concentrations measured in contact with spent fuels in long-term degradation experiments. In general, reliance on values derived from long-term degradation measurements would result in estimated radionuclide concentrations several orders of magnitude below those estimated from solubility measurements. These observations provide validation that the solubility model will bound the radionuclide concentrations.

**Colloids**—The colloid model abstraction is based on laboratory results from waste-form corrosion testing and testing of adsorption and desorption properties of plutonium and americium on clay and iron-(hydr)oxide colloids. The development of the conceptual model and implementation requires consideration of colloid generation, colloid-radionuclide interaction, colloid stability behavior, and to some extent, colloid transport/retardation behavior. Information used for groundwater colloids, waste-form colloids, and corrosion-product colloids was obtained primarily from Yucca Mountain-specific studies. Consequently, the colloid-concentration model is expected to be representative of Yucca Mountain behavior.

Field evidence of small concentrations of radionuclides associated with colloids migrating considerable distances has provided insight into possible colloid behavior at Yucca Mountain. At the Benham nuclear test site at the Nevada Test Site, colloid-associated plutonium appears to have

been rapidly transported (Kersting et al. 1999). At a point about 1.3 km (0.8 mi) from the blast site,  $1 \times 10^{-14}$  mol/L colloid-associated plutonium was detected 30 years after the detonation. It is plausible that the plutonium was transported as plutonium irreversibly attached to colloids, a possibility which underscores the potential significance of the irreversibility of radionuclide attachment to smectite colloids observed in Argonne National Laboratory waste form corrosion experiments (CRWMS M&O 2000dt, Figures 11 and 13). Irreversibly attached colloids are included in the abstracted model as a contribution to the colloid-associated radionuclide concentration.

#### 4.2.6.4 Total System Performance Assessment Abstraction

The process models described in Section 4.2.6.3 are not fully implemented until they are combined within the TSPA model, as shown in Figure 4-97. While the fundamental features specific to each process model are retained where possible in the TSPA, a number of further simplifications have been made. These are outlined in greater detail below.

##### 4.2.6.4.1 Inventory Abstraction

The radioisotope inventory abstraction provided the radioisotope inventory for TSPA. This abstraction is described in *Inventory Abstraction* (CRWMS M&O 2000ds) and nine supporting calculations. Three important aspects of the radionuclide inventory abstraction are (1) obtaining the radioisotope inventories of various fuels and wastes, (2) selecting the most important radionuclides for human dose out of the few hundred found within the fuel and waste, and (3) grouping the fuels and wastes into the waste packages selected for modeling in the TSPA-SR analysis.

**Data Sources**—Four main sources were used for inventory data: (1) commercial utilities, for commercial spent nuclear fuel (CRWMS M&O 1999a); (2) DOE National Spent Nuclear Fuel Program, for DOE spent nuclear fuel (DOE 1999d); (3) Yucca Mountain Environmental Impact Statement (EIS) program, for DOE high-level radioactive waste, mixed oxide, and plutonium

ceramic wastes (DOE 1999a); and (4) *Monitored Geologic Repository Project Description Document* (Curry 2001, Table 5-5).

**Isotope Selection**—The relative importance of individual radionuclides to offsite doses was evaluated for several waste types, time frames, and release scenarios (CRWMS M&O 2000bm, Section 3.1.1.1). This evaluation considered the effects of inventory abundance, radionuclide longevity, element solubility, and element transport affinity. Inventory abundance was addressed by examining eight waste types (average and bounding types for boiling water reactor, pressurized water reactor, high-level radioactive waste, and DOE spent nuclear fuel waste forms). To address radionuclide longevity, these fuels were evaluated between 100 years and 1 million years after repository closure. The elements were separated into two solubility groups—the relatively soluble and the relatively insoluble (americium, curium, zirconium, thorium, niobium, protactinium, and tin)—and three transport affinity groups: (1) highly sorbing, (2) moderately sorbing, and (3) slightly sorbing to nonsorbing. The isotopes within each group were ranked against one another in relative importance (CRWMS M&O 2000ds, Section 4.1.1.4). Three release scenarios were considered: nominal case, human intrusion, and direct volcanic release. Two time frames were considered: 100 years to 10,000 years and 100 years to 1 million years. The set of important isotopes was different for each scenario and time frame. The resulting 23 screened-in isotopes are shown in Table 4-19, along with isotope selection from previous performance assessments. The differences between the isotope selection in these performance assessments are primarily due to (1) modification made to remain consistent with licensing-related regulations concerning, for example, dose, groundwater protection, the time period—10,000 years or 1 million years, and human intrusion, (2) inventory data relied upon, and (3) screening techniques.

**Grouping of Fuels and Wastes**—The waste types, allocations, and waste packages for commercial spent nuclear fuel, high-level radioactive waste (including immobilized plutonium), and DOE spent nuclear fuel are shown in Figure 4-108.

For the base case, over 220,000 commercial spent nuclear fuel assemblies will need to be disposed, and each assembly will have a unique isotopic composition. In 1995, the utilities supplied historical information about reactor assembly discharges up through December 1995 and five-cycle forecasts for assembly discharges. With this information, the forecasts for assembly discharges over the lifetime of each commercial power reactor were developed for use in defining the commercial spent nuclear fuel inventory for the TSPA (CRWMS M&O 1999a). For the base case repository design of 70,000 MTHM, three alternative schedules were developed for shipping the assemblies to Yucca Mountain. Radionuclide activities for each assembly in the waste stream were estimated, and the waste package configuration that could accommodate the assembly based on its potential criticality level was determined.

The proposed technology for immobilization of the high-level radioactive waste is vitrification in a borosilicate glass. Because the reprocessed fuel at each of the vitrification sites differs, the radionuclide inventory of the waste and resultant glass product will vary slightly among the sites.

Up to approximately 33 metric tons of surplus plutonium will be fabricated into uranium-plutonium fuel (mixed-oxide fuel) and irradiated in commercial reactors. The spent fuel will be treated as part of the commercial waste stream. About 17 metric tons of surplus plutonium will be immobilized with neutron absorber material in small canistered ceramic disks. These disks will be placed within standard high-level radioactive waste canisters and the remaining void filled with high-level radioactive waste glass.

DOE spent nuclear fuel consists of more than 250 distinct types, and much like commercial spent nuclear fuel, radionuclide inventories for these fuels will vary widely depending on the history of the fuel. The National Spent Nuclear Fuel Program divided the fuels into 11 groups.

Arrival scenarios were developed for all fuels and wastes. The immobilized plutonium, DOE spent nuclear fuels, and high-level radioactive wastes will be packaged in the 10 canister designs listed in

Table 4-19. Isotope Selection

isotope	TSPA-SR <sup>a</sup> & Final EIS 2000	TSPA 1993 <sup>b</sup>	TSPA 1995 <sup>c</sup>	TSPA-VA 1998 <sup>d</sup>	NRC Iterative Performance Assessment 1995 <sup>e</sup>
<sup>227</sup> Ac	X	X	X		
<sup>108m</sup> Ag		X			
<sup>241</sup> Am	X	X	X		X
<sup>242m</sup> Am		X	X		
<sup>243</sup> Am	X	X	X		X
<sup>14</sup> C	X	X	X	X	X
<sup>36</sup> Cl		X	X		
<sup>243</sup> Cm		X			
<sup>244</sup> Cm		X	X		
<sup>245</sup> Cm		X	X		X
<sup>246</sup> Cm		X	X		X
<sup>135</sup> Cs		X	X		X
<sup>137</sup> Cs	X	X			X
<sup>129</sup> I	X	X	X	X	X
<sup>99</sup> Mo		X			
<sup>93m</sup> Nb			X		
<sup>94</sup> Nb		X	X		X
<sup>59</sup> Ni		X	X		X
<sup>63</sup> Ni		X	X		
<sup>237</sup> Np	X	X	X	X	X
<sup>231</sup> Pa	X	X	X	X	X
<sup>210</sup> Pb	X	X	X		
<sup>107</sup> Pd		X	X		
<sup>238</sup> Pu	X	X	X		
<sup>239</sup> Pu	X	X	X	X	X
<sup>240</sup> Pu	X	X	X		X
<sup>241</sup> Pu		X	X		
<sup>242</sup> Pu	X	X	X	X	
<sup>226</sup> Ra	X	X	X		X
<sup>228</sup> Ra			X		
<sup>79</sup> Se		X	X	X	X
<sup>151</sup> Sm		X	X		
<sup>121m</sup> Sn		X			
<sup>126</sup> Sn		X	X		
<sup>90</sup> Sr	X	X			
<sup>99</sup> Tc	X	X	X	X	X

Table 4-19. Isotope Selection (Continued)

Isotope	TSPA-SR <sup>a</sup> & Final EIS 2000	TSPA 1993 <sup>b</sup>	TSPA 1995 <sup>c</sup>	TSPA-VA 1995 <sup>d</sup>	NRC Iterative Performance Assessment 1995 <sup>e</sup>
<sup>229</sup> Th	X	X	X		
<sup>230</sup> Th	X	X	X		X
<sup>232</sup> Th			X		
<sup>232</sup> U	X	X	X		X
<sup>233</sup> U	X	X	X		X
<sup>234</sup> U	X	X	X	X	X
<sup>235</sup> U		X	X		
<sup>236</sup> U	X	X	X		
<sup>238</sup> U	X	X	X		X
<sup>93</sup> Zr		X	X		

NOTES: <sup>a</sup>CRWMS M&O 2000ds, Sections 7.1 and 7.2.

<sup>b</sup>Wilson, M.L. et al. 1994.

<sup>c</sup>CRWMS M&O 1995.

<sup>d</sup>DOE 1998, Volume 3.

<sup>e</sup>Wescott et al. 1995.

Source: CRWMS M&O 2000bm, Table 3.1-1.

Section 3.3 and Table 4-20. These canisters and the commercial spent nuclear fuel assemblies will be emplaced in the 10 waste package designs listed in Tables 3-2 and 4-21. The waste packages and canisters combine to give a total of 13 waste package configurations, as shown in Table 4-22.

Average and bounding inventories were developed for each package configuration recommended for the potential repository (CRWMS M&O 2000dw). Then, the package-specific radionuclide activities were combined, using the number of waste packages in each group as a weighting factor, to estimate the per-package radionuclide activities for TSPA modeling purposes (see Table 4-23). For each commercial spent nuclear fuel configuration, the average radionuclide activity is the number of assemblies multiplied by the average per-assembly radionuclide activity. For the TSPA representative commercial spent nuclear fuel waste package, a weighted average of these five configurations was used. For the TSPA representative codisposal waste package, the average radionuclide activity from DOE spent nuclear fuel is the number of DOE spent nuclear fuel canisters multiplied by the

average per canister radionuclide activity calculated. Similarly, the average radionuclide activity from high-level radioactive waste for one of these configurations is the number of waste canisters multiplied by the average per canister radionuclide activity calculated. This average was performed for all waste and fuel that was represented in the TSPA by the codisposal packages.

Because of its robust design (see Section 3.3.1), releases from naval spent nuclear fuel waste packages are very small (Mowbray 2000). Releases from naval spent nuclear fuel are significantly less than releases from commercial spent nuclear fuel (BSC 2001q). This comparison shows that it is very conservative to represent releases from naval spent nuclear fuel waste packages with releases from commercial spent fuel waste packages.

Three radionuclides appear in Table 4-23 that were not listed in Table 4-19: radium-228, thorium-232, and uranium-235. These isotopes were not identified as important contributors to dose. However, radium-228 and thorium-232 are required for the proposed groundwater protection scenario, and

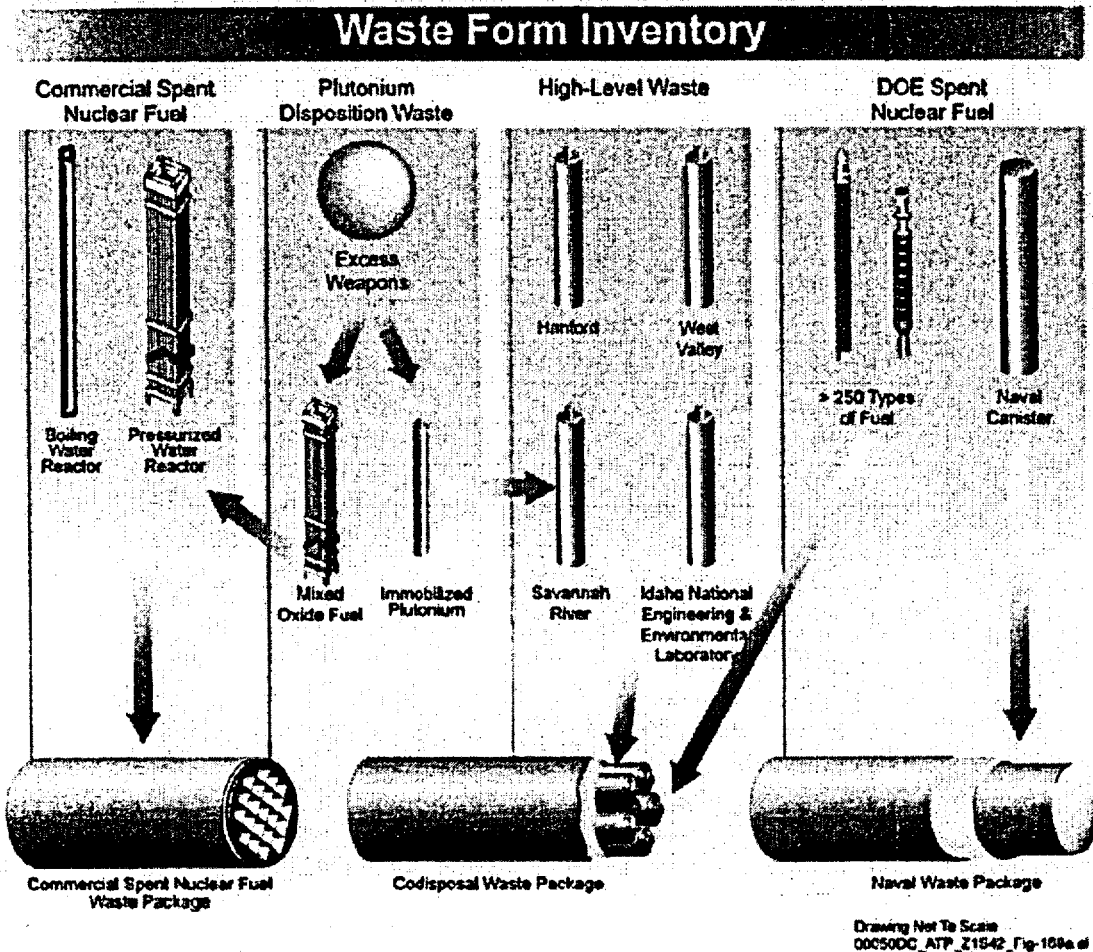


Figure 4-108. The Waste Form Inventory, Detailing Waste Types, Allocation, and Waste Packages  
Source: Adapted from CRWMS M&O 2000bm, Figure 3.1-1.

uranium-235 is required for calculations of the dose from protactinium-231.

Projected waste streams could differ from the actual waste streams in their fuel burnups, fuel ages, fuel enrichments, and utility efficiencies, which introduces some uncertainty in the model. However, the analysis performed for TSPA-SR is more detailed and flexible than previous analyses and is tied to the waste stream. Changes in waste package configurations or waste streams are more easily reflected in the per-package inventory of representative waste packages.

#### 4.2.6.4.2 In-Package Chemistry Abstraction

*Summary of In-Package Chemistry for Waste Forms* (CRWMS M&O 2000dm, Section 6) uses

reaction-path modeling to predict the broad range of effluent compositions emanating from a breached waste package and provides a basis from which to estimate radioisotope solubilities.

The analysis of calculated in-package fluid compositions reveals four common characteristics. Carbonate alkalinity increases with pH due to the assumed fixed partial pressure of carbon dioxide. System Eh decreases with pH due to the assumed constant partial pressure of oxygen. Low early pHs are only seen with low cladding failures, and alkalinities typically correlate with high ionic strengths associated with high glass dissolution and low flow rates. Typically, reaction times of less than 1,000 years result in relatively minor degradation of waste package components; hence, the concentrations of many radionuclides are often well below

their respective solubility limits. In effect, their concentrations depend directly on the dissolution rates of waste package components. At much greater time spans (over 1,000 years), many, but not all, radionuclides have reached saturation with at least one mineral phase. Once this has occurred, dissolved levels of the particular radionuclides will depend on the thermodynamics of secondary phase stability and much less directly upon the dissolution rates of the waste package components.

Table 4-20. Canister Designs

Canister Design	Canister Design Code
Naval short	C1
Naval long	C2
DSNF short	C3
DSNF long	C4
DSNF short, wide	C5
DSNF long, wide	C6
HLW short	C7
HLW long	C8
HLW short with Pu-ceramic	C9
Multicanister overpack	C10

NOTES: DSNF = DOE spent nuclear fuel; HLW = high-level radioactive waste.

Table 4-21. Waste Package Designs

Waste Package Design	Waste Package Design Code
21-PWR Absorber Plate	W1
21-PWR Control Rod	W2
12-PWR Long	W3
44-BWR	W4
24-BWR	W5
5-DHLW/DOE SNF Short	W6
5-DHLW/DOE SNF Long	W7
2-MCO/2-DHLW Long	W8
Naval SNF Short	W9
Naval SNF Long	W10

The abstraction of in-package processes consists of multiple linear regression analyses of the output from the EQ3/6 simulations described in the *In-Package Chemistry Abstraction* (CRWMS

M&O 2000dn). The multiple linear regression analyses take explicit account of the change in process control with time and treat results for times less than 1,000 years after waste package breach separately from those for later times.

The pH abstraction follows two lines of reasoning based on the waste package type (commercial spent nuclear fuel waste package or codisposal waste package) and the difference in kinetic rate laws between the two. The rate law for commercial spent nuclear fuel is proportional to the hydrogen ion activity, i.e., proportional to pH, such that at low pH the dissolution rate increases (CRWMS M&O 2000dm, Section 6.1.1). For high-level radioactive waste glass, the rate law is "U" shaped, with the minimum at pH 7 and the rate increasing above and below pH 7 (CRWMS M&O 2000dm, Section 6.1.1). For the commercial spent nuclear fuel, at times less than 1,000 years after waste package breach, minimum pH values for each flux/cladding/corrosion scenario were regressed to produce two abstractions of pH; one for low waste package corrosion rates and the other for high waste package corrosion rates. This process was repeated for times greater than 1,000 years after breach, where the average pH for the entire modeled duration (0 to 10,000 years after breach) was used to calculate the average pH.

The results are four response surfaces for each waste type, two surfaces for less than 1,000 years, and two for more than 1,000 years. The parameter space between two surfaces may be sampled by the TSPA code where pH can be calculated as a function of time, water flux  $Q$  ( $m^3/yr$ ), waste package corrosion rates, and cladding coverage, or glass dissolution rate for the case of codisposal waste packages. In the case of the commercial spent nuclear fuel, assuming the lowest observed pH for the less than 1,000-year period, and the averaged pH for greater than 1,000-year period is the most conservative, while still honoring the pH-time history. However, for the codisposal package using the lowest observed pH is conservative for the less than 1,000-year period but not for the greater than 1,000-year period when use of the maximum pH is conservative. The difference in the rate laws between glass and commercial spent nuclear fuel and the difference in the pH-time profiles for the

Table 4-22. Waste Configurations Used in the Inventory Abstraction

Configuration	Waste Package Design Code	Number <sup>a</sup>	DSNF Canisters per Waste Package	HLW Canisters per Waste Package
21-PWR Absorber Plate	W1	4500	—	—
21-PWR Control Rod	W2	100	—	—
12-PWR Long	W3	170	—	—
44-BWR	W4	3000	—	—
24-BWR	W5	90	—	—
<b>Total Commercial Spent Nuclear Fuel</b>		<b>7860</b>		
Pu-ceramic in HLW	W6	100	—	Five C7 (short)
Codisposal short	W6	1100	One C3 (short)	Five C7 (short)
Codisposal long	W7	1500	One C4 (long)	Five C8 (long)
Codisposal mixed	W7	130	One C3 (short)	Five C8 (long)
HLW-only	W7	600	—	Five C8 (long)
2-MCO/2-DHLW Long	W8	160	Two C10	Two C8 (long)
<b>Total Codisposal</b>		<b>3590</b>		
Naval SNF Short	W9	200	One C1 (short)	—
Naval SNF Long	W10	100	One C2 (long)	—
<b>Total Naval</b>		<b>300</b>		

NOTE: <sup>a</sup>Curry 2001, Table 5-5.

two waste forms predicate the use of different assumptions in the abstractions.

The balance of acid production from A516 carbon steel and base production from the glass determine the pH in codisposal waste packages. At early times (less than 1,000 years after breach), acid production dominates, but as the steel is consumed, base production overcomes the acid production. In most cases, this is not calculated to occur until considerably after 10,000 years after breach.

Total dissolved carbonate affects the solubilities of a number of actinide phases as well as the degradation rate of commercial spent nuclear fuel. The total dissolved carbonate is abstracted as a function of pH by assuming a partial pressure of  $10^{-3}$  atm for carbon dioxide and equilibrium between the carbonate, bicarbonate, and carbonic acid in solution. The system Eh is important in particular for determining the solubilities of many of the actinides. Calculating Eh directly from the pH and an assumed partial pressure of oxygen (0.20 atm) tends to be conservative, as it maximizes the solubilities of a number of radionuclides.

For the period before 1,000 years after breach, the minimum ionic strength was calculated for each flux/cladding and glass-rate/corrosion-rate

scenario. At times greater than 1,000 years after breach, the average value of ionic strength was used from each scenario to calculate the ionic strength range used in the colloid abstraction.

#### 4.2.6.4.3 Commercial Spent Nuclear Fuel Cladding Degradation Abstraction

The cladding degradation process models are abstracted to a family of distributions, lookup tables, or simple calculations for inclusion in the TSPA. The following summarizes this abstraction.

**Cladding Condition as Received**—The groups (bins) of waste packages have an average initial cladding failure distribution of 0.095 percent (range 0.0155 to 1.29 percent, triangular distribution).

**Creep Failures**—Table 5 of *Clad Degradation—Summary and Abstraction* (CRWMS M&O 2000dj) gives the percentage of rods failed as a function of peak waste package surface temperature. Because of the comparatively low temperatures of the design, the creep failures are due only to creep failures in dry storage and transportation to Yucca Mountain. This produces an initial cladding failure distribution of 2.44 percent (range 1.05 to 19.4 percent, triangular distributed).

Table 4-23. Average Radionuclide Inventory in Grams in Commercial Spent Nuclear Fuel and Codisposal Waste Packages for TSPA-SR

Isotope	Specific Activity (Ci/g)	Grams in TSPA-SR CSNF Packages	Grams in TSPA-SR Codisposal Packages	
			From Spent Fuel	From HLW glass
Actinium-227	$7.24 \times 10^1$	$3.09 \times 10^6$	$1.13 \times 10^4$	$4.67 \times 10^4$
Americium-241 <sup>a</sup>	$3.44 \times 10^0$	$1.09 \times 10^4$	$1.17 \times 10^2$	$6.57 \times 10^1$
Americium-243	$2.00 \times 10^{-1}$	$1.29 \times 10^3$	$1.49 \times 10^0$	$3.99 \times 10^{-1}$
Carbon-14	$4.46 \times 10^0$	$1.37 \times 10^0$	$4.96 \times 10^{-2}$	$6.43 \times 10^{-3}$
Cesium-137	$8.65 \times 10^1$	$5.34 \times 10^3$	$1.12 \times 10^2$	$4.51 \times 10^2$
Iodine-129	$1.73 \times 10^{-4}$	$1.80 \times 10^3$	$2.51 \times 10^1$	$4.80 \times 10^1$
Neptunium-237	$7.05 \times 10^{-4}$	$4.74 \times 10^3$	$4.79 \times 10^1$	$7.23 \times 10^1$
Protactinium-231	$4.72 \times 10^{-2}$	$9.87 \times 10^{-3}$	$3.25 \times 10^{-1}$	$7.95 \times 10^{-1}$
Lead-210	$7.64 \times 10^1$	$0.00 \times 10^0$	$1.40 \times 10^{-6}$	$1.14 \times 10^{-7}$
Plutonium-238	$1.71 \times 10^1$	$1.51 \times 10^3$	$6.33 \times 10^0$	$9.33 \times 10^1$
Plutonium-239	$6.21 \times 10^{-2}$	$4.38 \times 10^4$	$2.30 \times 10^3$	$3.89 \times 10^3$
Plutonium-240	$2.27 \times 10^{-1}$	$2.09 \times 10^4$	$4.89 \times 10^2$	$3.81 \times 10^2$
Plutonium-242	$3.93 \times 10^{-3}$	$5.41 \times 10^3$	$1.11 \times 10^1$	$7.77 \times 10^0$
Radium-226	$9.89 \times 10^{-1}$	$0.00 \times 10^0$	$1.87 \times 10^{-6}$	$1.67 \times 10^{-5}$
Radium-228	$2.72 \times 10^2$	$0.00 \times 10^0$	$6.98 \times 10^{-6}$	$3.19 \times 10^{-6}$
Strontium-90	$1.37 \times 10^2$	$2.24 \times 10^3$	$5.54 \times 10^1$	$2.88 \times 10^2$
Technetium-99	$1.70 \times 10^{-2}$	$7.68 \times 10^3$	$1.15 \times 10^2$	$7.29 \times 10^2$
Thorium-229	$2.14 \times 10^{-1}$	$0.00 \times 10^0$	$2.66 \times 10^{-2}$	$4.08 \times 10^{-3}$
Thorium-230	$2.06 \times 10^{-2}$	$1.84 \times 10^{-1}$	$1.06 \times 10^{-2}$	$7.82 \times 10^{-3}$
Thorium-232	$1.10 \times 10^{-7}$	$0.00 \times 10^0$	$1.49 \times 10^4$	$7.31 \times 10^3$
Uranium-232	$2.20 \times 10^1$	$1.01 \times 10^{-2}$	$1.47 \times 10^{-1}$	$8.23 \times 10^{-4}$
Uranium-233	$9.66 \times 10^{-3}$	$7.00 \times 10^{-2}$	$2.14 \times 10^2$	$1.11 \times 10^1$
Uranium-234	$6.24 \times 10^{-3}$	$1.83 \times 10^3$	$5.72 \times 10^1$	$4.72 \times 10^1$
Uranium-235	$2.16 \times 10^{-6}$	$6.28 \times 10^4$	$8.31 \times 10^3$	$1.70 \times 10^3$
Uranium-236	$6.47 \times 10^{-5}$	$3.92 \times 10^4$	$8.53 \times 10^2$	$3.98 \times 10^1$
Uranium-238	$3.36 \times 10^{-7}$	$7.92 \times 10^6$	$5.09 \times 10^5$	$2.61 \times 10^5$

NOTES: <sup>a</sup>Part of the americium-241 inventory is due to decay of plutonium-241 and curium-245.

Source: *Inventory Abstraction* (CRWMS M&O 2000ds, Section 7 and Attachment I). These numbers have been updated from the numbers used in TSPA-SR, which were provided in the initial version of *Inventory Abstraction* (CRWMS M&O 2000dx). CSNF = commercial spent nuclear fuel; HLW = high-level radioactive waste.

This failure rate is added to the cladding condition as received failures.

**Localized Corrosion**—This conservative model uses two severe assumptions. The first assumption is that there is no filling or flushing of the waste package by water. This is the worst case for concentration of aggressive species and breach of cladding. It is assumed that groundwater entry occurs while there is still significant heat and/or radiation. The water flow rate must nearly match the evaporation rate within the package. If the flow is too high, the package will fill and overflow. The scenario of a filled, well-mixed, overflowing

package is covered by the in-package chemistry model, which shows only moderate pH reduction. The scenario with flushing is the worst for transport of species out of the package but is not the worst for cladding performance. Filling the package with water displaces the nitrogen that otherwise might be radiolytically converted to nitric acid. Overflow will flush out aggressive species and prevent groundwater from concentrating to the point of promoting galvanic corrosion of the carbon steel basket materials. Oxygen influx is also greatly reduced in a flooded waste package, so the corrosion potential and corrosion rates are reduced, as are many radionuclide solubilities.

The second assumption is that aggressive species concentrate in the worst possible way. Because fluoride and chloride are consumed by reaction with Zircaloy (CRWMS M&O 2000df, Section 6.2.2.3.2) and carbon steel (McCright 1998, Section 2.1.8), respectively, it is assumed that aggressive species from incoming water will concentrate where they can do the most damage. For fluoride, this would be nearly total evaporation of incoming drops on a drop-width section of a single fuel rod. For chloride, this would be in a crevice between Zircaloy and carbon steel basket materials. It is assumed that the incoming water species are directed to a single rod, until they have breached that rod. Then it is assumed that new aggressive species are directed to another single rod until it is breached, and so on. In this approach, the fraction of cladding perforated is linearly dependent on the water inflow, which generally increases with time as the waste package degrades. Inflow, however, is also a function of other factors such as climate and location within the repository. The likelihood of significant concentration of aggressive species decreases with time; as decay heat and radioactivity decrease, likelihood of good galvanic connection to the Zircaloy decreases, and amount of reduced iron as an energy source for microbes decreases. The trend toward less aggressive conditions is ignored, however, as it is assumed that the aggressive species concentrate in the worst possible way for all time.

This conservative model estimates that the fraction of rods failed from localized corrosion is equal to the amount of water (in  $m^3$ ) that has entered the average waste package in a group (bin) divided by  $2,424 m^3$  ( $85,648 ft^3$ ). Thus, all rods will fail by the time  $2,424 m^3$  ( $85,648 ft^3$ ) of water has entered the package. This is evaluated at each time-step, and as the waste package corrodes, more water enters the waste package and more rods fail.

**Fast Release of Radionuclides**—When the waste package fails, the inventory of isotopes that have migrated to the gap between the fuel and cladding is modeled as instantly released. This was 1.4 percent of the cesium inventory and 4.2 percent of the iodine inventory. In addition, 0.2 percent (range of 0 to 0.4 percent uniformly distributed) of

the inventory of all radionuclides in failed commercial spent fuel rods was modeled as instantly released to account for spent fuel dissolution that occurs before wet unzipping starts.

**Wet Unzipping**—The fuel rods that have failed at time of waste package breach, or later fail from localized corrosion, are modeled as unzipping as the uranium dioxide fuel matrix reacts. The fraction of fuel that is reacted within the waste package is calculated each time step (after waste package failure) based on the intrinsic commercial spent nuclear fuel dissolution rate. The wet unzipping velocity is modeled as 40 times (range 1 to 240, triangular distributed) the intrinsic dissolution velocity. Unzipping starts at the rod center and progresses in both direction. The intrinsic dissolution velocity is evaluated using the in-package chemistry at each time step.

**Seismic Failures**—Seismic failures that are severe enough to fail the cladding are estimated to occur with a frequency of  $1.1 \times 10^{-6}$  per year. When such an event is predicted within a TSPA time-step, all the cladding is assumed to fail and start unzipping.

**Stainless Steel Cladding**—The waste packages that contain the stainless steel clad commercial spent nuclear fuel are treated as a special type of commercial spent nuclear fuel waste package in TSPA. These waste packages are modeled as 3.5 percent of the total number of commercial spent nuclear fuel waste packages and are assumed to contain 33 percent stainless steel clad fuel and 67 percent Zircaloy clad fuel. The stainless steel clad fuel within these packages is assumed to fail and start unzipping at waste package breach.

#### 4.2.6.4.4 Commercial Spent Nuclear Fuel Degradation Abstraction

The degradation rate function is combined with the in-package chemistry and waste package temperature to determine a rate, which is then directly used by the cladding degradation model (see Section 4.2.6.3.3) to determine the rate at which the fuel cladding splits open and exposes more of the fuel matrix. The abstracted dissolution model is shown in Figure 4-102.

#### 4.2.6.4.5 Glass Degradation Abstraction

Dissolution rates are independent of the glass composition within the limits prescribed by the high-level radioactive waste glass waste acceptance product specification, but high-level waste glass degradation rates do depend on pH and temperature. Abstracted degradation rates are shown in Figure 4-104. Uncertainty is included in all three terms of the abstracted model: the effective forward dissolution rate, the pH term, and the activation energy term. These are combined with the pH from abstracted codisposal package chemistry model and the waste package temperature to determine the rate of glass dissolution with time. The resulting uncertainty in the degradation rate included in the model is about four orders of magnitude with a log-uniform distribution.

#### 4.2.6.4.6 DOE Spent Nuclear Fuel and Other Waste Form Degradation Abstraction

The conservative Hanford N Reactor fuel model (1.75 kg/m<sup>2</sup>-day) was recommended as the surrogate to bound DOE spent nuclear fuel groups 2 through 11. Naval spent fuel can be bounded by commercial spent fuel, and immobilized plutonium degradation was bounded by high-level radioactive waste glass degradation.

#### 4.2.6.4.7 Solubility Abstraction

A systematic review of thermodynamic data and controlling phases was performed for a large range of chemical conditions. The amount of thermodynamic data available for the radionuclides, the sensitivity of solubilities to in-package chemistry, and the importance of radionuclides to total system performance is quite uneven. For these reasons, the implementation of solubility within the TSPA-SR analysis ranged from (1) multitermed functions of chemistry for uranium, neptunium, and americium; (2) distributions for plutonium, protactinium, lead, and nickel; and (3) constant bounding values for technetium, iodine, thorium, cesium, strontium, chlorine, carbon, niobium, zirconium, radium, and selenium. For the multitermed functions, the radionuclide solubility was calculated as a function of time for each simulation. For the distribution type,

a value for the simulation was sampled from the distribution and used for the entire simulation. For the last type, the same bounding value was used for all times in all simulations. Detailed discussions for each radionuclide are provided in *Summary of Dissolved Concentration Limits* (CRWMS M&O 2000dp). The concentration limits are given in Table 4-24.

In TSPA, solubilities were calculated for each computational cell, using the abstracted chemistry of that cell. Thus for isotopes whose solubilities were functions of chemistry, the solubilities varied spatially and with time.

Table 4-24. Dissolved Concentration Limits for TSPA-SR

Element	Distribution Type	Min (mol/L)	Max (mol/L)
Americium	Function	$\sim 10^{-7.7}$	$\sim 0.19$
Actinium	Function	$\sim 10^{-7.7}$	$\sim 0.19$
Samarium	Function	$\sim 10^{-7.7}$	$\sim 0.19$
Curium	Function	$\sim 10^{-7.7}$	$\sim 0.19$
Carbon	Constant	1	1
Chlorine	Constant	1	1
Cesium	Constant	1	1
Iodine	Constant	1	1
Niobium	Constant	$10^{-7}$	$10^{-7}$
Nickel	Log Uniform	$10^{-6.9}$	$10^{0.5}$
Neptunium	Function	$\sim 10^{-5.7}$	$\sim 10^{-1.8}$
Protactinium	Log Uniform	$10^{-10}$	$10^{-5}$
Lead	Log Uniform	$10^{-10}$	$10^{-5}$
Plutonium	Log Uniform	$10^{-10}$	$10^{-3.7}$
Radium	Constant	$10^{-6}$	$10^{-6}$
Tin	Constant	$10^{-7.3}$	$10^{-7.3}$
Strontium	Constant	1	1
Technetium	Constant	1	1
Thorium	Constant	$10^{-5}$	$10^{-5}$
Uranium	Function	$\sim 10^{-6.3}$	$\sim 10^{-3.4}$
Zirconium	Constant	$10^{-9.2}$	$10^{-9.2}$

Source: Excerpted from *Summary of Dissolved Concentration Limits* (CRWMS M&O 2000dp).

#### 4.2.6.4.8 Colloids Abstraction

The mobile colloidal radionuclide source term consists of three colloid types: waste-form colloids, corrosion-product colloids, and ground-water colloids. As illustrated in Figure 4-106, the mobile colloidal radionuclide source term is the sum of the radionuclide contribution from those colloid types. The total colloid mass concentration

is also provided for recalculating reversibly attached radionuclide concentrations as dissolved concentrations change during transport.

For codisposal packages, the colloidal source term includes (1) waste-form smectites produced from high-level radioactive waste glass, (2) iron-(hydr)oxide colloids produced from steel packaging material, and (3) naturally occurring groundwater colloids found in the infiltrating water. Plutonium and americium are bound irreversibly in waste form colloids, and along with their daughter products are permanently entrained within the colloid. Waste-form colloids can also serve as substrates for reversibly sorbed plutonium and americium. For commercial spent nuclear fuel packages, only iron-(hydr)oxide and naturally occurring groundwater colloids are available for uptake of radionuclides. Following the conceptual model, the TSPA calculations use in-package and in-drift pH and ionic strength conditions to calculate the generation and stability of waste-form colloids and the stability of corrosion-product and groundwater colloids.

#### 4.2.7 Engineered Barrier System Transport

The purpose of the engineered barrier system transport process model is to provide a description of radionuclide transport within the emplacement drift as a result of releases from one or more breached waste packages (CRWMS M&O 2000as). Radionuclide transport out of the waste form and waste package through the invert and into the unsaturated zone is dependent on a complex series of processes, including development of potential flow pathways through the engineered barrier system discussed in Section 4.2.5. This section emphasizes the mobilization and transport of dissolved or colloidal radionuclide species through the engineered barrier system by flowing or slowly dripping water or alternatively through continuous water films formed by adsorptive condensation of humidity on engineered barrier system materials (CRWMS M&O 2000a, Sections 3.6.1 and 3.6.2). In the TSPA-SR model, the principal processes included in the abstraction are diffusion (i.e., the diffusion barrier effect when advection is negligible) and advection without

sorptive retardation (when there is greater water content).

As noted in Section 4.1.4, the DOE has evaluated operation of the repository at lower temperatures. The conceptual basis and model abstractions presented in this section primarily reflect the effects of higher-temperature operating conditions described in Sections 4.2.2 through 4.2.6, specifically those implemented in the TSPA-SR model (CRWMS M&O 2000a, Section 3.6). Conservatism and conceptual uncertainties in the model have been reevaluated since the TSPA-SR model and are reported or summarized in *FY01 Supplemental Science and Performance Analyses* (BSC 2001a, Sections 10 and 15; BSC 2001b, Sections 3.2.8 and 4.2.8).

New or reevaluated processes modeled in the supplemental TSPA model and found to have a potential affect on radionuclide releases from the engineered barrier system include:

- Waste package diffusion, specifically in-package diffusion (BSC 2001a, Sections 10.3.1 and 10.4.1)
- Sorption of radionuclides to corrosion products derived from mild steel and stainless steel used in the waste package and in the structural support for the invert (BSC 2001a, Sections 10.3.4 and 10.4.4).

Uncertainties in the TSPA-SR colloidal transport model and invert diffusion model were also reevaluated in the supplemental TSPA model (BSC 2001a, Sections 10.3.3, 10.3.5, 10.4.3 and 10.4.5; BSC 2001b, Sections 3.2.8 and 4.2.8). In general, the supplemental TSPA model results suggest that the TSPA-SR model results are reasonable to conservative.

##### 4.2.7.1 Conceptual Basis

The waste form is the source of radionuclides considered for the engineered barrier system. Radionuclides can be transported downward from breached waste packages, through the invert, and into the unsaturated zone. Transport can occur through advection, by which dissolved chemical

species or colloidal particles are carried along by the fluid when there is a fluid flux through the waste package and invert. Transport can also occur by diffusion, whereby dissolved chemical species or colloidal particles migrate from zones of high to low concentration. Diffusion can occur in the absence of an advective liquid flux, if there is a continuous liquid pathway via thin films on the waste form, the waste package, and in the invert (CRWMS M&O 2000a, Section 3.6.2.2).

A one-dimensional transport model is used to represent advection and diffusion in the engineered barrier system. Further, because the duration of radionuclide releases from the waste package will generally be much greater than the travel time through the invert (when advective flow and release conditions pertain), transport dispersivity is neglected in the model. Also, the invert materials have little sorptive affinity for several important radionuclides, so in the TSPA-SR model no performance credit is taken for sorptive retardation (CRWMS M&O 2000a, Section 3.6.1.2).

The engineered barrier system elements through which radionuclides can migrate are conceptually similar to a laboratory column test. That is, radionuclides are introduced at the top of the "column" and migrate downward through materials representing the invert.

**Transport Modes Considered**—Transport of radionuclides through the waste package and into the invert can occur in several possible modes. Dissolved and colloidal radionuclides will diffuse through thin films of water and stress corrosion cracks in the waste package wall. They may also migrate by advection through larger patches formed by general corrosion. Migration through the invert may be by diffusion, advection, or both (CRWMS M&O 2000a, Sections 3.6.1 and 3.6.2; CRWMS M&O 2000dd, Section 6.1.2).

Colloid-facilitated transport of radionuclides is important for certain radionuclides that have limited solubility (as dissolved species) but strong affinity for colloidal-size particles that are mobile in water. Three types of colloids are expected in the engineered barrier system: (1) waste form colloids, (2) colloids produced from corrosion of repository

materials, and (3) groundwater colloids. Radionuclides may become irreversibly embedded in waste form colloids, reversibly attached by sorption, or both modes may exist. Radionuclide sorption to corrosion-product and groundwater colloids is likely to be reversible, although sorption of metal ions to iron-oxide colloids can be quite strong (CRWMS M&O 2000dd, Section 6.1.2).

#### 4.2.7.2 Summary State of Knowledge

##### 4.2.7.2.1 Hydrologic Properties of the Invert

The drip shield is designed to divert water flow to the invert (CRWMS M&O 2001c, Section 6.3). The invert ballast material will be crushed tuff derived from the excavated host rock and will exhibit the hydraulic characteristics of a porous medium. Permeability, porosity, thermal properties, and unsaturated hydrologic properties of candidate invert ballast materials have been measured (CRWMS M&O 2001c).

##### 4.2.7.2.2 Analogue Studies

**Advection**—Laboratory testing of radionuclide migration downward through a crushed-tuff column was performed with several radionuclides (neptunium-237, plutonium-239, tritium, and pertechnetate) in two groundwaters with different chemical compositions (Triay, Meijer et al. 1997, Section V.A). The purpose of the tests was mainly to compare column transport characteristics with radionuclide sorption parameters from batch-sorption tests. The tests, therefore, provided analogous information on advective transport modified by sorption. The engineered barrier system transport model is analogous to these laboratory tests.

**Diffusion**—A different series of tests was performed to gather information on the diffusive uptake of radionuclides by intact samples of tuff (Triay, Meijer et al. 1997, Section VI). It was observed that certain radionuclides could diffuse through minute water-filled pores, depending on the porosity, heterogeneity of the pore structure, and sorptive retardation. The tests show that diffusion through the intact tuff is a slow process, particularly for radionuclides with sorptive affinity

such as actinides. For unsaturated conditions, diffusive transport is very slow.

In another set of tests (Conca and Wright 1992), transport parameters including diffusion coefficients were measured in unsaturated gravels over a range of water content. It was observed that in granular materials, diffusive behavior depends on the presence of small amounts of water on grain surfaces, which presumably facilitate grain-to-grain contact. This was apparent even in materials consisting of grains with significant intra-granular porosity. The electrical conductivity of partially saturated materials was measured, from which the analogous solute diffusivity behavior (diffusion coefficient) was estimated using the Nernst-Einstein relation.

#### 4.2.7.2.3 Colloid-Facilitated Radionuclide Transport

**Colloid Stability at Engineered Barrier System Conditions**—For radionuclide-bearing colloids to affect repository performance, the colloidal dispersion must be stable for the duration of transport and must carry significant amounts of radionuclides. Transport times can range from days to years for advective transport out of a breached waste package and up to hundreds of thousands of years for retarded transport to the receptor location. Thus, some relatively unstable colloids generated at the waste form may persist long enough to be transported out of the waste package and through the invert, but not long enough to be transported a significant distance away from the potential repository. More stable colloids, however, may remain suspended for years and travel a much greater distance (CRWMS M&O 2000cn, Section 6.1.2).

Iron-(hydr)oxide colloids from corrosion of steel and naturally occurring in groundwater are least stable around pH 8.5, and at this pH they will tend to agglomerate (i.e., form larger, immobile particles) (CRWMS M&O 2000cn, Section 6.1.2). At higher or lower pH, however, iron-(hydr)oxide colloids may be more mobile, depending on other factors, such as ionic strength. It is anticipated that ionic strength of water in the drifts will be relatively low during the post-thermal period when

waste package breach is most likely, which will facilitate colloid mobility.

**Analogues**—There is field evidence that suggests colloid-facilitated transport of radionuclides. Buddemeier and Hunt (1988, p. 536) found plutonium and americium more than 30 m (100 ft) below a low-level waste site in unsaturated tuff after approximately 30 years of operation. At the Nevada Test Site, the isotope ratio of plutonium-240 to plutonium-239 in groundwater suggested that plutonium may have been colloidally transported more than 1.3 km (0.8 mi) over a 30-year period, although plutonium is strongly sorbing at the Nevada Test Site and assumed to be immobile (Kersting et al. 1999). In water samples from the Nevada Test Site, plutonium was found to be attached to colloids. In the Pahute Mesa drainage, Buddemeier and Hunt (1988, p. 537) found colloid concentrations of 0.8 to 6.9 mg/L for particles greater than 30 nm (0.000001 in.) in size.

Treated liquid wastes containing traces of plutonium and americium have been released into Mortandad Canyon at Los Alamos National Laboratory (Triay, Meijer et al. 1997, Section V.D). The shallow alluvium at that location is composed of sandy to silty clays formed from weathering of volcanic rocks. Detectable amounts of plutonium and americium have been observed in monitoring wells up to about 3.4 km (2.1 mi) downgradient from the discharge point. Sorption studies had predicted that movement of plutonium and americium would be restricted to a few meters. This suggests that plutonium and americium are strongly associated with colloid materials and that they can be mobile for large distances (Triay, Meijer et al. 1997, Section V.D).

#### 4.2.7.3 Engineered Barrier System Process Model Development

In this section, an overview of radionuclide transport in the engineered barrier system is presented. The engineered barrier system model is described more fully in *EBS Radionuclide Transport Model* (CRWMS M&O 2000dy), *EBS Radionuclide Transport Abstraction* (CRWMS M&O 2000dd), and *Total System Performance Assessment for the*

*Site Recommendation* (CRWMS M&O 2000a, Section 3.6).

The approach uses the analytical solution to the one dimensional advection–dispersion equation for a continuous source to determine radionuclide breakthrough curves for various postclosure scenarios. Breakthrough curves are plots of relative concentration (i.e., the downstream concentration relative to the concentration at the source) at the point of interest (the floor of the drift) versus the amount of time that has passed since the radionuclide was first released from the source (the waste form). Because of the effects of diffusion and dispersion, relative concentrations gradually increase from 0 to 1 as a contaminant front arrives. Breakthrough times for relative concentrations of 0.01 and 0.5 are used to facilitate comparison of the results (CRWMS M&O 2000dd, Section 6.3.3).

The primary hydrologic input to the engineered barrier system analysis is the pore water velocity, which in turn depends on the Darcy flux (volumetric flow rate per unit area) and the moisture content (fractional volume of the invert material that is occupied by water). This input was derived by inspecting output from *Multiscale Thermohydrologic Model* (CRWMS M&O 2000cf, Section 7).

In addition, a correlation based on laboratory-determined diffusion coefficients is used for calculating diffusive transport when the advective pore water velocity is negligible. This correlation is a power law similar to Archie's Law for electrical conductivity (CRWMS M&O 2000dz) that accounts for the effect of moisture content. In the TSPA calculations, the multiscale thermal-hydrologic model provides the invert water content from which the invert diffusion properties are calculated.

Transport calculations are made using the one-dimensional analytical solution and the average pore water velocity immediately beneath the waste package (i.e., at the drift centerline) (CRWMS M&O 2000dy, Section 6). Sensitivity calculations were performed to evaluate breakthrough times (defined by relative concentration of 50 percent) for various combinations of model input parameters. For advective transport, breakthrough is most

sensitive to the sorptive retardation coefficient. For diffusive transport, transport is most sensitive to the diffusion coefficient.

Model assumptions include one-dimensional vertical migration of radionuclides, negligible transport of radionuclides in the vapor phase, and negligible radioactive decay along the transport pathway (CRWMS M&O 2000dd, Sections 5.5 and 5.7). The invert material is assumed to be homogeneous. These assumptions are justified because the most direct pathway is used, and the pathway is short relative to downstream pathways through the host rock. Radionuclides which can contribute to potentially significant doses at the biosphere, do not form gaseous species at conditions present in the engineered barrier system when releases are most likely to occur.

#### 4.2.7.3.1 Limitations and Uncertainties

As noted in Sections 4.1.1.2 and 4.2.7, the DOE performed several activities to improve the treatment of uncertainty in TSPA-SR models. As stated in Section 4.2.7, uncertainties in the TSPA-SR colloidal transport model and invert diffusion model were reevaluated in the supplemental TSPA model (BSC 2001a, Sections 10.3.3, 10.3.5, 10.4.3, and 10.4.5; BSC 2001b, Sections 3.2.8 and 4.2.8).

Although sorptive distribution coefficients for invert materials are uncertain, this does not affect the modeling approach described here because the distribution coefficient for the TSPA-SR model is assumed to be zero: that is, no credit is taken for any retardation that may occur in the engineered barrier system. This assumption produces a conservative estimate of the transport of dissolved species out of the engineered barrier system (CRWMS M&O 2000dd, Section 5.2.7).

If advection is the dominant mode of transport, then differences in travel time at the center of the invert, compared to near the edges, could be important. However, advective travel times are relatively fast, on the order of a few tens of years or less. Therefore, the model is insensitive to the location of the fastest advective pathway through the invert. If advection is negligible (i.e., at low water content), then the invert can behave as a diffusion

barrier. However, by relying on a conservative diffusion coefficient model, the TSPA-SR model and supplemental model studies show limited diffusion resistance to radionuclide transport in the invert (BSC 2001b, Section 3.2.8).

#### 4.2.7.3.2 Alternative Conceptual Processes

Several concepts that could be examined as relevant alternatives were considered but, because they are improbable or not supported by available data, are not incorporated in the engineered barrier system analyses. Transport was represented using a one-dimensional model. Expanding the model to multiple dimensions would provide insights into the spreading of a radionuclide contaminant from a point source, but the resulting differences in the estimated rate of transport would probably be small.

It is possible that complete saturation could occur in the emplacement drift invert due to clogging in the invert or in the host rock that drains the invert. Drainage pathways could become clogged with fine materials by geochemical alteration of engineered barrier system materials or by precipitation of uranium compounds derived from the waste form. Possible consequences include an increased rate of radionuclide release and transport by saturated flow in a direction parallel to the drift axis. Radionuclides might then be transported laterally through the invert to a major fault or fracture zone where relatively rapid drainage through the host rock could occur. Transport of radionuclides through the unsaturated zone would potentially occur at higher velocity, and with fewer water-rock interactions, than if the drainage was more uniform. However, the fracture permeability and drainage capacity of the host rock are considered sufficient that complete saturation of the invert is unlikely, and this condition is excluded from the TSPA-SR model (CRWMS M&O 2001c, Section 6.2.5).

It is also possible that radionuclides could be sorbed by solids (e.g., steel corrosion products) in the engineered barrier system, and that episodes of increased fluid flux could cause temporarily increased rates of radionuclide release. As for episodes of increased flux, this process would

cause dilution downstream, which would tend to mitigate the effects on dose rates at the biosphere. Alternative conceptual processes were conservatively unaccounted for in the TSPA-SR model but were implemented in supplemental models to quantify conservatism. These processes included sorption of radionuclides to corrosion products in the emplacement drifts and in-package diffusion of radionuclides, which were found to have a beneficial affect on total performance. These conclusions have provided additional confidence in the TSPA-SR model (BSC 2001a, Sections 10.3.1, 10.3.3, and 10.3.4).

It is possible that precipitates and salts could accumulate in the invert early in the thermal period. The change in porosity could produce changes in the transport properties. However, the salts would be readily dissolved when water returned during cooldown, leaving the less soluble precipitates (consisting mainly of silica and calcite) at later times when waste package breach is most likely to occur. These precipitates constitute only a fraction of the maximum accumulation (CRWMS M&O 2000cg, Section 6.5) and would occupy only a portion of the available porosity (CRWMS M&O 2001c, Section 6.1). Consequently, the effect on transport properties of the invert ballast material would be limited.

Another possibility is that constituents of the waste form (e.g., uranyl compounds) could precipitate in the invert and change the transport properties. This is unlikely because the waters that contact the waste form will have already reacted with the host rock and because conditions that lead to advective flow through the waste package would be associated with additional water flow that is diverted to the invert and is available for dilution. This possibility is the subject of ongoing analysis.

Microbially facilitated radionuclide transport was considered but was screened out for the TSPA-SR model (CRWMS M&O 2001d, Section 6.4.61). Microbial action tends to increase colloid size, which would make them susceptible to gravitational settling and filtration. Consequently, exclusion of microbially facilitated transport may be considered conservative.

#### 4.2.7.3.3 Engineered Barrier System Radionuclide Transport Model Validation

The one-dimensional advection–dispersion equation is widely accepted for evaluating solute transport, and the analytical solution to this equation provides a robust and reliable method for evaluating transport through a homogeneous material like the invert ballast. Applicability of the model depends on understanding possible changes that could occur in the invert ballast material with time. The model relies on results from *Water Distribution and Removal Model* (CRWMS M&O 2001c, Section 6) for scoping of such changes.

#### 4.2.7.4 Engineered Barrier System Flow and Transport Abstraction

The following sections provide a summary of how the results of the engineered barrier system radionuclide transport process modeling were abstracted for use in the TSPA-SR model. The principal processes included are diffusion (i.e., the diffusion barrier effect when advection is negligible) and advection without sorptive retardation (when there is greater water content) (CRWMS M&O 2000a, Section 3.6).

Over tens of thousands of years the drip shields and waste packages will gradually degrade, leading to the release and transport of radionuclides through the engineered barrier system (Section 4.2.4.3). Water is expected to be the primary transport medium. Flowing water, or a continuous film of stationary water, is necessary for radionuclide transport out of the waste package, through the invert, and into the unsaturated zone (CRWMS M&O 2000a, Section 3.6).

After a waste package is breached, moisture may enter the waste package as vapor and form water films on the internal surfaces (Section 4.2.5.1). If the cladding is breached, radionuclides may dissolve in the water and be transported out of the waste package by diffusion (Figures 4-109 and 4-110). Breaches formed by general corrosion (“patches”) can provide a path for advective liquid flux to enter the waste package and mobilize radionuclides. Advective transport is anticipated to be

the main transport mechanism through corrosion patches. Diffusive transport will be the dominant mechanism through stress corrosion cracks because their small size and associated capillary forces resist advective flux.

The dissolved concentration of each mobilized radionuclide cannot exceed the radionuclide solubility limit, unless suspended colloids are present. Colloids are important because they can increase the concentration of radionuclides in the liquid. Colloids can also increase the transport velocity of radionuclides, although this will be a minor effect over the short distances in the engineered barrier system (CRWMS M&O 2000a, Section 3.6; see also Section 4.2.6.3).

Once outside the package, the radionuclides will be transported through the invert by diffusion if advection in the invert is sufficiently slow, or by advection if an appreciable amount of water is flowing through the invert. For TSPA-SR, the one-dimensional advection–diffusion transport model described previously combines these mechanisms. The conceptual model for the engineered barrier system flow and transport abstraction is summarized in Figure 4-111. The important elements for transport are the flow abstraction and the transport abstraction.

##### 4.2.7.4.1 Flow Abstraction

The source of advective inflow to the engineered barrier system is seepage flux, flowing from discrete fractures in the roof of the drift, falling vertically onto the drip shield and any other exposed components (Figure 4-109). The most important part of the engineered barrier system flow abstraction is the algorithm for splitting the seepage flux into the portion that flows through breaches in the drip shield or waste package and the remainder that flows around the drip shield or waste package (Sections 4.2.5.3 and 4.2.5.4). As discussed in Section 4.2.5.4, the result of the flow abstraction is that fluid flux occurs along eight pathways through the engineered barrier system. Only the flux through the waste package and the flux to the unsaturated zone are used directly in the transport calculations for the TSPA-SR model (CRWMS M&O 2000dd, Section 6.4).

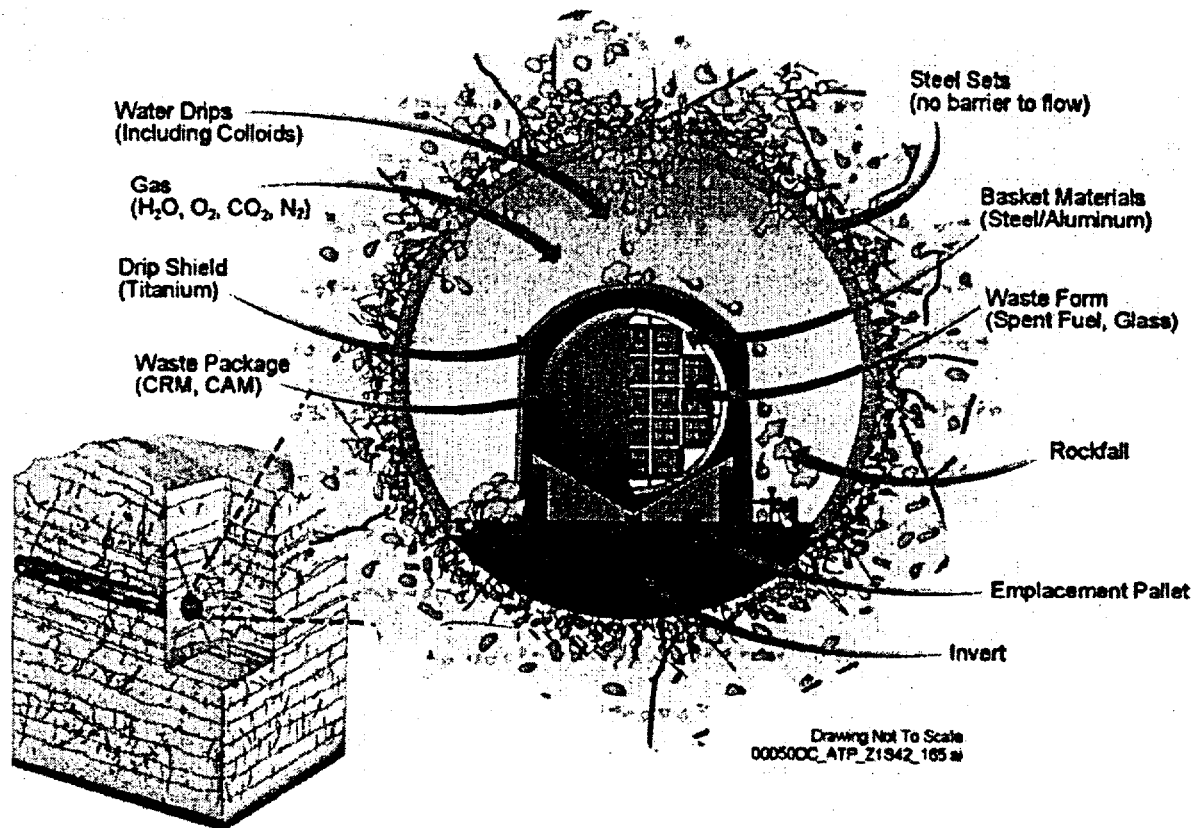


Figure 4-109. Conceptualization of an Emplacement Drift with the Major Components of the Engineered Barrier System, and Seepage Diverted by the Drip Shield  
CRM = corrosion-resistant material; CAM = corrosion-allowance material.

The flow abstraction is conservative in several aspects, as discussed in Sections 4.2.5.3 and 4.2.5.4. First, leakage of liquid water through the drip shield always falls on a waste package, although it is also possible that such leakage could be diverted as film flow on the underside of the drip shield. In addition, where seepage occurs, it is assumed to uniformly wet the surface of the drip shield or waste package. Thus, every breach is exposed to seepage; however, no breach is exposed to the full flow of dripping at a point. This approach is justified because it represents the average response of the many waste package locations where seepage can occur. It also accommodates the average response when seep locations move around with time. Finally, evaporation within and on the waste package is ignored. Either diffusive or advective transport will cease if

the liquid films on the waste form or the waste package evaporate. The potential for evaporation to eliminate radionuclide transport is conservatively ignored in the TSPA-SR model (CRWMS M&O 2000dd, Section 5.1.17).

Modifications to the flow abstraction are discussed in Section 4.2.5 of this report. These changes include a revised method for splitting the seepage flux through the engineered barriers. See Sections 4.2.5.3 and 4.2.5.4 of this report for further discussion.

#### 4.2.7.4.2 Engineered Barrier System Transport Abstraction

The waste form is the source of all radionuclides considered for the engineered barrier system. After

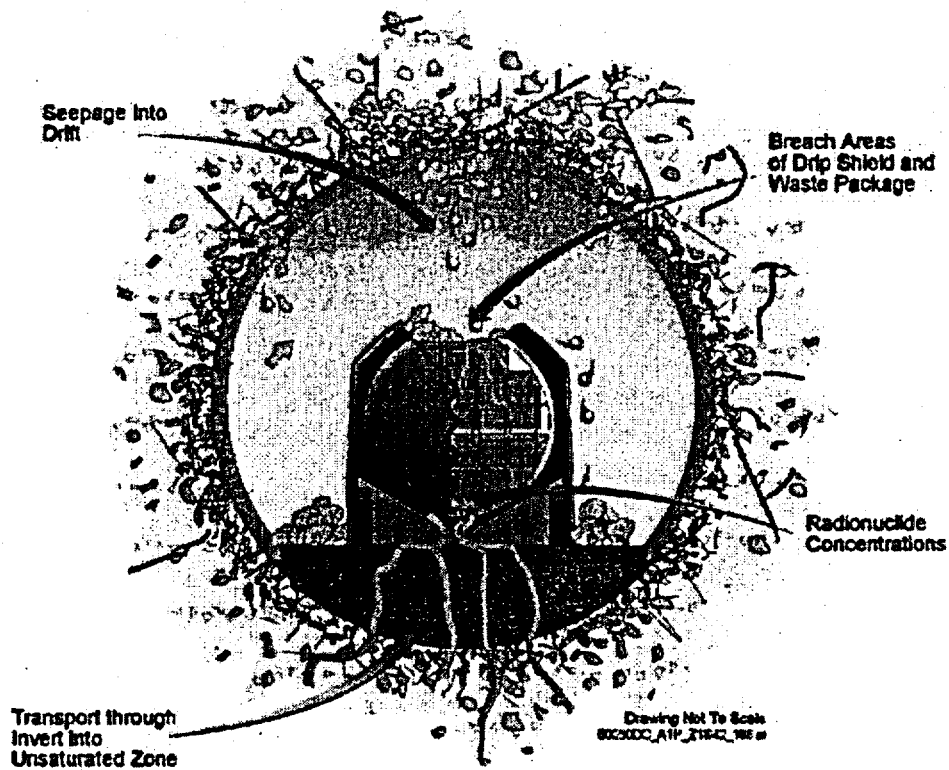


Figure 4-110. Conceptualization of an Emplacement Drift after the Drip Shield and Waste Package are Breached

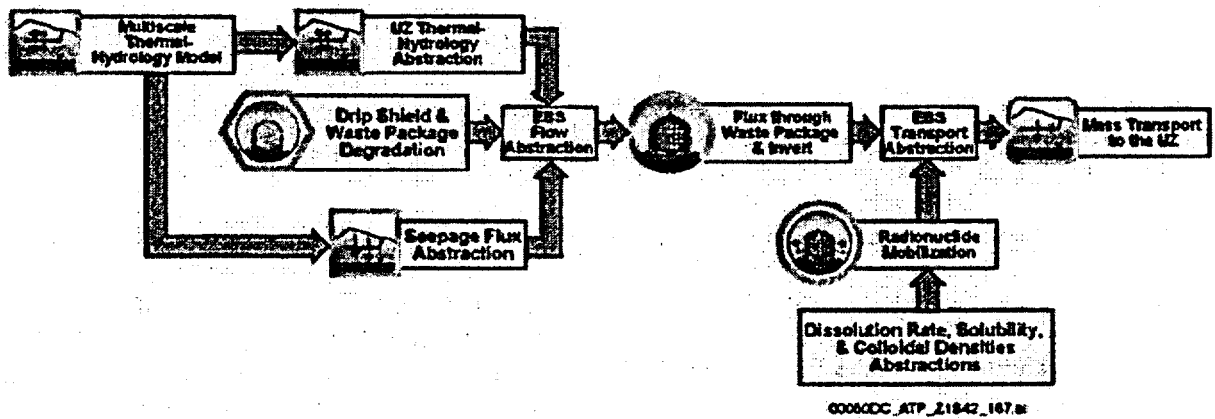


Figure 4-111. Schematic Representation of Inputs and Outputs of Engineered Barrier System Flow and Transport Model for Total System Performance Assessment  
UZ = unsaturated zone; EBS = engineered barrier system.

a breach of the drip shield and waste package, radionuclides could be transported downward, through the invert, and into the unsaturated zone (Figure 4-110). After stress corrosion cracks appear in the waste package, diffusive transport is allowed to commence regardless of whether conditions may be consistent with existence of a continuous liquid pathway. Radionuclides are then mobilized to the unsaturated zone when a significant advective liquid flux is present in the invert (CRWMS M&O 2000dd, Section 7.1).

Colloid-facilitated transport of radionuclides is included as an additional source term. Radionuclide transport from the waste package occurs in a fluid containing colloids and dissolved radionuclides. The total concentration for certain radionuclides, particularly plutonium and americium, can be increased well above the solubility limit by colloidal transport. Plutonium and americium are included on the basis of their transport behavior and observations from laboratory and field studies. Protactinium and thorium are highly sorptive and are included for conservatism. Selected daughters of these parent radionuclides are also included in the TSPA-SR model (CRWMS M&O 2000a, Section 3.5.6.2). Colloid-associated radionuclide concentrations, colloid masses, and water chemistry parameters (ionic strength and pH) from the waste package serve as inputs to the in-drift colloids model, where colloid stability and advective transport through the invert are modeled (CRWMS 2000co, Section 6.3.4).

Mixing cells are used in TSPA-SR to represent the waste package and the invert. A mixing cell is a fluid volume with well-mixed, homogeneous conditions throughout. Representation of radionuclide solubility, waste form dissolution rate, cladding performance, and inventory by waste package type are defined by other abstractions for the TSPA-SR (CRWMS M&O 2000a, Section 3.5).

The transport abstraction in the TSPA-SR model is also conservative in several aspects. Firstly, as mentioned in Section 4.2.7.3.1, there is no retardation of dissolved species in the waste package or invert (CRWMS M&O 2000dd, Section 5.2.7). Corrosion products from the waste package, structural steel in the drifts, and spent nuclear fuel have

the potential to be strong sorbents for actinides but are conservatively ignored. Secondly, diffusive transport cannot occur if liquids are not present, and the waste form may actually remain dry for hundreds or thousands of years after the waste package is breached. This effect is conservatively ignored, and diffusion is allowed to occur immediately when a breach occurs. In addition, the waste package is assumed to be in contact with the invert, providing a continuous liquid pathway for diffusion (CRWMS M&O 2000a, Section 3.6.2). Finally, release of radionuclides by advective transport is modeled to be independent of the location of breaches in the waste package. Thus, in the TSPA-SR abstraction, a waste package with only one penetration, or a waste package with one or more penetrations on its upper surface and none on its lower surface, would still have advective transport into the invert (CRWMS M&O 2000dd, Section 7.2).

The supplemental TSPA model has incorporated selected changes to the engineered barrier system transport model resulting from supplemental uncertainty analyses. These modifications include waste package diffusion (BSC 2001a, Sections 10.3.1 and 10.4.1) and sorption of radionuclides to corrosion products (BSC 2001a, Sections 10.3.4 and 10.4.4). The effects of these changes at the TSPA level are discussed in Volume 2, Section 4.2.8 of *FY01 Supplemental Science and Performance Analyses* (BSC 2001b). In general, inclusion of the supplemental models results in slight reductions in dose calculations by the supplemental TSPA model, indicating that the TSPA-SR model may be somewhat conservative.

#### 4.2.8 Unsaturated Zone Transport

In the event of radionuclide mobilization and migration away from the potential emplacement drifts at Yucca Mountain, the rate of radionuclide transport through the unsaturated zone is determined by the percolation flux and by the hydrologic properties and sorptive characteristics of tuff units. Water carrying radionuclides would percolate vertically through fractured tuff units, or it may be laterally diverted around low-permeability horizons (particularly where perched water occurs) to fault zones. Diffusion, sorption, and

dispersion would retard the radionuclide movement. Each of these processes potentially affects the distribution and concentration of radioactive particles at the water table.

Unsaturated zone transport depends on inputs from the unsaturated zone flow and seepage into drifts (described in Section 4.2.1) and on rates of radionuclide releases from the waste emplacement drifts (described in Sections 4.2.2 to 4.2.7). The unsaturated zone transport model supplies to the TSPA temporal evolutions and spatial distributions of radionuclide concentrations at the water table. The current understanding of transport in the unsaturated zone is documented in *Unsaturated Zone Flow and Transport Model Process Model Report* (CRWMS M&O 2000c, Sections 2.2 and 3.11), *Radionuclide Transport Models Under Ambient Conditions* (CRWMS M&O 2000ea, Section 6), *Unsaturated Zone and Saturated Zone Transport Properties (U0100)* (CRWMS M&O 2000eb, Sections 6.4 to 6.8), and *In Situ Field Testing of Processes* (CRWMS M&O 2000bu, Section 6.9; BSC 2001a, Section 11).

#### 4.2.8.1 Conceptual Basis of Unsaturated Zone Transport

This section summarizes basic concepts about transport through the unsaturated zone at Yucca Mountain. The transport of aqueous/colloidal radionuclide species can occur in both the fractures and the porous matrix. The flow pathways are determined by the characteristics of hydrogeologic units, faults, and perched water. These characteristics control the extent of downward versus lateral flow, fracture-matrix interaction, and the partitioning of flow between fractures and rock matrix. Fractures and faults can be fast flow paths, with diffusion into the matrix and sorption to the rock being the important processes for radionuclide retardation. Radionuclide retardation may be important to the safety of a potential repository at Yucca Mountain (CRWMS M&O 2000c, Section 3.11.1.1).

The concentration of radionuclides and their daughter products are diminished according to their radioactive decay rates, the extent of sorption onto the solid phase, and dilution as a result of

mixing (i.e., dispersion). The effects of advective flow processes, sorption (solutes) or filtration (colloids), matrix diffusion, hydrodynamic dispersion, and radioactive decay on unsaturated zone transport are summarized below.

**Advection** (CRWMS M&O 2000c, Section 3.11.2.2)—Advection is the movement of dissolved or colloidal species resulting from the bulk flow of fluid (Fetter 1993, p. 47). Flow and advective transport within Yucca Mountain are predominantly downward because of gravity. The presence of perched water may result in lateral flow and subsequent transport of the radionuclides. Advection through fractures is expected to dominate transport behavior in welded units and in the zeolitic portions of the Calico Hills nonwelded hydrogeologic unit and other lower tuff units. In some welded and zeolitic layers, the matrix permeability is insufficient to carry the net infiltration, which implies that a portion of the percolation is likely to be carried by fractures (CRWMS M&O 2000c, Section 3.6.3.1). Matrix flow dominates in the vitric Calico Hills nonwelded hydrogeologic unit.

**Matrix Diffusion** (CRWMS M&O 2000c, Section 3.11.2.5)—Matrix porosity, saturation, and mineralogy affect the extent of diffusion and sorption of species. Matrix diffusion can play an important role in radionuclide exchange between the fractures and the rock matrix. It depends on the effective contact area between fracture and matrix (CRWMS M&O 2000bq, Section 6.2). The presence of inactive and relatively dry fractures, accounted for with the active fracture model, would affect matrix diffusion. Radionuclide diffusion into the rock matrix and away from the fracture surface is driven by a concentration gradient, and it will slow the advance of radionuclides by removing them from the faster flowing fractures. The effective matrix diffusion coefficient can be expressed as the product of molecular diffusion coefficient (for diffusion process in aqueous solution), tortuosity (for measure of deviation from straight flow path through porous medium), porosity, and water saturation to account for the rock characteristics and saturation effects on matrix diffusion.

**Sorption** (CRWMS M&O 2000c, Section 3.11.2.4)—Sorption is a general term to describe the binding of a solute (radionuclide) onto the sorbent (either the immobile rock matrix or colloids). As a result of sorption onto the rock matrix, the advancing rate of sorbing radionuclides is retarded. In Yucca Mountain studies, the effective sorption distribution coefficient ( $K_d$ ) approach is employed to quantify the extent of radionuclide-sorbent interactions. This approach does not require identifying the specific underlying processes of sorption, such as surface adsorption, precipitation, and ion exchange.

**Hydrodynamic Dispersion** (CRWMS M&O 2000c, Section 3.11.2.3)—Hydrodynamic dispersion includes both mechanical dispersion arising from local velocity variations and molecular diffusion driven by concentration gradients. Hydrodynamic dispersion dilutes and smears sharp concentration gradients and reduces the breakthrough time of radionuclides to the water table. Dispersion of radionuclides occurs both along (longitudinally) and transverse to the average flow direction.

**Radioactive Decay and Daughter Products** (CRWMS M&O 2000c, Section 3.11.2.6)—The decay of the radioactive species of interest and their half-lives are well documented. The transport simulations must compute the total radioactivity distribution (i.e., the sum of the concentrations of all the members of the radioactive decay chain). This is especially significant if the daughters from the decay chains have long half-lives. The daughter products may have significantly different transport behavior than the parent radionuclide.

**Colloidal Transport** (CRWMS M&O 2000c, Section 3.11.2.7)—Colloids are very fine particles (e.g., clay minerals, metal oxides, viruses, bacteria, and organic macromolecules) that range in size from 1 to 10,000 nm (0.00000004 to 0.0004 in.) (McCarthy and Zachara 1989, pp. 496 to 502). Radionuclides can be transported as intrinsic colloids. Intrinsic colloids are also referred to as waste-form colloids or true colloids of elemental particles (e.g., plutonium colloidal forms plutonium (IV) and colloidal plutonium (V), with Roman numerals representing the valence or

oxidation states). Radionuclides can also be adsorbed to naturally occurring fine particles and be transported as radionuclide-bearing pseudo-colloids (e.g., for plutonium-239 and americium-243). The transport of colloidal species is further affected by their size, which determines the nature of pore exclusion and filtration processes. Colloidal transport differs from solute transport because of colloidal particle interactions (e.g., flocculation or formation of aggregated mass of suspended particles), pore exclusion, and surface reactions (e.g., deposition or attachment).

#### 4.2.8.2 Summary State of Knowledge

This section presents data that support the conceptual basis and modeling of radionuclide transport through the unsaturated zone. The in situ field tests in the Exploratory Studies Facility at Yucca Mountain and at the unsaturated transport test site at Busted Butte are first described in Section 4.2.8.2.1. The laboratory measurements of transport properties conducted on tuff samples from deep boreholes and from field sites are summarized in Section 4.2.8.2.2. In addition, natural analogues for unsaturated zone transport processes are discussed in Section 4.2.8.2.3.

##### 4.2.8.2.1 Field Tracer Tests

All liquids released in the alcove and niche test sites in the Exploratory Studies Facility contain tracers. The tracer analyses provide data and information on flow and transport processes. Some flow tests are summarized in Section 4.2.1.2 and in *Unsaturated Zone Flow and Transport Model Process Model Report* (CRWMS M&O 2000c, Section 2.2). The tracer transport data from seepage tests and fracture-matrix interaction tests are presented in *In Situ Field Testing of Processes* (CRWMS M&O 2000bu, Sections 6.3, 6.4, 6.6, and 6.7).

**Construction Water Migration** (CRWMS M&O 1998i)—Construction water used in the excavation of the Exploratory Studies Facility drifts contained lithium bromide as a tracer. The presence of the tracer (measured as bromide to chloride ratio, leached out of crushed borehole samples) is illustrated in Figure 4-112 along three construction

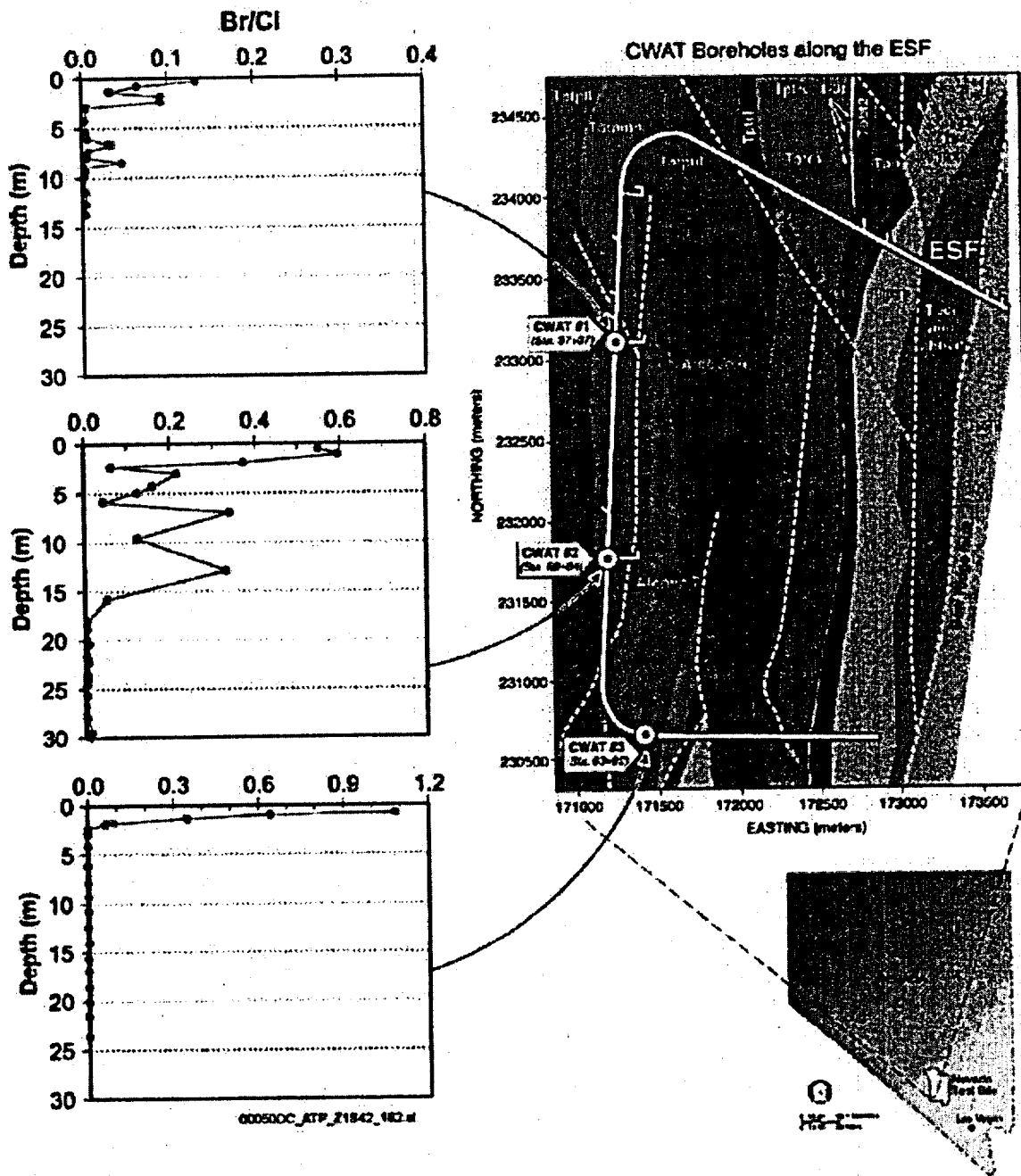


Figure 4-112. Construction Water Distribution below the Exploratory Facilities Drift  
Sources: Bromide to chloride ratios taken from Figure 3.1-1 of *Model Prediction of Local Plume Migration from the Cross Drift* (CRWMS M&O, 1998i); geologic framework map based upon the geologic framework model (CRWMS M&O 2000bs). ESF = Exploratory Studies Facility.

water boreholes (designated "CWAT") drilled in the Exploratory Studies Facility. The deepest tracer penetration was at borehole CWAT#2, in which construction water had reached the bottom of the hole (30 m, or 98 ft). CWAT#2 is located in an intensely fractured zone (illustrated in Figure 4-10) of the middle nonlithophysal zone of the Topopah Spring welded hydrogeologic unit. In CWAT#1, the construction water was detected in all samples to a depth of 2.4 m (8 ft) with two isolated peaks at greater depths. In CWAT#3, located in the upper lithophysal zone, the construction water was detected only in the top 2 m (7 ft).

Figure 4-112 also illustrates that the Exploratory Studies Facility main drift is primarily through the middle nonlithophysal zone, with the main potential repository block in the lower lithophysal zone located to the west of the main drift horizon. Both the variations in hydrologic properties of different tuff units and in the construction usage rates could have effects on the construction water penetrations. Another test was conducted in the upper lithophysal zone at the starter tunnel of the ECRB Cross-Drift. Wetting front signals were detected up to depths close to 10 m (33 ft) by electrical resistivity probes and psychrometers after the excavation by the tunnel boring machine (CRWMS M&O 2000bu, Section 6.9).

**Alcove 1 El Niño Infiltration and Seepage Tests (CRWMS M&O 2000bw, Section 6.8.1)**—A large-scale infiltration and seepage test in the Exploratory Studies Facility is located in Alcove 1 near the North Portal (Figure 4-113). In this test, a drip irrigation system on the outcrop above Alcove 1 is used to simulate large infiltration events associated with high precipitation during El Niño conditions. The crown of Alcove 1 is approximately 30 m (100 ft) below the ground surface. The infiltration test at Alcove 1 involved applying water at the ground surface. At a late stage of the test, lithium bromide at high concentration was introduced into the infiltrating water. Seepage into the alcove and the tracer arrival time were recorded. The tracer was first detected after 28 days.

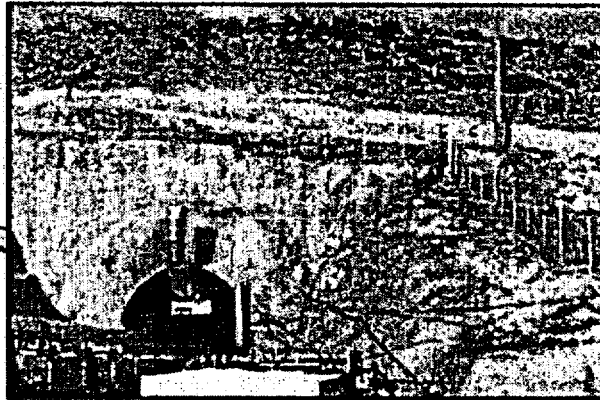
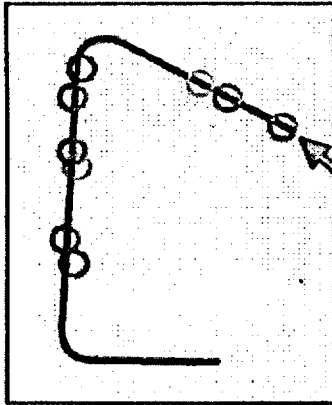
Hydrologic properties calibrated to earlier Alcove 1 seepage data were used in the tracer simulation. The simulated breakthrough curve closely matches

the tracer concentration data for a tortuosity value of 0.75, which is close to the value of 0.7 given by Francis (1997, p. 5). This relatively high tortuosity value is possibly related to the nearly saturated conditions in the test. Comparison with early test results indicate that the continuum approach is valid for modeling flow and transport in unsaturated fractured rock. An active fracture model can capture the major features of fingering flow and transport in fractures. Matrix diffusion has a large effect on the overall transport behavior in unsaturated fractured rock, while dispersion in fractures does not (CRWMS M&O 2000bw, Section 6.8.1.2).

Test results show that matrix diffusion is important in diluting the tracer concentration and increasing the tracer breakthrough times in the Tiva Canyon welded hydrogeologic unit (CRWMS M&O 2000bw, Section 6.8.1). Both the Tiva Canyon and Topopah Spring hydrogeologic units contain fractured and welded tuff rock. While the Alcove 1 test site in the Tiva Canyon welded hydrogeologic unit is above the potential repository horizon, the test results on the importance of matrix diffusion may be applied to the similarly fractured Topopah Spring welded hydrogeologic unit below the potential repository horizon.

**Alcove 8-Niche 3 Cross-Drift Tests (CRWMS M&O 2000bu, Section 6.9)**—Alcove 8 has been excavated in the ECRB Cross-Drift, approximately 20 m (66 ft) directly above Niche 3 in the main drift. Alcove 8 is for controlled liquid-release tests with Niche 3 instrumented for seepage detection, as illustrated in Figure 4-114. The Cross-Drift test block includes the interface between the upper lithophysal zone and the middle nonlithophysal zone of the Topopah Spring welded hydrogeologic unit. A localized release test has been initiated and a 3 m × 4 m (10 ft × 13 ft) areal liquid release plot will be used for the Cross-Drift tests. The test results, when available, would be used to understand large-scale flow and seepage processes across a tuff layer interface at the potential repository horizon.

Where the Cross-Drift crosses over the main drift, the migration of construction water from the excavation of the Cross-Drift was monitored, as



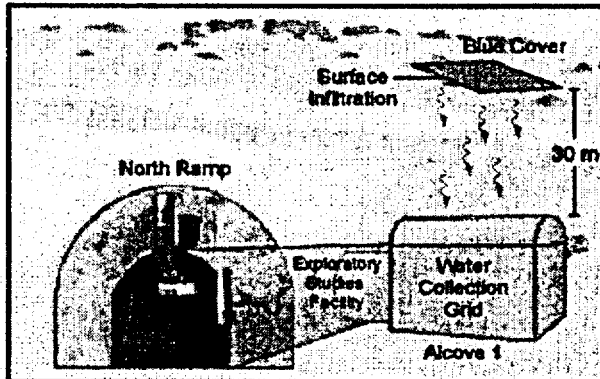
(a) Photograph of Exploratory Studies Facility North Portal and Infiltration Plot (Blue Cover)

**Objectives:**

- Quantify large-scale infiltration and seepage processes in the bedrock.
- Evaluate matrix diffusion mechanism in long-term flow and transport tests.

**Approaches:**

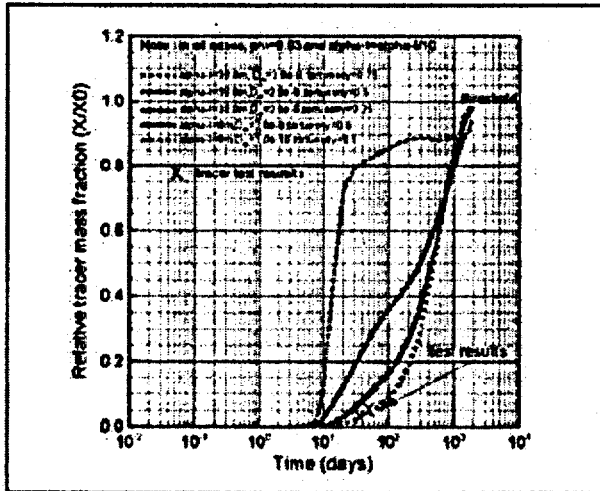
- Water applied on the surface 30 m directly above the alcove.
- Tests conducted in two phases: March - August 1998 and May 1999 - present, with Phase 1 focusing on flow and Phase 2 focusing on tracer transport.



(b) Schematic of Alcove 1 Infiltration Test

**Results:**

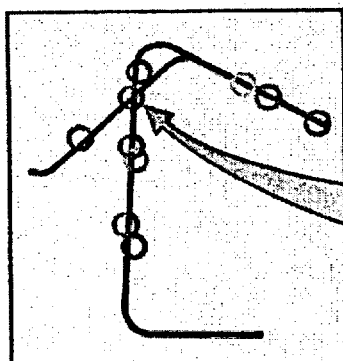
- Over 100,000 liters infiltrated in Phase 1, with observed seepage rates of up to 300 liters/day.
- First seepage was observed 58 days after Phase 1 test initiation. Pressure/flow response of the system was observed to be ~2 days once a nearly steady-state system had developed.
- High concentrations of LIBr were used in Phase 2 tracer test.
- First tracer breakthrough in Phase 2 observed in 28 days with a nearly steady-state flow system using a conservative tracer.
- Tracer recovery data were used to compare with model predictions and to evaluate the importance of matrix diffusion.



(c) Tracer Breakthroughs Test Results and Model Predictions with Matrix Diffusion

000500C\_ATP\_21642\_166a.m

Figure 4-113. El Niño Infiltration and Seepage Test at Alcove 1  
Source: CRWMS M&O 2000c, Figure 2.2-8.



**Objectives:**

- Quantify large-scale infiltration and seepage processes in the potential repository horizon.
- Evaluate matrix diffusion mechanism in long-term flow and transport tests across a lithophysal—nonlithophysal interface.

**Approaches:**

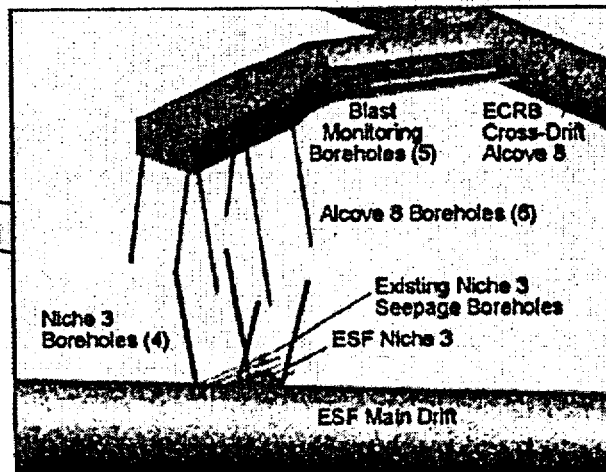
- Water releases are in Alcove 8 and seepage collections are in Niche 3.
- Niche 3 is instrumented with seepage collectors and wetting front sensors.
- Geophysical tomographs are conducted in vertically slanted boreholes.

**Status:**

- Drill-and-blast phase of Alcove 8 excavation was completed in 1999.
- Tests are prepared to be conducted after alcove excavation.

**Supporting Results:**

- Seepage tests at Niche 3 behind bulkhead demonstrate the existence of seepage threshold under high-humidity conditions.
- During ECRB Cross-Drift construction, no water was observed to seep into the ESF Main Drift 20 m below.



(a) Schematic of the Cross-Drift Test Bed



(b) Photograph of Partial Excavated Alcove 8 in ECRB Cross-Drift



(c) Photograph of Water Collection Trays on the Ceiling of the ESF Main Drift

00050DC\_ATP\_Z1542\_183c.ai

Figure 4-114. Alcove 8—Niche 3 Cross-Drift Tests

ESF = Exploratory Studies Facility. Source: CRWMS M&O 2000c, Figure 2.2-9.

illustrated in Figure 4-114. No seepage was observed when the tunnel boring machine passed over the main drift.

**Busted Butte Transport Tests (CRWMS M&O 2000c, Section 3.11.11.2)**—Transport processes in the vitric Calico Hills nonwelded hydrogeologic unit have been and are currently under investigation at the Busted Butte underground facility (Figure 4-115). The principal basis for the Busted Butte tests is that the test results can be extended to characterize the transport properties of the Calico Hills nonwelded geologic unit in the unsaturated zone beneath the potential repository. Busted Butte is located approximately 8 km (5 mi) southeast of the potential Yucca Mountain repository area. This facility consists of a drift complex excavated 70 m (230 ft) below the ground surface to reach a distal extension of the vitric Calico Hills nonwelded hydrogeologic unit below Yucca Mountain. Tracer-injection tests, partial mine-out, and geophysical measurements (ground-penetrating radar, electrical resistivity tomography, and neutron logging) were performed to map solute migration patterns. Results of the ongoing tests are presented in *Unsaturated Zone and Saturated Zone Transport Properties (U0100)* (CRWMS M&O 2000eb, Section 6.8).

Phase 1A results indicate that transport through the vitric Calico Hills nonwelded hydrogeologic unit is dominated by capillary-driven flow, with a well-defined plume developing after tracer injection. Plumes from the ongoing larger-scale Phase 2 test are tracked by sorbing pads in monitoring boreholes and by geophysical imaging techniques. Examples of a fluorescent plume photograph from the Phase 1A test and a ground-penetrating radar tomograph from Phase 2 are presented in Figure 4-115.

The radar data were acquired in two-dimensional planes defined by two boreholes. Regions with elevated moisture content correspond to regions of low transmission velocity of the radar signals. The radar tomographs, together with neutron logging and electrical resistivity tomography results, are compared with tracer breakthrough logs in boreholes. Injected fluid may displace the pore fluid

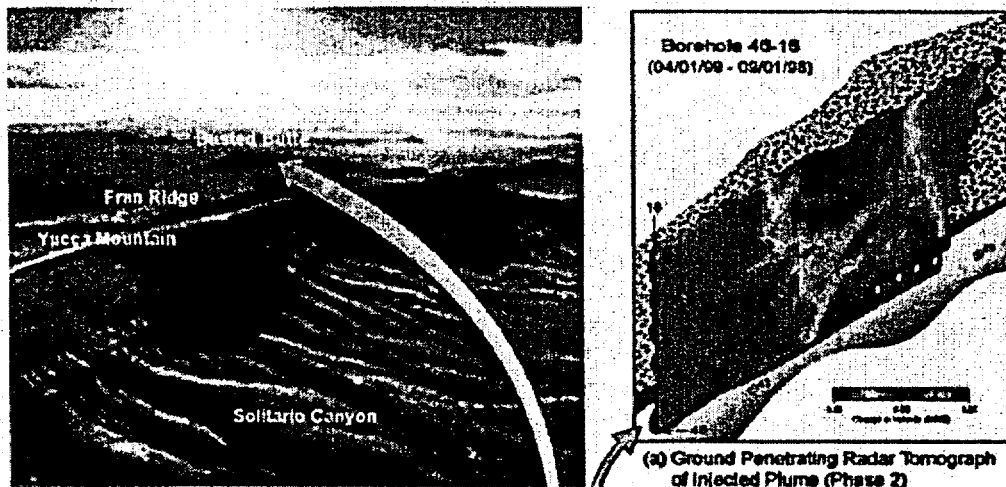
based on preliminary results of Phase 2 tests. Some fluid breakthrough occurred in the boreholes, but it did not contain injected tracers (CRWMS M&O 2000eb, Section 6.8.4.1.4).

Microspheres are used as a colloidal tracer at the Busted Butte transport test as well as in the saturated zone C-Wells tests (CRWMS M&O 2000eb, Section 6.9). Results of transport tests using sorbing tracers that represent sorbing radionuclides provide evidence of whether or not laboratory-measured retardation factors can be used to predict field-scale transport processes. The Busted Butte transport tests are discussed in more detail in *Unsaturated Zone Flow and Transport Model Process Model Report* (CRWMS M&O 2000c, Section 3.11.11.2), *Radionuclide Transport Models Under Ambient Conditions* (CRWMS M&O 2000ea, Section 6.10), and *Unsaturated Zone and Saturated Zone Transport Properties (U0100)* (CRWMS M&O 2000eb, Section 6.8).

#### 4.2.8.2.2 Transport Properties

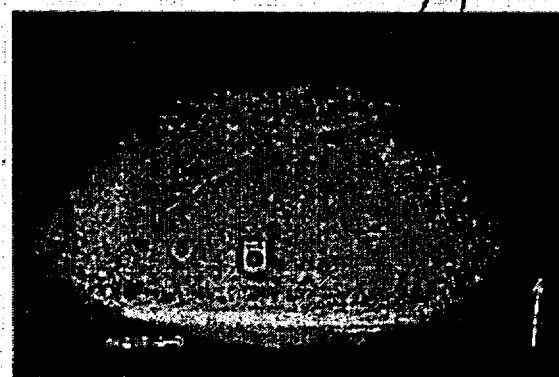
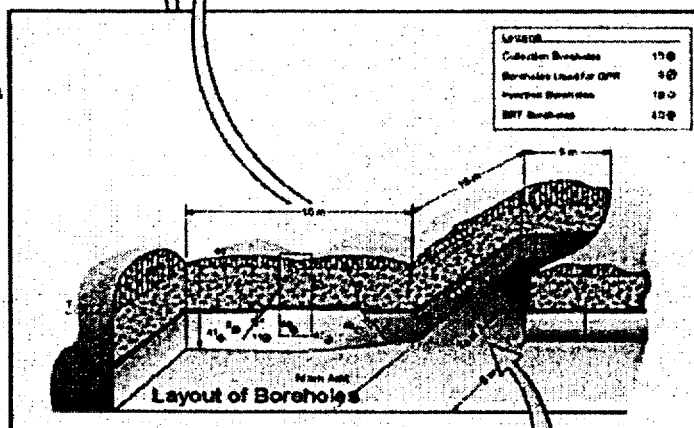
As described in Section 4.2.8.1, the unsaturated zone transport processes include advection, matrix diffusion, sorption, hydrodynamic dispersion, radioactive decay, and colloidal transport. The unsaturated zone flow properties affecting advective transport are discussed in Section 4.2.1 and will not be repeated in this section. This section describes unsaturated zone transport properties based primarily on laboratory measurements of tuff samples.

**Matrix Diffusion Coefficients**—The effective diffusion coefficient, which is the product of the molecular diffusion coefficient, tortuosity, porosity, and water saturation, is used to account for rock geometry and saturation effects on matrix diffusion. Some experimental data exist on the tortuosity distribution in the various hydrogeologic units at Yucca Mountain. *Radionuclide Transport Models Under Ambient Conditions* (CRWMS M&O 2000ea, Section 6.1.2.4) employed the approach of using the porosity value to approximate tortuosity. Tortuosity measurements on devitrified tuffs showed good agreement with this approximation.



- Objectives:**
- Quantify unsaturated zone transport processes in Calico Hills nonwelded unit.
  - Measure retardation coefficients in the field to compare with laboratory measured values.

- Approaches:**
- A test bed was excavated 70 m below the surface in mainly vitric CHn underlying the vitrophyre.
  - A mixture of conservative and sorbing tracers is used in tracer injection tests.
  - Absorbent pads are used to sample periodically the tracer distributions below injections.
  - Ground-penetrating radar tomography, together with electrical resistivity tomography and neutron logging, is used to track plume migrations.



- Results:**
- Phase 1A was conducted with single point injections from April 1998 to mineback in 1999. Capillary-driven flow mechanism is confirmed.
  - Phase 2 tests with aerial injections are ongoing with breakthroughs and plume migrations monitored.

000500C\_ATP\_Z1542\_157b.a

Figure 4-115. Unsaturated Zone Transport Test at Busted Butte  
ERT = electrical resistance tomography; GPR = ground penetrating radar. Source: CRWMS M&O 2000c, Figure 2.2-12.

A probabilistic description of matrix diffusion was developed using a beta distribution and the distribution parameters listed in Table 4-25 (CRWMS M&O 2000eb, Section 6.6.3). The assigned parameter values were developed based on analyses of data from literature reviews and limited laboratory data (CRWMS M&O 2000eb, Section 6.6.1.3, Table 16, and Figures 29 and 30). The cationic (positively charged and sorbing) radionuclides are assigned values representative of the coefficient for tritium. Based on measured diffusion behavior of cationic radionuclides, this is conservative (CRWMS M&O 2000eb, Section 6.6.1.3). The coefficient for technetium (as pertechnetate, the predominant aqueous species of technetium) is approximately 10 times lower than that for tritium. The anionic (negatively charged) radionuclides are more likely to be excluded from the matrix pores, which are also negatively charged.

Table 4-25. Distribution Parameters for Matrix Diffusion Coefficients

Radionuclide Type	Mean (m <sup>2</sup> /s)	Standard Deviation (m <sup>2</sup> /s)	Maximum (m <sup>2</sup> /s)	Minimum (m <sup>2</sup> /s)
Anionic	$3.2 \times 10^{-11}$	$1.0 \times 10^{-11}$	$1 \times 10^{-9}$	0
Cationic	$1.6 \times 10^{-10}$	$0.5 \times 10^{-10}$	$1 \times 10^{-9}$	0

Source: CRWMS M&O 2000eb, Section 6.6.3.

**Sorption Coefficients**—Most experimentally determined sorption values at Yucca Mountain have been derived from batch experiments using crushed tuff (crushed to 75 to 500  $\mu\text{m}$  [0.003 to 0.02 in.]) under water-saturated conditions (CRWMS M&O 2000eb, Section 6) for a variety of rock types and elements. Probabilistic descriptions and distribution parameters of sorption coefficients for selected radionuclides are given in Table 4-26 for three rock types: devitrified tuff (including welded tuff), vitric tuff, and zeolitic tuff (CRWMS M&O 2000eb, Table 2a). These distributions and parameter values were derived from an expert elicitation conducted in 1993 as modified by additional new data (CRWMS M&O 2000eb, Section 6.4.2). The water compositions from Wells J-13 and UE-25 p#1 were used to provide an adequate range of compositions to capture the influence of water compositional variability on sorption in the unsaturated zone. The effects of temperature were bounded by measurements at ambient tempera-

tures. The batch experimental approach with crushed tuff may overestimate the sorption values for unsaturated zone transport, as discussed in Section 4.2.8.3.5.2.

The assumptions used to develop values of sorption are discussed in *Unsaturated Zone and Saturated Zone Transport Properties (U0100)* (CRWMS M&O 2000eb, Section 5). The complete table (CRWMS M&O 2000c, Table 3.11-1; CRWMS M&O 2000eb, Table 2a) contains data for additional elements, and, in addition to tuff rocks, sorption coefficients for iron oxide are also presented for some elements. Sorption onto fracture surfaces can retard radionuclide migration. Laboratory sorption experiments showed that trace minerals might be effective at retarding the transport of neptunium-237 when they are concentrated on fracture surfaces (CRWMS M&O 2000eb, Section 6.5.3). Numerical simulations showed that the limited sorption on the fracture walls was sufficiently important to retard transport of strongly sorbing radionuclides (e.g., plutonium-239) (CRWMS M&O 2000ea, Section 6.17.1). However, sorption in fractures is not included in the TSPA transport evaluations because of limited data and the conservative nature of this approximation regarding radionuclide transport to the water table.

Experimental sorption coefficients ( $K_d$  values) were obtained using rock samples collected from the Topopah Spring welded and Calico Hills nonwelded hydrogeologic units at Busted Butte (Table 4-27). Sorption coefficients for neptunium and americium from Busted Butte (Table 4-27) are similar to values from batch experiments (Table 4-26); however, sorption values for plutonium are significantly larger.

**Dispersivities**—The dispersion coefficient is a function of dispersivity and flow velocity. Dispersivity has been shown to increase as a function of observation scale, attributed mainly to mixing as more heterogeneities are sampled at larger scales (Gelhar et al. 1992). Field measurements show that the transverse dispersivity is significantly less than longitudinal dispersivity (Fetter 1993, pp. 65 to 66).

Table 4-26. Sorption Coefficient Distributions for Unsaturated Zone Hydrogeologic Units from Batch Experiments

Element	Rock Type	$K_d$ (mL/g)			Coefficient of Variation	Distribution Type
		Minimum	Maximum	Mean		
Neptunium	Devitrified	0	1.0	0.3	0.3	Beta
	Vitric	0	1.0	0.3	1.0	Beta (exp)
	Zeolitic	0	3.0	0.5	0.25	Beta
Plutonium	Devitrified	5	70	—	—	Uniform
	Vitric	30	200	100	0.25	Beta
	Zeolitic	30	200	100	0.25	Beta
Uranium	Devitrified	0	2.0	0.5	0.3	Beta
	Vitric	0	1.0	0.5	0.3	Beta
	Zeolitic	0	10.0	4.0	1.0	Beta (exp)
Americium	Devitrified	100	2000	—	—	Uniform
	Vitric	100	1000	400	0.20	Beta
	Zeolitic	100	1000	—	—	Uniform
Chlorine, Technetium, Iodine	—	0	0	0	0	N/A

NOTE: N/A = not applicable. Source: Adapted from CRWMS M&O 2000eb, Table 2a.

Table 4-27. Summary of Radionuclide Sorption Results from Busted Butte Tests

Element	Geologic Unit	Model Layer	Sample Source	Approximate Average $K_d$ (mL/g)
Neptunium	Tptpv2	tsw39	Phase 1B, BH 7	1.1
	Tptpv1	ch1v	Phase 1A, BH 3	0.3
	Tac	ch2v	Phase 1A, BH 4	1.4
Plutonium	Tptpv2	tsw39	Phase 1B, BH 7	1100
	Tptpv1	ch1v	Phase 1A, BH 3	19
	Tac	ch2v	Phase 1A, BH 4	2500
Americium	Tptpv2	tsw39	Phase 1B, BH 7	460
	Tptpv1	ch1v	Phase 1A, BH 3	380
	Tac	ch2v	Phase 1A, BH 4	470

Source: Adapted from CRWMS M&O 2000c, Table 3.11-4.

No data are available to determine dispersivity in the unsaturated zone over the transport distance between the potential repository horizon and the water table. In transport simulations, longitudinal dispersion results in earlier arrival but generally lower concentration. Given this behavior, no simple conservative bound exists for the longitudinal dispersion. A distribution consistent with the dispersivity versus scale correlation of Neuman (1990) is used in TSPA calculations. Transverse dispersion acts only to reduce concentration, with generally little effect on breakthrough time. Therefore, a conservative value of zero for transverse dispersivity is used in TSPA.

The potential repository emplacement area is broad relative to the distance to the water table. For this reason, hydrodynamic dispersion is not expected to play an important role in unsaturated zone transport at Yucca Mountain (CRWMS M&O 2000bq, Section 6.2.5).

**Decay Chains**—The plutonium-239 decay chain (plutonium-239 → uranium-235 → protactinium-231) is particularly important because the daughter uranium-235 has significantly smaller  $K_d$  values compared to its parent plutonium-239, as shown in Table 4-26. The listed decay chain includes only the most important radioactive chain members and omits daughters with short half-lives. The neptunium-237 decay chain (neptunium-237

→ uranium-233 → thorium-229) has also been evaluated. The daughter contribution is less than 2 percent at 1 million years (CRWMS M&O 2000ea, Section 6.13.1.2). As such, daughter contributions to the neptunium-237 transport are relatively insignificant.

**Colloid-Facilitated Transport Parameters—** Anthropogenic colloids may be produced from the waste or from potential repository construction and sealing materials. This was demonstrated in an experiment on simulated weathering of a high-level radioactive waste glass, where the amounts of plutonium and americium released from waste forms were orders of magnitude greater than their respective concentrations in the dissolved phase (Bates et al. 1992). Constraints on these types of colloids are described in Section 4.2.7 and are treated in *Waste Form Degradation Process Model Report* (CRWMS M&O 2000bm, Section 3.8). Relative to waste form colloids, natural colloid-facilitated transport is much lower and plays a minor role in releases from the repository (CRWMS M&O 2000ec, Section 6.6).

The association of radionuclides with colloids is modeled using two end-member representations: (1) reversible equilibrium exchange with the aqueous phase and (2) irreversible attachment. Radionuclides associated with colloids in either condition (reversible or irreversible) may be subject to size exclusion for fracture-matrix exchange. Colloids are excluded from moving from a fracture into matrix pores smaller than the colloid diameter. This tends to keep colloids (and the associated radionuclides) in the fractures, which leads to more rapid transport of the radionuclides. The chance of exclusion of a colloid from the matrix during fracture-matrix exchange is computed using a probabilistic method that considers different colloid-size and pore-size distributions (CRWMS M&O 2000ec, Section 6.2.1).

The description of reversible, colloid-facilitated radionuclide transport for the particle-tracking transport model used in performance assessment is quantified through two parameters (CRWMS M&O 2000ed, Section 6.1.4). One parameter defines the equilibrium partitioning of radionu-

clides between the aqueous phase and colloids. The other parameter is a retardation factor that captures the details of an equilibrium balance between colloid deposition and resuspension. The retardation factor in the colloid model abstraction applies to the transport through fractures. The distribution of retardation factors used is derived from C-Wells data for saturated-zone colloid transport (CRWMS M&O 2000ed, Section 6.2.5). The accessibility factors of colloids of different sizes were evaluated for different geological units (CRWMS M&O 2000ec, Table 3). The linear kinetic model of colloid filtration was used, with the forward kinetic coefficient directly computed (CRWMS M&O 2000ea, Section 6.16).

Colloid concentrations have been measured in several groundwater samples from Yucca Mountain and from other areas at the Nevada Test Site. The measured particle concentrations vary between  $1.05 \times 10^6$  and  $2.72 \times 10^{10}$  particles per mL, with the lowest being for water from Well J-13 and the highest for water from Well U19q on Pahute Mesa (CRWMS M&O 2000ec, Section 6.2.2.2). These values are consistent with what has been reported in the literature for various groundwaters around the world.

#### 4.2.8.2.3 Analogues for Unsaturated Zone Radionuclide Transport

Natural and anthropogenic sites around the world potentially provide sources of long-term data on the behavior of radionuclides and various metals that may serve as analogues to radionuclide transport at Yucca Mountain (CRWMS M&O 2000c, Section 3.11.12). In this section, some of the more important analogue sites for transport in the unsaturated zone are discussed; additional discussion is presented by *Natural Analogs for the Unsaturated Zone* (CRWMS M&O 2000bp).

**Colloid Transport at the Nevada Test Site—** There is some field evidence for the occurrence of colloid-facilitated transport of radionuclides at or near the Nevada Test Site. In one case, migration of plutonium and americium, attributed to colloidal transport, was found more than 30 m (100 ft) downward through unsaturated tuff over the period of approximately 30 years below a low-level waste

site (Buddemeier and Hunt 1988, p. 536). In a saturated zone study at the Nevada Test Site, the isotopic ratio of plutonium-240 to plutonium-239 in groundwater showed that plutonium had been transported more than 1.3 km (0.8 mi) from an underground explosion cavity to a test well over a 30-year period, although plutonium is strongly sorbing at the Nevada Test Site and assumed to be immobile (Kersting et al. 1999). Filtration of groundwater samples from the test well indicated that the plutonium was on colloidal material. It is difficult to interpret the plutonium observed at the Nevada Test Site because it originated from an underground nuclear bomb test. The effects of the underground blast on the movement of plutonium are not fully understood.

**Uranium Migration at Peña Blanca, Mexico—** Since the 1980s, the Nopal I uranium deposit at Peña Blanca (see Figure 4-19b in Section 4.2.1) has been recognized as a natural analogue for the potential repository at Yucca Mountain. From the uranium–thorium age data, it appears that the primary transport of uranium occurred more than 300,000 years ago. Subsequently, there has been little redistribution of uranium-238 and uranium-235. The 300,000-year stability of uranium-235, uranium-238, thorium, and protactinium in fracture-fill minerals has survived recent hydrologic disturbances from surface water infiltration of the fractures. Recent data indicate that the geochemical system at Nopal I restricts actinide mobility in the unsaturated environment. By analogy, the tuffs at Yucca Mountain should have similar retentive properties and impede the mobility of oxidized uranium.

The McDermitt Caldera uranium deposits and other uranium deposits in northwestern Nevada and southeastern Oregon, together with many other uranium sites and contaminated sites worldwide, are discussed in *Natural Analogs for the Unsaturated Zone* (CRWMS M&O 2000bp). These natural analogue studies build confidence in the flow and transport process models.

**Artifact Preservation at Akrotiri, Greece—** Akrotiri, Greece has silicic volcanic rocks, a dry climate, and oxidizing, hydrologically unsaturated subsurface conditions that are similar to those at

Yucca Mountain. The Minoan eruption, an eruption of volcanic ash 3,600 years ago, buried bronze and lead artifacts under 1.5 to 2.0 m (5 to 6 ft) of ash. Researchers looked for plumes of copper, tin, and lead beneath the artifacts by selectively leaching packed earth and bedrock samples that were collected beneath the artifacts. Little of the bronze material had been transported away from the artifacts. Copper and lead plumes were found beneath the artifacts, but neither was detected below a depth of about 45 cm (18 in.). The Akrotiri study shows preservation of artifacts for a long period of time in an oxidizing environment, indicating that unsaturated systems in arid environments may provide favorable sites for geologic disposal of radioactive waste (Murphy et al. 1998).

#### **4.2.8.3 Unsaturated Zone Flow and Transport Process Models**

Section 4.2.1 described seepage into the drifts. In this section, additional understanding of flow diverted around drifts and of condensate shed away from the drifts is discussed in Section 4.2.8.3.1. After the radionuclides are transported to the tuff units below the potential repository horizon, the current understanding of the impact of perched water is summarized in Section 4.2.8.3.2. The modeling results on the temporal and spatial distributions of particle released from the potential waste emplacement drifts to the water table are described in Section 4.2.8.3.3. Alternative conceptual processes and limitations and uncertainties are discussed in Sections 4.2.8.3.4 and 4.2.8.3.5, respectively.

##### **4.2.8.3.1 Seepage Diversion and Condensate Shedding**

Both the advective and diffusive transport processes determine the rates of radionuclide releases in the drift and transport below the drift. With percolation flux below the seepage threshold and limited amount of seepage flux available (as described in Section 4.2.1.4.2) for advective transport, the release rate is sensitive to enhanced diffusive transport (CRWMS M&O 2000a, Sections 3.6.3.1 and 5.2.5.1). Figure 4-116 is a conceptual sketch that illustrates the concepts of the possible diffusion-dominated flow field or the

advection-dominated flow field in the zone below the drift, discussed in the following paragraphs. The results of analyses of drift seepage for performance assessment (CRWMS M&O 2000bx, Section 6.6.6) indicate that the drift acts as a barrier to downward percolation and that the region below the drift is a drier shadow zone, as illustrated in Figure 4-117. More recent modeling and analysis of the drift shadow zone are presented in Volume 1, Sections 11.2.1 and 11.3.1 of *FY01 Supplemental Science and Performance Analyses* (BSC 2001a).

As long as waste packages are warm enough to heat the air in emplacement drifts, the heat will tend to desaturate the rock around the drifts and redistribute the water. If liquid water is boiled away near the drift during the thermal period, little or no seepage into the drifts is expected. The functioning of the hot and dry barrier is illustrated in Figure 4-118, based on the thermal-hydrologic model and the thermal seepage model (CRWMS M&O 2000ci, Section 6.11.2; BSC 2001o, Section 6.3.5). The drift shadow zone remains relatively dry during the thermal period. The percolation and

seepage after the waste heat decays will be essentially equal to the preemplacement rates if the hydrologic properties and conditions are not significantly altered.

#### 4.2.8.3.2 Lateral Flow Associated with Perched Water Bodies

This section summarizes the effects of perched water bodies on the unsaturated flow field below the potential repository (CRWMS M&O 2000c, Section 3.7.3.3). The geological setting of perched water bodies was presented in Section 4.2.1.1.2 (and illustrated there in Figure 4-7). The occurrence of perched water indicates that the base of the Topopah Spring welded hydrogeologic unit and the zeolitic layers within the Calico Hills nonwelded hydrogeologic unit may serve as barriers to vertical flow and cause lateral diversion of flow. The spatial distribution of low-permeability zeolites has been modeled using mineralogic and petrologic data from several boreholes and is presented in *Integrated Site Model Process Model Report* (CRWMS M&O 2000i).

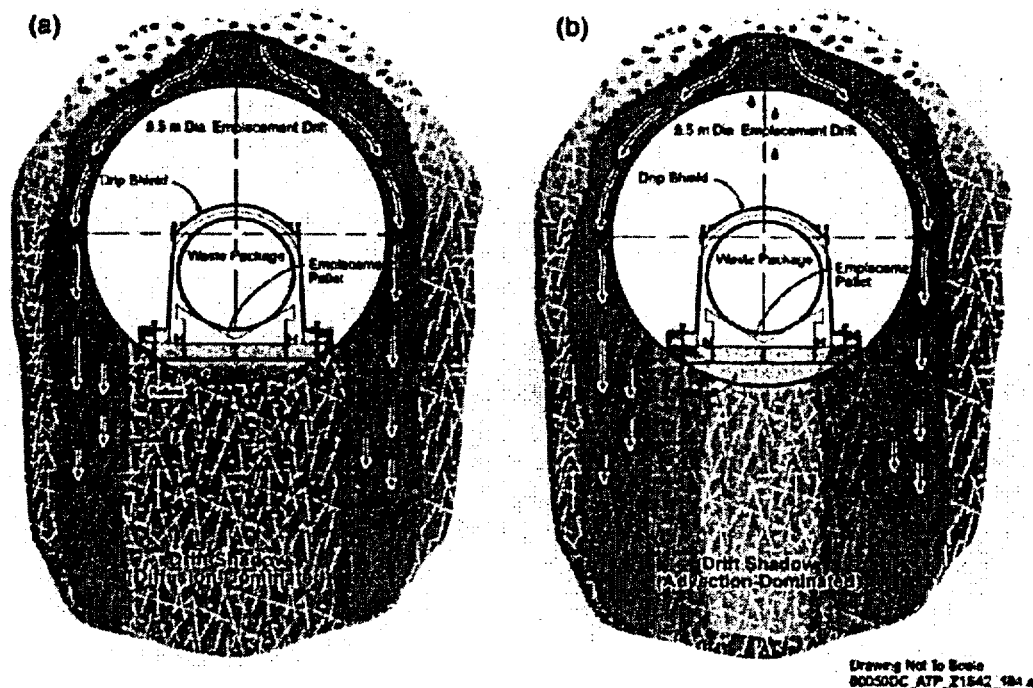


Figure 4-116. Schematic Diagram of Diffusion Barriers in Invert and Drift Shadow Zone  
(a) Schematic with diffusion barriers enhanced by seepage diversion and drip shield. (b) Schematic with diffusion barriers influenced by surface diffusion and advective transport. See also Section 2.4.1, Figures 2-71 and 2-72 for the invert structure selected for the potential emplacement drift.

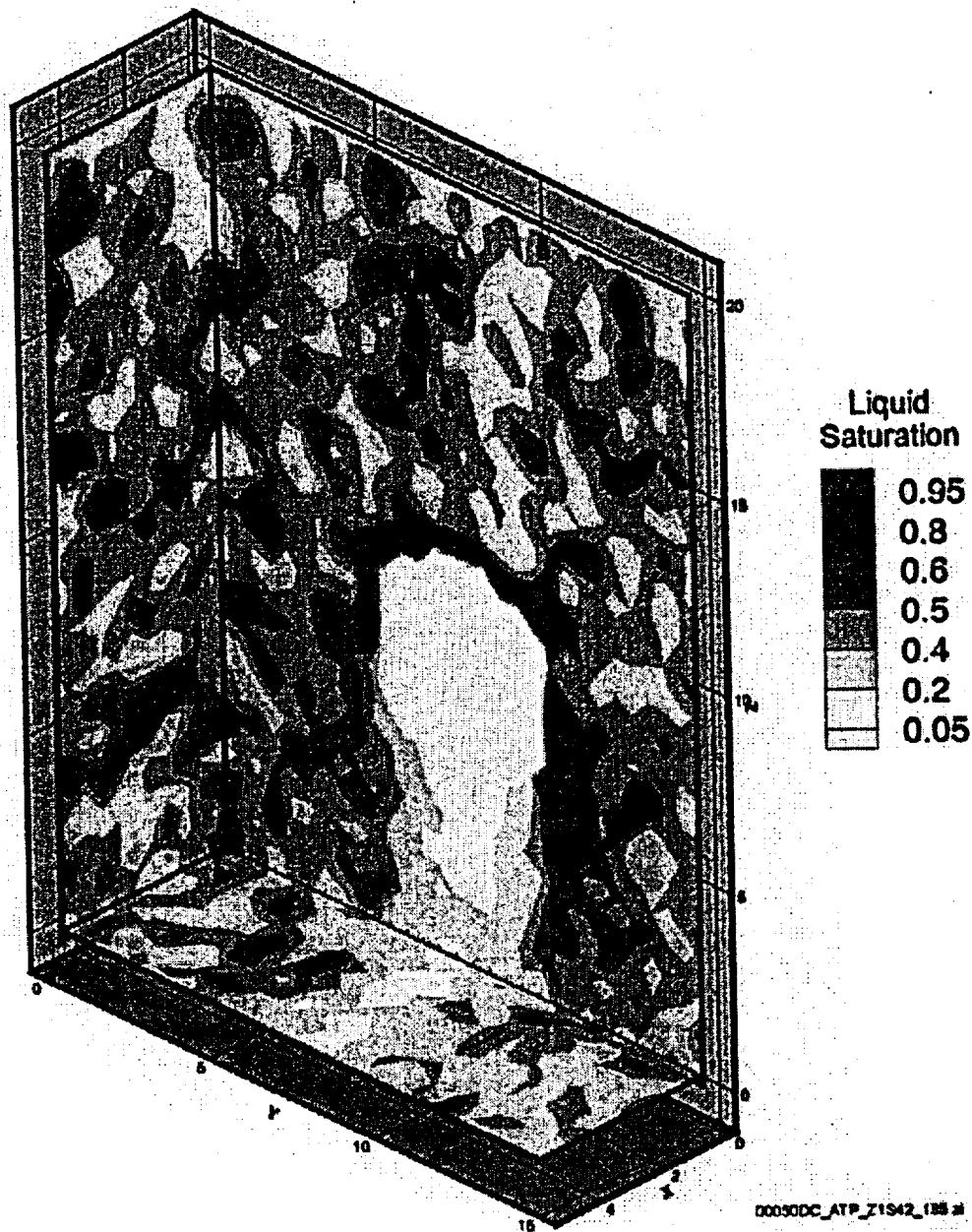


Figure 4-117. Saturation Profiles around a Drift from a Seepage Model for Performance Assessment  
Source: CRWMS M&O 2000bx, Figure 5.

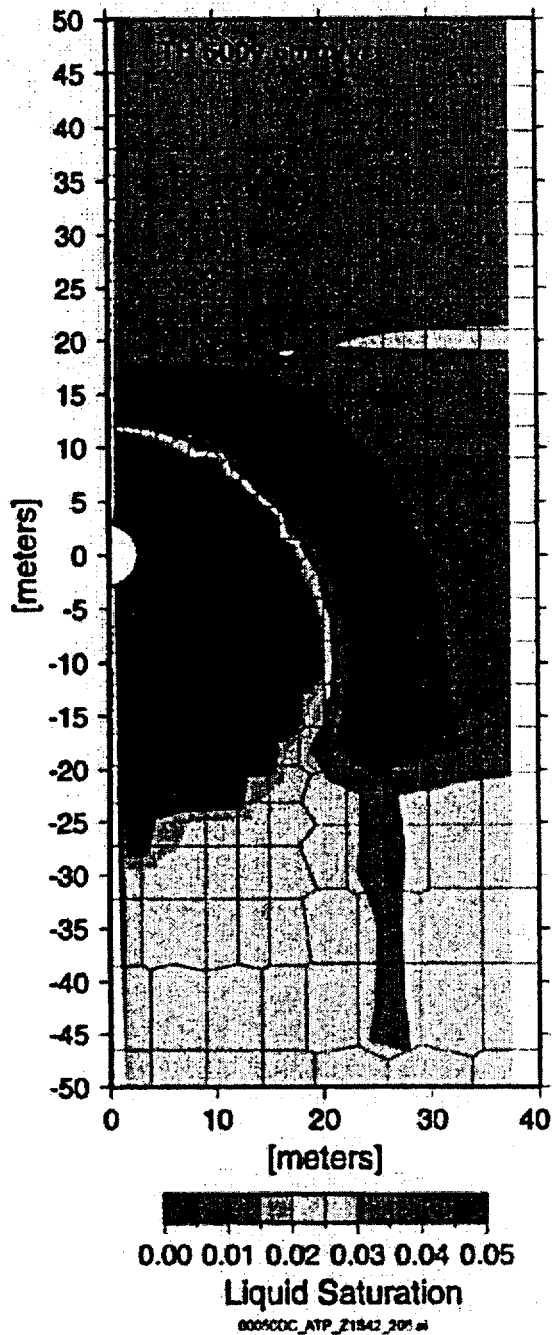


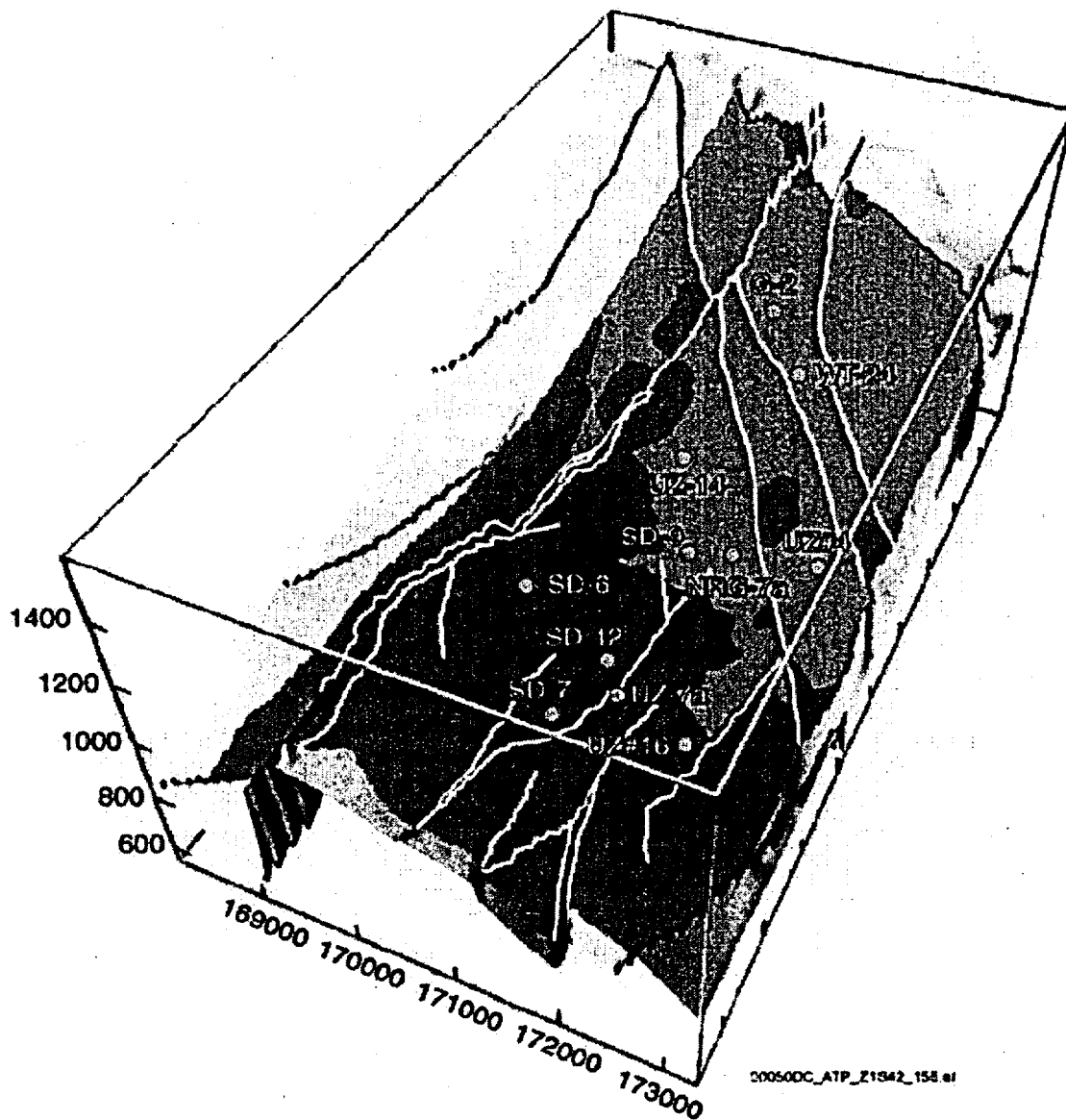
Figure 4-118. Condensate Shedding during the Thermal Period  
Source: BSC 2001c, Figure 32b.

Figure 4-13 (see Section 4.2.1.2.10) shows the modeled distribution of zeolites for layers within the lower Topopah Spring welded and the upper Calico Hills nonwelded hydrogeologic units. Areas with 3 percent or less zeolite by weight are considered vitric, or unaltered.

Zeolites within the Calico Hills nonwelded hydrogeologic unit are prevalent in the northern and eastern portion of the model domain (Figure 4-13). The areal extent of the vitric region diminishes with depth and is considered to be largely confined to the fault block bounded on the north and east by the Sundance and Ghost Dance faults, respectively, and in the west by the Solitario Canyon fault. The northern half of the potential repository area is underlain by the predominantly zeolitic Calico Hills nonwelded hydrogeologic unit, while the southern half is underlain by the predominantly vitric upper portion of the Calico Hills nonwelded unit. However, below the vitric Calico Hills nonwelded hydrogeologic unit (yet above the water table) are nonwelded portions of the Prow Pass, Bullfrog, and Tram tuffs that are pervasively altered to zeolites. Thus, there appears to be no direct vertical pathway from the potential repository horizon to the water table that does not intersect zeolitic units, except perhaps within fault zones.

The spatial distributions of vitric and zeolitic material within the Calico Hills nonwelded hydrogeologic unit, along with the characterization of the basal vitrophyre of the Topopah Spring welded hydrogeologic unit, are important for understanding the distribution of perched water and for determining potential flow paths for radionuclides. Figure 4-119 shows a perspective view of the extent of perched water in the lower Topopah Spring welded hydrogeologic unit based on three-dimensional simulations with mean, present-day infiltration rates.

Performance assessment analyses, described in *Analysis of Base-Case Particle Tracking Results of the Base-Case Flow Fields (ID: U0160)* (CRWMS M&O 2000cb, Sections 6.2.1 and 6.2.2), considered the particle breakthrough locations and times resulting from two perched water conceptual models. Figure 4-120 shows the particle-break-



**Figure 4-119. Perched Water at the Base of the Topopah Spring Welded Hydrogeologic Unit**  
Figure based on a simulation with present-day mean infiltration rates. Blue indicates 100 percent liquid saturation (perched water) within fractures; green indicates less than 100 percent fracture liquid saturation. Elevation is given in meters; horizontal coordinates are Nevada State Plane, Easting. Source: CRWMS M&O 2000bw, Figure 6-9.

through locations at the water table for an advective tracer (no diffusion, sorption, or dispersion) released uniformly as a pulse in the outlined potential repository region using the mean infiltration case for the glacial-transition climate. Both perched-water models show a large amount of lateral diversion of particles beneath the northern portion of the potential repository. Many of the diverted particles are concentrated in faults, which, based on the simulated fault properties, channel water to the water table. Perched-water model #2 (permeability barrier, unfractured zeolite model) shows more lateral diversion in the southern portion of the potential repository area because of the absence of enhanced fracture permeability in zeolitic units of the Calico Hills nonwelded hydro-

geologic unit. Perched-water model #1 (permeability barrier, fractured zeolite model) shows breakthrough over a large area in the southern half of the potential repository footprint because of enhanced fracture permeability in zeolitic portions of the Calico Hills nonwelded hydrogeologic unit in areas where perched water is absent.

Additional results from modeling studies that investigate flow distribution within the Calico Hills nonwelded hydrogeologic unit, perched water occurrence, and the effects on flow and transport of major faults below the potential repository horizon are summarized in Section 4.2.1.3.

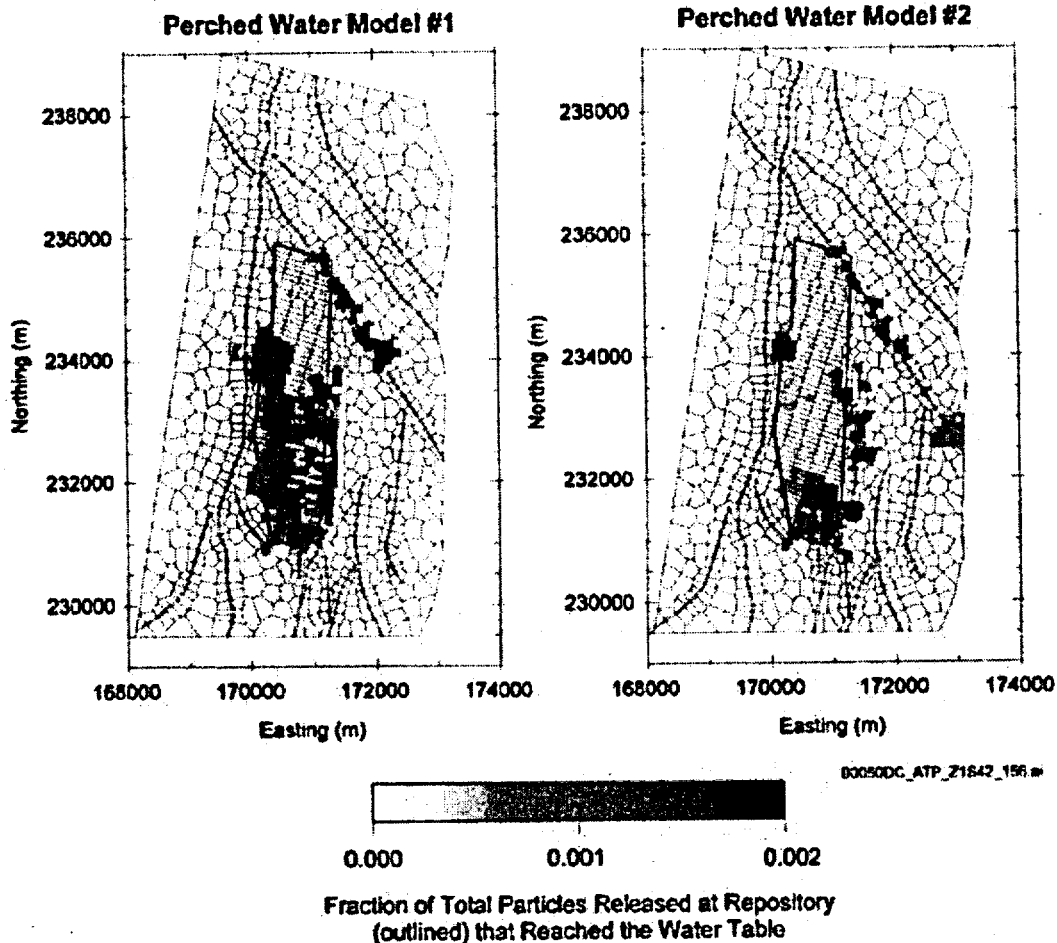


Figure 4-120. Locations of Particle Breakthrough at the Water Table for the Mean Infiltration, Glacial-Transition Climate Using Two Perched Water Models  
Source: CRWMS M&O 2000c, Figure 3.7-16.

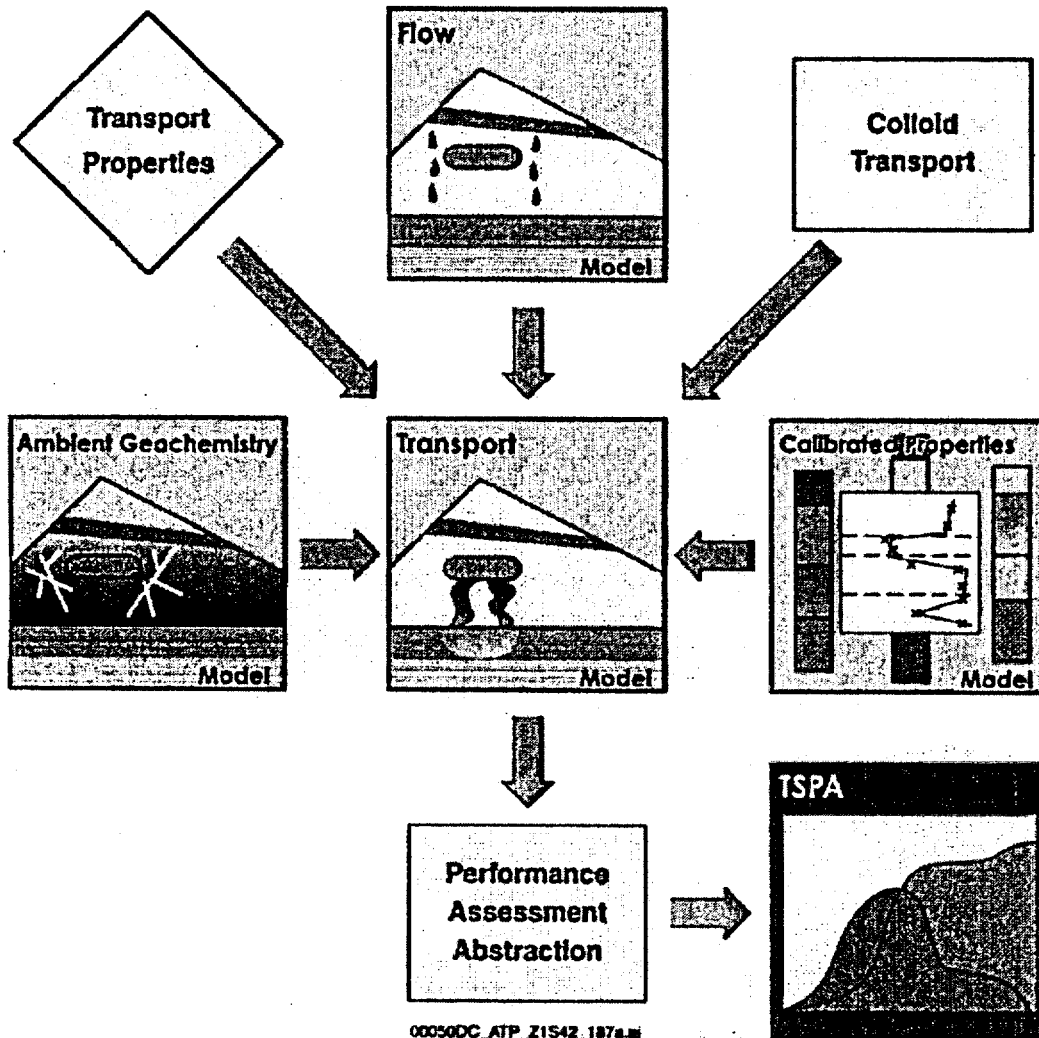
**4.2.8.3.3 Flow and Transport in Geological Layers below the Potential Repository**

In addition to unsaturated zone flow processes, radionuclide migration depends on transport properties, colloid transport mechanisms, and the geochemical environment. The relationship of other models and data feeds to the unsaturated zone transport model are schematically illustrated in Figure 4-121. Most of the model assumptions and approaches are similar to the corresponding unsaturated zone flow model components. The integrated flow and transport model is presented more fully in *Unsaturated Zone Flow and Trans-*

*port Model Process Model Report (CRWMS M&O 2000c, Section 3.11).*

**4.2.8.3.3.1 Transport of Nonsorbing and Sorbing Radionuclides through the Hydrogeologic Units**

For transport assessment, nonsorbing and weakly sorbing radionuclides with long half-lives are the primary concern. In sensitivity analyses, processes, properties, and model results are presented for the representative radionuclides: technetium-99 (nonsorbing), neptunium-237 (moderately sorbing), plutonium-239 (strongly sorbing), and its long-lived daughter uranium-235 (moderately



00050DC\_ATP\_Z1542\_187a.m

Figure 4-121. Relationships of Other Models and Data Inputs to the Unsaturated Zone Transport Model  
Source: CRWMS M&O 2000c, Figure 3.11-2.

sorbing). In these analyses, the radionuclides are released continuously at the top of the model domain (which coincides with the location of the potential repository), and the contaminant distribution is monitored over time for different percolation rates. In TSPA, the full inventory of radionuclides and their daughters are included to assess the total radioactivity distribution.

Flow in the zeolitic portions of the Calico Hills nonwelded hydrogeologic unit is judged to be dominated by fracture flow. In some welded and zeolitic layers, the matrix permeability is insufficient to carry the net infiltration, which implies that a portion of the percolation is likely to be carried by fractures (CRWMS M&O 2000c, Section 3.6.3.1). In vitric portions of the Calico Hills nonwelded hydrogeologic unit, matrix and fracture permeabilities are on the same order of magnitude; therefore, these layers behave as porous (rather than fractured) media, and flow is matrix-dominated. Fracture flow in the Topopah Spring welded hydrogeologic unit will be strongly attenuated.

transport velocities greatly reduced, and contact of dissolved radionuclides with the rock matrix enhanced by the slower velocities, longer contact time, and stronger fracture-matrix interaction, which leads to more retardation for sorbing radionuclides. Based on current understanding, the Prow Pass and Bullfrog tuffs are heterogeneous, with some zeolitic layers and some devitrified and unaltered layers (CRWMS M&O 2000c, Section 3.11.4).

#### 4.2.8.3.3.2 Two-Dimensional Radionuclide Transport at Representative Borehole Locations

The effect of geologic layers on radionuclide migration below the potential repository is illustrated in Figure 4-122, which illustrates, conceptually, flow and transport processes in two representative hydrogeologic profiles. Borehole USW UZ-14 is located in the northern part of the potential repository site, while borehole USW SD-6 is located in the southern part. Narrow-width

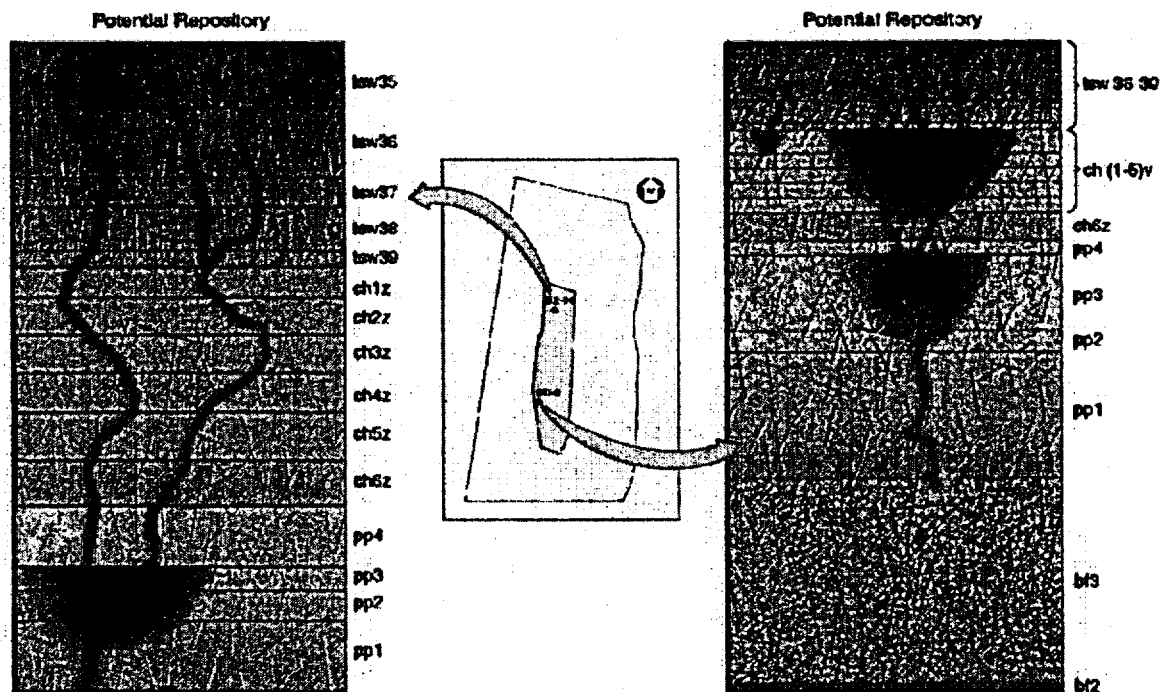


Figure 4-122. Flow and Transport in Two Representative Unsaturated Zone Hydrogeologic Profiles  
Source: CRWMS M&O 2000c, Figure 3.11-3.

cross-sectional (two-dimensional) models were developed at each of these locations. As radionuclides leave the potential repository, they could quickly migrate through the Topopah Spring welded hydrogeologic layers with limited matrix diffusion and sorption. Vitric layers could retard migration because of the matrix-dominated flow in these layers, while radionuclides could quickly pass through zeolitic layers due to the fracture-dominated flow (CRWMS M&O 2000c, Section 3.11.4).

The difference in the capacity to retard radionuclides between vitric and zeolitic tuffs is illustrated in Figure 4-123 for two-dimensional simulations with a percolation rate of 6 mm/yr (0.24 in./yr) (close to the mean present-day rate). At 10,000 years, the breakthrough to the water table for the moderately sorbing neptunium-237 occurs through zeolitic layers (in a cross section including borehole USW UZ-14) and does not occur through mainly vitric layers (in a cross section including borehole USW SD-6). Transport of other radionuclides through individual layers is summarized in *Unsaturated Zone Flow and Transport Model Process Model Report* (CRWMS M&O 2000c, Section 3.11.5). The two-dimensional simulations do not allow lateral diversion in the third dimension.

#### 4.2.8.3.3 Three-Dimensional Mountain-Scale Radionuclide Transport

In the three-dimensional model (CRWMS M&O 2000c, Section 3.11.6), the spatial distribution of percolation is heterogeneous with perched water and faults affecting the percolation distribution below the potential repository. Modeling of radionuclide transport using the mountain-scale three-dimensional grids (CRWMS M&O 2000ea, Sections 6.11 to 6.16) were performed, and breakthrough is described by a normalized release rate,  $R$ , (i.e., the ratio of radionuclide mass release rates at the water table versus that at the potential repository).

The normalized release rate for nonsorbing technetium-99 depends strongly on the infiltration rate (Figure 4-124). As the infiltration rate increases from lower-bound to mean present-day level, the

$t_{10}$  time, defined as the time at which  $R = 0.1$ , decreases from about 10,000 years to about 300 years. The  $t_{50}$ , the time at which  $R = 0.5$ , decreases from about 45,000 years to about 4,000 years. The upper-bound infiltration rate further reduces  $t_{10}$  and  $t_{50}$ . The maximum attainable normalized release rate decreases with the infiltration rate because lower infiltration results in lower velocities and slower transport, thus higher radioactive decay.

From  $t_{10}$  and  $t_{50}$  values, the moderate sorption and resulting retardation of neptunium-237 is sufficient to increase the time to reach the water table by a factor of about 40. The  $R = 1.0$  limit is not achieved within the simulation period. At 1 million years,  $R$  is 0.98, 0.86, and 0.42 for the upper-bound, mean, and lower-bound infiltration rates, respectively.

The normalized release rate for strongly sorbing plutonium-239 never reaches the 0.1 level, even after 1 million years of continuous release. The picture changes dramatically, however, if the daughter contributions to the release rate at the water table are accounted for in the computations. Given the half-life of plutonium-239 and the much longer half-life of uranium-235, the daughter contributions can become important. The relative flux fractions,  $M_R$ , are also shown in Figure 4-124. The plutonium contribution to the release rate starts declining rapidly after 1,000 years, and uranium-235 is by far the dominant species after 10,000 years (CRWMS M&O 2000ea, Section 6.14.1.2). After 1,000 years, the release at the water table consists mostly (over 95 percent) of uranium-235 under the lower-bound, present-day infiltration rate. The protactinium-231 contribution is negligible because of the very long half-life of uranium-235.

Direct comparison of perched-water hydrogeochronology and modeled radionuclide breakthrough times is hindered by the differences in the flowpaths of the water in both cases and the role and magnitude of retardation of the different radionuclides in the transport models. There are, nonetheless, some inferences that can be drawn about the percolation flux rates in the deep unsaturated zone and the style of flow in that region that

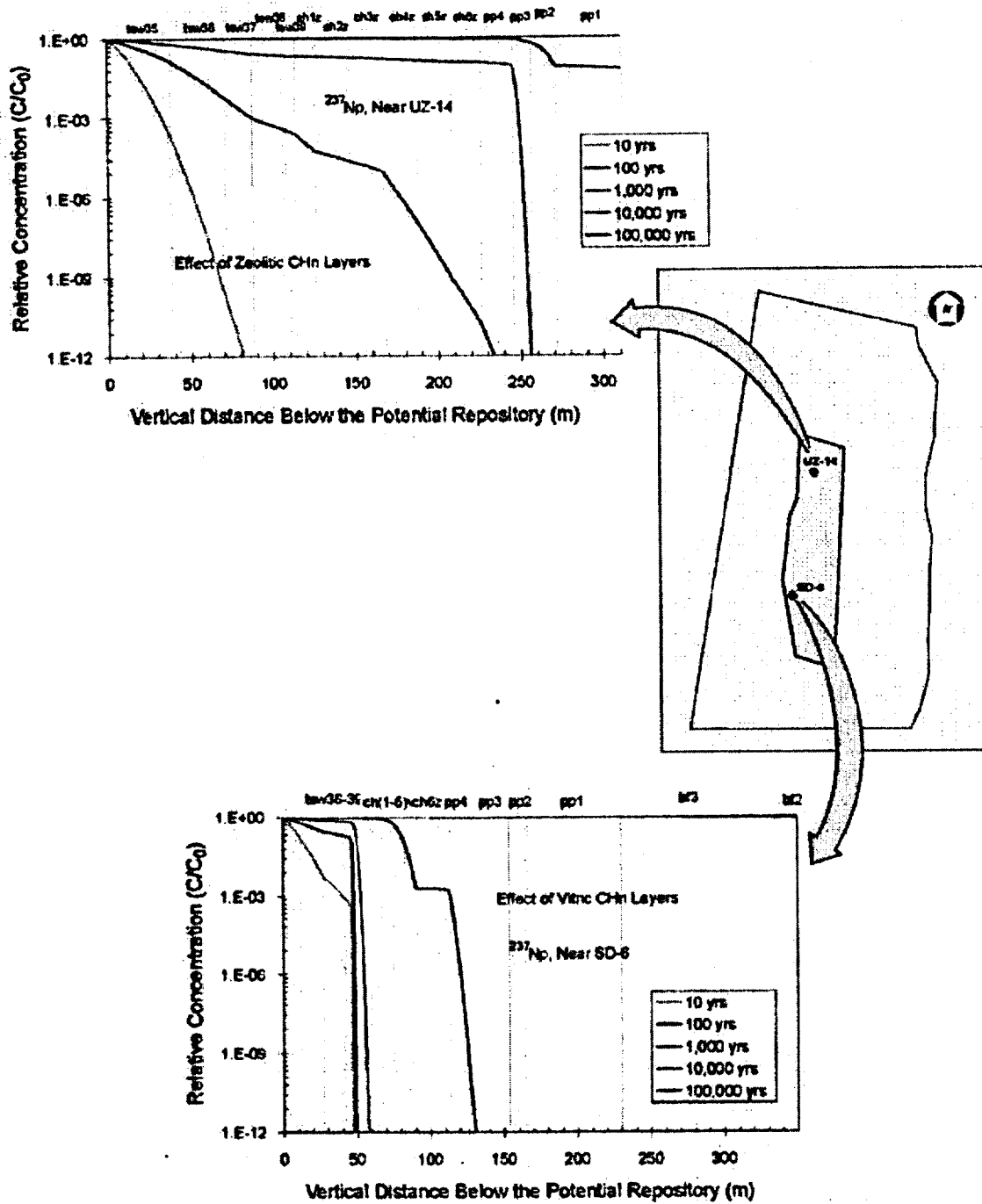


Figure 4-123. Comparison of Transport Characteristics in USW UZ-14 and USW SD-6  
The data shown in this figure are based on a model that is appropriately conservative for TSPA analysis and not intended to represent expected breakthrough of radionuclides of the water table. Source: CRWMS M&O 2000c, Figure 3.11-4.

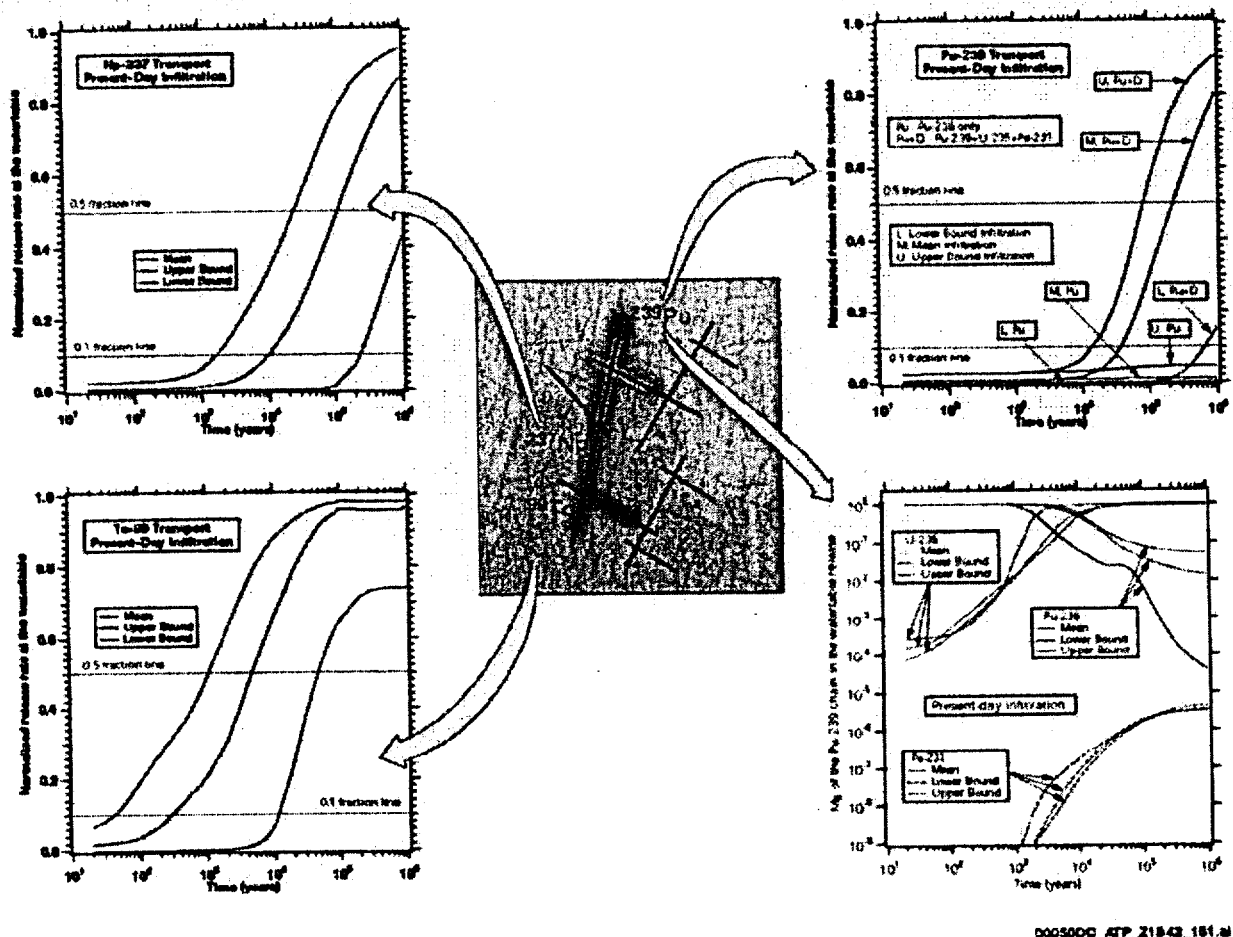


Figure 4-124. Normalized Release Rate and Dependence of Technetium-99 Transport on Infiltration Rates. The data shown in this figure are based on a model that is appropriately conservative for TSPA analysis and not intended to represent expected breakthrough of radionuclides at the water table. Source: CRWMS M&O 2000c, Figure 3.11-5.

are useful in supporting the understanding of unsaturated zone transport.

Perched water is a mixture of old and young water, with the oldest water perhaps being the product of flow during past wetter climates and the youngest water being the result of fast fracture flow. The chlorine-36 analyses of perched water indicate ages ranging from 2,000 to 12,000 years, in general agreement with the carbon-14-based ages (BSC 2001r, Section 6.6.3.6; Yang, Rattray et al. 1996). Variation in ages from place to place in the perched water bodies indicates incomplete mixing of old and young water. Pore water near fault zones (borehole UZ#16) is sometimes apparently some-

what younger than the water in nearby perched-water bodies (Yang, Rattray et al. 1996).

Major ion concentrations and uranium isotope data indicate that the perched-water bodies formed from water different from water in the matrix of the host rock and that little equilibration has taken place between these waters (BSC 2001r, Section 7.5). This suggests that perched water arrived at its present location by fracture flow in a flow system in which there was little liquid exchange between the fractures and the matrix. This observation supports the dual permeability model used in evaluating unsaturated zone transport.

The apparent radionuclide transport times from the repository horizon to the water table average about 5,000 years (CRWMS M&O 2000c, Section 3.11.8), falling at about the median age of perched water (BSC 2001s, Section 6.2.1.2). Although the flowpaths and details of radionuclide retardation are different, the fracture-dominated dual-permeability flow mechanism is comparable, and the youngest perched water is not much younger than the predicted breakthrough times. The hydrogeochronology of the perched water therefore permissively supports the modeled breakthrough times by demonstrating slow percolation in the deep unsaturated zone and the geochemistry of the fracture and matrix water supports the dual permeability model used in the breakthrough modeling.

Where transported radionuclides intersect perched water, the role of the perched-water bodies in transport includes the dilution of radionuclides and delay associated with residence time in the perched-water bodies. The residence times and subsequent transport flowpaths are represented by two conceptual models, one representing vertically downward flow and another representing lateral diversion to faults and subsequent rapid downward flow to the water table (BSC 2001s, Section 6.5.3.2). These are known as the flow-through and flow-by models. The flow-through model is used in performance assessment because it is slightly faster and therefore more conservative.

Results of the three-dimensional simulation indicate that flow is diverted above the zeolitic Calico Hills nonwelded hydrogeologic unit and that radionuclides move slowly through the perched water to faults and to the vitric Calico Hills nonwelded hydrogeologic unit. In the three-dimensional model, transport is controlled by faults, especially at the early times (approximately 100 years). The Ghost Dance (southern splay), Sundance, and Drill Hole Wash faults are the main transport-facilitating features, providing fast pathways to the water table (CRWMS M&O 2000ea, Section 6.12.2.2). The main Ghost Dance fault does not play an important role in transport at the bottom of the Topopah Spring welded hydrogeologic unit, as the technetium-99 does not reach the fault at this level even after 100,000 years (CRWMS M&O 2000ea, Section 6.12.2.2). This fault is more important at

the water table, where it acts as a barrier to lateral transport while facilitating downward migration into the water table.

The transport pattern illustrated in Figure 4-125 indicates that radionuclide transport to the groundwater is expected to be faster in the southern part of the potential repository block, where it is also areally concentrated. There are several reasons for this. First, the rates and direction of water flow dictate the advective transport pattern, and the maximum water flow within the footprint of the potential repository is in its southern part in perched water model #1. Second, the presence of the highly conductive faults (e.g., Splay G of the Solitario Canyon fault and the Ghost Dance fault splay) act as the venue for fast transport, despite the fact that the vitric Calico Hills nonwelded hydrogeologic unit behaves as a porous medium (with relatively lower water velocities). These faster transport pathways may be facilitated by flow focusing in the vitric Calico Hills nonwelded hydrogeologic unit, which has a funnel-shaped distribution in the south. Third, the low-permeability zones at the Topopah Spring welded-Calico Hills nonwelded hydrogeologic unit interface in the northern part of the potential repository, act as barriers to water drainage, and lead to low water velocities and the presence of perched water bodies. Radionuclides move slowly through the perched water before reaching the underlying conductive zeolitic Calico Hills nonwelded hydrogeologic unit, hence the delay in transport. Radionuclide breakthrough at the water table occurs before 1,000 years and over a large area by 10,000 years in the southern part of the potential repository block.

#### 4.2.8.3.3.4 Three-Dimensional Mountain-Scale Transport of Plutonium True Colloids

Plutonium, a major nuclear fuel element, can be present as a waste-form colloid (i.e., true or intrinsic colloid as elemental particle). The waste-form colloids will play a more significant role than natural colloids as pseudocolloids with radionuclides adsorbed to the naturally occurring fine particles (CRWMS M&O 2000ec, Section 7). Colloid size has an important effect on transport,

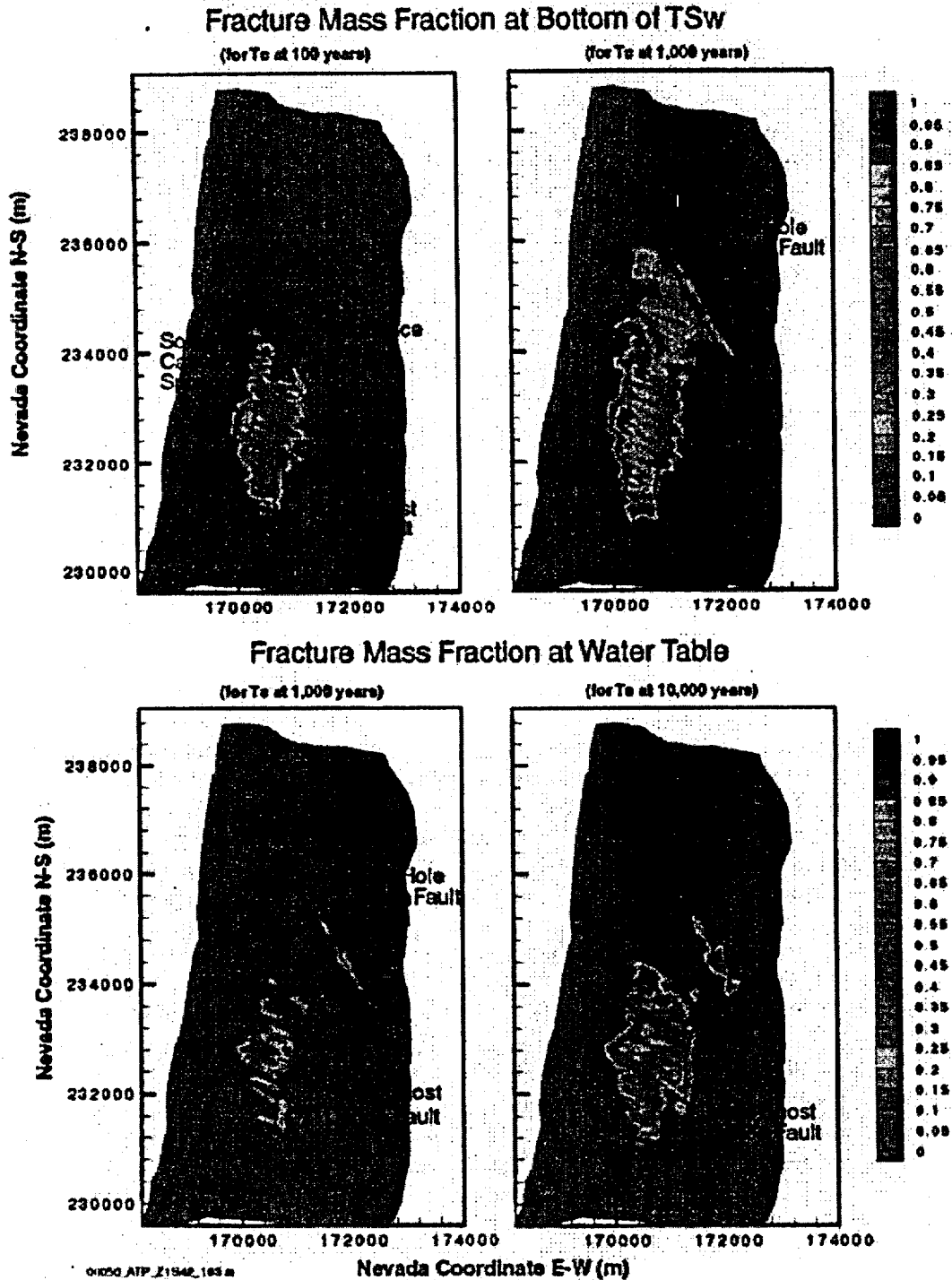


Figure 4-125. Normalized Mass Fraction Distribution of Technetium-99 in Fractures at the Bottom of the Topopah Spring Welded Hydrogeologic Unit and at the Water Table

The data shown in this figure are based on a model that is appropriately conservative for TSPA analysis and not intended to represent expected breakthrough of radionuclides at the water table. Source: CRWMS M&O 2000c, Figure 3.11-6.

and the size exclusion (inability of larger colloids to move into the matrix) results in enhanced transport to the groundwater. Smaller colloidal particles can diffuse more easily into the matrix, and their transport is thus more retarded. Size exclusion at the interfaces of different geologic units leads to colloid concentrations that can be significantly higher than that in the water released from the potential repository (CRWMS M&O 2000ea, Section 6.16). These high concentrations are observed behind (i.e., they do not penetrate) the interfaces because the large-size colloids cannot move across the interface.

#### 4.2.8.3.4 Alternative Conceptual Approaches

The alternative conceptual processes for unsaturated flow below the potential repository horizon, as described in Section 4.2.1.3.4, have the same large impacts on the unsaturated zone transport. These alternative processes include episodic flow within the Topopah Spring welded hydrogeologic unit, flow through the perched water into the Calico Hills nonwelded unit without significant lateral diversion, and faults in the Calico Hills unit and below having low permeabilities. The conservatism and optimism associated with the advective transport are similar to the discussions in Section 4.2.1.3.4 and are not reiterated in this section.

**Drift Shadow**—If the shadow zone of drier conditions exists below the drift, the advective and diffusive transport will be greatly reduced in the vicinity of the radionuclide release points, as illustrated in Figures 4-116 to 4-118. Omitting the shadow process from the unsaturated zone transport model results in a conservative evaluation. A realistic representation, with drift-scale processes below the drift taken into account, would likely result in performance analyses that indicate more retardation of radionuclide transport in the unsaturated zone. More recent modeling and analyses, which show that the drift shadow may increase the radionuclide transport time from the repository horizon to the water table by several orders of magnitude, are presented in Volume 1, Sections 11.2.1 and 11.3.1 of *FY01 Supplemental Science and Performance Analyses* (BSC 2001a).

**Matrix Diffusion**—Some previous hydrologic models of Yucca Mountain have ignored the effects of matrix diffusion, an assumption that is very conservative because it ignores the interaction between water in fractures and the rock matrix, particularly in unwelded tuffs. This results in unrealistically fast predictions of transport. The available analyses of Alcove 1 infiltration tests indicate that the inclusion of matrix diffusion is important in interpreting the data and in validating the models. Ongoing testing and modeling of the Alcove 8 to Niche 3 Cross-Drift test can further validate the importance of matrix diffusion. While neglecting matrix diffusion is conservative, the alternative process model with no matrix diffusion is not realistic. In the TSPA-SR abstraction, matrix diffusion is explicitly incorporated and modeled (CRWMS M&O 2000c, Section 3.11.13.1).

#### 4.2.8.3.5 Uncertainties and Limitations

The uncertainties and limitations for unsaturated flow, as described in Section 4.2.1.3.5—in climate, hydrologic properties in lower tuff units, geochemical analyses, and numerical approaches—are also applicable to unsaturated zone transport. In this section, uncertainties and limitations associated with field testing are first discussed, followed by evaluations of transport properties.

##### 4.2.8.3.5.1 Uncertainties and Limitations for Field Testing in Lower Hydrogeologic Units

The field tests in construction water monitoring and liquid release testing are mainly limited to the tuff units accessible from the Exploratory Studies Facility, in and above the middle nonlithophysal zone of the Topopah Spring welded hydrogeologic unit. Ongoing tests along the Cross-Drift are generating additional data for the lower lithophysal unit, with additional tests in the lower nonlithophysal and the western part of the potential repository block planned. Uncertainties about transport below the drift can be reduced with relevant data collected.

The unsaturated zone transport test site at Busted Butte is in a distal extension of the vitric Calico Hills nonwelded hydrogeologic unit. The site-

specific information about the zeolitic Calico Hills nonwelded hydrogeologic unit is based on borehole cores. The uncertainties and limitations are being assessed by comparing tests in fractured units and in vitric units to demonstrate that core-scale data are adequate for site-scale assessment.

#### 4.2.8.3.5.2 Uncertainties and Limitations in Transport Properties

Many conservative approximations are used in the performance assessments, leading to overestimation of radionuclide transport. Conservative assignments of transport parameters, potentially overconservative alternative models, and potentially optimistic (nonconservative) approaches all contribute to uncertainties in the assessment of transport processes in the unsaturated zone. In addition to the diffusion processes discussed in Section 4.2.8.3.4, some of the uncertainties and limitations of other flow and transport processes are further discussed below.

**Matrix Sorption**—The experimentally determined  $K_d$  values are mostly from batch experiments using crushed tuff under saturated conditions. These saturated conditions are not representative for ambient conditions in the unsaturated zone. The crushed rock tests can overestimate sorption, and fine particles generated in grinding can lead to irreproducible or high  $K_d$  values (CRWMS M&O 2000ea, Section 6.1.3.1). Measurements of tracer penetration into unsaturated core-size solid tuff samples can generate  $K_d$  values that are more directly related to processes of transport through fractured blocks observed in the field (CRWMS M&O 2000bu, Section 6.4).

**Rate-Limited Sorption**—Rate-limited sorption could be important, especially for fluid-radionuclide-rock systems with large sorption potential. Breakthrough curves for neptunium-237 transport in tuffs from the column experiments can only be analyzed by considering rate-limited sorption (Viswanathan et al. 1998, p. 267). This result indicates the existence of rate-limited sorption under flowing conditions. Nonlinear and irreversible sorption are also evident from the diffusion and transport studies in *Unsaturated Zone and Saturated Zone Transport Properties (U0100)*

(CRWMS M&O 2000eb, Sections 6.5 and 6.6). Overall, rate-limited sorption and nonlinear sorption are uncertainties in evaluating the validity of the linear equilibrium sorption adopted in unsaturated zone transport studies. Rate-limited sorption reduces sorption in the matrix and increases the concentration and duration of migration through the fractures. In the TSPA-SR, the sorption coefficients ( $K_{ds}$ ) of linear sorption for different radionuclides are represented by distribution functions to quantify the uncertainties (CRWMS M&O 2000a, Section 3.7.3).

**Colloid Declogging**—The kinetic declogging (reverse) coefficient,  $\kappa$ , is treated as a fraction of  $\kappa^*$  to examine the sensitivity of this parameter on colloidal transport (CRWMS M&O 2000c, Figure 3.11-7). When no declogging is allowed, no colloids reach the water table (CRWMS M&O 2000ea, Section 6.16). Small values of  $\kappa$  (i.e., slow declogging) lead to retardation of colloids and slow transport to the water table. Large values of  $\kappa$  (i.e., fast declogging) lead to fast transport to the water table for radioactive colloids. For the TSPA-SR, the colloid retardation factor is conservatively set to 1 for all colloids in the unsaturated zone.

**Surface Diffusion**—It is possible that surface diffusion can be supported in zeolites. Surface diffusion can be important for radionuclides that exhibit strong sorption (e.g., plutonium). A larger  $K_d$  clearly indicates stronger sorption, but this does not mean immobilization of the dissolved species when the fractured porous medium supports surface diffusion (Moridis 1999, Section 6.1.2). For the TSPA-SR, the uncertainties of molecular diffusion coefficients (as described in Section 4.2.8.2.2, based on sorbing tritium and nonsorbing technetium measurements) and the retardation factors are independently sampled. The uncertainties associated with surface diffusion may be large for media supporting surface diffusion.

**Desorption from Radioactive Decay**—Daughters of sorbed parents may be ejected from grain surfaces because of recoil from radioactive decay. The alpha decay is evaluated and the potential implications for kinetically controlled sorption are discussed in *Radionuclide Transport Models under Ambient Conditions* (CRWMS M&O 2000ea,

Section 6.2.8). For equilibrium sorption, this is not an issue.

**Particle Tracking**—Different approaches to represent matrix diffusion could yield different transport behavior. Comparisons between the FEHM V2.10 particle tracker and DCPT code were performed by *Analysis Comparing Advective-Dispersive Transport Solution to Particle Tracking* (CRWMS M&O 2000ee, Section 6.4). The two particle-tracking routines agree only if diffusion and dispersion are neglected. For the cases that include diffusion and dispersion, the median breakthrough for FEHM V2.10 occurs at times more than one or two orders of magnitude earlier. The difference is more pronounced for radionuclides undergoing sorption in the matrix. These differences stem from different implementations of the diffusive mass flow between fractures and the matrix in the two codes (CRWMS M&O 2000ee, Section 7). The conservative FEHM V2.10 particle tracker is used for the TSPA-SR abstraction. The flow fields derived from the three-dimensional site-scale model are inputs to the particle tracker and are used to calculate transport velocities.

#### 4.2.8.4 Total System Performance Assessment Abstraction

Unsaturated zone transport is important as the first natural barrier to radionuclides that escape from the potential repository. The unsaturated zone acts as a barrier by delaying radionuclide movement. If the transport time is long compared to the radionuclide half-life, then the unsaturated zone may have an important effect on decreasing the dose from that radionuclide at the biosphere. In this section, the abstraction of unsaturated zone process modeling results into the TSPA-SR is presented (CRWMS M&O 2000a, Section 3.7).

Within the unsaturated zone, radionuclides can migrate in groundwater as dissolved molecular species or associated with colloids (CRWMS M&O 2000a, Section 3.7.1). Five basic processes affect the movement of dissolved or colloidal radionuclides: advection, diffusion, sorption, hydrodynamic dispersion, and radioactive decay. Sorption is potentially important because it slows, or retards, the transport of radionuclides. Diffusion

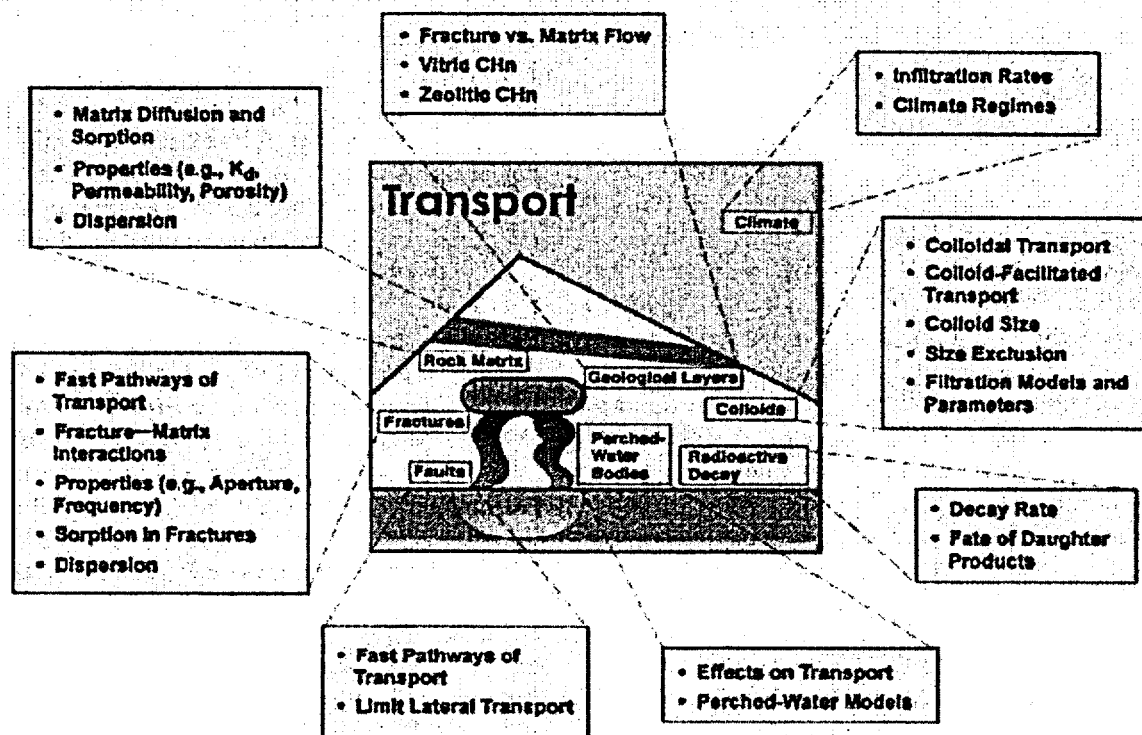
of radionuclides out of fractures into matrix pores is also a potential retardation mechanism because matrix transport is generally slower than fracture transport. However, sorption and matrix diffusion have less effect on colloids, so radionuclides can be more mobile if they are attached to colloids than if they are dissolved in the water. Radioactive decay is potentially important because daughter products may have sorption behavior different than that of the parent radionuclide, thus affecting transport. The key processes and issues for unsaturated zone transport are summarized in Figure 4-126. The unsaturated zone flow and transport model is used to represent the key processes, assess the uncertainties, and provide direct inputs to the TSPA-SR.

#### 4.2.8.4.1 Abstraction and Direct Use of the Unsaturated Zone Flow and Transport Fields

A dual-permeability model is used to represent mountain-scale unsaturated zone flow. The same concept is used to model radionuclide transport: a dual-continuum model in which fractures and matrix are distinct interacting continua that coexist at every point in the modeling domain. Each continuum is assigned transport properties in addition to its hydrologic properties. The properties can vary spatially.

The unsaturated zone transport model is directly coupled, that is, dynamically linked, with the TSPA-SR model (CRWMS M&O 2000a, Section 3.7.2). The unsaturated zone flow calculations are done ahead of time, and the flow fields are saved for use by the TSPA-SR model. During a TSPA simulation, radionuclide mobilization and transport through the engineered barrier system are calculated and the radionuclide mass flux at the engineered barrier system boundary at each time step is provided as the boundary condition for unsaturated zone transport.

The use of pregenerated flow fields implies the assumption of quasi-steady flow. That is, flow is modeled as a sequence of steady states (as an approximation). Mountain-scale unsaturated zone flow is represented as a sequence of steady states as determined by climate change and infiltration models. The transport calculation (particle



00050DC\_ATP\_Z1542\_158a.nl

Figure 4-126. Key Issues of Unsaturated Zone Transport  
Source: CRWMS M&O 2000c, Figure 3.11-1.

tracking) itself is fully transient, with radionuclides moving downward from the potential repository as they are released. Each TSPA realization uses one set of flow fields: low infiltration, mean infiltration, or high infiltration; each set has three flow fields, for present-day, monsoon, and glacial-transition climates.

The flow field is changed from one to another at the time of a climate change. The transport calculation then continues with the new flow field. In addition to the step change in the flow field, the location of the water table is also changed at the time of climate change. The water table for the future climates (monsoon and glacial-transition) is taken conservatively to be 120 m (390 ft) higher than the present-day water table (CRWMS M&O 2000ca, Section 6.2). When the water table rises with a climate change, radionuclides in the unsaturated zone between the previous and new water table elevations are moved to the saturated zone.

#### 4.2.8.4.2 Abstraction of Matrix Diffusion, Sorption, and Dispersion

The incorporation of matrix diffusion in the unsaturated zone transport model is simplified by conservatively neglecting flow in the matrix continuum in the diffusion calculation. This allows use of an analytical solution for matrix diffusion (CRWMS M&O 2000ed, Section 6.1.3). Fracture properties (aperture, spacing) are modified to take into account that only some fractures actively flow and transport radionuclides (CRWMS M&O 2000ed, Section 6.2.1). Colloids are larger than solute molecules, so they have much smaller diffusion coefficients. Because of this and possible size-exclusion effects, matrix diffusion is conservatively neglected for colloids. Anionic species such as pertechnetate (the predominant aqueous species of technetium) have lower diffusion coefficients than cationic species (CRWMS M&O 2000c, Section 3.11.3.2) and are assigned different diffusion coefficients.

In TSPA simulations, the sorption characteristics of the tuff units are taken to be constant in time. Changes in sorption (or other transport properties) brought about by thermal effects of the potential repository or from climate change have been considered and found to be insignificant (CRWMS M&O 2000ef, Sections 6.3.8 and 6.8).

In unsaturated zone TSPA transport calculations, dispersion in fractures is represented independently of that in the matrix (CRWMS M&O 2000a, Section 3.7.1.4). Dispersion is a way of including small-scale velocity variations in the transport model, but these small-scale variations are not very important to unsaturated zone transport because they have less effect over long distances than the large-scale velocity variations that are explicitly included in the model. Also, the explicitly modeled differences in transport velocity between fractures and matrix, and the transfer of radionuclides between them, introduce considerable dispersion into the transport simulations. Transverse dispersivities are normally small compared to longitudinal dispersivities (CRWMS M&O 2000a, Section 3.7.1.4). Any transverse dispersion (spreading) that occurs in the unsaturated zone is eliminated at the water table by starting the saturated zone transport model at a small number of discrete points.

#### 4.2.8.4.3 Abstraction of Colloidal Transport

Colloids diffuse more slowly than dissolved radionuclides because of their larger size, and as a result, matrix diffusion of colloids is neglected in TSPA. Colloids can, however, move between fractures and rock matrix advectively (i.e., moving with the water) as long as they are smaller than the matrix pores. Most of the pores in the welded and zeolitic tuffs are small, so most colloids remain in the fractures in those hydrogeologic units (CRWMS M&O 2000c, Section 3.11.3.4). Because transport in fractures is faster than transport in the matrix, this size-exclusion effect results in faster colloidal transport in those units. Most flow and transport in those units is through fractures, so the result of this effect is not large. In addition, a size-exclusion effect is possible at hydrogeologic unit interfaces. This exclusion is not applied to colloids transporting through fractures because fractures are

relatively large compared to matrix pores, but it is applied to colloids transported in the matrix from one hydrogeologic unit to another. In this situation a portion of the colloids, corresponding to the fraction of them that are smaller than the pores in the downstream unit, is stopped at the unit interface. This exclusion is taken to be a permanent filtration for irreversible colloids; it is not applied to reversible colloids because the radionuclides can desorb from the colloids and continue to move (CRWMS M&O 2000c, Section 3.11.13.3).

Colloids may be temporarily "detained" at the interface of fractures and matrix or sorbed to fracture walls (reversible filtration), and this interaction can be included in the colloid transport model as a retardation factor for colloid transport in the fracture system (CRWMS M&O 2000c, Section 3.11.13.3; CRWMS M&O 2000ed, Section 5.3). The effective transport velocity is reduced by this retardation factor. However, the data available on this effect are for the saturated zone, so the retardation factor is conservatively set to 1 in the unsaturated zone (i.e., no retardation due to this factor).

For reversible colloids, radionuclides sorbed to colloids are assumed to be in equilibrium with radionuclides in solution. The ratio of the concentration of a radionuclide sorbed to colloids to the concentration in solution is represented by a colloid partitioning factor in the models (CRWMS M&O 2000ed, Section 5.3). The ratio is a function of the concentration of colloids and the sorption coefficient for the given radionuclide onto the given type of colloid. Diffusion of dissolved radionuclides into the matrix can reduce the concentration in the fractures, which reduces the amount of radionuclides sorbed to the colloids in equilibrium with radionuclides in solution. Thus, matrix diffusion can effectively slow the transport. The colloid partitioning factor is one of the key transport parameters sampled in the TSPA-SR (CRWMS M&O 2000a, Section 3.7.3).

#### 4.2.8.4.4 Abstraction with Particle Tracking

Radionuclide transport modeling for the unsaturated zone uses the residence time transfer function particle-tracking technique (CRWMS M&O

2000c, Section 3.11.13.3). This technique is a cell-based approach in which particles move from cell to cell in a numerical grid. Particle locations within cells are not tracked as they are in some particle-tracking techniques, but rather movement from cell to cell is computed probabilistically based on transfer functions. The transfer functions are defined using analytical or semi-analytical solutions of the transport equations and represent probability distributions of the residence time (the amount of time that a particle resides in a cell). The probability that a particle will move to a neighboring cell is proportional to the water flow rate to that cell. Only outflows are included in this calculation; particles are not moved to a cell if water flows from that cell to the current cell. A dual-continuum conceptual model is used for transport, so there is a network of fracture cells and a network of matrix cells, with each fracture cell connected to a corresponding matrix cell.

#### 4.2.8.4.5 Abstraction of Spatial and Temporal Variabilities

Releases from the engineered barrier system are computed for 30 environmental groups that are based on infiltration, waste type, and seepage condition (CRWMS M&O 2000a, Section 3.7.2). Because infiltration is important for unsaturated zone transport, radionuclides are released into the unsaturated zone at locations consistent with the environmental group from which they are released. Each environmental group is associated with one of five infiltration categories that are based on the percolation at each spatial location during the glacial-transition climate. The ranges for the categories are 0 to 3 mm/yr (0 to 0.1 in./yr), 3 to 10 mm/yr (0.1 to 0.4 in./yr), 10 to 20 mm/yr (0.4 to 0.8 in./yr), 20 to 60 mm/yr (0.8 to 2.4 in./yr), and greater than 60 mm/yr (2.4 in./yr).

To avoid artificial dispersion, the model of radionuclide release into the unsaturated zone takes into account the number of failed waste packages within each of the five infiltration categories (CRWMS M&O 2000a, Section 3.7.2). If only one waste package has failed in a category, then releases for that category are put into a single unsaturated zone cell, sampled randomly from the cells in that category. If two waste packages fail,

then releases are put into two randomly selected cells. This process continues for additional waste packages until the number of failed waste packages is equal to the number of cells in the category; at that point the releases are spread over all cells in the category, and additional waste package failures cause no change in the release locations. For any number of failed waste packages in a particular category, releases are always divided evenly among the cells that have been selected. Artificial dispersion in the unsaturated zone is further reduced by gathering releases from the unsaturated zone into a few discrete locations at the water table for input to the saturated zone transport model.

In the unsaturated zone transport model, spatial variability is included by use of a three-dimensional model that incorporates the appropriate geometry and geology (CRWMS M&O 2000a, Section 3.7.3). Temporal variability is included by using different unsaturated zone flow fields for different climate states, but none of the other transport properties change with time.

#### 4.2.8.4.6 Uncertainty and Conservatism

Uncertainty is included in the unsaturated zone transport model by defining uncertainty distributions for a number of input parameters. Values of these parameters for each TSPA realization are sampled from the distributions. Thus, each realization of the total system has a unique set of input parameters, each of which is within the range that is considered to be defensible (CRWMS M&O 2000a, Section 3.7.3). Normally each realization is considered to be equally likely, but importance sampling may be used to emphasize some realizations (usually to increase the probability of sampling an unlikely parameter value).

Current performance assessment models of unsaturated zone transport consider and account for uncertainties and conservatisms. These are detailed in *Unsaturated Zone Flow and Transport Model Process Model Report* (CRWMS M&O 2000c); they include:

- The significance of fracture flow in the vitric Calico Hills nonwelded hydrogeologic unit

- The effectiveness of perched water to divert water away from the zeolitic Calico Hills nonwelded hydrogeologic unit
- The reduction of fracture–matrix interaction along fractured flow paths within the Topopah Spring welded hydrogeologic unit
- The extrapolation of properties for the fault intervals in the Calico Hills nonwelded hydrogeologic unit and the Crater Flat undifferentiated hydrologic unit from fault data collected in the Topopah Spring welded hydrogeologic unit
- The use of a conservative particle tracker for performance assessment.

This conservatism may be partially offset by the use of batch-derived retardation factors (obtained from crushed-rock samples) for radionuclide migration, which may overestimate sorption (CRWMS M&O 2000c, Section 3.11.10.2). In general, the abstraction represents a balance of conservative assumptions and nominal parameters and processes to yield a reasonably realistic representation and assessment.

As noted in Section 4.1.1.2, the DOE has completed several activities to improve the treatment of uncertainty in current models, and the results are reported in *FY01 Supplemental Science and Performance Analyses* (BSC 2001a; BSC 2001b). Modeling based on new information and one-off sensitivity studies were focused on model aspects that were identified as unevaluated or that were perceived as having overly conservative estimates of uncertainty associated with them (BSC 2001b, Table 1.3-1). Descriptions of each analysis are contained in Volume 1 of *FY01 Supplemental Science and Performance Analyses* (BSC 2001a) and an assessment of the impact of the analyses on performance is presented in Volume 2 (BSC 2001b). In addition, analyses and assessments were carried out that provide a basis for evaluation of the role of repository thermal operating mode on performance and uncertainty. Analyses of performance of thermal modes are presented in Volume 2, Section 4 of *FY01 Supplemental Science and*

*Performance Analyses* (BSC 2001b). The supplemental analyses indicate that the TSPA-SR model is generally conservative to reasonable. The sensitivity studies are also briefly described in Section 4.4.5.5.

#### 4.2.9 Saturated Zone Flow and Transport

Yucca Mountain is part of the Alkali Flat–Furnace Creek subbasin of the Death Valley flow system. Recharge within the Death Valley flow system occurs at high altitudes, where relatively large amounts of snow and rainfall occur. Water inputs to the Alkali Flat–Furnace Creek subbasin include groundwater inflow along the northern boundary of the subbasin, recharge from precipitation in high-elevation areas of the subbasin, and recharge from surface runoff in Fortymile Canyon and Fortymile Wash. North and northeast of Yucca Mountain, recharge from precipitation is believed to occur also at Timber Mountain, Pahute Mesa, Rainier Mesa, and Shoshone Mountain (CRWMS M&O 2000bn, Section 3.2).

The geologic strata at Yucca Mountain form a series of alternating volcanic aquifers and confining units above the regional carbonate aquifer. The volcanic rocks generally thin toward the south, away from their eruptive sources in the vicinity of Timber Mountain. The volcanic aquifers and confining units are intercalated with undifferentiated valley-fill and the valley-fill aquifer to the south and southeast of Yucca Mountain (USGS 2000d, Section 6.1).

The general conceptual model of saturated zone flow in the site-scale saturated zone flow and transport model area is that groundwater flows to the south from recharge areas of higher precipitation at higher elevations north of Yucca Mountain, through the Tertiary volcanic rocks into the valley-fill aquifer, and toward the Amargosa Desert. Within the site-scale model area, recharge occurs from infiltration of precipitation and infiltration of flood flows from Fortymile Wash and its tributaries. Outflow from the model area mostly occurs across the southern boundary of the model, and to pumpage by irrigation wells in the Amargosa Farms area (CRWMS M&O 2000bn, Section 3.2).

In the event of waste mobilization and migration away from the potential emplacement drifts at Yucca Mountain, the rate of radionuclide transport through the saturated zone is determined by the groundwater flux, the hydrologic properties, and sorptive properties of tuff and alluvium units.

The objective of the saturated zone flow and transport process model and the corresponding components of the TSPA-SR is to evaluate the migration of radionuclides from their introduction at the water table below the potential repository to

the release point to the biosphere, as illustrated in Figures 4-127 and 4-128. The release point is at the accessible environment downgradient (i.e., the direction of groundwater flow) from the site. The main output of the saturated zone flow and transport process models used directly by the TSPA is an assessment of the concentration of radionuclides in groundwater and the time it takes for various radionuclides to be transported from areas beneath the potential repository to the accessible environment. The current understanding of saturated zone transport is documented in *Saturated Zone Flow*

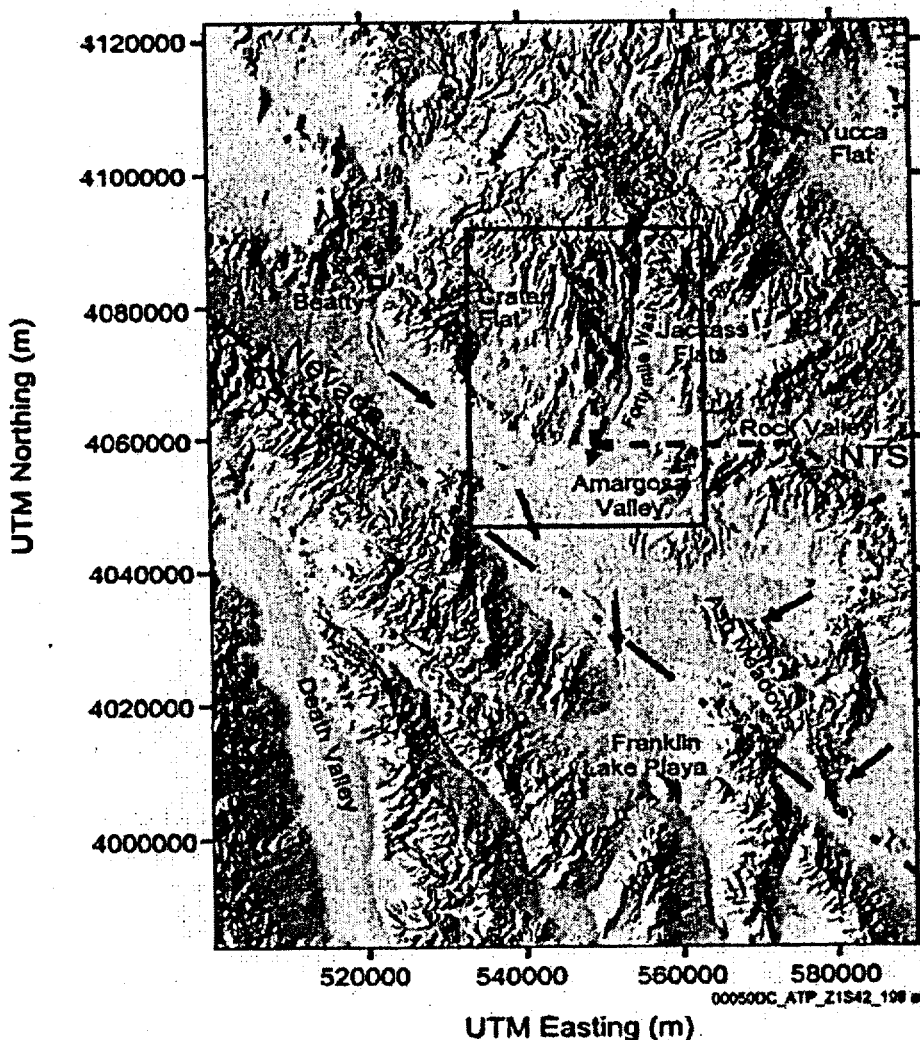


**Figure 4-127. Regional Map of the Saturated Zone Flow System Showing Direction of Flow and Outline of the Three Dimensional Saturated Zone Flow Model Domain**  
Arrows give direction of flow from regional flow models. The solid rectangle shows the boundary of the site-scale three-dimensional saturated zone flow model. Flow from Yucca Mountain is southeast to Fortymile Wash and then south to the site-scale model boundary. NTS = Nevada Test Site. Source: (CRWMS M&O 2000a, Figure 3.8-4).